Manganese-driven Oxidation of Amino(poly)phosphonates – Processes, Product Formation and Quantification

Dissertation

der Mathematisch-Naturwissenschaftlichen Fakultät

der Eberhard Karls Universität Tübingen

zur Erlangung des Grades eines

Doktors der Naturwissenschaften

(Dr. rer. nat.)

vorgelegt von

Anna Magdalena Röhnelt

aus Düsseldorf

Tübingen

2024

Gedruckt mit Genehmigung der Mathematisch-Naturwissenschaftlichen Fakultät der Eberhard Karls Universität Tübingen.

Tag der mündlichen Qualifikation:	14.02.2025
Dekan:	Prof. Dr. Thilo Stehle
1. Berichterstatter/-in:	Prof. Dr. Stefan B. Haderlein
2. Berichterstatter/-in:	Prof. Dr. Christian Zwiener

Abstract

Aminopolyphosphonates (APPs) are widely used chelating agents in industrial and household applications, with increasing environmental release raising concerns due to their reported recalcitrance and potential transformation into controversial compounds like aminomethylphosphonate (AMPA). Despite their widespread use, significant knowledge gaps exist regarding the environmental fate and transformation pathways of APPs, particularly in the presence of common environmental constituents like manganese oxides. The complex surface processes involved in APP transformations and the lack of comprehensive analytical methods for simultaneous quantification of APPs and their transformation products have hindered a full understanding of their environmental impact. This thesis aims to address these knowledge gaps by providing insights into the transformation products and mechanisms of manganese-driven APP transformation, and in turn their potential environmental fate and implications, while also addressing the analytical challenges associated with these investigations.

The first part of this work investigated the mechanism of iminodi(methylene phosphonate) (IDMP) oxidation by manganese dioxide (MnO_2). IDMP is a major transformation product of numerous commercially used APPs and a precursor for AMPA. The research successfully determined the transformation pathways and surface processes involved in IDMP oxidation by MnO_2. Through batch experiments at pH 6, part 1 revealed AMPA and phosphate as the main transformation products, with a phosphorus mass balance of 80-92%. The proposed mechanism involves initial C-P bond cleavage, formation of *N*-formyl-AMPA as a stable intermediate, followed by C-N bond cleavage leading to AMPA formation. Notably, part one identified the formation of IDMP-Mn^{2+} surface bridging complexes as MnO_2 reduction progressed, resulting in the passivation of the mineral surface for IDMP oxidation. Compound-specific stable carbon isotope analysis (carbon CSIA) further supported this hypothesis, indicating that either sorption of IDMP to the mineral surface or electron transfer from IDMP to Mn^{IV} could be the rate-limiting step, depending on the Mn^{2+} surface concentration. This research provided evidence for the potential contribution of abiotic oxidative transformation of APPs by MnO_2 to elevated AMPA concentrations in the environment.

The second part of this study addressed the analytical challenges in quantifying APPs and their transformation products. Recognizing the need for a green, low-cost approach for simultaneous quantification in laboratory experiments, a novel analytical method using ion chromatography (IC) coupled to integrated pulsed amperometric detection (IPAD) was developed. This method

successfully quantified six A(P)Ps, including AMPA, glyphosate, IDMP, aminotris(methylene phosphonate) (ATMP), ethylenediamine tetra(methylene phosphonate) (EDTMP), and diethylenetriamine penta(methylene phosphonate) (DTPMP), within a 35-minute runtime. The method detection limits ranged from 0.014 µM for AMPA to 0.14 µM for DTPMP. A key advantage of this approach is its environmental friendliness, eliminating the need for derivatization agents and organic solvents while employing a low-energy detector. Although the detector's inherent non-specific nature presents some limitations, the method offers a sustainable alternative to existing techniques, facilitating more comprehensive studies of APP transformations in controlled laboratory settings.

The third part, by combining insights and developments from part one and two, investigated the manganese-driven oxidation of DTPMP, a widely used complexing agent in household and industrial applications. DTPMP transformation in the presence of MnO_2 (with and without dissolved O_2) and in the presence of Mn^{2+} and O_2 in buffered ultra-pure water (pH 6) and in sterile-filtered wastewater (pH 8) was examined. A groundbreaking discovery was made, demonstrating that glyphosate, a broad-spectrum herbicide, is a stable transformation product during this process. Maximum glyphosate yields ranged from 0.03 to 0.42 mol-%, varying with reaction conditions. Importantly, both glyphosate and AMPA concentrations were found to be stable well beyond complete DTPMP transformation, even in the wastewater matrix.

The widespread occurrence of manganese in both natural environments and wastewater treatment plants (WWTPs) underscores the potential significance of manganese-mediated DTPMP transformation and subsequent glyphosate formation under environmentally relevant conditions. These results lend support to recent hypotheses suggesting that municipal wastewaters could be a previously unrecognized source of glyphosate in European surface waters, with APPs as potential precursors, highlighting manganese as a potential key factor. Although additional applied research is necessary to definitively establish the role of manganese in glyphosate formation within technical and natural systems, this study challenges the traditional understanding of herbicide application as the single source for glyphosate concentrations in the environment. The results of this study suggest that the pathways of glyphosate introduction into ecosystems may be more complex and diverse than previously thought.

Collectively, this work significantly advances our understanding of APP transformation, provides new analytical tools for their study, and reveals an unexpected pathway for the formation of the controversially discussed contaminant glyphosate. Polyphosphonates, including APPs, are generally described as chemically stable compounds due to their stable C-P bonds. The results

of this study together with recently published literature on APP transformation and behavior in WWTPs strongly suggest revising those assumptions. In this context, the widely accepted assumption that APPs are primarily removed from WWTPs through sorption processes should be re-evaluated and subjected to further investigation. This work provides evidence suggesting that APPs may undergo significant transformation within wastewater treatment systems and/or the environment. Those findings might have important implications for environmental risk assessment, monitoring, and the regulation of APPs and their transformation products.

Kurzfassung

Aminopolyphosphonate (APPs) finden als Chelatbildner breite Anwendung in Industrie und Haushalt. Ihre zunehmende Freisetzung in die Umwelt gibt jedoch Anlass zur Sorge, da sie als persistent gelten und möglicherweise zu kontrovers diskutierten Verbindungen wie Aminomethylphosphonat (AMPA) umgewandelt werden können. Trotz ihres weitverbreiteten Einsatzes bestehen erhebliche Wissenslücken hinsichtlich des Umweltverhaltens und der Transformationswege von APPs, insbesondere in Gegenwart ubiquitärer Umweltkomponenten wie Manganoxide. Die komplexen Oberflächenprozesse bei APP-Transformationen und der Mangel an umfassenden analytischen Methoden zur simultanen Quantifizierung von APPs und ihren Transformationsprodukten haben bisher ein vollständiges Verständnis ihrer Umweltauswirkungen verhindert. Diese Arbeit zielt darauf ab, diese Wissenslücken zu schließen und Einblicke in die Transformationsprodukte, -mechanismen und mögliche Umweltauswirkungen von APPs sowie die damit verbundenen analytischen Herausforderungen zu gewinnen.

Der erste Teil dieser Arbeit untersuchte den Mechanismus der Oxidation von Iminodi(methylenphosphonat) (IDMP) an Mangandioxid (MnO_2). IDMP ist ein bedeutendes Haupttransformationsprodukt zahlreicher kommerziell genutzter APPs und ein potenzieller Vorläufer für AMPA. Die Untersuchungen identifizierten erfolgreich die Umwandlungswege und Oberflächenprozesse, die an der IDMP-Oxidation durch MnO_2 beteiligt sind. Batch-Experimente bei pH 6 zeigten, dass AMPA und Phosphat die Haupttransformationsprodukte sind, mit einer Phosphor-Massenbilanz von 80-92%. Der vorgeschlagene Mechanismus umfasst die initiale C-P-Bindungsspaltung, die Bildung von *N*-Formyl-AMPA als stabiles Zwischenprodukt und die anschließende C-N-Bindungsspaltung, die zur AMPA-Bildung führt. Ein wichtiges Ergebnis war die Identifizierung von IDMP-Mn^{2+}-Oberflächenbrückenkomplexen, die sich mit fortschreitender MnO_2-Reduktion bildeten und zur Passivierung der Mineraloberfläche für die IDMP-Oxidation führten. Die verbindungsspezifische Analyse stabiler Kohlenstoffisotope (Kohlenstoff-CSIA) unterstützte diese Hypothese und deutete darauf hin, dass entweder die Sorption von IDMP an die Mineraloberfläche oder der Elektronentransfer von IDMP zu Mn^{IV} der geschwindigkeitsbestimmende Schritt sein könnte, abhängig von der Mn^{2+}-Oberflächenkonzentration. Dieser Teil der Arbeit lieferte Hinweise auf den möglichen Beitrag der abiotischen oxidativen Umwandlung von APPs durch MnO_2 zu erhöhten AMPA-Konzentrationen in der Umwelt.

Der zweite Teil der Studie widmete sich den analytischen Herausforderungen bei der Quantifizierung von APPs und ihren Transformationsprodukten. Angesichts der Notwendigkeit eines umweltfreundlichen und kostengünstigen Ansatzes zur simultanen Quantifizierung in Laborexperimenten wurde eine neuartige Analysemethode entwickelt. Diese Methode basiert auf der Kopplung von Ionenchromatographie (IC) mit integrierter gepulster amperometrischer Detektion (IPAD). Mit diesem Verfahren konnten sechs A(P)Ps erfolgreich quantifiziert werden, darunter AMPA, Glyphosat, IDMP, Aminotris(methylenphosphonat) (ATMP), Ethylendiamin-tetra(methylenphosphonat) (EDTMP) und Diethylentriamin-penta(methylenphosphonat) (DTPMP), innerhalb einer Laufzeit von 35 Minuten. Die Nachweisgrenzen der Methode lagen zwischen 0,014 µM für AMPA und 0,14 µM für DTPMP. Ein wesentlicher Vorteil dieses Ansatzes ist seine Umweltverträglichkeit, da er ohne Derivatisierungsreagenzien und organische Lösungsmittel auskommt und einen energieeffizienten Detektor verwendet. Trotz gewisser Einschränkungen aufgrund der inhärenten Unspezifität des Detektors bietet die Methode eine nachhaltige Alternative zu bestehenden Techniken. Sie ermöglicht somit umfassendere Untersuchungen von APP-Umwandlungen unter kontrollierten Laborbedingungen.

Der dritte Teil der Arbeit kombinierte die Erkenntnisse und Entwicklungen aus den vorherigen Teilen und untersuchte die mangangesteuerte Oxidation von DTPMP, einem weitverbreiteten Komplexbildner in Haushalts- und Industrieanwendungen. Die DTPMP-Transformation wurde in Gegenwart von MnO_2 (mit und ohne gelösten O_2) sowie in Anwesenheit von Mn^{2+} und O_2, jeweils in gepuffertem ultrareinem Wasser (pH 6) und in sterilfiltriertem Abwasser (pH 8) untersucht. Eine bedeutende Entdeckung war der Nachweis, dass Glyphosat, ein Breitspektrumherbizid, als stabiles Umwandlungsprodukt während dieses Prozesses entsteht. Die maximalen Glyphosat-Ausbeuten variierten je nach Reaktionsbedingungen zwischen 0,03 und 0,42 Mol-%. Bemerkenswert war, dass sowohl die Glyphosat- als auch die AMPA-Konzentrationen auch nach vollständiger DTPMP-Umwandlung stabil blieben, selbst in der Abwassermatrix.

Das ubiquitäre Vorkommen von Mangan sowohl in natürlichen Umgebungen als auch in Kläranlagen unterstreicht die potenzielle Bedeutung der manganvermittelten DTPMP-Transformation und der daraus resultierenden Glyphosat-Bildung unter umweltrelevanten Bedingungen. Diese Ergebnisse stützen jüngste Hypothesen, die darauf hindeuten, dass kommunale Abwässer eine bisher unerkannte Quelle für Glyphosat in europäischen Oberflächengewässern darstellen könnten, wobei APPs als potenzielle Vorläufer fungieren und Mangan als möglicher Schlüsselfaktor identifiziert wird. Obwohl weitere anwendungsorientierte Forschung erforderlich ist, um die Rolle von Mangan bei der Glyphosatbildung in technischen und

natürlichen Systemen abschließend zu klären, stellt diese Studie das traditionelle Verständnis der Herbizidanwendung als einzige Quelle für Glyphosatkonzentrationen in der Umwelt in Frage. Die Ergebnisse dieser Untersuchung deuten darauf hin, dass die Eintragswege von Glyphosat in Ökosysteme möglicherweise komplexer und vielfältiger sind als bisher angenommen.

Insgesamt trägt diese Arbeit wesentlich zum Verständnis der APP-Transformation bei, stellt neue analytische Werkzeuge für deren Untersuchung bereit und deckt einen unerwarteten Bildungsweg für den kontrovers diskutierten Schadstoff Glyphosat auf. Polyphosphonate, einschließlich APPs, werden aufgrund ihrer stabilen C-P-Bindungen allgemein als chemisch stabile Verbindungen beschrieben. Die Ergebnisse dieser Studie zusammen mit kürzlich veröffentlichten Erkenntnissen zur APP-Transformation und zum Verhalten in Kläranlagen legen jedoch nahe, diese Annahmen zu überdenken. In diesem Zusammenhang sollte die weithin akzeptierte Annahme, dass APPs hauptsächlich durch Sorptionsprozesse aus Kläranlagen entfernt werden, neu bewertet und weiteren Untersuchungen unterzogen werden. Diese Arbeit liefert Hinweise darauf, dass APPs möglicherweise signifikante Umwandlungen innerhalb von Abwasserbehandlungssystemen und/oder in der Umwelt durchlaufen. Diese Erkenntnisse könnten bedeutende Auswirkungen auf die Umweltrisikobewertung, das Monitoring und die Regulierung von APPs und ihren Transformationsprodukten haben.

Contents

List of Figures

List of Schemes

List of Tables

1 General Introduction

1.1 Polyphosphonates and Aminopolyphosphonates

1.1.1 General Introduction

Polyphosphonates including aminopolyphosphonates (APPs) are a class of organophosphorus compounds characterized by the presence of more than one phosphonate (-C-PO(OH)$_2$) group and, in the case of APPs, nitrogen atoms connecting those phosphonate moieties. Due to their multiple phosphonate (and amine) groups, they exhibit multiple pKa values and therefore multiple pH species. Polyphosphonates exhibit strong chelating properties for di- and trivalent metal cations[1,2] and are described to be highly chemically stable[3–6], making them valuable in a range of industrial and household applications[7]. APP structures often resemble those of the well-known aminopolycarboxylates, such as e.g. ethylenediaminetetraacetic acid (EDTA) and ethylenediaminetetra(methylene phosphonic acid) (EDTMP) (see Fig. 1.1). APP complexation constants with metal cations are usually a little higher than for their carboxylic analogues, as for example EDTMP shows log K values ranging from 9.3 for Mg^{2+} (EDTA: 8.8) to 21.7 for Cu^{2+} (EDTA 18.8)[8].

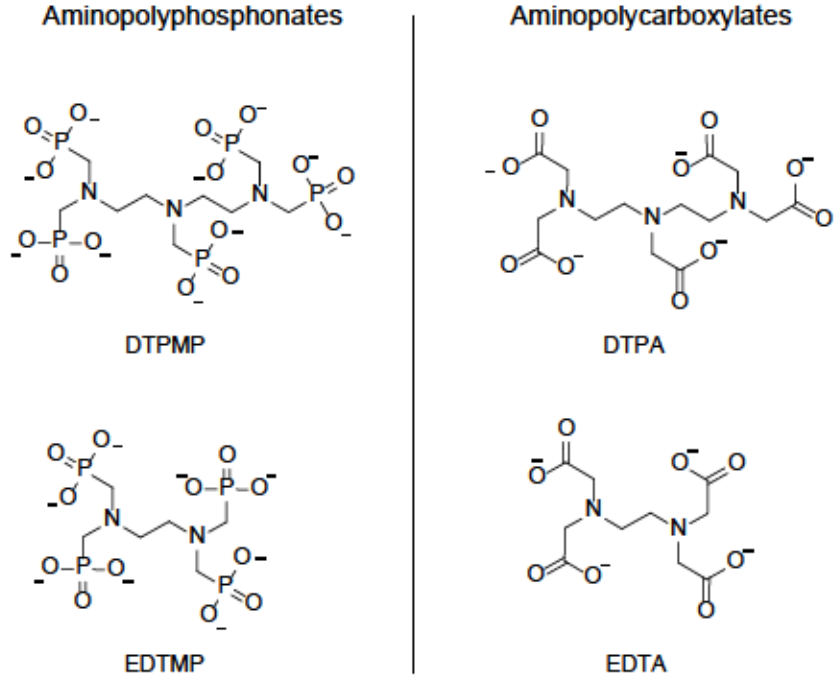

Figure 1.1 Fully deprotonated structures of the two APPs ethylenediaminetetra(methylene phosphonate) (EDTMP, dieethylenetriaminepenta(methylene phosphonate) (DTPMP) and their carboxylate equivalents ethylenediaminetetraacetate (EDTA) and diethylenetriaminepentaacetate (DTPA).

1.1.2 Use and Applications

Polyphosphonates have been used since the mid-20th century in various industrial and domestic applications due to their excellent scale inhibition and metal ion sequestration properties[1,7,9]. Early applications included i) industrial water treatment, as e.g. the conditioning of cooling water or as antiscalants in water boilers, ii) bleaching stabilization in the textile and paper industry by inactivating metal ions catalyzing peroxide decomposition and iii) additives in industrial and household detergents by chelating metal cations and reducing water hardness. Over time, their use has expanded to iv) oil drilling (as scale and corrosion inhibitors), v) personal care (as preservatives and stabilizers) and vi) medical products (as Ca^{2+}-binders for bone disease treatment)[4,7,8,10]. Their strong chelating capabilities and sub-stoichiometric effectiveness (threshold inhibition) allow for them to be used in quite low concentrations (0.1-5 %)[4,10]. They are used as substitutes for polycarboxylates and polyphosphates in detergents and water treatment[7,9], due to the reportedly high chemical stability due to the C-P bond[4,6,11] and therefore no contribution to eutrophication[12]. In the EU, phosphate-containing additives are banned from household detergents since 2013 (laundry) resp. 2017 (dishwasher)[13].

1.1.3 Quantitatively most relevant

Among the most commonly used polyphosphonates are 1-hydroxyethane-1,1-diphosphonic acid (HEDP), and the APPs aminotris(methylene phosphonic acid) (ATMP), ethylenediaminetetra(methylenephosphonic acid) (EDTMP) and diethylenetriaminepenta(methylenephosphonic acid) (DTPMP)[7,12]. Regional differences are remarkable, with DTPMP being the main phosphonate additive in european detergents followed by EDTMP, while HEDP is mostly used in the USA for industrial water treatment, such as scaling inhibition in cooling water systems or boilers[4,7]. Global phosphonate consumption increased from 56.000 t/a in 1998[11,14] to 94,000 t/a in 2012[7], with Europe accounting for >50 % of the global phosphonate use[7], which might be due to the ongoing use of polyphosphates in the US[15].

1.1.4 Environmental Behavior and Fate

Entry into the environment and Environmental Concentrations

Polyphosphonates enter receiving waters either directly, e.g. from cooling water cycles where phosphonate removal is not a standard yet, or indirectly via wastewater treatment plants (WWTPs)[7].

Polyphosphonate concentrations in German wastewater effluents were detected between 1.1 µg/L (ATMP) and 34.1 µg/L (PBTC)[16]. Additionally, polyphosphonate concentrations in the sediment of the receiving river were found to be significantly increased after wastewater discharge [16,17].

In the environment, polyphosphonates are mostly found adsorbed to particulate matter and soils[11,16,18]. Trace level quantification of ATMP, EDTMP and DTPMP determined the phosphonate loads of solid phases to be around 3 orders of magnitude higher than the respective liquid phases from e.g. river samples[16]. Up to 6.2 mg/kg DTPMP and 0.7 mg/kg ATMP have been found in suspended matter of german river water, while phosphonate concentrations in the aqueous phase were usually below the detection limit (sub to low ug/L range)[16]. Sorption of polyphosphonates onto minerals seems to be enhanced further by the presence of metal-cations by altering the mineral surface charge or even forming ternary complexes[3,19,20]. The detection of polyphosphonates in a Rhine River sediment sample from 66 cm depth indicates that polyphosphonates strongly sorb to sediment particles and accumulate there[17].

Elimination and transformation in Wastewater Treatment Plants and the Environment

In wastewater treatment, polyphosphonates are described to be mainly removed by sorption onto sewage sludge[7,21,22]. This is supported by the strong sorption onto mineral phases, as exemplary investigated for goethite[18], with Fe-(hydr)oxides being ubiquitously present in sewage sludge [23,24]. Even in the presence of 20-fold excess of phosphate, ATMP sorption onto goethite (pH 7) was just diminished by 8 %, while EDTA in the same experiment desorbed almost completely[18]. Removal efficiencies of phosphonates from 60 % to >90 % were reported for different sludge adsorption experiments (differing in starting concentrations, sludge and time), summed up by Rott et al. (2018)[7] to a general phosphonate removal efficiency of 80-95 % from WWTPs. While those numbers apply to industrial and consumer wastewaters entering water treatment, removing phosphonates from water conditioning and industrial processes is not a standard procedure yet. Here, Rott et al. (2018)[7] estimated phosphonate removal rates around 30-60 %. Next to adsorption onto sewage sludge, abiotic transformation probably plays an important role in polyphosphonate removal in WWTPs. A study investigating the relevance of biotic versus abiotic processes in sewage plant effluent and natural waters identified abiotic processes to be the main driver of APP transformation even occurring in the dark, even though biotic processes enhance further transformation and even mineralization of abiotic transformation products[22]. Accordingly,

residues of polyphosphonates as well as transformation products are released into the environment.

While the monophosphonates glyphosate (anthropogenic) and 2-aminoethylphosphonic acid (2-AEP) (biogenic) are readily degraded microbially by C-P bond cleaving bacteria strains such as e.g. *Pseudomonas* sp.[10,25,26], the biotic degradation of polyphosphonates is not so straightforward[11,12]. This is probably due to size, multiple negative (and positive) charges and complex speciations[11]. A few studies report biotransformation of polyphosphonates under P-limiting conditions[6,22,27–29], but no mineralization due to pure biotic processes was reported so far [4,11,22,30]. In WWTPs as in the environment biotransformation processes probably play – if at all – a marginal role, as phosphonates will never present the exclusive P-source[11].

Instead, a number of abiotic processes leading to transformation of APPs have been identified:

IDMP, ATMP, EDTMP and DTPMP have been found to be transformed by UV light (photolysis)[31–34]. Photolysis of DTPMP was even found to be enhanced by the presence of bivalent metal cations (Fe^{2+}, Ca^{2+}, Mg^{2+})[34]. A technical process leading to transformation of EDTMP is ozonation[35].

Additionally, ATMP, EDTMP and DTPMP were shown to be transformed by manganese: By Mn^{2+} in the presence of O_2 and in the presence of MnOOH (with and without oxygen)[36–38]. While early work reported ATMP, EDTMP and DTPMP degradation in the presence of Ca, Mg and Fe^{II} [39], Nowack & Stone (2000)[40] found Ca^{2+}, Zn^{2+} and Cu^{2+} to hinder the transformation by Mn^{2+}/O_2. For more details on manganese oxides please see subchapter 1.2.

1.1.5 Toxicity and Environmental Concerns

The acute toxicity of polyphophonates is generally reported to be very low[4,7,9]. For aquatic organisms acute toxicity usually occurs at concentrations >100 ppm [4,8], while no-effect levels as high as 100 mg EDTMP/kg/day over 2 years has been determined for rats[41]. Such high concentrations do not occur in wastewater or nature[7,16,17]. Despite this low acute toxicity, there are indirect toxicity concerns for polyphosphonates due to their chelating properties: Inhibition of algal growth probably by chelating important micronutrients was observed for HEDP, EDTMP and DTPMP, with EDTMP being the most effective inhibitor[4]. On the other hand, polyphosphonates could also protect aquatic organisms by effectively chelating heavy metals and inhibiting their uptake. Concerns about heavy metal remobilization[10] are probably unsubstantiated due to i) the high polyphosphonate concentrations needed, which won't occur in natural environments and ii)

the polyphosphonates high partitioning to sediments[4,7]. Despite their use as polyphosphate replacements to prevent eutrophication and their low usage numbers, polyphosphonate contribution to eutrophication should not be underestimated[7,10].

However, despite the low acute toxicity of APPs, there are significant environmental concerns related to their transformation products (TPs). In all the above-mentioned transformation processes the main quantified TPs are phosphate, IDMP and AMPA[31–33,35,38,40]. Additionally, multiple minor TPs like *N*-formyl-IDMP[40], ethylamino(bismethylenephosphonic acid) (EABMP)[33] and even *N*-(phosphonomethyl)glycine (glyphosate)[35] were detected. Recent studies have detected negative removal efficiencies of AMPA and glyphosate in WWTPs and elevated concentrations after WWTP effluent discharge into surface waters[42,43]. This suggests that APP transformation, rather than direct glyphosate input, may contribute to these elevated levels.

Environmental concerns related to these transformation products include i) persistence of AMPA in the environment[44] and ii) the formation of glyphosate[43], a controversial herbicide with ongoing debates about its long-term effects and potential carcinogenicity[45].

Glyphosate

Glyphosate is a compound of major societal interest and therefore demands its own short introduction to understand the implications of this work. While glyphosate belongs to the subgroup of amino**mono**phosphonates and is therefore structurally related to the APPs, it is by far the most used phosphonate in the world. Global glyphosate usage rose from 67,000 t in 1995 to 826,000 t in 2014[46]. Glyphosate – or *N*-phosphonomethylglycine – is the most widely used broadband herbicide due to its unique mode of action (non-selective), its reported low acute toxicity and the spread of glyphosate-tolerant genetically modified crops[47–50]. Glyphosate is used for weed control and exhaustive vegetation clearance in agriculture and private applications[47,49]. Glyphosate acts via inhibition of the enzyme 5-enolpyruvyl-shikimate-3-phosphate synthase (EPSPS) of the shikimate pathway, which probably kills plants by insufficient aromatic amino acid production[47].

In the environment, glyphosate is mainly transformed microbially. There are two pathways leading to different TPs: The oxidoreductase (AMPA) and the C-P lyase (sarcosine, glycine) pathway[48]. The dominance of one pathway or the other depends on the microbial cultures present in soil, while *Pseudomonas* species (oxidoreductase) are considered the most important, leading to AMPA as glyphosate's main TP in the environment[44,48,51]. Typical half-lifes for i) glyphosate and ii) AMPA in soils are given with i) 47 days[48,52] resp. ii) 121 days[44], while the actual half-life varies

a lot depending on soil physical, chemical and biological properties[48,50,53–55]. By now, residues of i) glyphosate and ii) AMPA are found in almost all soybeans from fields planted with glyphosate-resistent soybeans, with mean concentrations of i) 3.3 and ii) 5.7 mg/kg [50,56].

Glyphosate's acute toxicity for mammals (oral, dermal, inhalation) is generally low to very low[52,57], especially compared to other pesticides[47]. For humans, ingestion of concentrated glyphosate formulations can cause corrosive effects in the mucous membranes, but is generally associated with only mild and transient features, severe toxicity just occurring at ingestion volume of >85 mL of concentrated herbicide formulation[58].

However, toxicity, health and safety data on long-term exposure of glyphosate and AMPA are still lacking, even though chronic, sub-chronic and reproductive toxicity might be far more important, due to much lower effect levels and the frequent occurrence of glyphosate and AMPA in soil, water and even foods[44,54]. While a plethora of genotoxicity assays has been conducted in the past decades, taking into account studies with different outcomes led to quite diverging assessments by different authorities[45]: While the International Agency for Research on Cancer (IARC) workgroup of the World Health Organization (WHO) declared glyphosate to be "probably carcinogenic to humans", based on sufficient evidence from animal research[59,60], the United States Environmental Protection Agency (EPA) and the European Food Safety Authority (EFSA) classified glyphosate as "not likely to be carcinogenic to humans *at doses relevant for human health risk assessment*"[61,62]. Scientists analyzing the studies considered by the EPA and EFSA, remark that most of these are registrant-conducted studies and that threshold values in the US and Germany are based on outdated studies[45,50]. Just in 2023, the European Union approved glyphosate usage for another 10 years[63].

The debate surrounding the chronic toxicity and potential carcinogenicity of glyphosate and its primary metabolite, AMPA, remains unresolved[45,64]. This ongoing controversy extends to APPs (specifically DTPMP and EDTMP), as their transformation into glyphosate introduces an indirect pathway for potential environmental and health risks.

1.2 Manganese Oxides

The transformation of APPs in the environment is influenced by various factors, with manganese oxides potentially playing a significant role. As discussed in previous sections, APPs can undergo transformation through several pathways, including photolysis, ozonation, and manganese-driven oxidation.

Manganese is the tenth most abundant element and the second most common heavy metal in the Earth's crust after iron[65]. Manganese is non-uniformly distributed in the crust and therefore, concentrations vary greatly[66]. In soils, manganese concentrations are described to typically range from 450 mg/kg to 4,000 mg/kg, varying with pH and redox conditions[67,68]. Notably, manganese is also present in engineered systems[66]. In sewage sludge concentrations ranging from 46 to 251 mg/kg Mn per dry mass have been reported in Poland[69] and 600-1,500 mg/kg Mn per dry mass in Germany[70]. Manganese oxides have also been found in water pipelines[66,71].

1.2.1 Manganese Oxidation States and Redox

Manganese occurs in several oxidation states, ranging from Mn^{II} to Mn^{VII}, with Mn^{II}, Mn^{III}, and Mn^{IV} being the most common in natural systems[72]. The stability of these oxidation states depends on environmental conditions: Mn^{II} is most stable under reducing conditions and in acidic environments, typically as the Mn^{2+} ion. Mn^{III} and Mn^{IV} oxides are more stable under oxidizing conditions and at higher pH values.[68,69,73,74] Mn^{III} is usually unstable in aqueous solution and disproportionates to Mn^{II} and Mn^{IV}, but can be stabilized by ligands such as citrate, pyrophosphate, and siderophores[66].

The oxidation of Mn^{II} to higher oxidation states can occur through both abiotic and biotic processes. Chemical homogenous oxidation of Mn^{II} to Mn^{III} (one electron transfer) is thermodynamically unfavourable at pH values <9[74,75]. Chemical oxidation of Mn^{II} to Mn^{IV} (two electron transfer) is thermodynamically feasible at pH values >3, but faces kinetic limitations at pH values <9 due to the first electron transfer step (Mn^{II} → Mn^{III}) [66,75]. Bacterially mediated oxidation of Mn^{II} in the presence of O_2 has been found to achieve oxidation rates 10.000 to 100.000 times higher than the abiotic process[66,76,77]. Consequently, in natural and technical environments, Mn^{II} oxidation is largely catalyzed by microorganisms[74,78].

1.2.2 Microbial Manganese Oxidation

Microorganisms, including bacteria and fungi, play a crucial role in manganese oxidation. The microbial oxidation of Mn^{II} primarily yields $Mn^{IV}O_2$ through two consecutive one-electron transfers, with molecular oxygen serving as the electron acceptor[74]. The stoichiometry of this process can be represented by the following equation[78,79]:

$$Mn^{2+} + \frac{1}{2}O_2 + H_2O \rightarrow MnO_2 + 2H^+$$

Microbial Mn^{II} oxidation is facilitated by multicopper oxidase-like enzymes[78]. The intermediate Mn^{III} is thermodynamically unstable in aqueous media, but microorganisms produce organic ligands, or exhibit enzymes or cellular structures that can bind and stabilize Mn^{III} [74,78]. The reasons for microbial Mn^{II} oxidation are diverse, including energy generation, protection from reactive oxygen species (ROS), and the production of reactive MnO_2 for breaking down large organic materials into more accessible carbon sources[74].

1.2.3 Distribution of Manganese Species in the Natural Water Bodies

In natural water bodies, the distribution of manganese species is closely tied to the vertical stratification and redox conditions in different zones, including pH, salinity, O_2 concentration, temperature, light, and concentration of organic matter[66,76,80–83]. Generally, in the well-oxygenated epilimnion (surface layer), manganese primarily exists as insoluble Mn^{IV} oxides, often in the form of suspended particles or colloids[80,82]. Some Mn^{III} species may also be present as intermediates in oxidation processes[66,84]. In the hypolimnion (bottom layer), especially under anoxic conditions, soluble Mn^{II} becomes the dominant form. Mn^{II} accumulates in the water column during periods of stratification, as Mn^{IV} oxides are reduced, and can precipitate as e.g. the carbonate salt[81,82]. Mn^{III} complexed by organic ligands, may also exist to a high percentage of total Mn in suboxic zones[84]. The sediment-water interface is a particularly dynamic zone for manganese cycling. Here, Mn^{IV} oxides in sediments can be reduced to Mn^{II} under anoxic conditions, with Mn^{II} diffusing upward into the water column[82,83]. This vertical distribution of manganese species is not static but undergoes seasonal changes due to lake turnover events, which mix the water column and redistribute oxygen and manganese species throughout the lake[66,80,81,85].

1.2.4 Structure and Properties of Manganese Oxides

The different stable oxidation states of manganese lead to the formation of various manganese oxides (MnOx), such as manganite (MnOOH), hausmannite (Mn_3O_4), birnessite (MnO_2), and pyrolusite (MnO_2), with x ranging between 1.0 and 2.0. These oxides vary in their crystallography, while the main building block of Mn oxides are MnO_6 octahedra, which can be edge-sharing or corner-sharing. Mn oxides exhibit either layered or tunnel-like structures, with varying degrees of long-range order and intercalation of foreign cations and water molecules[65]. Due to their capacity for forming minerals with varying oxidation states and their cation and oxygen storage capacity in the mineral lattice, MnO_x can be re-oxidized by molecular oxygen after reduction and therefore

act as electron mediators, which makes them effective catalysts. The crystalline structure, surface morphology and microstructure as well as surface active oxygen species all contribute to the catalytic performance and/or the reaction mechanism of MnO_x.[65,73] For instance, birnessite – the most common Mn oxide – is composed of layers of edge-sharing MnO_6 octahedra, forming octahedral sheets similar to clay minerals[86]. Birnessite is known for its high specific surface area and its contribution to a variety of redox and cation-exchange processes[65]. Biogenic Mn oxides are mostly amorphous $Mn^{IV}O_2$. While they exhibit a high degree of disorder, there are some crystalline domains, often in a birnessite-like structure. Biogenic Mn oxides are associated with higher proportions of Mn^{III}, higher surface areas and therefore higher reactivity compared to abiotic Mn oxides[72,87].

1.2.5 Environmental Significance of Manganese Oxides

MnOx containing Mn^{III} and Mn^{IV} are among the strongest environmental oxidants[65,72,75,88] and play crucial roles in biogeochemical cycles[74,78]. Their redox properties are influenced by factors such as pH, oxygen concentration, cation concentration, and microbial activity. MnO_x are known to sorb and/or oxidize a wide range of organic compounds and sorb and therefore control the concentration of heavy metals[72,89].

Next to their relevance in natural biogeochemical cycles, MnO_x are powerful oxidants capable of transforming various anthropogenic organic compounds[90] including phenols[91,92], anilines[93], antibiotics[94], and emerging contaminants like bisphenol A[95], glyphosate[96–98] and AMPA[99].

Furthermore, Mn oxides can catalytically activate oxidants such as hydrogen peroxide, ozone, and persulfates, generating reactive oxygen species (ROS) that enhance the degradation of recalcitrant pollutants[90,100–102].

The strong sorbing and oxidative properties of MnO_x offer promising characteristics for their application in wastewater treatment for metal cation and organic contaminant removal[89,103,104].

This versatility in environmental reactions and technological applications underscores the importance of Mn oxides in both natural systems and engineered solutions for environmental remediation.

1.3 Analytical Challenges

APPs pose specifically difficult analytes: They possess multiple negative (and positive) charges, strong chelating and sorption characteristics – therefore a plethora of different species – and show no analytically useful functionalities like chromophoric groups, therefore few suitable analytical methods are avaible[4,9,16]. All aminophosphonates – even the monophosponates – show multiple pKa values for the phosphonate, amino and – in case of glyphosate – carboxyl groups (see Figure A.1). The monophosphonates glyphosate and AMPA can therefore occur in the cation as well as the zwitterionic form[105]. When using anion chromatography to separate amino**mono**- to **poly**phosphonates, one needs to apply a sufficiently high pH to yield all compounds in their anionic form, even glyphosate and AMPA[16,105]. For the mere analysis of **poly**phosphonates, it is in general more advisable to use an acidic pH, to reduce the negative charges and therefore reduce the affinity to metal cations and complex formation, which hamper the analysis[106–108]. Unsymmetrical peak shapes, double peaks and shoulders in published methods underline the difficulty of chromatographic separation and detection of those analytes[16,109,110].

For the mere analysis of the monophosphonates AMPA and glyphosate, one can make use of the primary resp. secondary amine function for derivatization[111,112] (see LC-QQQ after FMOC derivatization).

A variation of analysis methods with different benefits and limitations have been developed over the past years. Several quantification methods have been employed in this work in order to fulfill different needs/serve different purposes. To allow for smooth reading some methods will be explained in more detail in the following section.

1.3.1 IC-PAD

IC coupled to amperometric detection takes on a special position in this work. On the one hand, IDMP and AMPA have been quantified using this method throughout the work, on the other hand, chapter 3 describes method development for six different amino(poly)phosphonates (A(P)Ps) on this system.

The specialty of amperometric detection lies in its sensitivity and selectivity yet low energy consumption. Compounds to be detectable with amperometric detection need to be electroactive and sorb to the working electrode surface, so that they can be oxidized/reduced upon application of a specific potential between working electrode (WE) and counter electrode CE) (except for indirect "mode III" detection)[113]. The detector geometry used in this work (Wall-Jet cell) is depicted in Fig. 1.2. The partial reduction/oxidation of the analytes at the WE causes a current, which is

proportional to the analyte concentration in a certain range[114]. In case of aminophosphonates, it is made use of the amine-function, so that a detector method (waveform) found useful for the detection of amines and amino acids – integrated pulsed amperometric detection (iPAD)[114] – is deployed[113,115]. Details about pulsed amperometric detection will be given in chapter 3.

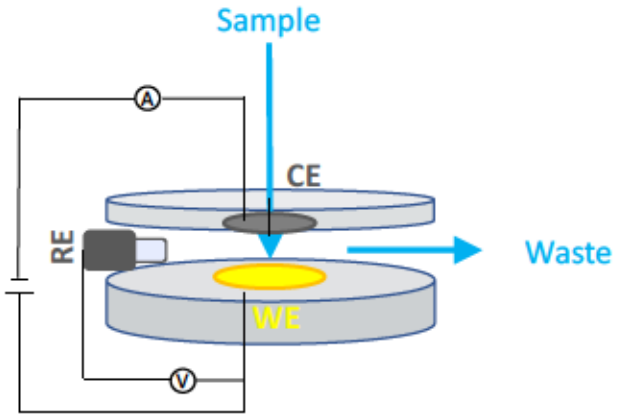

Figure 1.2 Schematic depiction of the amperometric detector geometry (Wall-Jet cell) used within this work. Gold served as the WE material, while Pt was used for the CE. As RE material either Pd or Ag/AgCl was used.

The use of solely aqueous eluents, low energy consumption, sufficient detection limits and relatively low acquisition costs made IC-PAD the workhorse for most AMPA and IDMP quantifications within this thesis. Furthermore, it presented a promising tool for the simultaneous quantification of aminomono- and polyphosphonates and was therefore chosen for method development in chapter 3.

1.3.2 LC-QQQ after FMOC derivatization

In order to detect traces of AMPA and glyphosate, the trace level determination method for AMPA and glyphosate involving derivatization at the (primary or secondary) amine function with 9-fluorenylmethoxycarbonyl chloride (FMOC Cl) (see Fig. 1.3) has been employed. This trace-level quantification method well described in literature[111,112,116] allows quantification of glyphosate and AMPA in the low µg/L range, and after preconcentration even in the low ng/L range[111]. The derivatized compounds glyphosate-FMOC and AMPA-FMOC are retained on the RP column, while underivatized (e.g. tertiary amines or no amine containing) TPs are not retained and therefore cannot hamper the quantification. The use of a triple quadruple (QQQ) mass spectrometer allows for tandem mass spectrometry (MS/MS) experiments and therefore for the unequivocal identification of compounds.

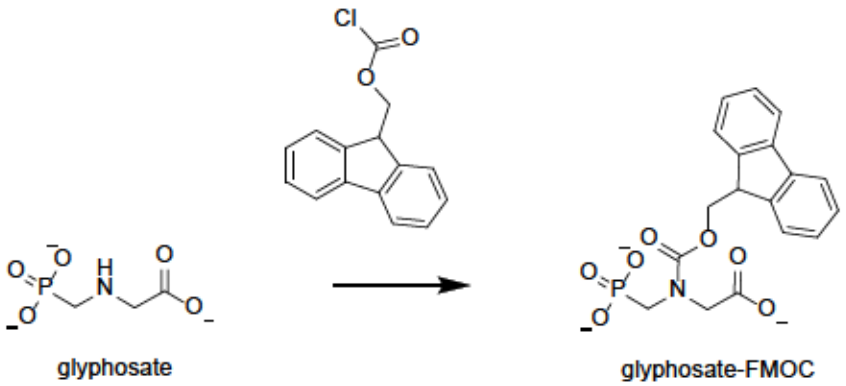

Figure 1.3 Glyphosate derivatization using FMOC Cl. Glyphosate and glyphosate-FMOC are depicted in their fully deprotonated forms.

This analysis method was chosen for the transformation experiments conducted in **chapter 4**, as AMPA and glyphosate needed to be i) unequivocally identified and ii) quantified in low concentrations in a highly concentrated matrix containing a plethora of other amine-containing transformation products.

1.3.3 Molybdenum Blue Method for PO_4^{3-} quantification

The Molbydenum Blue (MB) method is the most common method for phosphate quantification in waters[117–119]. It is based on the formation of a blue-coloured species around the phosphate (phosphate molybdenum blue, PMB), which is then measured photometrically.

It is a two-step reaction: The first step is the formation of a Keggin ion around the analyte ion. In case of phosphate as the analyte ion, the Keggin ion is the 12-molybdophosphoric acid (12-MPA) involving Mo^{VI} and P^{V} (see (**1**)). In the next step, this Keggin ion is reduced and polymerises, forming the blue PMB (see (**2**)[117]. Photometric detection is mostly conducted at either 710 or 880 nm after reduction using ascorbic acid[117,118].

$$PO_4^{3-} + 12Mo_4^{2-} + 27H^+ \rightarrow H_3PO_4(MoO_3)_{12} + 12H_2O \quad (1)$$

$$H_3PMo_{12}^{IV}O_{40} + \text{reductant} \rightarrow [H_4PMo_8^{IV}Mo_4^{V}O_{40}]^{3-} \quad (2)$$

The most widely used methods apply ammonium molybdate, antimony potassium tartrate and sulfuric acid together with ascorbic acid as the reducing agent, even though the final concentrations differ a little[117–119]. Sulfuric acid is used for acidification, while antinomy is used for accelerated reduction of the 12-MPA and stabilization of the PMB[117,118].

It should be mentioned that MB is also reported as a phosphonate detection method: After chromatographic separation, the P-containing species are quantitatively oxidized to PO_4^{3-} and then transformed to the PMB species[3,120].

Interferences with organic acids forming a 5- or 6-membered coordination ring around Mo^{VI} are reported[117,121]. Most recently, strong interference in the presence of DTPMP excess was observed[122]. Therefore, the MB method was just applied for solutions containing IDMP and monophophosnates. For PO_4^{3-} determination in the presence of DTPMP, an appropriate quantification technique needed to be found.

1.3.4 IC-ICP-MS

Due to the discovery of phosphonate quantification issues by the molybdenum blue method (MB) in the presence of higher APPs[122] – especially DTPMP – another quantification method was sought for PO_4^{3-} quantification in excess DTPMP matrices. The analysis of PO_4^{3-} by means of IC coupled to ICP-MS (QQQ) presented a suitable and sensitive quantification method. A separation and quantification method for Gd-based contrast agents provided the basis for the phosphonate method used[123]. After atomization and ionization, P was reacted with O_2 in the second quadrupole and measured as the PO^+ adduct ion. Next to PO_4^{3-}, other P-containing compounds of interest have been identified and quantified in the reaction suspensions of chapter 4.

1.3.5 LC-IRMS (CSIA)

As the use of compound-specific stable isotope analysis (CSIA) by means of liquid-chromatography (LC) coupled to isotope-ratio mass spectrometry (IRMS) is rather seldom, some more details will be provided on this method.

CSIA is a useful tool to detect little changes in the isotopic composition of one element in one compound (not spatially resolved). Therefore, the compounds need to be separated by chromatography first, and then analyzed individually for their isotopic composition. Usually, due to the instrument construction concerning oxidation reactor and mass analyzer, the isotope analysis is limited to one element.[124] In this work, the isotope composition of carbon ($^{13}C/^{12}C$) was investigated.

Following the method of Martin et al. (2020)[125], the separation of the polar phosphonates was achieved by means of anion exchange chromatography which was then coupled to the interface and further to the IRMS (see Figure 3). After chromatographic separation, the compounds are oxidized to CO_2 using sodium persulfate and phosphoric acid at 99.9 °C. The CO_2 gas is then

extracted and dried before it is transferred to the ion source. A sector field mass spectrometer serves as the mass analyzer, using three faraday cups set to the mass/charge (m/z) ratios 44, 45 and 46 (see Figure 1.4).

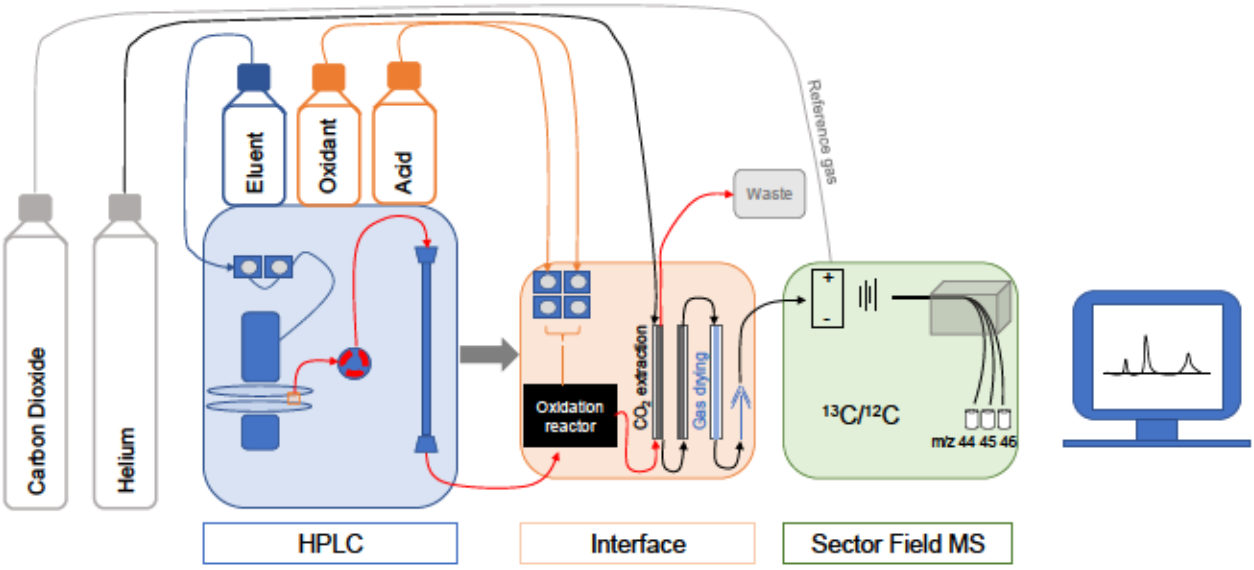

Figure 1.4 Schematic depiction of the LC-IRMS instrument used within chapter 1 of this work. The elute from the HPLC part (blue) enters the interface (orange), where all carbonaceous material is oxidized to CO_2. The dried CO_2 gas is then passed on to the mass spectrometer (green), where it is analyzed for the ^{13}C and ^{12}C content.

CSIA is a useful tool to analyze the environmental behavior of organic contaminants[126,127]. The basis for those investigations lies in the differential behavior of different isotopologues of one compound during chemical or physical reactions[128]. To prove the degradation of an organic contaminant contrary to sorption or leaching, one can make use of the kinetic isotope effect (KIE)[126]. Typically, bonds involving the lighter isotope are broken more easily than bonds involving the heavy isotope, which is then called "normal" KIE[124,128]. During a proceeding bond cleavage reaction (irreversible), the heavy isotope is enriched in the precursor/parent compound. In general, the isotope fraction caused by physical processes is insignificant compared to chemical reactions[126,129], hence the isotopic composition of the remaining fraction provides information about the nature of the occurring processes. More accurately, the isotopic enrichment in the remaining fraction can provide information about the difference in activation energies between different isotopologues (see Figure 1.4). This, of course, is just applicable if the fractionating step is not masked by a much slower or reversible not fractionating step in a multi-step reaction.[126,129]

Therefore, measuring the isotopic fractionation in the parent compound can provide insights into the underlying transformation mechanism, e.g. which bond is broken or which step is reversible or rate-limiting[126]. Figure 1.5 schematically depicts a heterogenous three-step oxidation reaction

involving sorption, electron transfer and bond cleavage as in the experiments conducted for this thesis. While sorption is reversible, electron transfer and bond cleavage are irreversible. If there is any isotope fractionation visible, it is caused by the bond cleavage step (step 3, irreversible), as sorption and electron transfer do not involve carbon atoms (if isotope fractionation is not masked by a slow previous step). Figure 1.5 holds two scenarios: I) the activation energy for electron transfer (step 2) is higher than for sorption (step 1) (black). II) the activation energy for electron transfer is lower than for sorption (blue), which will lead to a greater share of the molecules proceeding via electron transfer than in I). Isotope fractionation from step 3 (bond cleavage) will be mirrored in pool B, as step 2 and 3 are both irreversible. In scenario I) sorbed compounds in pool B will desorb again (step 1) and gather in pool A. This happens to a greater extent than in scenario II), where a higher percentage will react further via electron transfer (step 2) due to the lower activation energy (blue) for electron transfer. This means, that in scenario I) pool A (unsorbed parent compound) and pool B (sorbed parent compound, partly enriched in heavy isotopes) are mixed. Thus, the measured isotope fractionation in pool A (aqueous) and B (sorbed phase) holds information about the relative relationship between the activation energies along the reaction path, not just the fractionating step.

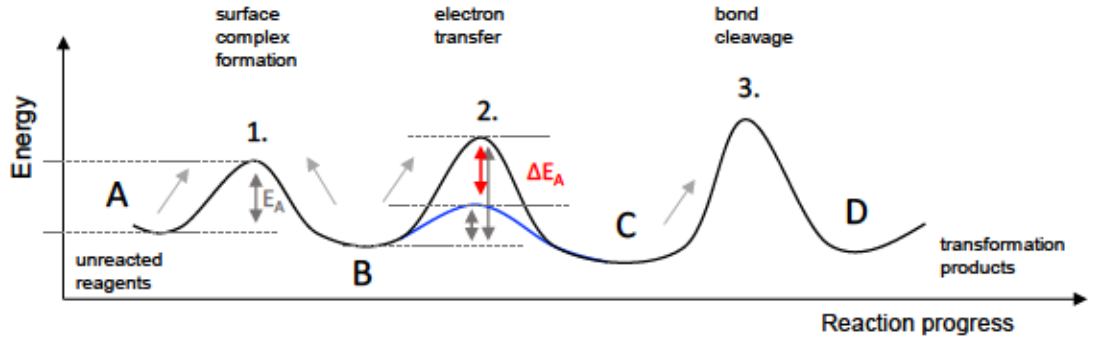

Figure 1.5 Energy diagram of a three-step oxidation reaction of an organic compound on a mineral involving two different scenarios (black and blue), which differ in their activation energy for the electron transfer.

For more details, it is referred to Elsner (2010)[126] and Hofstetter *et al.* (2024)[127].

1.3.6 Manganese Analysis

Manganese in solution was quantified by means of microwave plasma atomic emission spectroscopy (MP-AES). Mn^{2+} is a product of $Mn^{IV}O_2$ reduction and is therefore released when MnO_2 serves as an oxidant, which is why Mn^{2+} release was used as a proxy for reaction progress in previous studies[130]. However, Mn^{2+} can in turn sorb to the MnO_2 mineral surface, either by

electrostatic sorption or undergoing comproportionation with Mn^{IV} forming Mn^{III} [95,131,132]. Hence, the pure aqueous manganese concentration does not provide sufficient information on Mn release and/or reduction[133]. Therefore, in this thesis sorption isotherms for Mn^{2+} sorption onto MnO_2 have been recorded and the experimental data was fitted using the Freundlich model[134]. This Freundlich isotherm then served as a foundation to calculate sorbed Mn and in turn total Mn release in **chapter 2**. Due to IDMP transformation and therefore Mn^{2+} release, sorption isotherms of Mn^{2+} on MnO_2 cannot be recorded in the actual medium – hence, this approach presents an approximation.

1.4 Aims and Scope

APPs have gained significant importance in various industrial and domestic applications over the past decades[7]. Initially considered stable due to their C-P bond, recent research has revealed that APPs are more susceptible to transformation than previously thought[32,34,135]. This discovery, coupled with the potential role of APPs in the formation of glyphosate and AMPA in WWTPs[42,43], underscores the urgent need for a comprehensive understanding of their environmental fate and transformation processes.

This thesis focuses on fundamental research into the environmental behavior and transformation of APPs under controlled laboratory conditions, providing a foundation for future studies in more complex environmental matrices. All experiments were conducted at environmentally relevant pH levels (6 or 8) to ensure applicability to natural systems. Key aspects within the scope of this research include:

1. Detailed elucidation of the IDMP oxidation mechanism on MnO_2 surfaces
2. Development and validation of a green analytical method for simultaneous quantification of multiple A(P)Ps without the need of derivatisation
3. Exploration of glyphosate formation from DTPMP oxidation by MnO_2

The overarching aim of this thesis is to elucidate manganese-driven transformation of APPs under environmentally relevant conditions. This research seeks to contribute to a comprehensive understanding of APP degradation pathways, improve analytical methods for their quantification, and investigate the potential formation of glyphosate and AMPA as transformation products.

The specific objectives and approaches of each part will be discussed below:

Despite extensive research on APP transformation, the exact mechanism of oxidative transformation on manganese dioxide remains unclear. Understanding this process is crucial for predicting the environmental fate of APPs and their transformation products. **Chapter 2** addresses this knowledge gap, and elucidates the heterogenous oxidation of APPs on manganese dioxide with the bisphosphonate IDMP as a model compound. IDMP reacts with MnO_2 but does not react with Mn^{2+}/O_2. This eliminates one complexity dimension present for higher APPs[40] and allows the pure investigation of the heterogenous oxidation. Additionally, the formation of TPs is limited compared to e.g. DTPMP and the complete transformation of IDMP on MnO_2 proceeds in an adequate time range (100-400 h).

Chapter 2 aims to shed light on this multi-step reaction, which includes e.g. sorption, electron transfer, bond cleavage, desorption and resorption of transformation products. Therefore, the oxidation of IDMP on MnO_2 was investigated in 10 laboratory batch experiments, differing i) in the type of MnO_2 used and ii) in the MnO_2 concentration. As sorption on and redox potential of MnO_2 are pH-dependent, the experimental pH was controlled at 6 using MES buffer. The main analysis tools employed were quantification of IDMP and its main TPs AMPA and PO_4^{3-}, as well as quantification of released Mn^{2+}. CSIA has been employed as a special tool to investigate the succession of the different reaction steps and to explain differences in behavior when altering the MnO_2 concentration and/or when using a different mineral.

Current analytical methods for quantifying APPs and their TPs exhibit notable constraints in terms of environmental sustainability and multi-analyte detection capabilities. These limitations impede investigations of APP transformation and sorption in lign with the principles of green analytical chemistry (GAC). To overcome these challenges, **chapter 3** aims at developing a green simultaneous quantification method for the six aminophosphonates AMPA, Glyphosate, IDMP, ATMP, EDTMP and DTPMP. In the **chapter 2**, IDMP and AMPA concentrations were routinely analyzed by IC-PAD. IC-PAD offers numerous advantages in terms of GAC, such as low energy consumption, no need for derivatization, and the use of purely aqueous eluents. Therefore, the aim was to expand the previous AMPA/IDMP method to include glyphosate and APPs. An anion exchange column already proven suitable for the separation of APPs (Dionex IonPac AS16)[16] was employed for this purpose.

The method aims to quantify APPs and selected TPs in laboratory batch experiments. Therefore, contrary to requirements for ultra-trace environmental analysis methods, it was primarily focused on simplicity, greenness, and low cost. Method validation focused on reproducibility, while applicability was shown using a DTPMP transformation experiment on MnO_2. Further, the greenness of this method is compared to another recently published APP quantification method using a generic greenness metric system for analytical methods. A great deal of time went into maintenance and regeneration of the IC system and column to assure robustness of the system.

Recent studies suggested that municipal wastewaters could be a previously unrecognized source of glyphosate in surface waters, with APPs as potential precursors. However, the formation of glyphosate from APPs under environmentally relevant conditions has not been demonstrated until now. To address this critical knowledge gap, **chapter 4** investigates the formation of AMPA and glyphosate during DTPMP oxidation by MnO_2. It builds upon the two previous studies, as it combines the knowledge derived about IDMP oxidation on MnO_2 in **chapter 2** and applies the APP quantification method described in **chapter 3**.

Chapter 4 elucidates if and under which conditions the formation of glyphosate from DTPMP via manganese-driven oxidation is chemically possible. Several findings from literature and **chapter 2** indicated glyphosate formation from DTPMP using a strong oxidant being plausible, thus it was explicitly searched for glyphosate as a minor TP using a trace-level quantification method (LC-QQQ after FMOC-derivatization). The effect of O_2 and MnO_2 concentration on AMPA and glyphosate formation was investigated, as well as glyphosate formation from DTPMP in the presence of Mn^{2+}/O_2. Last but not least, the environmental relevance of manganese-driven DTPMP oxidation was primarily assessed by repeating the experiments in a wastewater matrix. Next to LC-QQQ, IC-PAD was employed for the quantification of DTPMP. IC-ICP-MS served for the quantification of PO_4^{3-} and provided an overview of all P-containing products formed within an experiment. The outcomes of this study shall serve – as for **chapter 2** – as a basis for further research in environmental and technical systems.

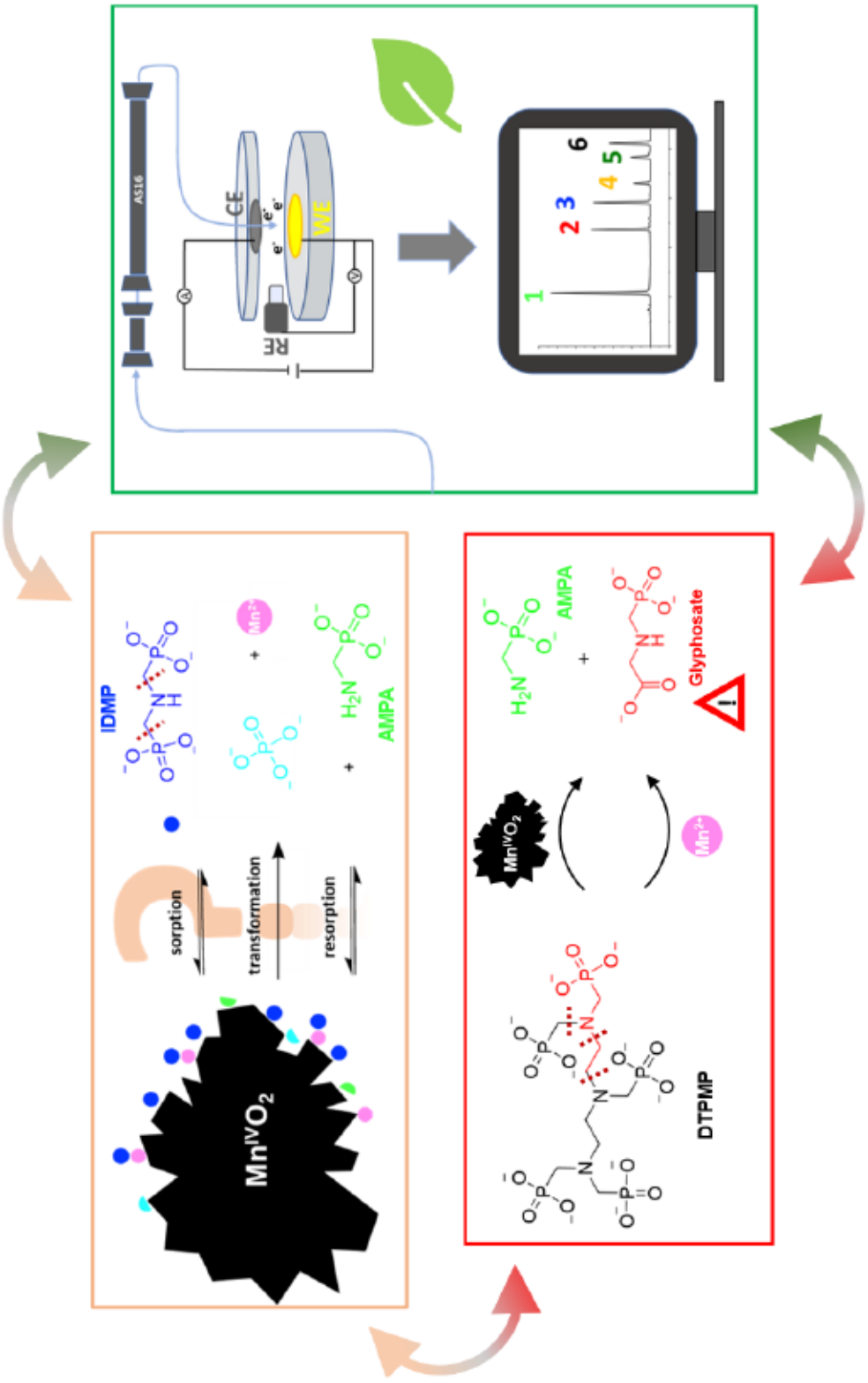

Figure 1.6 Graphical abstract summarizing the major contents of this work.

1.6 References

(1) Nowack, B.; Vanbriesen, J. M. *Chelating Agents in the Environment*; UTC, 2005; Vol. 4. https://pubs.acs.org/sharingguidelines.

(2) Popov, K.; Rönkkömäki, H.; J Lajunen, L. H. *Critical Evaluation of Stability Constants of Phosphonic Acids (IUPAC Technical Report)*; Brazil, 2001; Vol. 73.

(3) Nowack, B.; Stone, A. T. The Influence of Metal Ions on the Adsorption of Phosphonates onto Goethite. *Environ Sci Technol* **1999**, *33* (20), 3627–3633. https://doi.org/10.1021/es9900860.

(4) Gledhill, W. E.; Feijtel, T. C. J. Environmental Properties and Safety Assessment of Organic Phosphonates Used for Detergent and Water Treatment Applications. In *The Handbook of Environmental Chemistry – Detergents*; 1992; pp 261–285. https://doi.org/10.1007/978-3-540-47108-0_8.

(5) Ruffolo, F.; Dinhof, T.; Murray, L.; Zangelmi, E.; Chin, J. P.; Pallitsch, K.; Peracchi, A. The Microbial Degradation of Natural and Anthropogenic Phosphonates. *Molecules* **2023**, *28* (19). https://doi.org/10.3390/molecules28196863.

(6) Schowanek, D.; Verstraete, W. Phosphonate Utilization by Bacterial Cultures and Enrichments from Environmental Samples. *Appl Environ Microbiol* **1990**, *56* (4), 895–903.

(7) Rott, E.; Steinmetz, H.; Metzger, J. W. Organophosphonates: A Review on Environmental Relevance, Biodegradability and Removal in Wastewater Treatment Plants. *Science of The Total Environment* **2018**, *615*. https://doi.org/10.1016/j.scitotenv.2017.09.223.

(8) Knepper, T. P. Synthetic Chelating Agents and Compounds Exhibiting Complexing Properties in the Aquatic Environment. *TrAC - Trends in Analytical Chemistry* **2003**, *22* (10), 708–724. https://doi.org/10.1016/S0165-9936(03)01008-2.

(9) Jaworska, J.; Van Genderen-Takken, H.; Hanstveit, A.; Van De Plassche, E.; Feijtel, T. Environmental Risk Assessment of Phosphonates, Used in Domestic Laundry and Cleaning Agents in the Netherlands. *Chemosphere* **2002**, No. 47, 655–665.

(10) Studnik, H.; Liebsch, S.; Forlani, G.; Wieczorek, D.; Kafarski, P.; Lipok, J. Amino Polyphosphonates - Chemical Features and Practical Uses, Environmental Durability and Biodegradation. *N Biotechnol* **2015**, *32* (1), 1–6. https://doi.org/10.1016/j.nbt.2014.06.007.

(11) Nowack, B. Environmental Chemistry of Phosphonates. *Water Res* **2003**, *37* (11), 2533–2546. https://doi.org/10.1016/S0043-1354(03)00079-4.

(12) European Phosphonates Association. *Input to the Revision of the EU Ecolabels Related to Detergents*; 2015. https://www.phosphonates.org/images/Images/Documents/EPA%20phosphonate%20input%20detergent%20Ecolabel.pdf (accessed 2022-11-28).

(13) European Commission. *EP supports ban of phosphates in consumer detergents*. Press release. https://ec.europa.eu/commission/presscorner/detail/en/ip_11_1542 (accessed 2024-12-03).

(14) Davenport, B.; Dubois, F.; Kishi, A. Report: Chelating Agents. In *Chemical Economics Handbook (CEH)*; Menlo Park, CA, USA, 2000.

(15) US Environmental Protection Agency. *Sodium Salts of Polyphosphates Supply Chain – Executive Summary*; 2022. https://www.epa.gov/system/files/documents/2023-03/Sodium%20Salts%20of%20Polyphosphate%20Supply%20Chain%20Profile.pdf (accessed 2024-12-03).

(16) Armbruster, D.; Rott, E.; Minke, R.; Happel, O. Trace-Level Determination of Phosphonates in Liquid and Solid Phase of Wastewater and Environmental Samples by IC-ESI-MS/MS. *Anal Bioanal Chem* **2019**, *412* (20), 4807–4825. https://doi.org/10.1007/s00216-019-02159-5.

(17) Rott, E.; Happel, O.; Armbruster, D.; Minke, R. Behavior of PBTC, HEDP, and Aminophosphonates in the Process of Wastewater Treatment. *Water (Switzerland)* **2020**, *12* (1). https://doi.org/10.3390/w12010053.

(18) Nowack, B.; Stone, A. T. Competitive Adsorption of Phosphate and Phosphonates onto Goethite. *Water Res* **2006**, *40* (11), 2201–2209. https://doi.org/10.1016/j.watres.2006.03.018.

(19) Nowack, B.; Stone, A. T. Adsorption of Phosphonates onto the Goethite-Water Interface. **1999**.

(20) Martínez, R. J.; Farrell, J. Understanding Nitrilotris(Methylenephosphonic Acid) Reactions with Ferric Hydroxide. *Chemosphere* **2017**, *175*, 490–496. https://doi.org/10.1016/j.chemosphere.2017.02.015.

(21) Nowack, B. The Behavior of Phosphonates in Wastewater Treatment Plants of Switzerland. *Water Res* **1998**, *4* (12), 1271–1279.

(22) Steber, J.; Wierich, P. Properties of Aminotris(Methylenephosphonate) Affecting Its Environmental Fate: Degradability, Sludge Adsorption, Mobility in Soils, and Bioconcentration. *Chemosphere* **1987**, *16* (6), 1323–1337.

(23) Zhou, X.; Jiang, G.; Wang, Q.; Yuan, Z. Role of Indigenous Iron in Improving Sludge Dewaterability through Peroxidation. *Sci Rep* **2015**, *5*. https://doi.org/10.1038/srep07516.

(24) Navratil, J. D. Wastewater Treatment Technology Based on Iron Oxides. In *Natural Microporous Materials in Environmental Technology*; Misaelides, P., Macášek, P., Pinnavaia, T., Colella, C., Eds.; Springer Netherlands: Dordrecht, 1999; Vol. 362, pp 417–424. https://doi.org/10.1007/978-94-011-4499-5_31.

(25) Ternan, N. G.; Mc Grath, J. W.; Mullan, G. M.; Quinn, J. P. Review: Organophosphonates: Occurrence, Synthesis and Biodegradation by Microorganisms. *World J Microbiol Biotechnol* **1998**, *14*, 635–647.

(26) Murphy, A. R. J.; Scanlan, D. J.; Chen, Y.; Adams, N. B. P.; Cadman, W. A.; Bottrill, A.; Bending, G.; Hammond, J. P.; Hitchcock, A.; Wellington, E. M. H.; Lidbury, I. D. E. A. Transporter Characterisation Reveals Aminoethylphosphonate Mineralisation as a Key Step in the Marine Phosphorus Redox Cycle. *Nat Commun* **2021**, *12* (1). https://doi.org/10.1038/s41467-021-24646-z.

(27) Riedel, R.; Commichau, F. M.; Benndorf, D.; Hertel, R.; Holzer, K.; Hoelzle, L. E.; Mardoukhi, M. S. Y.; Noack, L. E.; Martienssen, M. Biodegradation of Selected Aminophosphonates by the Bacterial Isolate Ochrobactrum Sp. BTU1. *Microbiol Res* **2024**, *280*. https://doi.org/10.1016/j.micres.2024.127600.

(28) Riedel, R.; Meißner, K.; Kaschubowski, A.; Benndorf, D.; Martienssen, M.; Braun, B. Laundry Isolate Delftia Sp. UBM14 Capable of Biodegrading Industrially Relevant Aminophosphonates. *Microorganisms* **2024**, *12* (8). https://doi.org/10.3390/microorganisms12081664.

(29) Riedel, R.; Krahl, K.; Buder, K.; Böllmann, J.; Braun, B.; Martienssen, M. Novel Standard Biodegradation Test for Synthetic Phosphonates. *J Microbiol Methods* **2023**, *212*. https://doi.org/10.1016/j.mimet.2023.106793.

(30) Nowack, B. Aminopolyphosphonate Removal during Wastewater Treatment. *Water Res* **2002**, *36*, 4636–4642.

(31) Marks, R. G. H.; Drees, F.; Rockel, S.; Kerpen, K.; Jochmann, M. A.; Schmidt, T. C. Mechanistic Investigation of Phosphonate Photolysis in Aqueous Solution by Simultaneous LC-IRMS and HRMS Analysis. *J Photochem Photobiol A Chem* **2023**, *439*, 114582. https://doi.org/10.1016/j.jphotochem.2023.114582.

(32) Marks, R. G. H.; Rockel, S. P.; Kerpen, K.; Somnitz, H.; Martin, P. R.; Jochmann, M. A.; Schmidt, T. C. Effects of PH-Dependent Speciation on the Photolytic Degradation Mechanism of Phosphonates. *J Photochem Photobiol A Chem* **2023**, 115327. https://doi.org/10.1016/j.jphotochem.2023.115327.

(33) Kuhn, R.; Jensch, R.; Bryant, I. M.; Fischer, T.; Liebsch, S.; Martienssen, M. The Influence of Selected Bivalent Metal Ions on the Photolysis of Diethylenetriamine Penta(Methylenephosphonic Acid). *Chemosphere* **2018**, *210*, 726–733. https://doi.org/10.1016/j.chemosphere.2018.07.033.

(34) Kuhn, R.; Jensch, R.; Bryant, I. M.; Fischer, T.; Liebsch, S.; Martienssen, M. Photodegradation of Ethylenediaminetetra(Methylenephosphonic Acid) – The Effect of the System Configuration. *J Photochem Photobiol A Chem* **2020**, *388*. https://doi.org/10.1016/j.jphotochem.2019.112192.

(35) Klinger, J.; Lang, M.; Sacher, F.; Brauch, H. J.; Maier, D.; Worch, E. Formation of Glyphosate and AMPA during Ozonation of Waters Containing Ethylenediaminetetra(Methylenephosphonic Acid). *Ozone Sci Eng* **1998**, *20* (2), 99–110. https://doi.org/10.1080/01919519808547279.

(36) Nowack, B.; Stone, A. T. Homogeneous and Heterogeneous Oxidation of Nitrilotrismethylenephosphonic Acid (NTMP) in the Presence of Manganese(II, III) and Molecular Oxygen. *Journal of Physical Chemistry B* **2002**, *106* (24), 6227–6233. https://doi.org/10.1021/jp014293+.

(37) Nowack, B.; Stone, A. T. Manganese-Catalyzed Degradation of Phosphonic Acids. *Environ Chem Lett* **2003**, *1* (1), 24–31. https://doi.org/10.1007/s10311-002-0014-3.

(38) Martin, P. R.; Buchner, D.; Jochmann, M. A.; Elsner, M.; Haderlein, S. B. Two Pathways Compete in the Mn(II)-Catalyzed Oxidation of Aminotrismethylene Phosphonate (ATMP). *Environ Sci Technol* **2022**, *56* (7), 4091–4100. https://doi.org/10.1021/acs.est.1c06407.

(39) Schowanek, D.; Verstraete, W. Hydrolysis and Free Radical Mediated Degradation of Phosphonates. *J. Environ. Quality* **1991**, *20*, 769–776.

(40) Nowack, B.; Stone, A. T. Degradation of Nitrilotris(Methylenephosphonic Acid) and Related (Amino)Phosphonate Chelating Agents in the Presence of Manganese and Molecular Oxygen. *Environ Sci Technol* **2000**, *34* (22), 4759–4765. https://doi.org/10.1021/es0000908.

(41) Calvin, G.; Long, P. H.; Stitzel, K. A.; Anderson, R. L.; Balmbra, R.; Bruce, R. D.; Bhatt, A.; Miller, P. M.; Broadmeadow, A. Ethylenediaminetetra(Methylenephosphonic Acid): Genotoxicity, Biodistribution, and Subchronic and Chronic Toxicity in Rats. *Fd. Chem. Toxic.* **1988**, *26* (7), 601–6111.

(42) Venditti, S.; Kiesch, A.; Hansen, J. Fate of Glyphosate and Its Metabolite AminoMethylPhosponic Acid (AMPA) from Point Source through Wastewater Sludge and Advanced Treatment. *Chemosphere* **2023**, *340*. https://doi.org/10.1016/j.chemosphere.2023.139843.

(43) Schwientek, M.; Rügner, H.; Haderlein, S. B.; Schulz, W.; Wimmer, B.; Engelbart, L.; Bieger, S.; Huhn, C. Glyphosate Contamination in European Rivers Not from Herbicide Application? *Water Res* **2024**, *263*, 122140. https://doi.org/10.1016/j.watres.2024.122140.

(44) Grandcoin, A.; Piel, S.; Baurès, E. AminoMethylPhosphonic Acid (AMPA) in Natural Waters: Its Sources, Behavior and Environmental Fate. *Water Research*. Elsevier Ltd 2017, pp 187–197. https://doi.org/10.1016/j.watres.2017.03.055.

(45) Benbrook, C. M. How Did the US EPA and IARC Reach Diametrically Opposed Conclusions on the Genotoxicity of Glyphosate-Based Herbicides? *Environ Sci Eur* **2019**, *31* (1). https://doi.org/10.1186/s12302-018-0184-7.

(46) Benbrook, C. M. Trends in Glyphosate Herbicide Use in the United States and Globally. *Environ Sci Eur* **2016**, *28* (1), 1–15. https://doi.org/10.1186/s12302-016-0070-0.

(47) Duke, S. O.; Powles, S. B. Glyphosate: A Once-in-a-Century Herbicide. *Pest Manag Sci* **2008**, *64* (4), 319–325. https://doi.org/10.1002/ps.1518.

(48) András Székács; Béla Darvas. Forty Years with Glyphosate. In *Herbicides: Properties, Synthesis and Control of Weeds*; 2012; pp 247–287.

(49) Maggi, F.; la Cecilia, D.; Tang, F. H. M.; McBratney, A. The Global Environmental Hazard of Glyphosate Use. *Science of the Total Environment* **2020**, *717*. https://doi.org/10.1016/j.scitotenv.2020.137167.

(50) Myers, J. P.; Antoniou, M. N.; Blumberg, B.; Carroll, L.; Colborn, T.; Everett, L. G.; Hansen, M.; Landrigan, P. J.; Lanphear, B. P.; Mesnage, R.; Vandenberg, L. N.; Vom Saal, F. S.; Welshons, W. V.; Benbrook, C. M. Concerns over Use of Glyphosate-Based Herbicides and Risks Associated with Exposures: A Consensus Statement. *Environmental Health* **2016**, *15* (1). https://doi.org/10.1186/s12940-016-0117-0.

(51) Borggaard, O. K.; Gimsing, A. L. Fate of Glyphosate in Soil and the Possibility of Leaching to Ground and Surface Waters: A Review. *Pest Manag Sci* **2008**, *64* (4), 441–456. https://doi.org/10.1002/ps.1512.

(52) Henderson, A. M. ; Gervais, J. A. ; Luukinen, B. ; Buhl, K. ; Stone, D. ; Strid, A. ; Cross, A. ;; Jenkins, J. *Glyphosate Technical Fact Sheet*. http://npic.orst.edu/factsheets/archive/glyphotech.html (accessed 2024-06-11).

(53) Bento, C. P. M.; Yang, X.; Gort, G.; Xue, S.; van Dam, R.; Zomer, P.; Mol, H. G. J.; Ritsema, C. J.; Geissen, V. Persistence of Glyphosate and Aminomethylphosphonic Acid in Loess Soil under Different Combinations of Temperature, Soil Moisture and Light/Darkness. *Science of the Total Environment* **2016**, *572*, 301–311. https://doi.org/10.1016/j.scitotenv.2016.07.215.

(54) Bai, S. H.; Ogbourne, S. M. Glyphosate: Environmental Contamination, Toxicity and Potential Risks to Human Health via Food Contamination. *Environmental Science and Pollution Research* **2016**, *23* (19), 18988–19001. https://doi.org/10.1007/s11356-016-7425-3.

(55) Giesy, J. P.; Kannan, K. Global Distribution of Perfluorooctane Sulfonate in Wildlife. *Environ Sci Technol* **2001**, *35* (7), 1339–1342. https://doi.org/10.1021/es001834k.

(56) Bøhn, T.; Cuhra, M.; Traavik, T.; Sanden, M.; Fagan, J.; Primicerio, R. Compositional Differences in Soybeans on the Market: Glyphosate Accumulates in Roundup Ready GM Soybeans. *Food Chem* **2014**, *153*, 207–215. https://doi.org/10.1016/j.foodchem.2013.12.054.

(57) Williams, G. M.; Kroes, R.; Munro, I. C. Safety Evaluation and Risk Assessment of the Herbicide Roundup and Its Active Ingredient, Glyphosate, for Humans. *Regulatory*

Toxicology and Pharmacology **2000**, *31* (2), 117–165. https://doi.org/10.1006/rtph.1999.1371.

(58) Bradberry, S. M.; Proudfoot, A. T.; Vale, J. A. Glyphosate Poisoning. *Toxicol Rev* **2004**, *23* (3), 159–167. https://doi.org/10.2165/00139709-200423030-00003.

(59) IARC. Some Organophosphate Insecticides and Herbicides. *IARC Monogr Eval Carcinog Risks Hum* **2017**, *112*.

(60) Guyton, K. Z.; Loomis, D.; Grosse, Y.; El Ghissassi, F.; Benbrahim-Tallaa, L.; Guha, N.; Scoccianti, C.; Mattock, H.; Straif, K.; Blair, A.; Fritschi, L.; McLaughlin, J.; Sergi, C. M.; Calaf, G. M.; Le Curieux, F.; Baldi, I.; Forastiere, F.; Kromhout, H.; 't Mannetje, A.; Rodriguez, T.; Egeghy, P.; Jahnke, G. D.; Jameson, C. W.; Martin, M. T.; Ross, M. K.; Rusyn, I.; Zeise, L. Carcinogenicity of Tetrachlorvinphos, Parathion, Malathion, Diazinon, and Glyphosate. *Lancet Oncol* **2015**, *16* (5), 490–491. https://doi.org/10.1016/S1470-2045(15)70134-8.

(61) EPA's Office of Pesticide Programs. *Glyphosate Issue Paper: Evaluation of Carcinogenic Potential*; 2016. https://www.epa.gov/sites/default/files/2016-09/documents/glyphosate_issue_paper_evaluation_of_carcincogenic_potential.pdf (accessed 2024-12-03).

(62) European Food Safety Authority. *EFSA Explains the Scientific Assessment Glyphosate*; 2023. https://www.efsa.europa.eu/sites/default/files/2023-07/glyphosate_factsheet.pdf (accessed 2024-06-11).

(63) European Commision. *Status of glyphosate in the EU*. https://food.ec.europa.eu/plants/pesticides/approval-active-substances-safeners-and-synergists/renewal-approval/glyphosate_en (accessed 2024-12-03).

(64) Davoren, M. J.; Schiestl, R. H. Glyphosate-Based Herbicides and Cancer Risk: A Post-IARC Decision Review of Potential Mechanisms, Policy and Avenues of Research. *Carcinogenesis* **2018**, *39* (10), 1207–1215. https://doi.org/10.1093/carcin/bgy105.

(65) Post, J. E. Manganese Oxide Minerals: Crystal Structures and Economic and Environmental Significance. *Proc. Natl. Acad. Sci. USA* **1999**, *96*, 3447–3454.

(66) Hansel, C. M.; Learman, D. R. Geomicrobiology of Manganese. In *Ehrlich's Geomicrobiology*; Ehrlich, H. L., Newman, D. K., Kappler, A., Eds.; CRC Press, Taylor & Francis Group: Boca Raton, FL, USA, 2016; pp 401–452.

(67) Li, J.; Jia, Y.; Dong, R.; Huang, R.; Liu, P.; Li, X.; Wang, Z.; Liu, G.; Chen, Z. Advances in the Mechanisms of Plant Tolerance to Manganese Toxicity. *Int J Mol Sci* **2019**, *20* (20). https://doi.org/10.3390/ijms20205096.

(68) Sparrow, L. A.; Uren, N. C. Manganese Oxidation and Reduction in Soils: Effects of Temperature, Water Potential, PH and Their Interactions. *Soil Research* **2014**, *52* (5), 483–494. https://doi.org/10.1071/SR13159.

(69) Jakubus, M. Distribution of Oxyphinic Elements in Sewage Sludge Fractions Based on Manganese and Nickel. *Journal of Ecological Engineering* **2021**, *22* (6), 72–82. https://doi.org/10.12911/22998993/137359.

(70) Andrea Roskosch; Patric Heidecke. *Klärschlamm Entsorgung in Der Bundesrepublik Deutschland*; Dessau-Roßlau, 2018. https://www.umweltbundesamt.de/sites/default/files/medien/376/publikationen/2018_10_08_uba_fb_klaerschlamm_bf_low.pdf (accessed 2024-06-11).

(71) Sly, L. I.; Hodgkinson, M. C.; Arunpairojana, V. Deposition of Manganese in a Drinking Water Distribution System Following the Commissioning in 1983 of the Molendinar. *Appl Environ Microbiol* **1990**, *56* (3), 628–639.

(72) Remucal, C. K.; Ginder-Vogel, M. A Critical Review of the Reactivity of Manganese Oxides with Organic Contaminants. *Environmental Sciences: Processes and Impacts* **2014**, *16* (6), 1247–1266. https://doi.org/10.1039/c3em00703k.

(73) Ghosh, S. K. Diversity in the Family of Manganese Oxides at the Nanoscale: From Fundamentals to Applications. *ACS Omega* **2020**, *5* (40), 25493–25504. https://doi.org/10.1021/acsomega.0c03455.

(74) Geszvain, K.; Butterfield, C.; Davis, R. E.; Madison, A. S.; Lee, S. W.; Parker, D. L.; Soldatova, A.; Spiro, T. G.; Luther, G. W.; Tebo, B. M. The Molecular Biogeochemistry of Manganese(II) Oxidation. *Biochem Soc Trans* **2012**, *40* (6), 1244–1248. https://doi.org/10.1042/BST20120229.

(75) Luther, G. W. The Role of One- and Two-Electron Transfer Reactions in Forming Thermodynamically Unstable Intermediates as Barriers in Multi-Electron Redox Reactions. *Aquat Geochem* **2010**, *16* (3), 395–420. https://doi.org/10.1007/s10498-009-9082-3.

(76) Nealson, E. H.; Tebo, B. M.; Rosson, Reinhar. A. Occurrence and Mechanisms of Microbial Oxidation of Manganese. *Adv Appl Microbiol* **1988**, *33*, 279–318.

(77) Tebo, B. M. Manganese(II) Oxidation in the Suboxic Zone of the Black Sea. *Deep-Sea Research* **1991**, *38* (2), 883–905.

(78) Tebo, B. M.; Bargar, J. R.; Clement, B. G.; Dick, G. J.; Murray, K. J.; Parker, D.; Verity, R.; Webb, S. M. Biogenic Manganese Oxides: Properties and Mechanisms of Formation. *Annu Rev Earth Planet Sci* **2004**, *32*, 287–328. https://doi.org/10.1146/annurev.earth.32.101802.120213.

(79) Adams, L. F.; Ghiorse, W. C. Oxidation State of Mn in the Mn Oxide Produced by Leptothrix Discophora SS-1. *Geochim Cosmochim Acta* **1988**, *52* (8), 2073–2076. https://doi.org/10.1016/0016-7037(88)90186-X.

(80) Davison, W. Iron and Manganese in Lakes. *Earth Sci Rev* **1993**, *34*, 119–163.

(81) Godwin, C. M.; Zehnpfennig, J. R.; Learman, D. R. Biotic and Abiotic Mechanisms of Manganese (II) Oxidation in Lake Erie. *Front Environ Sci* **2020**, *8*. https://doi.org/10.3389/fenvs.2020.00057.

(82) Scholtysik, G.; Dellwig, O.; Roeser, P.; Arz, H. W.; Casper, P.; Herzog, C.; Goldhammer, T.; Hupfer, M. Geochemical Focusing and Sequestration of Manganese during Eutrophication of Lake Stechlin (NE Germany). *Biogeochemistry* **2020**, *151* (2–3), 313–334. https://doi.org/10.1007/s10533-020-00729-9.

(83) Schaller, T.; Wehrli, B. Geochemical-Focusing of Manganese in Lake Sediments-An Indicator of Deep-Water Oxygen Conditions. *Aquat Geochem* **1997**, *2*, 359–378.

(84) Trouwborst, R. E.; Clement, B. G.; Tebo, B. M.; Glazer, B. T.; Luther, G. W. Soluble Mn(III) in Suboxic Zones. *Science (1979)* **2006**, *313* (5795), 1955–1957. https://doi.org/10.1126/science.1132876.

(85) Aguilar, C.; Nealson, K. H. Biogeochemical Cycling of Manganese in Oneida Lake, New York: Whole Lake Studies of Manganese. *J Great Lakes Res* **1998**, *24* (1), 93–104. https://doi.org/10.1016/S0380-1330(98)70802-0.

(86) Arias, N. P.; Becerra, M. E.; Giraldo, O. Structural and Electrical Studies for Birnessite-Type Materials Synthesized by Solid-State Reactions. *Nanomaterials* **2019**, *9* (8). https://doi.org/10.3390/nano9081156.

(87) Morales, E.; Shaner, S. E.; Stone, K. L. Characterizing Biogenic MnOx Produced by Pseudomonas Putida MnB1 and Its Catalytic Activity towards Water Oxidation. *Life* **2024**, *14* (2). https://doi.org/10.3390/life14020171.

(88) Ulrich, H.-J.; Stone, A. T. Oxidation of Chlorophenols Adsorbed to Manganese Oxide Surfaces. *Environ Sci Technol* **1989**, *23* (4), 421–428.

(89) Islam, M. A.; Morton, D. W.; Johnson, B. B.; Mainali, B.; Angove, M. J. Manganese Oxides and Their Application to Metal Ion and Contaminant Removal from Wastewater. *Journal of Water Process Engineering* **2018**, *26*, 264–280. https://doi.org/10.1016/j.jwpe.2018.10.018.

(90) Salvestrini, S.; Fenti, A.; Qian, L.; Kopinke, F. D. Oxidation of Organic Pollutants over MnO2 in Cold Water Assisted by Peroxydisulfate. *Chemical Engineering Journal* **2024**, *479*. https://doi.org/10.1016/j.cej.2023.147170.

(91) Nico, P. S.; Zasoski, R. J. Mn(III) Center Availability as a Rate Controlling Factor in the Oxidation of Phenol and Sulfide on δ-MnO2. *Environ Sci Technol* **2001**, *35* (16), 3338–3343. https://doi.org/10.1021/es001848q.

(92) Hu, E.; Pan, S.; Zhang, W.; Zhao, X.; Liao, B.; He, F. Impact of Dissolved O2 on Phenol Oxidation by δ-MnO2. *Environ Sci Process Impacts* **2019**, *21* (12), 2118–2127. https://doi.org/10.1039/c9em00389d.

(93) Klausen, J.; Haderlein, S. B.; Schwarzenbach, R. P. Oxidation of Substituted Anilines by Aqueous MnO2 : Effect of Co-Solutes on Initial and Quasi-Steady-State Kinetics. *Environ Sci Technol* **1997**, *31*, 2642–2649.

(94) Chen, W. R.; Ding, Y.; Johnston, C. T.; Teppen, B. J.; Boyd, S. A.; Li, H. Reaction of Lincosamide Antibiotics with Manganese Oxide in Aqueous Solution. *Environ Sci Technol* **2010**, *44* (12), 4486–4492. https://doi.org/10.1021/es1000598.

(95) Liu, J.; Zhang, Y.; Gu, Q.; Sheng, A.; Zhang, B. Tunable Mn Oxidation State and Redox Potential of Birnessite Coexisting with Aqueous Mn(II) in Mildly Acidic Environments. *Minerals* **2020**, *10* (8), 1–15. https://doi.org/10.3390/min10080690.

(96) Barrett, K. A.; McBride, M. B. Oxidative Degradation of Glyphosate and Aminomethylphosphonate by Manganese Oxide. *Environ Sci Technol* **2005**, *39* (23), 9223–9228. https://doi.org/10.1021/es051342d.

(97) Paudel, P.; Negusse, A.; Jaisi, D. P. Birnessite-Catalyzed Degradation of Glyphosate: A Mechanistic Study Aided by Kinetics Batch Studies and NMR Spectroscopy. *Soil Science Society of America Journal* **2015**, *79* (3), 815–825. https://doi.org/10.2136/sssaj2014.10.0394.

(98) Li, H.; Wallace, A. F.; Sun, M.; Reardon, P.; Jaisi, D. P. Degradation of Glyphosate by Mn-Oxide May Bypass Sarcosine and Form Glycine Directly after C-N Bond Cleavage. *Environ Sci Technol* **2018**, *52* (3), 1109–1117. https://doi.org/10.1021/acs.est.7b03692.

(99) Li, H.; Joshi, S. R.; Jaisi, D. P. Degradation and Isotope Source Tracking of Glyphosate and Aminomethylphosphonic Acid. *J Agric Food Chem* **2016**, *64* (3), 529–538. https://doi.org/10.1021/acs.jafc.5b04838.

(100) Pal, A.; Mahamallik, P.; Saha, S.; Majumdar, A. Degradation of Tetracycline Antibiotics by Advanced Oxidation Processes: Application of MnO2 Nanomaterials. *Natural Resources & Engineering* **2018**, 1–11. https://doi.org/10.1080/23802693.2018.1434397.

(101) Lyu, Y.; Li, C.; Du, X.; Zhu, Y.; Zhang, Y.; Li, S. Catalytic Oxidation of Toluene over MnO2 Catalysts with Different Mn (II) Precursors and the Study of Reaction Pathway. *Fuel* **2020**, *262*, 116610. https://doi.org/10.1016/j.fuel.2019.116610.

(102) Watts, R. J.; Asce, A. M.; Howsawkeng, J.; Teel, A. L. Technical Note: Destruction of a Carbon Tetrachloride Dense Nonaqueous Phase Liquid by Modified Fenton's Reagent. *J. Environm. Eng.* **2005**, *131*, 1114–1119. https://doi.org/10.1061/ASCE0733-93722005131:71114.

(103) Zhu, S.; Ho, S. H.; Jin, C.; Duan, X.; Wang, S. Nanostructured Manganese Oxides: Natural/Artificial Formation and Their Induced Catalysis for Wastewater Remediation. *Environ Sci Nano* **2020**, *7* (2), 368–396. https://doi.org/10.1039/c9en01250h.

(104) Jia, L.; Zhou, Q.; Li, Y.; Wu, W. Application of Manganese Oxides in Wastewater Treatment: Biogeochemical Mn Cycling Driven by Bacteria. *Chemosphere* **2023**, *336*. https://doi.org/10.1016/j.chemosphere.2023.139219.

(105) Graf, H. G.; Biebl, S. M.; Müller, L.; Breitenstein, C.; Huhn, C. Capillary Electrophoresis Applied for the Determination of Acidity Constants and Limiting Electrophoretic Mobilities of Ionizable Herbicides Including Glyphosate and Its Metabolites and for Their Simultaneous Separation. *J Sep Sci* **2022**, *45* (5), 1128–1139. https://doi.org/10.1002/jssc.202100952.

(106) Wong, D.; Jandik, P.; Jones, W. R.; Hagenaars, A. Ion Chromatography of Polyphosphonates with Direct Refractive Index Detection. *J Chromatogr* **1987**, *389*, 279–285.

(107) Weiss, J.; Hägele, G. Lonen-Chromatographische Analyse Anorganischer Und Organischer Komplexbildner. *Fresenius Z Anal Chem* **1987**, *348*, 46–50.

(108) Fürhacker, M.; Lesueur, C.; Pfeffer, M.; Köllensperger, G.; Popp, M.; Mentler, A. *Phosphonate - AMPA (Aminomethylphosphonsäure). Herkunftsabschätzung, Umweltkonzentrationen Und Photolyseabbau*; Vienna, 2005.

(109) Tewari, M.-J. K.; van Stroe-Bieze, S. Analysis of Amine-Containing Phosphonates in Detergent Powders by Anion-Exchange Chromatography with Pulsed Amperometric Detection. *J Chromatogr A* **1997**, *771*, 155–161.

(110) Schmidt, C. K.; Raue, B.; Brauch, H. J.; Sacher, F. Trace-Level Analysis of Phosphonates in Environmental Waters by Ion Chromatography and Inductively Coupled Plasma Mass Spectrometry. *Int J Environ Anal Chem* **2014**, *94* (4), 385–398. https://doi.org/10.1080/03067319.2013.831410.

(111) Hanke, I.; Singer, H.; Hollender, J. Ultratrace-Level Determination of Glyphosate, Aminomethylphosphonic Acid and Glufosinate in Natural Waters by Solid-Phase Extraction Followed by Liquid Chromatography–Tandem Mass Spectrometry: Performance Tuning of Derivatization, Enrichment and Detection. *Anal Bioanal Chem* **2008**, *391* (6), 2265–2276. https://doi.org/10.1007/s00216-008-2134-5.

(112) Poiger, T.; Buerge, I. J.; Bächli, A.; Müller, M. D.; Balmer, M. E. Occurrence of the Herbicide Glyphosate and Its Metabolite AMPA in Surface Waters in Switzerland Determined with On-Line Solid Phase Extraction LC-MS/MS. *Environmental Science and Pollution Research* **2017**, *24* (2), 1588–1596. https://doi.org/10.1007/s11356-016-7835-2.

(113) LaCourse, W. R. *Pulsed Electrochemical Detection in High Performance Liquid Chromatography*, 1st ed.; Wiley & Sons Ltd: New Jersey, 1997.

(114) Weiss, J. *Handbook of Ion Chromatography*, 4th ed.; Wiley-VCH: Weinheim, 2016.

(115) Läubli, M.; Bastian Brand; Aeschlimann, A.; Zierfels, G. Glyphosat Und AMPA in Trinkwasser. *Metrohm Whitepaper* **2016**.

(116) Ibáñez, M.; Pozo, Ó. J.; Sancho, J. V.; López, F. J.; Hernández, F. Residue Determination of Glyphosate, Glufosinate and Aminomethylphosphonic Acid in Water and Soil Samples by Liquid Chromatography Coupled to Electrospray Tandem Mass Spectrometry. *J Chromatogr A* **2005**, *1081* (2), 145–155. https://doi.org/10.1016/j.chroma.2005.05.041.

(117) Nagul, E. A.; McKelvie, I. D.; Worsfold, P.; Kolev, S. D. The Molybdenum Blue Reaction for the Determination of Orthophosphate Revisited: Opening the Black Box. *Anal Chim Acta* **2015**, *890*, 60–82. https://doi.org/10.1016/j.aca.2015.07.030.

(118) Murphy, J.; Riley, J. P. A Modified Single Solution Method for the Determination of Phosphate in Natural Waters. *Anal Chim Acta* **1962**, *27*, 31–36. https://doi.org/10.1016/S0003-2670(00)88444-5.

(119) *ISO 6878:2004: Water Quality - Determination of Phosphorus - Ammonium Molybdate Spectrometric Method*; 2004.

(120) Vaeth, E.; Sladek, P.; Kenar, K. Ionen-Chromatographie von Polyphosphaten Und Phosphonaten. *Fresenius Z Anal Chem* **1987**, *329*.

(121) Cavaleiro, A. M. S. V.; Gil, V. M. S.; Pedrosa de Jesus, J. D. N.m.r. Studies of Complexes of Molybdenum(VI) with Tartaric Acid in Aqueous Solution. *Transition Met. Chem* **1983**, *9* (3), 62–67.

(122) Guo, R.; Röhnelt, A. M.; Martin, P. R.; Haderlein, S. B. Phosphate Quantification by the Molybdenum Blue Method Is Impaired by the Presence of (Poly)Phosphonate Chelating Agents. *submitted to Talanta* **2024**.

(123) Macke, M.; Quarles, C. D.; Sperling, M.; Karst, U. Fast and Automated Monitoring of Gadolinium-Based Contrast Agents in Surface Waters. *Water Res* **2021**, *207*. https://doi.org/10.1016/j.watres.2021.117836.

(124) Maik A. Jochmann; Torsten C. Schmidt. *Compound-Specific Stable Isotope Analysis*; The Royal Society of Chemistry, 2012.

(125) Martin, P. R.; Buchner, D.; Jochmann, M. A.; Haderlein, S. B. Stable Carbon Isotope Analysis of Polyphosphonate Complexing Agents by Anion Chromatography Coupled to Isotope Ratio Mass Spectrometry: Method Development and Application. *Anal Bioanal Chem* **2020**, *412* (20), 4827–4835. https://doi.org/10.1007/s00216-019-02251-w.

(126) Elsner, M. Stable Isotope Fractionation to Investigate Natural Transformation Mechanisms of Organic Contaminants: Principles, Prospects and Limitations. *Journal of Environmental Monitoring* **2010**, *12* (11), 2005–2031. https://doi.org/10.1039/c0em00277a.

(127) Hofstetter, T. B.; Bakkour, R.; Buchner, D.; Eisenmann, H.; Fischer, A.; Gehre, M.; Haderlein, S. B.; Höhener, P.; Hunkeler, D.; Imfeld, G.; Jochmann, M. A.; Kümmel, S.; Martin, P. R.; Pati, S. G.; Schmidt, T. C.; Vogt, C.; Elsner, M. Perspectives of Compound-Specific Isotope Analysis of Organic Contaminants for Assessing Environmental Fate and Managing Chemical Pollution. *Nature Water* **2024**, *2* (1), 14–30. https://doi.org/10.1038/s44221-023-00176-4.

(128) Aelion, C. M.; Höhener, P. Fundamentals of Environmental Isotopes and Their Use in Biodegradation. In *Environmental Isotopes in Biodegradation and Bioremediation*; CRC Press, Taylor & Francis Group: Boca Raton, FL, USA, 2009; Vol. 1, pp 3–22.

(129) Hunkeler, D.; Elsner, M. Principles and Mechanisms of Isotope Fractionation. In *Environmental Isotopes in Biodegradation and Bioremediation*; Aelion, C. M., Höhener, P., Hunkeler, D., Aravena, R., Eds.; CRC Press, Taylor & Francis Group: Boca Raton, FL, USA, 2009; pp 43–78.

(130) Stone, A. T.; Morgan, J. Reduction and Dissolution of Mn(Iii) and Mn(Iv) Oxides by Organics. 1. Reaction with Hydroquinone. *ACS Committee on Environmental Improvement Anal. Chem* **1984**, *18* (3), 1919–1980.

(131) Zhao, H.; Zhu, M.; Li, W.; Elzinga, E. J.; Villalobos, M.; Liu, F.; Zhang, J.; Feng, X.; Sparks, D. L. Redox Reactions between Mn(II) and Hexagonal Birnessite Change Its Layer Symmetry. *Environ Sci Technol* **2016**, *50* (4), 1750–1758. https://doi.org/10.1021/acs.est.5b04436.

(132) Elzinga, E. J. Reductive Transformation of Birnessite by Aqueous Mn(II). *Environ Sci Technol* **2011**, *45* (15), 6366–6372. https://doi.org/10.1021/es2013038.

(133) Zhang, H.; Huang, C. H. Oxidative Transformation of Triclosan and Chlorophene by Manganese Oxides. *Environ Sci Technol* **2003**, *37* (11), 2421–2430. https://doi.org/10.1021/es026190q.

(134) Sigg, L.; Stumm, W. *Aquatische Chemie - Einführung in Die Chemie Natürlicher Gewässer*; vdf Hochschulverlag AG an der ETH Zürich, 2016. https://doi.org/10.3218/3768-5.

(135) Drzyzga, D.; Forlani, G.; Vermander, J.; Kafarski, P.; Lipok, J. Biodegradation of the Aminopolyphosphonate DTPMP by the Cyanobacterium Anabaena Variabilis Proceeds via a C–P Lyase-Independent Pathway. *Environ Microbiol* **2017**, *19* (3), 1065–1076. https://doi.org/10.1111/1462-2920.13616.

2 Transformation of Iminodi(methylene phosphonate) on Manganese Dioxides – Passivation of the Mineral Surface by (Formed) Mn2+

Anna M. Röhnelt[1], Phillipp R. Martin[1], Daniel Buchner[1], Stefan B. Haderlein[1]

[1]Environmental Mineralogy, Center for Applied Geoscience, University of Tübingen, Schnarrenbergstraße 94-96, 72076 Tübingen, Germany

Status in the publication process: Manuscript published August 1, 2023.

Journal: Environmental Science & Technology

Reprinted (adapted) with permission from American Chemical Society (ACS) Publications:

Röhnelt, A. M., Martin, P. R., Buchner, D., & Haderlein, S. B. (2023). Transformation of Iminodi(methylene phosphonate) on Manganese Dioxides - Passivation of the Mineral Surface by (Formed) Mn2+. *Environmental Science and Technology*, *57*(32), 11958–11966. https://doi.org/10.1021/acs.est.3c01838

Author Contributions:

A.M.R.: Conceptualization, Methodology, Validation, Formal Analysis, Investigation, Writing – Original Draft, Visualization

P.R.M.: Conceptualization, Methodology, Validation, Writing – Review & Editing

D.B.: Funding Acquisition, Writing – Review & Editing

S.B.H.: Funding Acquisition, Supervision, Resources, Writing – Review & Editing

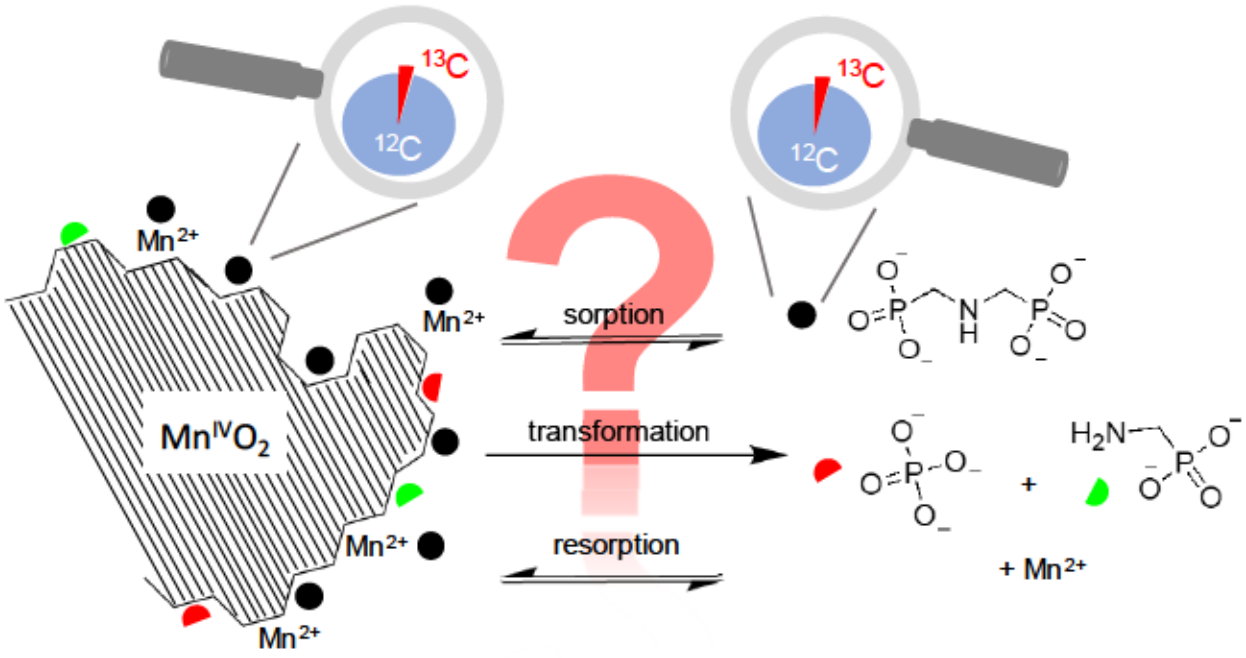

Scheme 2.1 Graphical abstract schematically summarizing the main findings and methodological approach of chapter 2.

2.1 Abstract

Aminopolyphosphonates (APPs) are strong chelating agents with growing use in industrial and household applications. In this study we investigated the oxidation of the bisphosphonate iminodi(methylene phosphonate) (IDMP) – a major transformation product (TP) of numerous commercially used APPs and a potential precursor for aminomethylphosphonate (AMPA) – on manganese dioxide (MnO_2). Transformation batch experiments at pH 6 revealed AMPA and phosphate as main TPs, with a phosphorous mass balance of 80 to 92 % throughout all experiments. Our results suggest initial cleavage of the C–P bond and formation of the stable intermediate *N*-formyl-AMPA. Next, C–N bond cleavage leads to the formation of AMPA, which exhibits lower reactivity than IDMP. Reaction rates together with IDMP and Mn^{2+} sorption data indicate formation of IDMP-Mn^{2+} surface bridging complexes with progressing MnO_2 reduction, leading to the passivation of the mineral surface regarding IDMP oxidation. Compound-specific stable carbon isotope analysis of IDMP in both sorbed and aqueous fractions further supported this hypothesis. Depending on the extent of Mn^{2+} surface concentration the isotope data indicated either sorption of IDMP to the mineral surface or electron transfer from IDMP to Mn^{IV} to be the rate-limiting step of the overall reaction.

Our study shed further light on the complex surface processes during MnO_2 redox reactions and revealed abiotic oxidative transformation of APPs by MnO_2 as a potential process contributing to widespread elevated AMPA concentrations in the environment.

2.2 Introduction

Aminopolyphosphonates (APPs) are increasingly used as chelating agents in a wide range of fields in industrial as well as household applications, such as scaling inhibition in membrane filtration or cooling water systems and bleaching stabilization in bleaching liquors.[1] Since the 1980s, APPs serve as alternatives for polyphosphates and polycarboxylates such as ethylenediaminetetraacetate (EDTA), which are controversially discussed due to adverse environmental effects.[1,2] Such concerns including heavy metal remobilization, complexation of trace nutrients or contribution to eutrophication, however, also exist for APPs.[1,3]

APPs appear to be poorly biodegradable but nevertheless are subject to significant elimination during waste water treatment by sorption to sewage sludge.[1,4,5] Several abiotic transformation processes such as oxidation by H_2O_2 (i), ozonation (ii), photolysis (UV) (iii), oxidation by Mn^{2+}/O_2 (iv) or MnOOH (v)[6–12] are described for APPs leading to (potentially) persistent and (eco-) toxicologically problematic transformation products (TPs) including phosphate (all), aminomethylphosphonate (AMPA) (i, ii, iii) and iminodi(methylene phosphonate) (IDMP) (iii, v).[6–12]

MnO_x minerals are among the strongest naturally occurring oxidants and are widespread in soils and sediments, primarily formed by microbial Mn^{II}-oxidation.[13] They are known to oxidize a broad range of organic substances such as phenols, anilines or different types of antibacterial agents, and are further known as strong sorbents for metals and oxyanions, e.g., phosphates.[13,14] Some of those oxidation reactions have been investigated intensively regarding their mechanism (e.g. for phenols), while others remain just partially understood. In general, oxidation of organic compounds on manganese oxides involves surface complex formation (step 1) followed by electron transfer (step 2) and a subsequent third step such as bond cleavage or polymerization.[10,13,14] However, thorough understanding of interfacial electron transfer processes is challenging due to a lack of suitable methods and techniques.[22] Hence, for many compounds the rate-limiting steps are not identified, yet.

Regarding APP transformation in natural environments, oxidation on MnO_x is considered a relevant pathway.[10,11] Nowack & Stone[11] investigated oxidation of the triphosphonate ATMP on MnOOH and identified phosphate and IDMP as major TPs. Because the sorbed phase has not

been investigated, factors such as the relevance of sorption/desorption or further rate-determining steps remain unknown.[13–15]

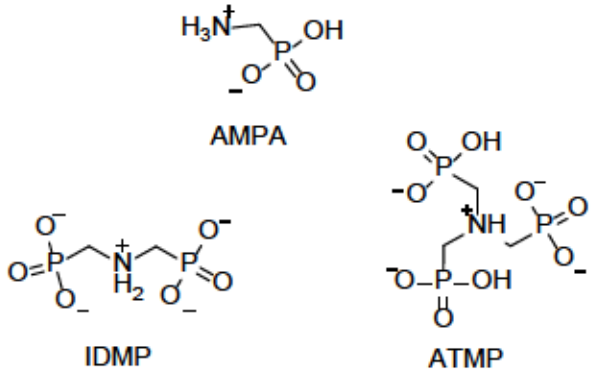

Figure 2.1 Structures of three aminophosphonates: aminotris(methylene phosphonate) (ATMP), iminodi(methylene phosphonate) (IDMP) and aminomethylphosphonate (AMPA) in their dominant species at pH 6. For speciation diagrams see Figure B.1.

In the presented work, we investigated the transformation of IDMP on MnO_2. IDMP was chosen as a model compound for higher APPs as it appears to be a key TP in the heterogeneous transformation of higher aminopolyphosphonates by MnO_x as demonstrated for ATMP[10,11] and contains two phosphonate and one amine moiety (see Figure 2.1). Thus, based on the molecular structure and transformation pathways described for other APPs, IDMP can be considered as a possible precursor of AMPA. However, in contrast to AMPA or glyphosate[15–18], transformation of IDMP in solution by Mn^{2+}/O_2 or at Mn (hydr)oxide minerals has not been reported yet. To shed light on the heterogenous transformation mechanism we monitored the transformation of IDMP and quantified IDMP and its main TPs in the aqueous as well as in the sorbed phase.

In addition to concentration analyses we conducted compound-specific stable carbon isotope analysis (carbon CSIA) as a complementary technique to gain insights into the reaction mechanism of IDMP oxidation on MnO_2.[19,20] Carbon CSIA of the sorbed analyte in a heterogenous oxidation reaction has been performed for the first time. In general, the cleavage of a carbon bond can lead to an enrichment of ^{13}C in the remaining substrate fraction (normal kinetic isotope effect, KIE).[19] The extent of isotopic fractionation depends on the discrimination of ^{13}C and ^{12}C in the bond cleavage step. However, isotope fractionation can also be masked if a step preceding bond cleavage, such as sorption, is rate limiting or irreversible. Therefore, CISA can provide information about the rate determining step (RDS) within a multistep reaction. A graphical depiction of the kinetic isotope effect during C bond cleavage reactions can be found in the SI (Figure B.2). For

detailed explanations of the isotope concept, we refer to Elsner[19], Aelion *et al.*[21] and Jochmann & Schmidt[20].

To evaluate the role of MnO_x minerals as potential sinks for IDMP and the related reaction mechanism and transformation products, we investigated the transformation of IDMP on such minerals in kinetic batch experiments at pH 6. We applied ion chromatography coupled to electrochemical detection (IC-ECD) to quantify IDMP as well as AMPA and UV/vis spectrometry (molybdenum blue method[22]) to quantify phosphate. Carbon CSIA of the remaining fraction of IDMP using liquid chromatography isotope ratio mass spectrometry (LC-IRMS) was applied to further elucidate the multistep transformation reaction at the mineral-water interphase.

2.3 Materials and Methods

Chemicals

If not described differently, chemicals have been purchased from Merck (Darmstadt, Germany) in the highest available purity (inorganic acids and bases in the respective commercial solute concentrations). Sodium acetate (≥99.5 %) was bought from Chemsolute (Renningen, Germany), MES buffer (≥99 %) at Carl Roth (Karlsruhe, Germany), while IDMP (97 %) has been purchased from Sigma Aldrich (Burlington (MA), USA).

The commercial MnO_2 ($MnO_{2/com}$) (Manganese^{IV}-oxide, ≥98 %) was purchased from Carl Roth, while synthetic MnO_2 ($MnO_{2/syn}$) was synthesized via the approach published by Villegas *et al.*[23] (see SI).

Design of transformation experiments

Each experimental setup contained an IDMP starting concentration of 1 mM and 20 mM MES buffer. The pH was adjusted to 6 using 1 M NaOH. Usage of MES buffer had no impact on sorption and transformation of IDMP (Figure B.3). To start the reaction, varying amounts of MnO_2 ($MnO_{2/com}$ or $MnO_{2/syn}$) were added to the reaction vessel. 0.3 to 6.0 g/L, resulting in molecular MnO_2:IDMP ratios from 8:1 to 46:1 and in surface area concentrations from 97.8 to 717.2 m^2/L.

The experiments were conducted in 50 mL PP centrifugation tubes placed in an overhead shaker, running at 26 rpm at room temperature (21 ± 1 °C). All experiments were prepared in duplicates.

At defined time points derived from pilot tests, a well suspended 4 mL aliquot of the suspension was taken, centrifuged (15 min, 20 000 rcf) and filtered (0.2 µM PES syringe filter, BGB Analytik, Lörrach, Germany). The reagents were desorbed from residue adapted from Paudel *et al.*[15], shaking the residues in 0.1 M NaOH for minimum 12 h. Subsequently, IDMP, AMPA and phosphate were quantified in the aqueous and sorbed phase, separately, while manganese was quantified solely in the aqueous phase. Samples were stored in the dark at 4 °C until analysis.

Concentration analysis of IDMP and its transformation products

IDMP and AMPA were quantified using a 930 Compact IC Flex ion chromatograph equipped with a high-capacity anion-exchange column (Metrosep Carb 2, 100x4.0 mm) and an electrochemical detector (all Metrohm, Herisau, Switzerland). The method included a flow gradient using 345 mM sodium acetate and 15 mM NaOH as eluent and the detector running in pulsed amperometric detection (PAD) mode (see Table S1). An exemplary chromatogram can be found in the SI (Figure B.4). *Ortho*-phosphate was quantified photometrically following the molybdenum blue method after Murphy and Riley[22] measuring the complex at λ = 710 nm in a concentration range between 0.2 and 10 mg/L PO_4^{3-}. Aqueous manganese was quantified by microwave-plasma atomic emission spectroscopy (MP-AES) using the measurement wavelength 403.307 nm (for further information, see SI).

Compound-specific stable carbon isotope analysis of IDMP

Stable carbon isotope ratios of IDMP were analyzed using liquid chromatography coupled to isotope ratio mass spectrometry (LC-IRMS), similar to Martin *et al.*[9]. The limit of precise isotope analysis was determined to be 50 µM IDMP (see Figure B.5).

Investigation of further TPs was conducted using LC-IRMS hyphenated to a high-resolution mass spectrometer (LC-IRMS-HRMS) after Marks *et al.*[24]. All instruments and measurement conditions for LC-IRMS and LC-IRMS-HRMS can be found in the SI.

Calculations

Isotope enrichment factors ε were determined by linearizing the isotope data using the double logarithmic Rayleigh distillation equation[19]:

$$\ln\left(\frac{R_t}{R_0}\right) = \ln\left(\frac{\delta^{13}C_t + 1}{\delta^{13}C_0 + 1}\right) = \varepsilon_C \ln\left(\frac{c_t}{c_0}\right) = \varepsilon_C \ln(f)$$

R_t stands for the isotope ratio ($^{13}C/^{12}C$) at timepoint t, which is then normalized to timepoint zero. The relative concentration c_t/c_0 is defined as the fraction *f* of the compound of interest still present compared to timepoint zero. $\delta^{13}C$ values have not been normalized to an international reference standard, as not the absolute values but the relative enrichment is of interest.

2.4 Results and Discussion

The transformation of IDMP on two types of MnO_2 at pH 6 was investigated in ten laboratory batch experiments. To resemble conditions found in natural waters, experiments were conducted at an environmentally relevant pH value of 6 using MES buffer, which did not interfere with sorption or transformation of IDMP and the applied analytical methods, (for details see SI, Figure B.3). Among the wide range of known Mn oxide minerals, we selected two specimen that are of environmentally relevance and cover a range of decisive surface properties. The chosen MnO_2 minerals ($MnO_{2/com}$, $MnO_{2/syn}$) were similar concerning Mn^{III} content (see SI) and impurities of other cations (see SI). Furthermore, they showed an amorphous structure (see Figure B.6 for XRD diffractograms) and therefore provide good model minerals for naturally occurring MnO_x which are often of low crystallinity[25]. On the other hand, the two used minerals differed significantly regarding their specific surface area ($MnO_{2/com}$: 64.5 ± 0.2 m^2/g, $MnO_{2/syn}$: 326 ± 1 m^2/g) and their point of zero charge (pH_{PZC}, $MnO_{2/com}$: 5.6 ± 0.1, $MnO_{2/syn}$: 2.3 ± 0.1), – two parameters substantially defining their reactivity towards organic pollutants[13]. Thus, the two minerals allowed us to correlate observed certain reactivity characteristics to specific mineral properties (i.e., pH_{PZC} and SSA) while ruling out potential effects of other mineral properties e.g. Mn^{III} content or impurities, which allowed us to investigate the significance of the latter properties regarding their relevance on the minerals' reactivity.

To obtain insights into the reaction progress and mechanism, IDMP and its two main TPs AMPA and PO_4^{3-} were analyzed in aqueous solution and on the mineral surface (sorbed phase). Dissolved Mn^{2+} formed during the reduction of Mn^{IV} minerals[12,36–38] was also quantified but cannot be used as parameter to monitor the progress of IDMP transformation due to significant sorption of Mn^{2+} to the mineral surface [39–41].

Concentration profiles of IDMP and its transformation products in the aqueous and mineral phase

In a typical experiment containing 1 mM IDMP and 1.7 g/L $MnO_{2/com}$ (ratio 1:20) IDMP was almost completely transformed within 460 hours, with a decreasing transformation rate over the course of the reaction (see Figure 2.2a). Simultaneously, total AMPA and phosphate concentrations continuously increased. The calculated phosphorous mass balance (P MB) including IDMP, AMPA and PO_4^{3-} (aqueous and sorbed phase) ranging between 83 and 100 % throughout the whole experiment, pinpoints AMPA and phosphate as the main TPs but also suggest the formation of minor amounts of other phosphorous containing TPs. In samples of one selected experiment (unbuffered, 1.7 g/L $MnO_{2/com}$), *N*-formyl-AMPA (F-AMPA) was identified and quantified via high-resolution mass spectrometry (HRMS) [24] (m/z $[M+H^+]$ 140.01029, Figure B.8 and B.9). The concentration of F-AMPA increased up to 76 µM after 360 h (88 % $IDMP_{transf.}$), accounting for 8 % of the total P MB. Despite this significant contribution of F-AMPA, the P MB is not entirely closed, suggesting minor formation of further P-containing TPs, such as hydroxymethylphosphonate (HMP) (see Figure B.9 and B.10). Furthermore, the concentration of $PO_4^{3-}{}_{tot}$ always exceeded the total AMPA concentration. While PO_4^{3-} is formed stoichiometrically (one PO_4^{3-} for one degraded IDMP molecule), AMPA is formed sub-stoichiometrically, reaching approximately 70 % of the amount of transformed IDMP at the end of the reaction. Observation beyond the point of complete IDMP transformation revealed subsequent AMPA transformation and further PO_4^{3-} formation, albeit at a much slower rate than IDMP transformation (Figure B.11).

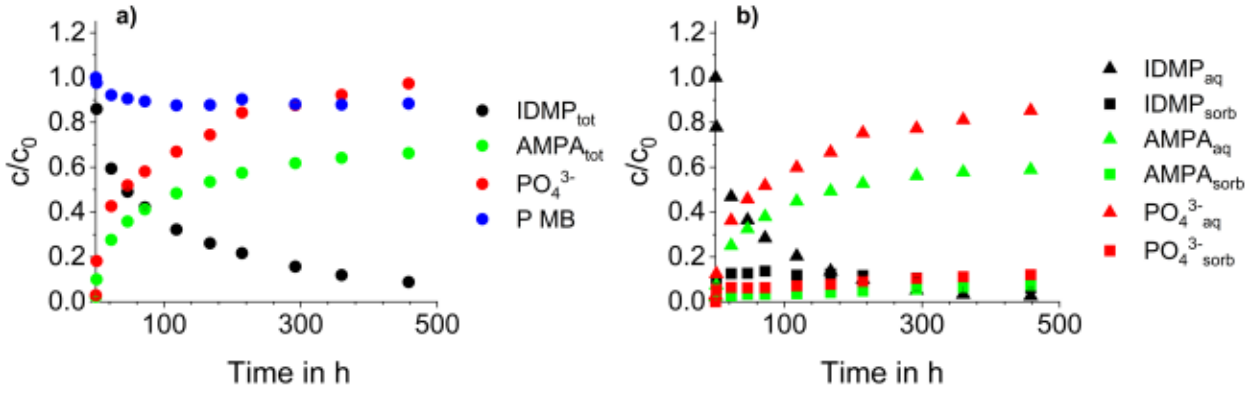

Figure 2.2 Full data set of one IDMP transformation experiment (1 mM IDMP, 1.7 g/L $MnO_{2/com}$, pH 6, 20 mM MES); **a)** display of total concentrations (aqueous + sorbed phase) of IDMP, AMPA, phosphate and the phosphorous mass balance (P MB); **b)** separate display of aqueous and sorbed phase of IDMP, AMPA and phosphate. Error bars (smaller than data points if not visible) display absolute error of duplicates.

The separate analysis of sorbed and aqueous phase revealed the major fraction of IDMP, AMPA and PO_4^{3-} to be present in the aqueous solution (Figure 2.2b). Interestingly, while the aqueous IDMP ($IDMP_{aq}$) concentration continuously decreased within the timeframe of the experiment (460 hours) the sorbed concentration of IDMP ($IDMP_{sorb}$) remained almost constant for 200 hours ($c_{sorb}/c_0 = 0.12 \pm 0.01$). The $IDMP_{sorb}$ concentration started to decrease when $IDMP_{aq}$ and $IDMP_{sorb}$ equalized followed by a simultaneously decrease of the two phases in the further course of the experiment. This quasi-steady state concentration of IDMP on the mineral ($IDMP_{sorb,max}$) was observed in all experiments. For PO_4^{3-} and AMPA, aqueous and – to a lesser extent – sorbed concentrations continuously increased. In contrast to IDMP, no quasi-steady state concentrations were observed for the two TPs. Further, also the sorbed PO_4^{3-} concentration always exceeded the respective AMPA concentrations.

While IDMP transformation to AMPA and phosphate was observed in all experiments, varying TP stoichiometries were calculated for varying mineral types and concentrations.

Dependency of TP formation on MnO_2 type and amount

Batch experiments with the two different MnO_2 mineral preparations were conducted with different mineral concentrations and subsequently different mineral surface areas. Accordingly, a typical experiment containing 218 m^2/L mineral surface area is equivalent to 0.67 g/L of $MnO_{2/syn}$ or 3.4 g/L of $MnO_{2/com}$ due to the different specific surface areas of the two minerals.

In all ten conducted experiments the ratio of formed PO_4^{3-} to transformed IDMP was almost stoichiometric (86 to 106%), while the ratio of formed AMPA to transformed IDMP was always sub-stoichiometric (62 to 87%) (Table 2.1). This observation indicates a stable intermediate forming on the way from IDMP to AMPA, which likely is F-AMPA as shown in the experiment without buffer. These findings imply that the proposed reaction mechanism by Nowack & Stone[10] for ATMP transformation at MnOOH with initial C–P and subsequent C–N bond cleavage including the intermediate *N*-formyl-IDMP is also applicable for IDMP oxidation on manganese dioxide, leading to F-AMPA formation. This is in accordance with the formation of F-IDMP and F-AMPA during ATMP transformation by UV light and OH radicals as recently described by Marks *et al.*[12].

Table 2.1 Molar ratios of the TPs formed ($PO_4^{3-}_{form}$ and $AMPA_{form}$) vs. transformed IDMP ($IDMP_{transf}$) together with the phosphorous mass balance (P MB) in the ten IDMP transformation experiments conducted. Displayed are the ratios at time points with maximum transformation of IDMP ($IDMP_{transf.}$) and negligible observable AMPA degradation. Errors represent absolute errors between duplicates.

Experiment	$PO_4^{3-}_{form.}$:$IDMP_{transf.}$ in %	$AMPA_{form.}$:$IDMP_{transf.}$ in %	P MB in %	$IDMP_{transf.}$ in %
6.0 g/L $MnO_{2/com}$	94 ± 2	62 ± 1	80 ± 1	93 ± 1
4.0 g/L $MnO_{2/com}$	86 ± 2	67 ± 2	83 ± 1	75 ± 2
3.4 g/L $MnO_{2/com}$	104 ± 3	72 ± 1	89 ± 3	93 ± 4
2.5 g/L $MnO_{2/com}$	93 ± 0	66 ± 3	83 ± 0	88 ± 0
1.7 g/L $MnO_{2/com}$	104 ± 1	70 ± 1	88 ± 2	91 ± 1
2.2 g/L $MnO_{2/syn}$	90 ± 5	67 ± 2	80 ± 4	96 ± 3
1.7 g/L $MnO_{2/syn}$	105 ± 3	71 ± 1	87 ± 2	96 ± 0
1.0 g/L $MnO_{2/syn}$	92 ± 2	78 ± 2	86 ± 2	96 ± 2
0.67 g/L $MnO_{2/syn}$	96 ± 1	87 ± 1	92 ± 2	99 ± 1
0.3 g/L $MnO_{2/syn}$	94 ± 1	88 ± 2	92 ± 1	65 ± 0

For $MnO_{2/syn}$, the ratio of formed AMPA to transformed IDMP steadily decreased with increasing MnO_2 concentration, while $PO_4^{3-}_{form.}$:$IDMP_{transf.}$ remained stoichiometric. This dependency of the $AMPA_{form.}$:$IDMP_{transf.}$ ratio on the available $MnO_{2/syn}$ surface reflects an accumulation of transient products and possibly varying reaction paths after the initial C–P bond cleavage, see below.

IDMP transformation kinetics

To evaluate experiments with different mineral surface areas regarding their IDMP reaction rates, we calculated zero-order reaction rates k_x (with x = type of mineral; initial MnO_2 concentration in

g/L) for $IDMP_{tot}$ in the quasi-steady state range (see Figure B.12). Table 2.2 compiles such rate constants normalized to the surface concentration of the minerals ($k_{x,norm}$).

For both minerals, $k_{x,norm}$ values increased disproportionately more than the provided mineral surface area. For example, for a surface area of 109.7 m^2/L (1.7 g/L $MnO_{2/com}$) the zero-order reaction rate was calculated to be $k_{com,1.7}$ = 1.4 µM/h, while doubling the surface area (219.3 m^2/L; 3.4 g/L $MnO_{2/com}$) lead to $k_{com,3.4}$ = 5.3 µM/h, i.e., a 3.8-fold increase of the reaction rate. For the synthetic $MnO_{2/syn}$, the zero-order reaction rate was $k_{syn,0.67}$ = 4.0 µM/h at 218.4 m^2/L (0.67 g/L). For this mineral. However, an increase of the surface area by factor 2.5 (554.2 m^2;1.7 g/L $MnO_{2/syn}$) lead to an 18.8-fold increase of the reaction rate ($k_{syn,1.7}$ = 75.1 µM/h). In summary, the kinetic data revealed i) higher concentrations of the same mineral lead to faster transformation kinetics, ii) the increase in reaction rate differs for the two investigated minerals ($MnO_{2/syn}$ > $MnO_{2/com}$) and iii) an increase in the surface area normalized zero-order reaction rate, indicating that another parameter governs the transformation of IDMP at the mineral surface. To elucidate how a mere concentration change can have such effects on the reaction kinetics, different parameters will be correlated in the following sections.

Table 2.2 Maximum sorbed concentrations of IDMP in µmol/L (to compare with the aqueous fraction), zero-order reaction rates (k_x), zero-order reaction rates normalized to the MnO_2 surface concentration in m^2/L ($k_{x,norm}$) and sorbed concentrations of Mn^{2+}, calculated based on measured Mn_{aq} and the respective sorption isotherm. Errors for $c(IDMP)_{sorb,max}$ and Mn^{2+}_{sorb} represent the absolute deviations between duplicates. Zero order reaction rates were calculated for $c(IDMP)_{tot}$ in the quasi-steady-state area; errors of k_x represent standard errors of the linear fitting.

Experiment	$IDMP_{sorb,max}$ in µM	k_x (0^{th} order) in µM/h	$k_{x,norm}$ (0^{th} order) in nmol/(m^2 h)	Mn^{2+}_{sorb} in µmol/m^2
6.0 g/L $MnO_{2/com}$	278 ± 2	38 ± 13	53.7 ± 7.8	2.75 ± 0.23
4.0 g/L $MnO_{2/com}$	228 ± 3	9.2 ± 1.0	35.6 ± 3.9	2.92 ± 0.90
3.4 g/L $MnO_{2/com}$	218 ± 2	5.3 ± 0.8	24.4 ± 3.8	4.55 ± 0.91
2.5 g/L $MnO_{2/com}$	163 ± 16	5.5 ± 1.2	34.1 ± 7.2	4.35 ± 0.23
1.7 g/L $MnO_{2/com}$	131 ± 2	1.4 ± 0.2	12.3 ± 1.8	4.98 ± 0.65
2.2 g/L $MnO_{2/syn}$	70 ± 4	107.4 ± 26.3	149.8 ± 36.7	1.68 ± 0.28
1.7 g/L $MnO_{2/syn}$	71 ± 3	75.1 ± 8.3	135.5 ± 15.0	1.88 ± 0.22
1.0 g/L $MnO_{2/syn}$	110 ± 10	12.9 ± 2.4	39.6 ± 7.3	4.12 ± 0.85
0.67 g/L $MnO_{2/syn}$	153 ± 3	4.0 ± 0.9	18.3 ± 4.3	5.84 ± 0.68
0.3 g/L $MnO_{2/syn}$	85 ± 2	5.0 ± 1.1	51 ± 11	4.47 ± 0.58

Effect of mineral surface properties on IDMP sorption & reaction rate

Generally, it can be assumed that the amount of IDMP sorbed to the mineral surface and consequently the reaction rate increases with increasing mineral loading due to an increase of available surface sites. To verify this hypothesis, we correlated the zero-order reaction rates normalized to the surface concentration ($k_{x,norm}$) with the quasi-steady state concentrations of sorbed IDMP ($IDMP_{sorb,max}$ in µmol/L) (Table 2.2). For $MnO_{2/com}$, the behavior followed the general assumption and $IDMP_{sorb,max}$ correlated positively with the mineral surface: In the experiment with 109.7 m^2/L surface area (1.7 g/L $MnO_{2/com}$) the $IDMP_{sorb,max}$ was observed at 131 ± 2 µM, whereas for a surface area of 258 m^2/L (4.0 g/L $MnO_{2/com}$) an $IDMP_{sorb,max}$ concentration of 228 ± 3 µM was determined.

In the system containing $MnO_{2/syn}$, however, an opposite trend was observed. While an increase in the provided surface area resulted in higher reaction rates, the sorbed concentration of IDMP decreased. For example, for 218.4 m^2/L (0.67 g/L $MnO_{2/syn}$) and 717.2 m^2/L (2.2 g/L $MnO_{2/syn}$) the normalized zero-order rate constant increased by factor eight. In contrast, the maximum sorbed IDMP concentration was 153 ± 3 µM (0.67 g/L $MnO_{2/syn}$) whereas only 70 ± 4 µM IDMP sorbed to 2.2 g/L $MnO_{2/syn}$. Thus, the increase in reaction rate cannot be explained by a higher sorption capacity for IDMP.

Comparing the sorption of IDMP on the two minerals, it is noticeable that the surface area of $MnO_{2/syn}$ is six times higher than the surface area of $MnO_{2/com}$, but still, $MnO_{2/syn}$ experiments show lower $IDMP_{sorb,max}$ values than $MnO_{2/com}$ experiments. Even though 3.4 g/L $MnO_{2/com}$ and 0.67 g/L $MnO_{2/syn}$ exhibit the same surface area, the sorbed IDMP concentrations differ by 43 % (228 ± 3 $MnO_{2/com}$ vs 153 ± 3 µM $MnO_{2/syn}$). This observation can be explained by the more negatively charged surface of $MnO_{2/syn}$ compared to $MnO_{2/com}$ due to its lower pH_{PZC} (2.3 vs 5.6). This leads to a higher affinity of $MnO_{2/com}$ for negatively charged IDMP molecules at pH 6. Accordingly, the calculated zero-order rate constant $k_{x,norm}$ is 33 % higher for 3.4 g/L $MnO_{2/com}$ compared to 0.67 g/L $MnO_{2/syn}$.

Another driving factor appeared to be bivalent manganese (Mn^{2+}), which is formed during the reaction and can sorb to the mineral surface to a certain extent.[13] As the breakdown of IDMP on $Mn^{IV}O_2$ to PO_4^{3-} (C–P) and AMPA (C–N bond cleavage) is associated with the transfer of two electrons[11,26], the formation of one Mn^{2+} for one oxidized IDMP molecule can be assumed. The sorbed Mn^{2+}-concentration was calculated based on sorption isotherms for Mn^{2+} on the two different minerals (Figure B.13) using the measured concentrations for aqueous Mn^{2+}.

Normalizing this sorbed Mn^{2+}-concentration to the surface area of the suspended minerals results in the Mn^{2+} concentrations per m^2 (Mn^{2+}_{sorb}/m^2) shown in Table 2.2.

Mn^{2+}_{sorb}/m^2 and the zero-order reaction rates $k_{x,norm}$ were inversely related, i.e., an increase in $k_{x,norm}$ correlated with a decrease in Mn^{2+}_{sorb}/m^2. This indicates a higher reactivity of the Mn^{2+}-free mineral, i.e, a passivation of the mineral surface by adsorption of Mn^{2+} from the aqueous phase. This is in line with previous studies, where sorption of Mn^{2+}_{aq} to MnO_2 surfaces resulted in a decreased oxidation potential towards organic reductants.[27,28] This was assigned to i) blocking of active surface sites by Mn^{2+} on the mineral or ii) reaction of Mn^{II} with Mn^{IV} and therefore competition for reactive surface sites and/or a decrease of the average oxidation state of Mn in the MnO_2. [13,27–30] To further investigate this phenomenon, a control experiment (4.0 g/L $MnO_{2/com}$) containing a Mn^{2+} (added as $MnCl_2$) starting concentration of 1 mM was conducted. In line with the results discussed earlier, a decrease in the reaction rate from 35.6 ± 3.9 nmol/(m^2 h) to 13.9 ± 2.0 nmol/(m^2 h) (with initial Mn^{2+}) along with an increase in $IDMP_{sorb,max}$ from 228 ± 3 µM to 478 ± 45 µM (with initial Mn^{2+}) was observed. (A graphical display of Mn^{2+}_{sorb}/m^2 vs zero-order rate constant and $IDMP_{sorb,max}$ can be found in Figure B.14.)

The increase in $IDMP_{sorb,max}$ with increasing Mn^{2+}_{sorb}/m^2 and decreasing $k_{x,norm}$ was observed for all $MnO_{2/syn}$ experiments (except 0.3 g/L). It seems plausible that the sorption of Mn^{2+}_{aq} shifts the surface charge of the mineral to more positive values and therefore increases the sorption affinity for the negatively charged IDMP. Martinez *et al.*[31] described Ca^{2+} to act as a bridge-cation between FeOOH and ATMP. Even though Ca^{2+} differs from Mn^{2+} with respect to e.g., ionic radius and charge density, it is conceivable that also Mn^{2+} serves as a bridge-cation between MnO_2 and IDMP, as Mn^{2+} was shown to form inner-sphere complexes with birnessite[32]. Additionally, we found a strong positive correlation between sorbed Mn^{2+} and IDMP sorption-capacity in experiments where we loaded the mineral with different amounts of Mn^{2+} prior to IDMP addition (see Figure B.15). The formation of such ternary IDMP-Mn^{2+}-surface complexes, however, is consistent with both, enhanced IDMP sorption and hinderance of electron transfer from IDMP to Mn^{IV} centers of the mineral.

Summarizing, the synthetic $MnO_{2/syn}$ showed a disproportionate increase in reaction rate with the surface area provided, respectively a decreasing Mn^{2+}_{sorb}/m^2, and showed a considerably different relationship concerning $IDMP_{sorb,max}$ and reaction rate compared to $MnO_{2/com}$. Those differences between the two minerals can partly be explained by the difference in pH_{PZC}. Due to its higher pH_{PZC}, $MnO_{2/com}$ is less negatively charged at pH 6 and probably possesses a higher IDMP sorption affinity than $MnO_{2/syn}$. At the same time, the higher pH_{PZC} leads to a lower Mn^{2+} sorption

affinity, compared to $MnO_{2/syn}$. If Mn^{2+} is now formed during the reaction, the stronger sorption to the $MnO_{2/syn}$ mineral surface causes a more positive charge – which i) eases IDMP sorption but also ii) passivates the surface over the course of the reaction. This explains why the observed effect is more pronounced for $MnO_{2/syn}$ than for $MnO_{2/com}$. On the other hand, Mn^{2+}_{sorb}/m^2 data reveal similar values for the two minerals exhibiting the same surface concentrations. Thus, other mineral characteristics like morphology and crystallography might also contribute to the observed differences in mineral reactivity.[13] To further elucidate the role of surface sites reactivities and rate-limiting step in this multi-step reaction, carbon CSIA of IDMP has been applied as a complementary technique.

Carbon isotope analysis of sorbed and dissolved IDMP reveals rate-limiting steps

In general, oxidation of organic compounds on manganese oxides involves surface complex formation (step 1) followed by electron transfer (step 2) and subsequent bond cleavage (step 3).[10,26,33] To further investigate the rate determining steps for the oxidation of IDMP at MnO_2, we analyzed ^{13}C-enrichment of IDMP in the aqueous ($\delta^{13}C_{aq}$) as well as in the sorbed ($\delta^{13}C_{sorb}$) phase, separately (Figure 2.3).

For the oxidation of IDMP on MnO_2 surfaces it is reasonable to assume that only the bond cleavage (step 3) is associated with a (significant) carbon isotope fractionation, as no carbon atom is involved in surface complex formation or electron transfer. This assumption is supported by insignificant isotope fractionation of IDMP observed in sorption experiments with the redox inert mineral Al_2O_3 (ε_C < -1.0 ‰, Figure B.16). Therefore, the two following scenarios can be resolved based on the isotopic composition of IDMP in the aqueous and solid phase. (I) Electron transfer is rate-limiting: In this case comparable $\delta^{13}C_{sorb}$ and $\delta^{13}C_{aq}$ values are expected, as fast (de-)sorption kinetics quickly establish an equilibrium between sorbed and aqueous IDMP and hence the isotopic imprint of IDMP transformed at the mineral surface is visible in the aqueous phase. (II) (De-)sorption is rate-limiting: In this case a pronounced deviation of $\delta^{13}C_{sorb}$ and $\delta^{13}C_{aq}$ values is expected, as the electron transfer is faster compared to desorption, preventing the establishment of an equilibrium between the aqueous and sorbed IDMP pools. Here, a pronounced ^{13}C enrichment in the sorbed phase is expected. A graphical depiction of those two scenarios is provided in the SI (Figure B.17).

For the three concentrations of $MnO_{2/com}$, similar $\delta^{13}C$ values and subsequently isotope enrichment in the aqueous and the sorbed phase were observed (see Figure 2.3 a). The

enrichment factors for all three $MnO_{2/com}$ experiments ranged between -5.7 ± 0.6 and -6.6 ± 0.6 ‰ for the aqueous ($\varepsilon_{C,aq}$) and between -5.1 ± 0.7 and -5.6 ± 0.6 ‰ for the sorbed phases ($\varepsilon_{C,sorb}$, see Table S2). Thus, isotope analysis revealed (de-)sorption to be faster than e^- transfer for the experiments conducted with the commercial MnO_2 meeting scenario I.

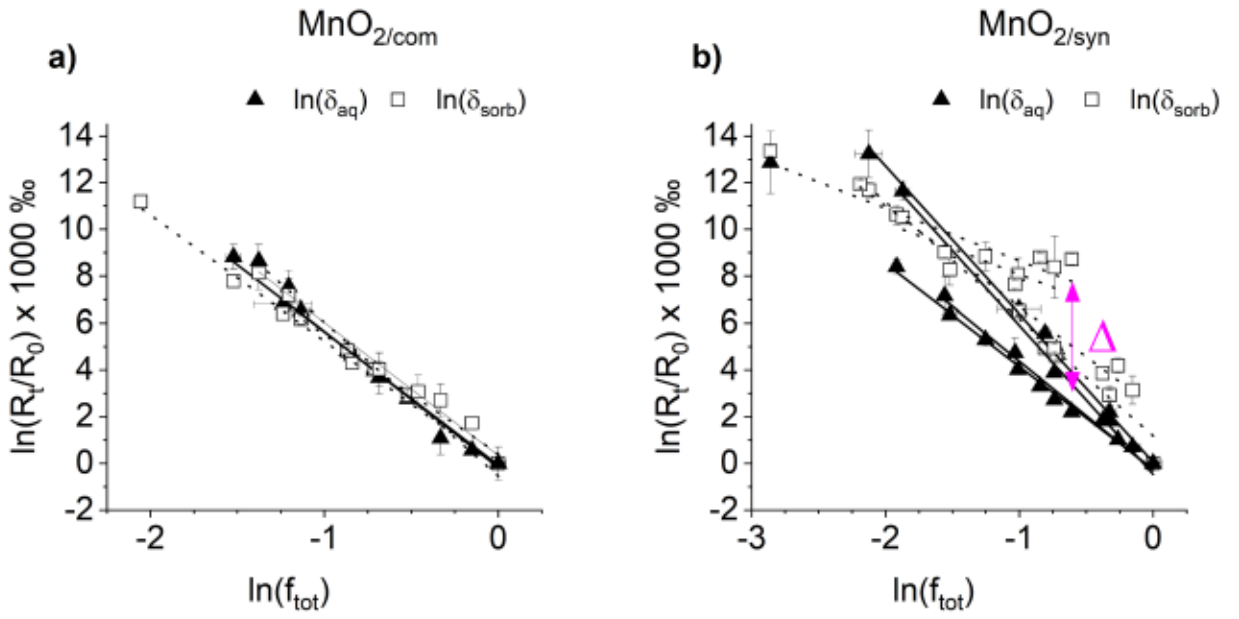

Figure 2.3 Double logarithmic Rayleigh plots of aqueous and sorbed IDMP phases of seven IDMP transformation experiments: **a)** $MnO_{2/com}$ in concentrations of 1.7, 3.4 and 4.0 g/L, **b)** $MnO_{2/syn}$ in concentrations of 0.67, 1.0, 1.7 and 2.2 g/L (a more detailed graphic can be found in Figure B.18). The δ-values are plotted versus the total remaining fraction of IDMP ($m_{tot} = m_{aq} + m_{sorb}$). Linear regressions are indicated by solid (aq) and dashed (sorb) lines, respectively. Errors of the normalized isotopic composition represent the standard deviations of all six isotopic measurements (triplicate analyses of duplicate experiments), while errors of the fraction represent the errors of IDMP quantification between duplicates. The pink delta indicates the deviation between aqueous and sorbed phase.

For the experiment containing 0.67 g/L synthetic $MnO_{2/syn}$, $\delta^{13}C$-values of IDMP in aqueous and sorbed phase were still comparable ($\varepsilon_{C,sorb}(0.67)$ = -5.0 ± 0.4 ‰ and $\varepsilon_{C,aq}(0.67)$ = -6.3 ± 0.4 ‰). With increasing $MnO_{2/syn}$ concentrations, however, the $\delta^{13}C$ values of IDMP in the sorbed phase significantly exceeded those in the aqueous phase, implying that ^{13}C enrichment in the sorbed phase was much stronger. At 1.0 g/L $MnO_{2/syn}$ the maximum difference between ^{13}C enrichment in the aqueous and the sorbed phase ($\Delta\delta^{13}C_{max}$) was 3.4 ± 0.4 ‰, while at 2.0 g/L $MnO_{2/syn}$ $\Delta\delta^{13}C_{max}$ further increased to 6.5 ± 0.3 ‰ (Figure 2.3b). The isotope data therefore indicates that increasing $MnO_{2/syn}$ surface areas lead to a shift of the rate-limiting step from electron transfer (step 2) to surface complex formation (step 1). Therefore, the $MnO_{2/syn}$ gradual shifts from scenario I (electron transfer is rate limiting) to scenario II and subsequently (de-)sorption becomes rate limiting.

While $\delta^{13}C_{sorb}$ and $\delta^{13}C_{aq}$ values differ particularly at the start of the transformation reaction ($\Delta\delta^{13}C_{max}$), they converge over the course of the reaction. Thus, isotope enrichment factors of IDMP in the sorbed fraction were much higher than those in the aqueous fraction (see Table S2).

Furthermore, for the $MnO_{2/syn}$ experiments the isotope data is in line with the quasi-steady state sorbed IDMP concentrations, normalized zero-order rate constants and sorbed Mn^{2+}. The more the IDMP $\delta^{13}C$-values of sorbed and aqueous phase diverge (the higher $\Delta\delta^{13}C_{max}$), the lower $IDMP_{sorb,max}$, but the higher $Mn^{2+}{}_{sorb}/m^2$ and $k_{x,norm}$. Therefore, the isotope data supports the hypothesis of MnO_2 passivation (self-poisoning) by sorption of Mn^{2+}. Free (Mn^{IV}) surface sites not occupied by Mn^{2+} sorb IDMP and are highly reactive, resulting in a fast e^- transfer compared to desorption. Attachment of Mn^{2+} to Mn^{IV} surface sites, however, increases IDMP sorption but e^- transfer from IDMP to Mn^{IV} is hindered. Due to the fast conversion of IDMP on free Mn^{IV} sites and comparably slow desorption, higher ^{13}C enrichment is observed in the sorbed IDMP phase compared to the aqueous phase. Those findings further strengthen the hypothesis of the ternary bridging complex scenario. Figure 2.4 illustrates the interplay of sorption, surface speciation and reactivity of the MnO_2 mineral-water interphase. The overall picture of progressive passivation of the MnO_2 surface by sorbed Mn^{2+} along with decreasing IDMP transformation rates is also reflected and thus supported by the convergence of $\delta^{13}C_{sorb}$ and $\delta^{13}C_{aq}$ over the course of the reaction (see Figure 2.3).

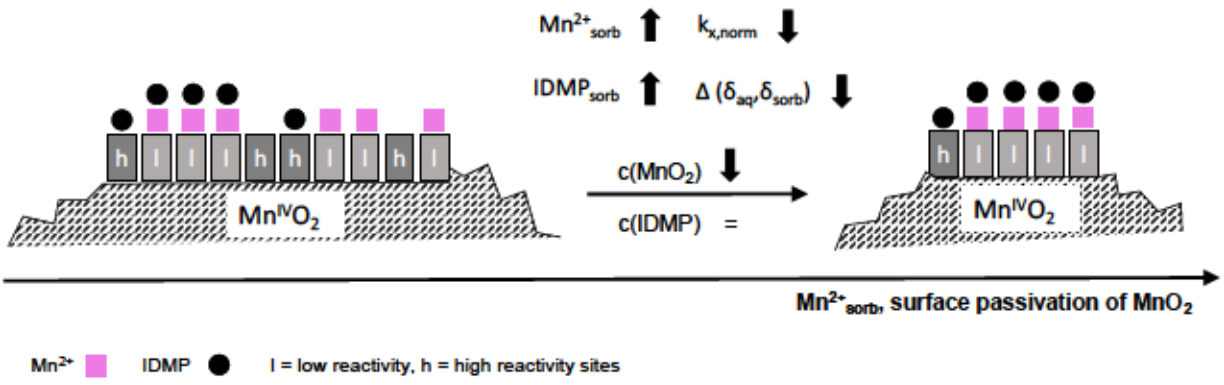

Figure 2.4 Schematic depiction of the effects of decreasing mineral concentration on i) Mn2+ loading of the mineral and therefore ii) IDMP sorption onto high (h) and low (l) reactivity sites, iii) transformation kinetics and the difference in δ13C values of IDMP in the sorbed vs the aqueous phase

2.5 Environmental Implications

Our work demonstrates that IDMP, a major transformation product of widely applied aminopolyphosphonates, can rapidly be oxidized by manganese oxide minerals with AMPA as major organic transformation product. AMPA – also known as a key metabolite of glyphosate[34] – is regarded as environmentally persistent, enriches in soils, and raises eco(toxico)logical concerns.[35–39]

Considering the high-volume production and emission of aminopolyphosphonates in Europe and elsewhere[1,5], conversion of only a small fraction to AMPA by manganese minerals would result in a significant amount of AMPA formed as transformation product. Thus, we describe here an alternative process and source of AMPA potentially contributing to its widespread occurrence in the environment. The heterogenous transformation of aminopolyphosphonates at MnO_x minerals potentially occurs in soils and sediments under dynamic redox conditions, where Mn^{III} and Mn^{IV} oxides are primarily formed by microbial activity.[13] As biogenic MnO_x are regarded to be even more reactive than abiotically synthesized MnO_x[13], they bear an even higher potential for rapid APP transformation than the synthetic MnO_2 minerals used in this study. Although microbial degradation of higher APPs currently is considered to be insignificant, microbial activity driving environmental conditions towards formation and transformation of Mn-minerals may indirectly contribute to the environmental fate of such compounds.

However, our study also revealed that the formation and adsorption of Mn^{2+} can lead to passivation of the mineral surface. This self-poisoning of manganese dioxides during redox reactions, as well as possible further passivation by other divalent cations such as Ca^{2+} or Zn^{2+} can potentially increase APP sorption but retard or inhibit its oxidation. Therefore, further research is needed to elucidate the role of environmental factors such as co-sorbents controlling APP interaction with and oxidation by MnO_2 minerals.

2.6 References

(1) Rott, E.; Steinmetz, H.; Metzger, J. W. Organophosphonates: A Review on Environmental Relevance, Biodegradability and Removal in Wastewater Treatment Plants. *Science of The Total Environment* **2018**, *615*. https://doi.org/10.1016/j.scitotenv.2017.09.223.

(2) Sillanpää, M. Environmental Fate of EDTA and DTPA; 1997; pp 85–111. https://doi.org/10.1007/978-1-4612-1964-4_3.

(3) Jaworska, J.; Van Genderen-Takken, H.; Hanstveit, A.; Van De Plassche, E.; Feijtel, T. Environmental Risk Assessment of Phosphonates, Used in Domestic Laundry and Cleaning Agents in the Netherlands. *Chemosphere* **2002**, No. 47, 655–665.

(4) Nowack, B. Aminopolyphosphonate Removal during Wastewater Treatment. *Water Res* **2002**, *36*, 4636–4642.

(5) Rott, E.; Happel, O.; Armbruster, D.; Minke, R. Behavior of PBTC, HEDP, and Aminophosphonates in the Process of Wastewater Treatment. *Water (Switzerland)* **2020**, *12* (1). https://doi.org/10.3390/w12010053.

(6) Greenlee, L. F.; Freeman, B. D.; Lawler, D. F. Ozonation of Phosphonate Antiscalants Used for Reverse Osmosis Desalination: Parameter Effects on the Extent of Oxidation. *Chemical Engineering Journal* **2014**, *244*, 505–513. https://doi.org/10.1016/j.cej.2014.02.002.

(7) Lesueur, C.; Pfeffer, M.; Fuerhacker, M. Photodegradation of Phosphonates in Water. *Chemosphere* **2005**, *59* (5). https://doi.org/10.1016/j.chemosphere.2004.10.049.

(8) Klinger, J.; Lang, M.; Sacher, F.; Brauch, H. J.; Maier, D.; Worch, E. Formation of Glyphosate and AMPA during Ozonation of Waters Containing Ethylenediaminetetra(Methylenephosphonic Acid). *Ozone Sci Eng* **1998**, *20* (2), 99–110. https://doi.org/10.1080/01919519808547279.

(9) Martin, P. R.; Buchner, D.; Jochmann, M. A.; Elsner, M.; Haderlein, S. B. Two Pathways Compete in the Mn(II)-Catalyzed Oxidation of Aminotrismethylene Phosphonate (ATMP). *Environ Sci Technol* **2022**, *56* (7), 4091–4100. https://doi.org/10.1021/acs.est.1c06407.

(10) Nowack, B.; Stone, A. T. Homogeneous and Heterogeneous Oxidation of Nitrilotrismethylenephosphonic Acid (NTMP) in the Presence of Manganese(II, III) and

Molecular Oxygen. *Journal of Physical Chemistry B* **2002**, *106* (24), 6227–6233. https://doi.org/10.1021/jp014293+.

(11) Nowack, B.; Stone, A. T. Manganese-Catalyzed Degradation of Phosphonic Acids. *Environ Chem Lett* **2003**, *1* (1), 24–31. https://doi.org/10.1007/s10311-002-0014-3.

(12) Marks, R. G. H.; Drees, F.; Rockel, S.; Kerpen, K.; Jochmann, M. A.; Schmidt, T. C. Mechanistic Investigation of Phosphonate Photolysis in Aqueous Solution by Simultaneous LC-IRMS and HRMS Analysis. *J Photochem Photobiol A Chem* **2023**, *439*, 114582. https://doi.org/10.1016/j.jphotochem.2023.114582.

(13) Remucal, C. K.; Ginder-Vogel, M. A Critical Review of the Reactivity of Manganese Oxides with Organic Contaminants. *Environmental Sciences: Processes and Impacts* **2014**, *16* (6), 1247–1266. https://doi.org/10.1039/c3em00703k.

(14) Islam, M. A.; Morton, D. W.; Johnson, B. B.; Mainali, B.; Angove, M. J. Manganese Oxides and Their Application to Metal Ion and Contaminant Removal from Wastewater. *Journal of Water Process Engineering* **2018**, *26*, 264–280. https://doi.org/10.1016/j.jwpe.2018.10.018.

(15) Paudel, P.; Negusse, A.; Jaisi, D. P. Birnessite-Catalyzed Degradation of Glyphosate: A Mechanistic Study Aided by Kinetics Batch Studies and NMR Spectroscopy. *Soil Science Society of America Journal* **2015**, *79* (3), 815–825. https://doi.org/10.2136/sssaj2014.10.0394.

(16) Li, H.; Joshi, S. R.; Jaisi, D. P. Degradation and Isotope Source Tracking of Glyphosate and Aminomethylphosphonic Acid. *J Agric Food Chem* **2016**, *64* (3), 529–538. https://doi.org/10.1021/acs.jafc.5b04838.

(17) Li, H.; Jaisi, D. P. Competition of Sorption and Degradation Reactions during Glyphosate Degradation by Ferrihydrite/δ-Manganese Oxide Composites. *ACS Earth Space Chem* **2019**, *3* (7), 1362–1370. https://doi.org/10.1021/acsearthspacechem.9b00127.

(18) Barrett, K. A.; McBride, M. B. Oxidative Degradation of Glyphosate and Aminomethylphosphonate by Manganese Oxide. *Environ Sci Technol* **2005**, *39* (23), 9223–9228. https://doi.org/10.1021/es051342d.

(19) Elsner, M. Stable Isotope Fractionation to Investigate Natural Transformation Mechanisms of Organic Contaminants: Principles, Prospects and Limitations. *Journal of Environmental Monitoring* **2010**, *12* (11), 2005–2031. https://doi.org/10.1039/c0em00277a.

(20) Maik A. Jochmann; Torsten C. Schmidt. *Compound-Specific Stable Isotope Analysis*; The Royal Society of Chemistry, 2012.

(21) Aelion, C. M.; Höhener, P. Fundamentals of Environmental Isotopes and Their Use in Biodegradation. In *Environmental Isotopes in Biodegradation and Bioremediation*; CRC Press, Taylor & Francis Group: Boca Raton, FL, USA, 2009; Vol. 1, pp 3–22.

(22) Murphy, J.; Riley, J. P. A Modified Single Solution Method for the Determination of Phosphate in Natural Waters. *Anal Chim Acta* **1962**, *27*, 31–36. https://doi.org/10.1016/S0003-2670(00)88444-5.

(23) Villegas, J. C.; Garces, L. J.; Gomez, S.; Durand, J. P.; Suib, S. L. Particle Size Control of Cryptomelane Nanomaterials by Use of H2O2 in Acidic Conditions. *Chemistry of Materials* **2005**, *17* (7), 1910–1918. https://doi.org/10.1021/cm048391u.

(24) Marks, R. G. H.; Jochmann, M. A.; Brand, W. A.; Schmidt, T. C. How to Couple LC-IRMS with HRMS—A Proof-of-Concept Study. *Anal Chem* **2022**, *94* (6), 2981–2987. https://doi.org/10.1021/acs.analchem.1c05226.

(25) Tebo, B. M.; Bargar, J. R.; Clement, B. G.; Dick, G. J.; Murray, K. J.; Parker, D.; Verity, R.; Webb, S. M. Biogenic Manganese Oxides: Properties and Mechanisms of Formation. *Annual Review of Earth and Planetary Sciences*. 2004, pp 287–328. https://doi.org/10.1146/annurev.earth.32.101802.120213.

(26) Zhang, H.; Chen, W. R.; Huang, C. H. Kinetic Modeling of Oxidation of Antibacterial Agents by Manganese Oxide. *Environ Sci Technol* **2008**, *42* (15), 5548–5554. https://doi.org/10.1021/es703143g.

(27) Zhang, H.; Huang, C. H. Oxidative Transformation of Triclosan and Chlorophene by Manganese Oxides. *Environ Sci Technol* **2003**, *37* (11), 2421–2430. https://doi.org/10.1021/es026190q.

(28) Chen, G.; Zhao, L.; Dong, Y. hua. Oxidative Degradation Kinetics and Products of Chlortetracycline by Manganese Dioxide. *J Hazard Mater* **2011**, *193*, 128–138. https://doi.org/10.1016/j.jhazmat.2011.07.039.

(29) Liu, J.; Zhang, Y.; Gu, Q.; Sheng, A.; Zhang, B. Tunable Mn Oxidation State and Redox Potential of Birnessite Coexisting with Aqueous Mn(II) in Mildly Acidic Environments. *Minerals* **2020**, *10* (8), 1–15. https://doi.org/10.3390/min10080690.

(30) McKendry, I. G.; Kondaveeti, S. K.; Shumlas, S. L.; Strongin, D. R.; Zdilla, M. J. Decoration of the Layered Manganese Oxide Birnessite with Mn(Ii/Iii) Gives a New Water Oxidation Catalyst with Fifty-Fold Turnover Number Enhancement. *Dalton Transactions* **2015**, *44* (29), 12981–12984. https://doi.org/10.1039/c5dt01436k.

(31) Martínez, R. J.; Farrell, J. Understanding Nitrilotris(Methylenephosphonic Acid) Reactions with Ferric Hydroxide. *Chemosphere* **2017**, *175*, 490–496. https://doi.org/10.1016/j.chemosphere.2017.02.015.

(32) Li, Y.; Zhao, X.; Wu, J.; Gu, X. Surface Complexation Modeling of Divalent Metal Cation Adsorption on Birnessite. *Chem Geol* **2020**, *551*. https://doi.org/10.1016/j.chemgeo.2020.119774.

(33) Ulrich, H.-J.; Stone, A. T. Oxidation of Chlorophenols Adsorbed to Manganese Oxide Surfaces. *Environ Sci Technol* **1989**, *23* (4), 421–428.

(34) Ojelade, B. S.; Durowoju, O. S.; Adesoye, P. O.; Gibb, S. W.; Ekosse, G. I. Review of Glyphosate-Based Herbicide and Aminomethylphosphonic Acid (AMPA): Environmental and Health Impacts. *Applied Sciences (Switzerland)*. MDPI September 1, 2022. https://doi.org/10.3390/app12178789.

(35) Grandcoin, A.; Piel, S.; Baurès, E. AminoMethylPhosphonic Acid (AMPA) in Natural Waters: Its Sources, Behavior and Environmental Fate. *Water Res* **2017**, *117*. https://doi.org/10.1016/j.watres.2017.03.055.

(36) Williams, G. M.; Kroes, R.; Munro, I. C. Safety Evaluation and Risk Assessment of the Herbicide Roundup and Its Active Ingredient, Glyphosate, for Humans. *Regulatory Toxicology and Pharmacology* **2000**, *31* (2), 117–165. https://doi.org/10.1006/rtph.1999.1371.

(37) Minnesota Department of Health. *Toxicological Summary for: Aminomethylphosphonic Acid*; Minnesota, 2022. https://www.health.state.mn.us/communities/environment/risk/docs/guidance/gw/ampasumm.pdf (accessed 2022-10-10).

(38) Reddy, K. N.; Rimando, A. M.; Duke, S. O. Aminomethylphosphonic Acid, a Metabolite of Glyphosate, Causes Injury in Glyphosate-Treated, Glyphosate-Resistant Soybean. *J Agric Food Chem* **2004**, *52* (16), 5139–5143. https://doi.org/10.1021/jf049605v.

(39) Antunes, A. M.; Rocha, T. L.; Pires, F. S.; de Freitas, M. A.; Leite, V. R. M. C.; Arana, S.; Moreira, P. C.; Sabóia-Morais, S. M. T. Gender-Specific Histopathological Response in Guppies *Poecilia Reticulata* Exposed to Glyphosate or Its Metabolite Aminomethylphosphonic Acid. *Journal of Applied Toxicology* **2017**, *37* (9), 1098–1107. https://doi.org/10.1002/jat.3461.

3 Green Quantification of Amino(poly)phosphonates using Ion Chromatography coupled to Integrated Pulsed Amperometric Detection

Anna M. Röhnelt[1], Phillipp R. Martin[1,#], Robert G. H. Marks[2], Daniel Buchner[1], Joachim Weiss[3], Torsten C. Schmidt[2], Stefan B. Haderlein[1]

[1]*Environmental Mineralogy, Center for Applied Geoscience, University of Tübingen, Tübingen, Germany*

[2]*Instrumental Analytical Chemistry, University of Duisburg-Essen, Essen, Germany*

[3]*Institute of Analytical Chemistry and Radiochemistry, Leopold-Franzens University Innsbruck, Inssbruck, Austria*

[#]*Current address: Division for Environmental Geosciences, Centre for Microbiology and Environmental Systems Science of Vienna, Vienna, Austria*

Status in the publication process: Manuscript published.

Röhnelt, A. M., Martin, P. R., Marks, R. G. H., Buchner, D., Weiss, J., Schmidt, T. C., & Haderlein, S. B. (2025). Green quantification of amino(poly)phosphonates using ion chromatography coupled to integrated pulsed amperometric detection. *Analytical and Bioanalytical Chemistry*. https://doi.org/10.1007/s00216-025-05747-w

Author Contributions:

A.M.R.: Conceptualization, Methodology, Validation, Formal Analysis, Investigation, Writing – Original Draft, Visualization

P.R.M.: Conceptualization, Methodology, Funding Acquisition, Writing – Review & Editing

R.G.H.M.: Conceptualization, Writing – Review and Editing

D.B.: Funding Acquisition, Writing – Review & Editing

J.W.: Validation, Writing – Review and Editing

T.C.S.: Supervision, Writing – Review and Editing

S.B.H.: Funding Acquisition, Supervision, Resources, Writing – Review & Editing

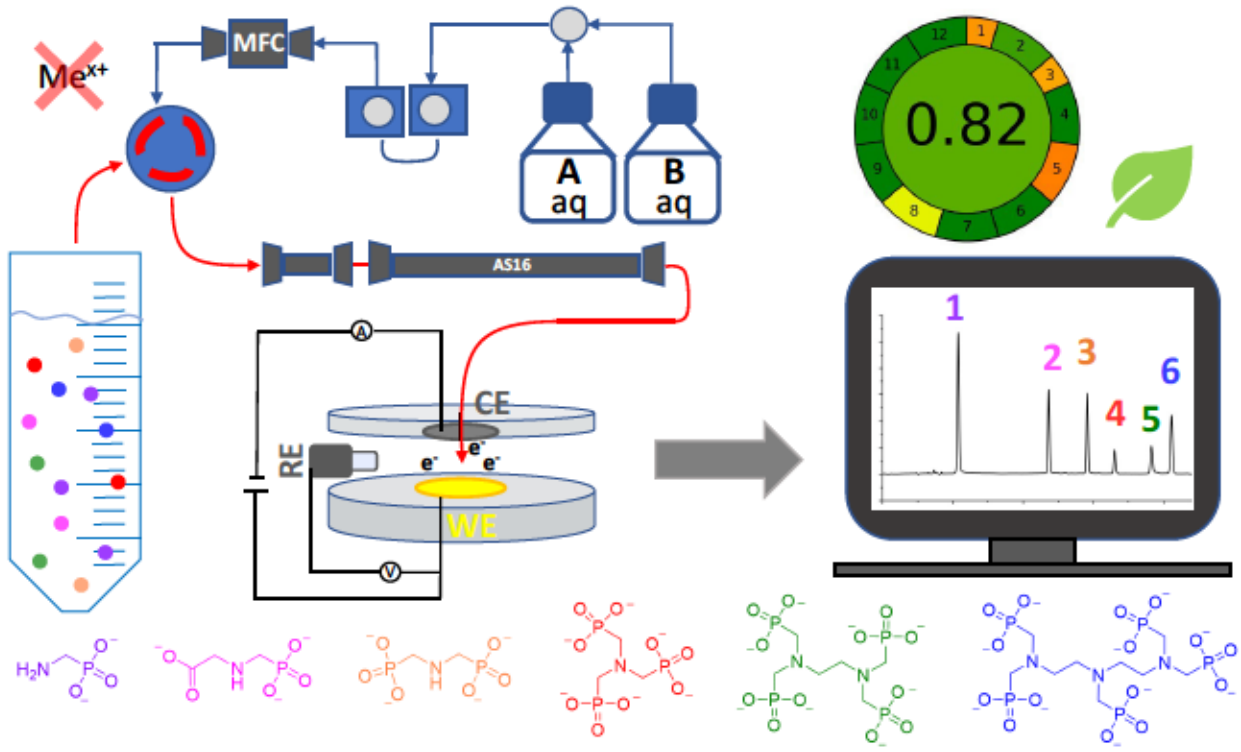

Scheme 3.1 Graphical abstract describing the main results and methodological approach of chapter 3.

3.1 Abstract

Aminopolyphosphonates (APPs) are widely used as chelating agents, and their increasing release into the environment has raised concerns due to their transformation into aminomethylphosphonic acid (AMPA) and glyphosate, compounds of controversial environmental impact. This transformation highlights the urgent need for detailed studies under controlled conditions. Despite the availability of various methods for quantifying individual aminopolyphosphonates and aminomonophosphonates, a green, low-cost approach for the simultaneous quantification of APPs and their transformation products in laboratory experiments has been lacking. In this study, we present a novel analytical method utilizing ion chromatography (IC) coupled to integrated pulsed amperometric detection (IPAD) to simultaneously quantify the six aminophosphonates AMPA, glyphosate, iminodi(methylene phosphonate) (IDMP), aminotrismethylene(phosphonates) (ATMP), ethylenediamine

tetra(methylene phosphonate) (EDTMP), and diethylenetriamine penta(methylene phosphonate) (DTPMP). This method achieves separation within a 35-min run time and method detection limits (MDLs) ranging from 0.014 µM for AMPA to 0.104 µM for DTPMP. The method's applicability was successfully shown by monitoring DTPMP, IDMP and AMPA during DTPMP transformation on manganese dioxide. A key advantage of this method is its environmental friendliness compared to existing aminophosphonate quantification techniques. Next to the simultaneous analysis, it avoids the use of derivatization agents and organic solvents and employs an energy-efficient detector. While the method's limitations lie in the detector's inherent non-specific nature, it offers a low-cost and sustainable alternative to existing methods.

3.2 Introduction

Aminopolyphosphonates

Aminopolyphosphonates (APPs) are strong chelating agents for di- and multivalent cations that are used in many household and industrial applications. The most important APPs by quantity are ethylenediamine tetra(methylene phosphonate) (EDTMP) and diethylenetriamine penta(methylene phosphonate) (DTPMP)[1]. APPs are constituents of, e.g., cleaning and bleaching agents, and are used as scale inhibitors in water treatment [1,2]. Global phosphonate consumption was at 94,000 t in 2012 – with 49,000 t thereof in Europe as reported by the European phosphonate association[1,3]. The German "Industrial Association for Personal Care and Detergents" (IKW)[4] stated the total German phosphonate use in washing, care and cleaning products with 7,613 t/a in 2019.

While phosphonates (including aminophosphonates (APs)) are generally assumed to be mainly removed from wastewater by adsorption onto sewage sludge[1,5,6], transformation of APPs under conditions relevant for environmental and technical systems is well described in literature, too. Studied reactions include i) oxidation of ATMP in the presence of Mn^{II} and oxygen [7], ii) oxidation of ATMP at MnOOH[8,9], iii) ozonation of EDTMP[10], and iv) UV photolysis of free and complexed APPs[11–15]. The transformation products primarily include orthophosphate, aminomethylphosphonic acid (AMPA) and iminodi(methylene phosphonate) (IDMP). Furthermore, selected studies reported the minor formation of the controversially discussed herbicide glyphosate from EDTMP or DTPMP (see Figure 3.1)[10,16].

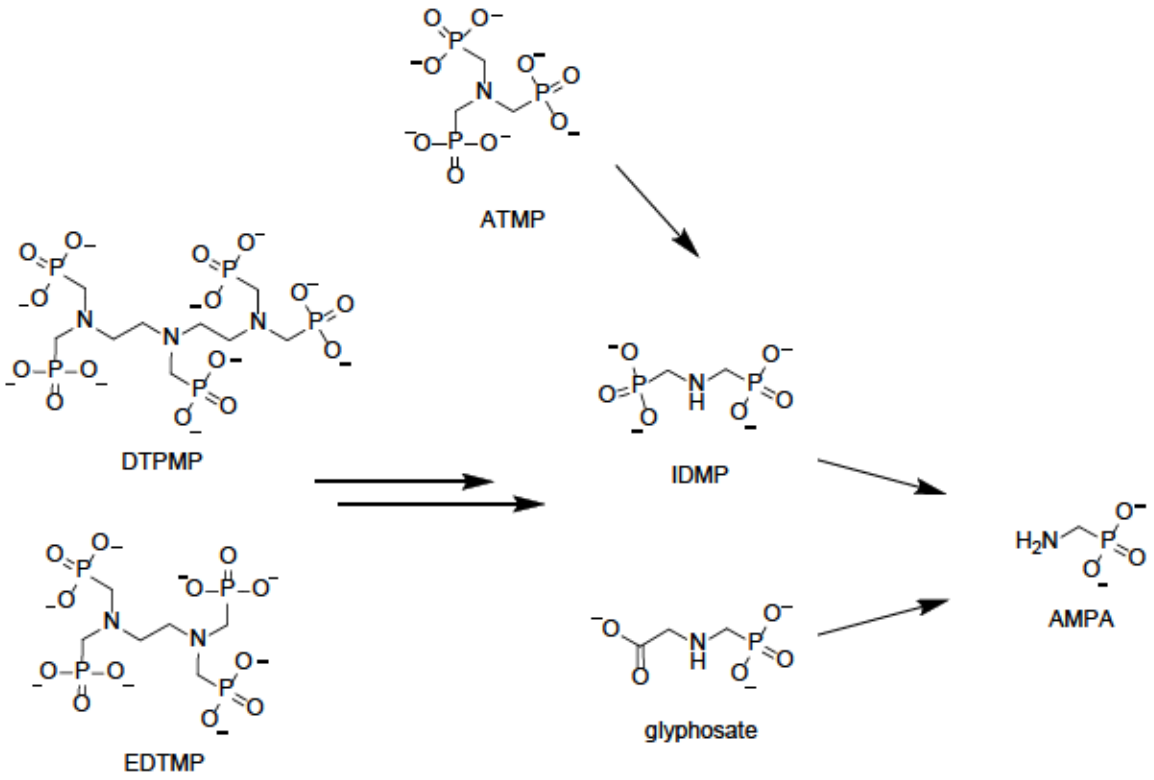

Figure 3.1 Fully deprotonated structures of DTPMP, EDTMP and ATMP and their transformation products IDMP, AMPA and – in case of EDTMP and DTPMP – glyphosate.

This suggests that household products may serve as a source of both glyphosate and AMPA, a conclusion that has been reinforced by recent studies which showed that WWTPs are sources of AMPA and glyphosate[17,18]. Those observations emphasize the need to further investigate different APP transformation pathways. Such mechanistic studies call for well-designed laboratory batch experiments.

Existing methods and greenness for polyphosphonate quantification

To investigate the transformation or sorption behavior of APPs in laboratory experiments, a green, easy, and low-cost quantification method is essential for the simultaneous quantification of APPs and their respective transformation products.

While green chemistry and atom economy are well-established tools in science and industry to sustainably design products and processes[19–21], the importance of green analytical chemistry has long been overlooked [22]. In the last years, green analytical chemistry (GAC) is increasingly gaining attention[23,24]. Despite the efforts of several scholars to develop evaluation systems, the

differences in purpose and the difference of the analytical methods itself for a long time made it quite difficult to derive exact "numbers of greenness"[20]. In the following, we refer to the 12 principles of GAC by Pena-Pereira *et al.* (2020)[24], who designed a general metric system and software to evaluate the greenness of analytical methods (AGREE).

Previous APP quantification methods generally do not perform well in AGREE, as they often require the use of a mass spectrometer (MS)[3,25–28]. These MS-based methods are energy-intensive (and not cost-efficient), contravening principle 9 of GAC, "energy minimization." Less expensive and less energy-intensive detectors can adequately monitor APP concentrations in, for instance, laboratory samples with a controlled matrix composition.

In addition, certain established methods require a pre-column derivatization with toxic compounds such as trimethylsilyldiazomethane or diazomethane[3,27]. This process is time-consuming, introduces potential error sources, and generates toxic waste, violating principle 6 "Derivatization should be avoided", principle 11 "Toxic reagents should be eliminated or replaced", and principle 1 "Direct analytical techniques should be applied to avoid sample treatment." As an example of nontoxic derivatization for non-MS methods, Fe^{III} is used for UV/Vis absorption detection, applied either post-column[29] or pre-column[30].

In general, APPs present significant analytical challenges, given their multiple negative charges, complex formation with bi- and multivalent cations[31–33], and lack of chromophores or reactive groups [28]. Thus, IC methods using alkaline eluents without pre-column derivatization often exhibit suboptimal peak shapes, sometimes attributed to impurities in the phosphonate chemicals[30,34,35].

A compilation of published and validated APP quantification methods and their key parameters can be found in the SI (Table C.1).

AMPA and Glyphosate Quantification Methods

The individual quantification of glyphosate and AMPA can be carried out with a variety of methods. Broadly used examples are i) the use of liquid chromatography (LC) coupled to MS after derivatization with fluorenylmethyloxycarbonyl (FMOC) chloride[36–39], fluorescence detection after derivatization and separation using FMOC[40] or fluorescence detection after IC separation with post-column derivatization using o-phthaldialdehyde and Thiofluor®[41]. Described quantification methods without the need for derivatization are for example IC coupled to amperometric detection[42], capillary electrophoresis coupled to MS (CE-MS)[43], or hydrophilic interaction chromatography (HILIC) coupled to MS[14,15,44].

None of the methods published so far described the simultaneous quantification of glyphosate, AMPA, and IDMP together with ATMP, EDTMP and DTPMP, which contrasts principle 8 "Multianalyte or multiparameter methods are preferred versus methods using one analyte at a time"[24].

Amperometric Detection

Electrochemical/amperometric techniques are promising in regards of greenness and specifically for the minimization of hazardous chemical usage[19]. For APs, amperometric detection is favorable in terms of low energy consumption but high sensitivity and selectivity[45]. The essential requirement for substances to be detectable via amperometry is their electroactivity, either given by aromaticity or the presence of oxidizable or reducible functional groups. For APs, this criterion is met by the presence of oxidizable hydroxyl and amino groups[46]. This allows for selective monitoring of APs and their electroactive transformation products. Compounds without electroactive groups, e.g. phosphate or methylene phosphonate, show no response and therefore cannot interfere with APP quantification[47].

Amperometric detectors comprise a three-electrode arrangement with a working electrode (WE), a counter electrode (CE), and a reference electrode (RE). The electrochemical reaction takes place at the WE, which is usually made of platinum or gold. In DC amperometry, a constant working potential is applied, by which the analytes are oxidized/reduced, and the resulting current is measured. However, for analytes precipitating or strongly sorbing at the electrode, constant working potential amperometry is not applicable due to baseline drift, increased background noise and a constantly changing electrode surface resulting in a changing response [48]. Developments regarding the applied potential sequence (waveform) led to "pulsed amperometric detection" (PAD), usually involving a gold WE[48]. In contrast to amperometry with a constant working potential, PAD involves the repetitive application of a short potential sequence, typically lasting <1 second, including a high oxidation and a low reducing potential. This potential sequence impedes electrode fouling or in other words "facilitates electrochemical cleaning" of the electrode surface in preparation for the next measurement interval. For further details on PAD waveforms, see the Supporting Information.

Especially, developments in the field of amino acid detection using integrated pulsed amperometric detection (IPAD)[45,47] and an IC-IPAD application note for glyphosate and AMPA

with detection limits (LODs) below 2 µg/L[42,49] suggested the suitability of IPAD for the quantification of APPs in aqueous solutions.

Integrated PAD (IPAD)

IPAD is a variant of PAD. The waveforms developed for IPAD allow the simultaneous oxidation of the electrode surface and the analyte, also known as "mode II detection"[45–47]. The different potentials applied in IPAD are explained in Table C.2. IPAD is predominantly used for the detection of amino acids, amines, and organic sulfur compounds. Their oxidation on metal electrodes is catalyzed by metal oxide formation[46]. While in pulsed amperometry the Faraday current is measured at a fixed oxidation potential, the integration part of the potential waveform in IPAD can have the form of a triangle or trapez (see Figure C.1 **b**), i.e., it is generally alternated between a high and a low potential[48]. While the surface oxide formation is necessary to catalyze analyte oxidation, the oxide formation produces a current itself – leading to high background currents.

In addition, concentration gradients are also the origin for high background currents caused by changes in the background electrolyte concentration throughout the gradient run[45,47].

When IPAD is employed, baseline disturbances caused by pH gradients, ionic strength variations, and metal oxide formation are minimized. Because the oxidation of the electrode surface is a reversible process, while the oxidation of analytes is not, the resulting signal is mainly characterized by the contribution of the analyte oxidation. When integrating the current yield during the cycle, the net signal for the respective analyte is obtained[45,47,48,50].

The oxidative detection of amino acids using IPAD is reported to be most effective on gold electrodes at strong alkaline pH[45,47]. This provided the rationale for coupling anion-exchange chromatography with amperometric detection using a gold WE, employing eluents in the pH range of 11-13. Despite the sensitivity of this method to trace amounts of metal cations in the system due to strong complex formation with higher APPs, the alkaline pH range was chosen to simultaneously analyze aminomono, -bi-, and -polyhosphonates.

Aim of this work

In summary, existing methods for the quantification of APPs have significant limitations concerning their greenness and especially the number of analytes that can be analyzed in a single chromatographic run. To address these shortcomings a green and low-cost method for the simultaneous quantification of six APPs was developed. We describe here the systematic development and evaluation of an IC-IPAD quantification method, offering a cost-efficient, green and sensitive approach. The applicability of the method will be demonstrated by monitoring the above-mentioned analytes in a DTPMP transformation experiment.

3.3 Experimental Section

Chemicals

DTPMP (a) and EDTMP (b) have been purchased as solid acids from Zschimmer and Schwarz (Lahnstein, Germany) under the names "Cublen D 900 GR" (a) and "Cublen ELC 950" (b) (CAS: 15827-60-8 (a) and 1429-50-1 (b)). To ascertain the purity of the purchased substances, $^{31}P-\{^{1}H\}$-NMR measurements were conducted, showing a purity of >98.6 % for DTPMP and 96.6 % for EDTMP (nuclear magnetic resonance spectroscopy (NMR) measurements and results are described in the Supporting Information, Figures C.2, C.3 and C.4). Glyphosate (≥98.0 %, analytical standard), AMPA (99 %, analytical standard), IDMP (≥97 %) and ATMP (≥97.0 %), 2-aminoethylphosphonic acid (2-AEP, 99 %), methylphosphonic acid (MPA, 99 %), editronic acid (HEDP, ≥95 %), phosphonoacetic acid (PAA, 98 %), and phenylphosphonic acid (PPA, 98 %) were purchased as solids from Sigma Aldrich (St Louis, MO, USA).

Sodium hydroxide (NaOH) for eluent preparation and analyte desorption from the manganese dioxide was purchased as a 49-51 % solution from Supelco (Merck, Darmstadt, Germany), while sodium acetate (NaOAc) was purchased from Chemsolute (Renningen, Germany). MES buffer (≥99%) and MnO_2 (manganese^{IV}oxide) for the DTPMP transformation experiments were purchased from Carl Roth (Karlsruhe, Germany).

The cation-exchange resin in proton form (Dowex™ 50W X8 200-400, ≥1.7 eq/L) used to treat the experimental samples was purchased from Roth (Karlsruhe, Germany).

The water used has been purified by an ultrapure water purification system (Barnstead, GenPure Pro, Thermo Fisher Scientific, Waltham (MA), USA) down to a conductivity below 0.06 µS/cm.

Instrumentation

A 930 Compact IC Flex ion chromatograph (Metrohm, Herisau, Switzerland) was used, equipped with a high-capacity anion-exchange column (Dionex™ IonPac™ AS16, 2x250 mm), a suitable guard column (Dionex™ IonPac™ AS16, 2x50 mm) and a metal-free trap column (Dionex™ MFC 500, all from Thermo Fisher Scientific, Waltham (MA), USA). Some tests have also been carried out using the anion-exchange column Metrosep A Supp 18 (4x150 mm, Metrohm) with the respective guard column (4x5 mm). The column temperature was set to 30 °C. The MFC 500, if used, was inserted between the pulse damper and the six-port injection valve.

The amperometric detector cell with a Wall-Jet geometry was equipped with a gold working electrode, platinum counter electrode and a palladium or Ag/AgCl reference electrode (all Metrohm, see Figure C.5). All columns, the detector and electrodes have been used in the commercial state without any modifications. The detector temperature was set to 35 °C. The dosing units for i) sample uptake and ii) concentration gradient were both an "800 Dosino" (Metrohm), with i) 2 mL and ii) 5 mL cylinder volume.

To prevent CO_2 dissolution into the eluents, an overpressure of 0.4 bar N_2 was applied to both eluent bottles (gas-tight plastic bottles, Metrohm). The concentration gradient was achieved by an HPLC pump and a dosing unit comparable to a syringe pump (dosino). The dosino doses a defined amount of eluent B into a mixing piece, where it is mixed with eluent A. The eluent mixture is then conveyed by the HPLC pump. In order to prevent CO_2 to dissolve in eluent B while the liquid is trapped in the dosino, the dosino is emptied completely at the start of each run and then filled just with the amount needed for one run (3 mL). For IC Maintenance, please see the Supporting Information.

In this work, all chromatograms are displayed in Ampere on the y-axis, although IPAD is often displayed in Coulomb. To convert from nA to nC, the value in nA can be multiplied by the integration time in seconds, which is 0.380 s in the optimized method presented in this work.

Maintenance

Due to the highly concentrated eluents and resulting salt precipitations, the HPLC pump head (although a chemically inert PEEK pump head) was rinsed weekly with deionized water (flow rate of 2 mL/min for at least 15 min), disassembled, and manually cleaned every 2-3 months.

Bi- and multivalent cations need to be removed from the IC system and column. Therefore, the system including the analytical column was rinsed fortnightly using 0.05 M ethylenediaminetetra(acetic acid) (EDTA, ≥97 %, p.a., Roth (Karlsruhe, Germany)) at pH 6.5 to chelate and remove Fe (flow rate 0.5 mL/min, 1.5 hours). Additionally, great attention must be paid to the metal parts in the system which can corrode even if they are not in contact with the eluent, because the smallest leaks (e.g., from scratches due to salt precipitation) allow Fe to enter the IC system and hamper the quantification of ATMP, EDTMP, and DTPMP. Therefore, the MFC 500 (metal-free trap column) is placed directly after the pulse damper, to trap any Fe that may leak from the pump head or the pulse damper. Fortnightly, the MFC 500 was regenerated with 20 mL 1.5 M HNO_3 and then rinsed with eluent A for 30 min.

Cyclovoltammograms

The cyclovoltammograms have been recorded with the amperometric detector (Wall-Jet Cell) of the IC as described above, equipped with a gold working electrode, platinum counter electrode and palladium reference electrode. The detector temperature was set to 35 °C. The sweep was perfomed from a minimum of -0.35 V to a maximum of +0.75 V with a sweep rate of 0.1 V/s and a range of 20 mA (cycle length: 22 s). The respective phosphonate was present at a concentration of 0.5 mM in a background solution of 0.1 M NaOH. The average of three consecutive sweeps was taken.

Method validation

To validate the analytical performance, calibration standards of all APs were prepared in ultrapure water. For EDTMP and DTPMP the pH was adjusted to a value of ≥ 5 in order to dissolve them. Due to observed analyte transformation at room temperature and under light, the standards were stored at –18 °C in the dark until analysis. The calibration ranged from 0.05 µM to 20 µM for each compound. For two standards (1 µM and 10 µM), ten replicates were measured consecutively to show repeatability. In order to validate the repeatability of the calibration, four calibration measurements have been performed on different days.

The method detection limits (MDLs) for all compounds were determined using the MDL procedure described by the US environmental protection agency (US EPA, Revision 2, 2016)[51]. At an S/N ratio of ~5, the respective standards have been prepared in deionized water and measured eight times (n = 8) consecutively, hence the MDL could be calculated using the singe-

tailed Student's t-value with a confidence level of 99 % and the standard deviation of the eight replicates.

Design of DTPMP transformation experiments

The experiments have been conducted in 50-mL centrifugation tubes (polypropylene, Fisher Scientific, Waltham, MA, USA) in an anaerobic glovebox (N_2 atmosphere) from MBRAUN (Garching, Germany). First, DTPMP stock solution, MES buffer solution, and ultrapure water have been purged with N_2 for one hour and were then transferred to the glovebox together with the solid MnO_2. Afterwards, DTPMP, MES buffer, and water were mixed to yield concentrations of 1 mM DTPMP and 20 mM MES. After taking the timepoint zero aliquot, MnO_2 (1 g/L) has been added to start the reaction. The sampling procedure described in Röhnelt *et al.*[16] was followed. In the end, there were two phases for each sampling point – the aqueous and the sorbed phase. The analytes were desorbed from the MnO_2 residue, using 0.1 M NaOH and 0.1 M NaH_2PO_4 in the ultrasonic bath for 30 minutes. After the desorption step, the desorbed analytes were in an aqueous phase again and are thus given in the unit µM, too. Samples were stored in the dark at -20 °C until analysis. Prior to analysis, samples were defrosted, diluted 1:50, and treated with cation-exchange resin.

The aqueous and sorbed phases were quantified separately and the analyte concentrations summed after analysis ($c_{tot} = c_{aq} + c_{sorb}$).

3.4 Results and Discussion

Chromatographic separation

The separation of all six analytes (AMPA, Glyphosate, IDMP, ATMP, EDTMP and DTPMP) on the Dionex™ IonPac™ AS16 column requires a concentration gradient, as already shown for some polyphosphonates with NaOH gradients[35]. This column is hydroxide-selective, i.e., it has been designed to be used with hydroxide mobile phases, thus previous methods describe the use of pure hydroxide eluents for the separation of e.g. perchlorate[52] and polyphosphates[53]. Yet, with the analytical setup used in this study no satisfactory separation could be achieved with eluents consisting purely of NaOH. In addition, pure NaOH eluents up to a concentration of 120 mM result in a high background signal and comparably low sensitivity for IDMP, EDTMP, and DTPMP (see Figure C.6). Therefore, sodium acetate (NaOAc) was tested as an alternative,

as it has proven to be particularly suitable for eluting the more strongly retained analytes in ion chromatography of amino acids[54]. Furthermore, NaOAc is not electroactive and thus compatible with integrated pulsed amperometric detection.

Hence, eluent B was amended with NaOAc as the main eluting agent. Initial experiments have been carried out with a combined NaOH and NaOAc concentration gradient. However, increasing the NaOH concentration from 15 to 50 mM during the chromatographic run, a significant baseline shift due to the change in pH was observed. By applying a NaOAc concentration gradient while keeping the NaOH concentration constant at 15 mM, the baseline shift could be eliminated. Additionally, a significant increase in the analyte response of ATMP, EDTMP and DTPMP could be achieved. Figure C.7 shows a comparison of the analyte response using a pure NaOAc gradient (0-400 mM) with constant NaOH concentration (15 mM) (**B**) and a combined NaOH (15-50 mM) and NaOAc (0-400 mM) gradient (**A**).

The optimized chromatogram was achieved by 15 mM NaOH (eluent A) and 15 mM NaOH plus 400 mM NaOAc (eluent B) and the gradient profile shown in Figure 3.2. This chromatographic setup led to the elution order AMPA < glyphosate < IDMP < ATMP < EDTMP < DTPMP.

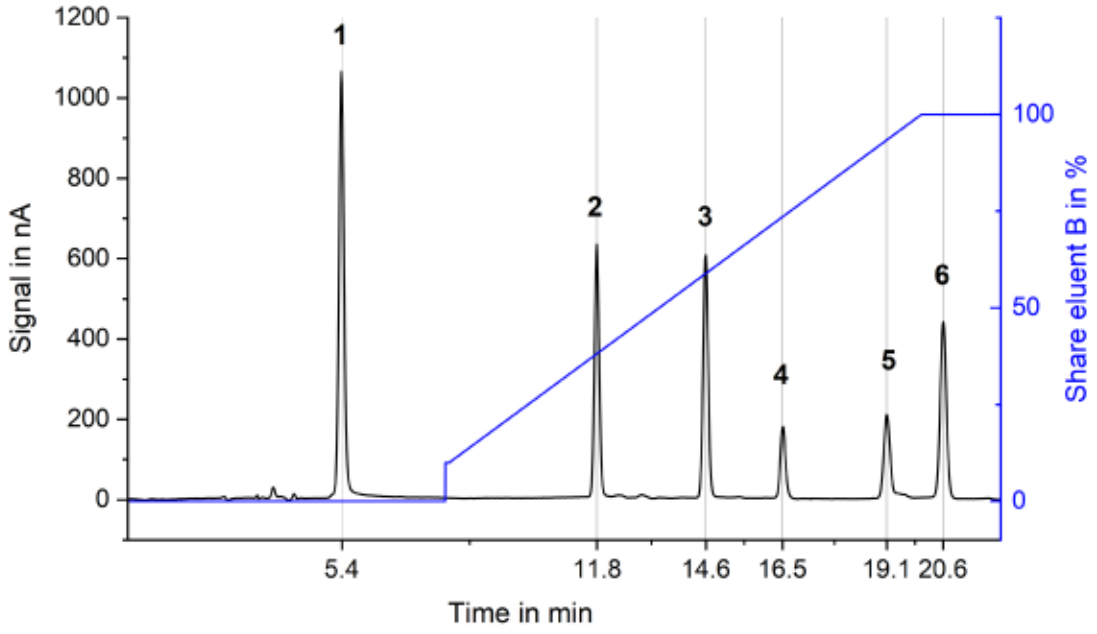

Figure 3.2 Optimized separation of a 10 µM multi-phosphonate standard using optimized chromatographic and amperometric parameters, shown after blank subtraction. Column: Thermo Scientific Dionex AS16 (2x5 + 2x250 mm) at 30 °C; MFC 500 inserted between pulse damper and six-port injection valve; eluents **A**: 15 mM NaOH, **B**: 15 mM NaOH + 400 mM NaOAc; flow rate: 0.3 mL/min; gradient profile: 0-6 min 0 % B, 6-18 min 10-100 % B, 18-21 min 100 % B, 21.1-22 min 0 % B, post run: 9 min with 100 % eluent A at 0.6 mL/min; detection: amperometric detector

with gold WE, Pt CE and Ag/AgCl RE, 35 °C; waveform: see Figure 3.5 3); injection volume: 50 µL; 10 µM of: 1 = AMPA, 2 = glyphosate, 3 = IDMP, 4 = ATMP, 5 = EDTMP, 6 = DTPMP.

An inherent problem of NaOH eluents – manually prepared from NaOH concentrates – are carbonate impurities[55]. At low hydroxide concentrations, divalent carbonate ions accumulate at the stationary phase of an anion exchanger, thus reducing the anion-exchange capacity of the column over time, which results in a general RT decrease and a change in the elution order between IDMP and ATMP (Figure C.8). Since analytes are identified via RT assignment, it is crucial to avoid carbon dioxide contamination in the eluent as much as possible to produce stable retention times. Therefore, several measures were taken to prevent CO_2 contamination, such as e.g., N_2 overpressure in the eluent bottles (see Experimental Section). With those measures in place reproducible RTs were obtained, with standard deviations ≤0.16 min (for DTPMP) and a maximum relative standard deviation of 1.3 % for AMPA within 38 hours (see Figure C.9). However, over a longer period of time a trend toward shorter RTs for all analytes was observed, which was compensated by the continuous measurement of external standards after six to ten sample runs (check standards). When strong retention time shifts were observed and two compounds were not separated to baseline anymore, the column was regenerated with freshly prepared NaOH (c = 300 mM) at a flow rate of 0.5 mL/min for 12 hours.

APPs form strong complexes with bi- and multivalent metal cations, such as copper and iron[32]. Therefore, bi- and multivalent cations need to be eliminated from the IC system and column. If metals are not eliminated, EDTMP and DTPMP show unreproducible chromatographic behavior, in the form of e.g., two peaks or no peak in the chromatogram and/or distorted peak shapes and therefore their quantification is impaired. If e.g., Fe is present in the system, different Fe complexes can be formed depending on the analytes and analyte concentrations present in the standard/sample. Figure 3.3 depicts chromatograms of EDTMP and DTPMP influenced by Fe in the IC system. To achieve metal elimination, the system and column have been rinsed regularly with 0.05 M EDTA and a metal-trap column has been inserted between pulse damper and six-port injection valve (see Experimental Section, Maintenance).

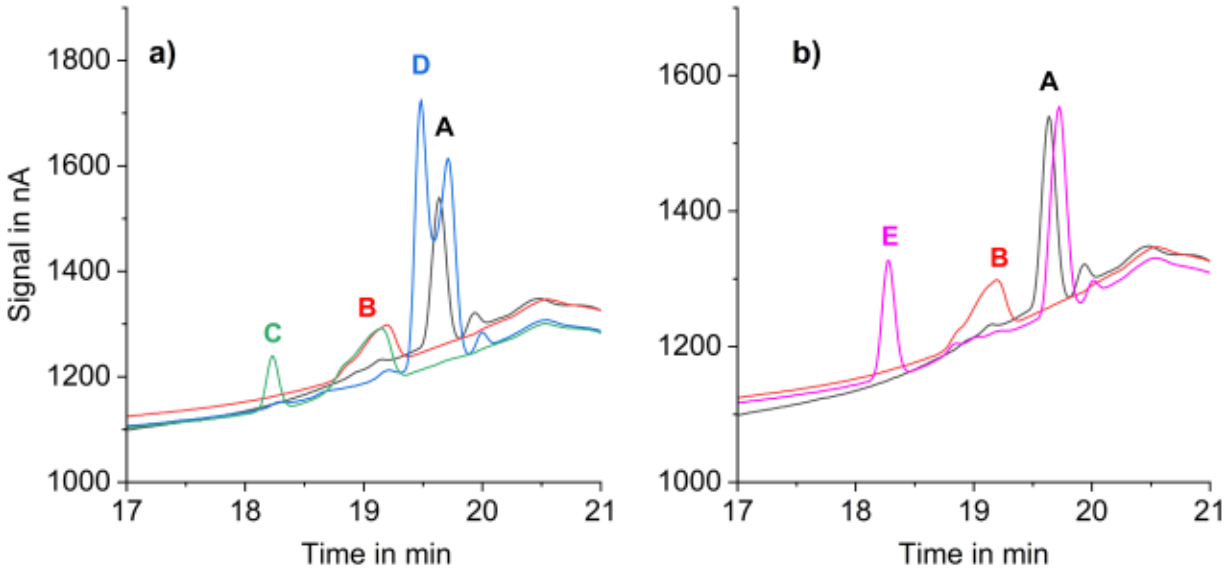

Figure 3.3 Chromatograms of EDTMP and DTPMP standards in a system with iron contamination. **a)** A: 10 µM DTPMP, B: 10 µM EDTMP, C: 20 µM EDTMP, D: 20 µM, DTPMP; **b)** A: 10 µM DTPMP, B: 10 µM EDTMP, E: 10 µM EDTMP + 10 µM DTPMP. Chromatographic conditions: column: Thermo Scientific Dionex AS16 (2x5 + 2x250 mm) at 30 °C; eluents **A**: 15 mM NaOH, **B**: 50 mM NaOH + 400 mM NaOAc; flowr ate: 0.3 mL/min; gradient profile: 0-6 min 0 % B, 6-14 min 10-30 % B, 14-18 min 30-100 % B, 18-19 min 100 % B, 20.1-22 min 0 % B, post run: 8 min with 100 % eluent A at 0.6 mL/min; detection: amperometric detector with gold WE, Pt CE, and Ag/AgCl RE, 35 °C; waveform: see Figure 5 3); injection volume: 50 µL.

Electrochemical Detection

After the chromatographic separation, the detection parameters were optimized. A gold working electrode (WE) was chosen because of the strong adsorptive interaction between amines and the gold surface due to its unsaturated *d*-orbitals[47]. Platinum was chosen as counter electrode (CE, here: cathode) material due to its inert character. For the reference electrode (RE), palladium has been chosen as a starting point[42].

However, the majority of the aminophosphonate analytes under investigation are not readily oxidized between -0.3 and +0.75 V utilizing DC amperometry at the gold electrode (see cyclovoltammograms in Figure C.10). Except for AMPA, the voltammograms of all other analytes (0.5 mM each) cannot be distinguished from the voltammogram of the background electrolyte (0.1 M NaOH). The peak in the positive scan in the cyclovoltammogram of 0.1 M NaOH corresponds to the formation of surface oxide at the gold electrode, while the peak in the negative scan corresponds to the reduction of surface oxide[46,56].

Hence, APPs cannot be detected by applying the classical waveforms for pulsed amperometric detection (see Figure 3.5 (1) and 3.5 (2)) that was originally developed for the detection of

carbohydrates[48]. On the other hand, the free electrons of the amine group in APPs can be oxidized utilizing IPAD waveforms on a gold working electrode.

Choice of the type of reference electrode

First, a Pd RE was utilized as it was already successfully used for IC-IPAD analysis of glyphosate and AMPA[42,49]. However, it did not turn out to be suitable for APP analysis as peak areas strongly increased for all six analytes (up to +80 % for EDTMP) within 32 hours. As an example, Figure 3.4**a** illustrates the peak area increase over time for 10 µM glyphosate. Insufficient cleaning of the working electrode was ruled out, as this would lead to a decrease in sensitivity. Therefore, it was hypothesized that the instable signal was caused by the sorption of APPs onto the reference electrode, altering the oxidation potential from the set value. To minimize the sorption of APPs an Ag/AgCl RE has been tested as described for EDTMP and DTPMP[34] and carbohydrates[55]. Using an Ag/AgCl instead of a Pd RE and applying the identical potential sequence, peak areas were significantly more stable (see Figure 3.4 **b**).

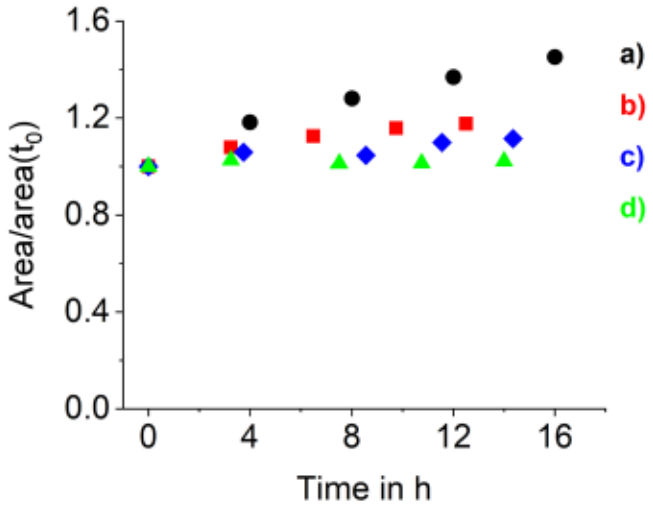

Figure 3.4 Normalized peak areas of glyphosate (10 µM) over time for different reference electrodes (RE) and potential waveforms. The used waveforms (**1**, **2** and **3**) are depicted in Figure 3.5. **a)** Pd RE and waveform **1**, **b)** Ag/AgCl RE and waveform **1**, **c)** Ag/AgCl RE and waveform **2**, **d)** Ag/AgCl RE and waveform **3**. Chromatographic parameters: column: Metrohm Metrosep A Supp18 (4x5 + 4x150mm), 30 °C; eluents: A 20 mMNaOH, B 50 mM NaOH + 400 mM NaOAc; gradient profile: 0-3 min 5 % B, 3-16 min 5-36% B, 16.1-18 min 50% B, 18.1-25min 0% B. Detection: amperometric detector with gold WE and Pt CE; RE and waveform as denoted; detector temperature: 35 °C; injection volume: 50 µL.

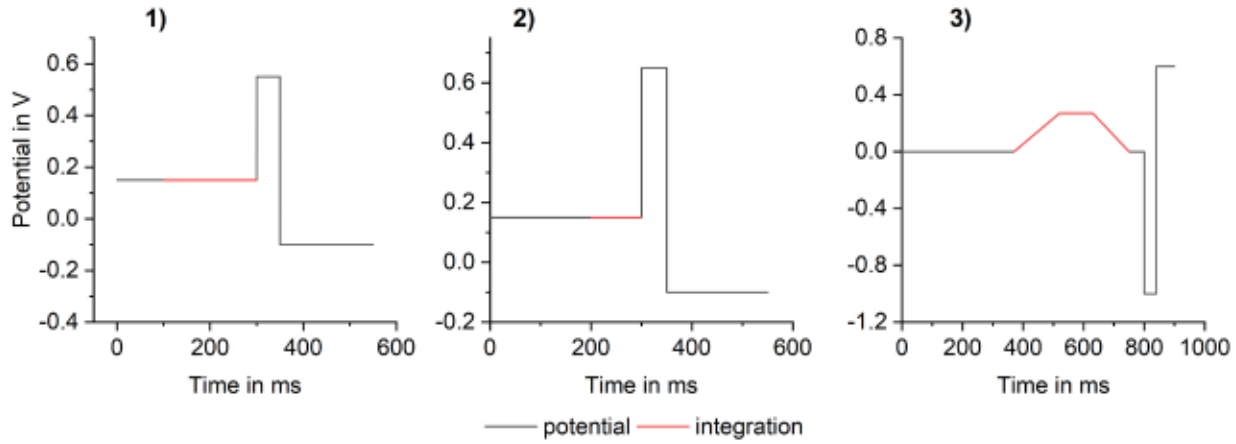

Figure 3.5 Waveforms used for the measurements presented in Figure 3.4: **1)** PAD with E_1 = +0.15 V, E_2 = +0.55 V, E_3 = -0.1 V and integration time of 200 ms, **2)** PAD with E_1 = +0.15 V, E_2 = +0.65 V, E_3 = -0.1 V and integration time of 100 ms, **3)** IPAD with E_1 = 0.00 V, E_2 = +0.27 V, E_3 = -1.0 V, E_4 = +0.60 V and integration time of 380 ms; the exact potential sequence of **3)** is presented in Table C.4.

Effect of IPAD wave forms

IPAD is the method of choice for detecting amino compounds, including amino acids, due to the necessity of mode II detection[46]. Using IPAD together with the Ag/AgCl RE resulted in constant peak areas with marginal increases within 15 hours (see Figures 3.4**d** and 3.5 **3**). Additionally, the advantages of IPAD include lower background signal, a lower gradient-induced background increase when applying a concentration gradient, and increased analyte signals (peak areas) compared to tested PAD waveforms (see Figures 3.5 **1** and **2**). Chromatograms recorded using PAD compared to IPAD are depicted in Figure C.11.

To prepare the WE surface for the next oxidation reaction, a series of reduction and oxidation potentials are applied after every cycle like in standard PAD mode. The optimized IPAD waveform with a maximum detection potential (E_2) of 0.27 V and an integration time of 750 ms is shown in Figure 3.5 **3)**. This sequence resulted in low background signal, a high signal-to-noise ratio, symmetric peak shapes (see Figure 3.2), and low method detection limits (MDLs) (see "Method validation").

IPAD waveforms are described in literature to be very effective for amino compounds, but not showing a great response for alcohols or carbohydrates[46]. In order to assess which TPs can be detected using IC-IPAD, the phosphonate compounds 2-aminoethylphosphonic acid (2-AEP), etidronic acid (HEDP), methylphosphonic acid (MPA), phosphonoacetic acid (PAA), and phenylphosphonic acid (PPA) were tested. While two of them did not show any response at the

before-mentioned detector (MPA, PAA), three of them showed a response (PPA, 2-AEP, HEDP), but one order of magnitude lower than the AMPA response: while 10 µM AMPA resulted in a peak area of approximately 260 nA*min, 20 µM HEDP (resp. 2-AEP, PPA) yield less than 10 % of that (HEDP: 23 nA*min, 2-AEP: 27 nA*min, PPA: 7 nA* min, see Figure 3.6).

Thus, the chosen detection method will primarily detect amino compounds with small signals for compounds bearing hydroxide groups or phenyl groups. The comparably low response of 2-AEP, which exhibits a primary amine function, needs further investigation.

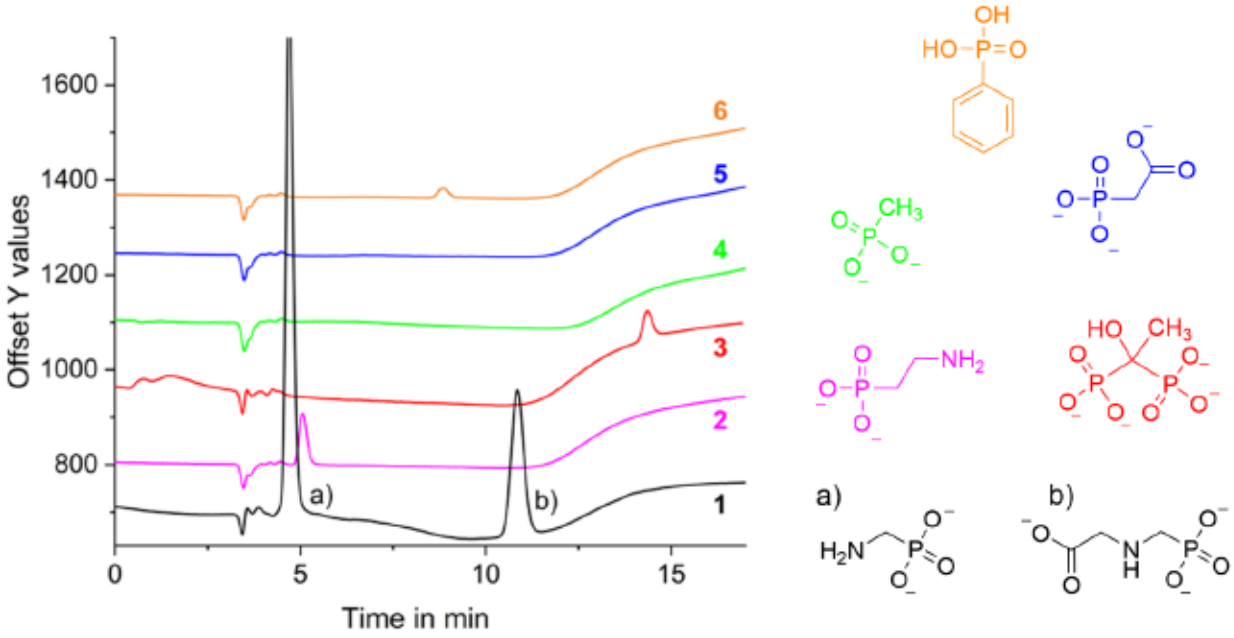

Figure 3.6 Chromatograms of seven different phosphonates. 20 µM of each compound: 1 = AMPA (a) and glyphosate (b), 2 = 2-aminoethylphosphonic acid (2-AEP), 3 = 1-hydroxyethylidene-1,1-diphosphonic acid (HEDP), 4 = methylphosphonic acid (MPA), 5 = phosphonoacetic, acid (PAA), 6 = phenylphosphonic acid (PPA). Chromatographic conditions: column: Thermo Scientific Dionex AS16 (2x5 + 2x250 mm) at 30 °C; eluents A: 15 mM NaOH, B: 50 mM NaOH + 400 mM NaOAc; flow rate: 0.3 mL/min; gradient profile: 0-5 min 10 % B, 5-10 min 10-30 % B, 10.1-15 min 0 % B; detection: amperometric detector with gold WE, Pt CE and Ag/AgCl RE, 35 °C; waveform: see Figure 3.5 3) with E_2 = 0.25 V.

Method validation

All APs were calibrated in the range of 0.05 – 20 µM. Calibration curves were measured four times over three days to assess repeatability. Applying linear regression, the coefficient of determination (r^2) showed values of ≥0.9960 for all six compounds. Over three days, the slopes of the linear calibration curves increased significantly, most pronounced for EDTMP and DTPMP, which is to be expected as the electrode surface is continuously altered throughout a

measurement sequence. This underlines the need for continuous injection of check standards and/or new system calibration. However, the consistent high linearity of the single calibration curves proves the suitability of the method for external calibration.

To verify the repeatability of consecutively measured samples, the 1 µM and the 10 µM standard were measured eight times sequentially. The relative standard deviations (σ_r) of the peak areas of those consecutive measurements were ≤5 % (1 µM) and ≤3 % (10 µM), respectively. The MDL was calculated according to the US EPA (Revision 2, 2016) using standards of the respective analyte with an S/N ratio of ~5.

Those analytical key figures are presented in Table 3.1. The peak width at half height was ≤0.13 min (glyphosate) for the 20 µM multi-standard. To assess the method's analytical performance metrics, they will be compared with the figures of merit of other non-MS-based APP quantification techniques listed in Table C.1.

Table 3.1 Analytical figures of merit of the optimized IC-IPAD method. σ_r denotes the relative standard deviation (n = 8) of the peak areas at the given concentration, r^2 is the coefficient of determination for the linear regression of one standard curve in the given concentration range. MDL denotes the method detection limit.

	AMPA	Glyph	IDMP	ATMP	EDTMP	DTPMP
σ_r (1 µM) in %	2.2	1.9	2.5	4.9	2.6	4.9
σ_r (10 µM) in %	1.0	0.8	1.0	1.7	0.3	2.3
r^2 (0.05–20 µM)	0.9996	0.9991	0.9991	0.9997	0.9929	0.9987
MDL in µM	0.014	0.064	0.049	0.065	0.062	0.104

Nowack (1997)[30] reported detection limits (LODs) of 0.05 µM for ATMP and EDTMP, and 0.1 µM for DTPMP using pre-column Fe^{III} complexation and UV/vis detection. Weiss & Hägele (1987)[29] stated quantification limits (LOQs) in the lowest ppm range for ATMP, EDTMP, and DTPMP (single digit µM range). Tewari & van Stroe-Bieze (1997)[34], using amperometric detection, described their method as easily applicable to 25 mg/L (43.7 µM DTPMP), without stating explicit LODs.

The MDLs achieved in this study are comparable to those reported by Nowack (1997)[30], despite the use of a larger injection volume (200 µL) and broader DTPMP peaks (>5 min width at 5 µM). Compared to the value provided by Tewari & van Stroe-Bieze (1997)[34], our method achieves MDLs approximately 100 times lower.

It is worth noting that these previous studies did not investigate method repeatability, which is crucial given the challenges associated with APP quantification[28,57,58]. Our detailed examination of repeatability and system maintenance provides valuable information for researchers in the APP field. The primary advantage of our method, however, lies in its green approach and simultaneous analysis of aminomono- and polyphosphonates, which will be discussed in subsequent sections.

Greenness

To evaluate the greenness of the presented method in comparison to other published methods, the "Analytical GREEnness Metric Approach and Software" (AGREE)[24] has been used, which was recently employed (in an adapted version) in a number of studies[59–62]. This approach is based on the 12 principles of GAC and provides a score from zero (not green) to one (maximum green). Some aspects are briefly explained and conceptualized in the Supporting Information to ensure transparency of the comparison.

For this comparison, the IC-ESI-MS quantification method published by Armbruster *et al.* in 2019[28] and the LC-UV/vis method published by Nowack in 1997[30] served as references. These methods were chosen, as both describe the analysis of the three APPs ATMP, EDTMP and DTPMP. The IC-ESI-MS method represents a novel approach using mass spectrometry without derivatization. This allows for a comparison with a state-of-the-art technique. The LC-UV/vis method employs pre-column derivatization (complexation with Fe^{III}), but no use of a mass spectrometer. By selecting these two methods, we can evaluate the greenness of our new IC-IPAD method against both a modern mass spectrometry-based technique and a simpler approach based on Fe^{III}-APP complex formation.

The IC-IPAD method (Figure 3.7a) outperforms the other two methods (Figure 3.7 b and c) in several aspects. Regarding energy usage (principle 9), IC-IPAD consumes only about 0.035 kWh per sample, compared to over 1.5 kWh for IC-ESI-MS[24]. In terms of waste and toxic reagents (principles 7 and 11), the IC-IPAD method avoids the use of organic solvents like methanol or acetonitrile and the use of the ion-pair reagent tetrabutylammonium (TBA), which are used in the other methods[28,30]. The sample preparation for the LC-UV/vis method requires a multi-step protocol, comprising cation exchange, Fe^{III}-APP complexation, sequestration of excess Fe^{III} with NTA, and subsequent addition of a carbonate/TBA buffer. This elaborate procedure is time-intensive and contravenes the principles of integrating analytical processes

(principle 4) and avoiding derivatization (principle 6). In contrast, the IC-IPAD method employs a less complex sample preparation protocol (solely cation exchange) and eschews the utilization of derivatization procedures.

Finally, the IC-IPAD method can simultaneously analyze six aminophosphonates, compared to three in the other methods (principle 8).

While the IC-ESI-MS method provides additional compound-specific information, this is not always necessary depending on the research requirements. The IC-IPAD method offers a good balance between analytical performance and greenness, making it particularly suitable for routine analysis of laboratory samples with known matrices.

It is important to note that the selection of an appropriate quantification method should be based on the specific research needs, and existing methods should be evaluated for potential improvements in greenness while considering these requirements.

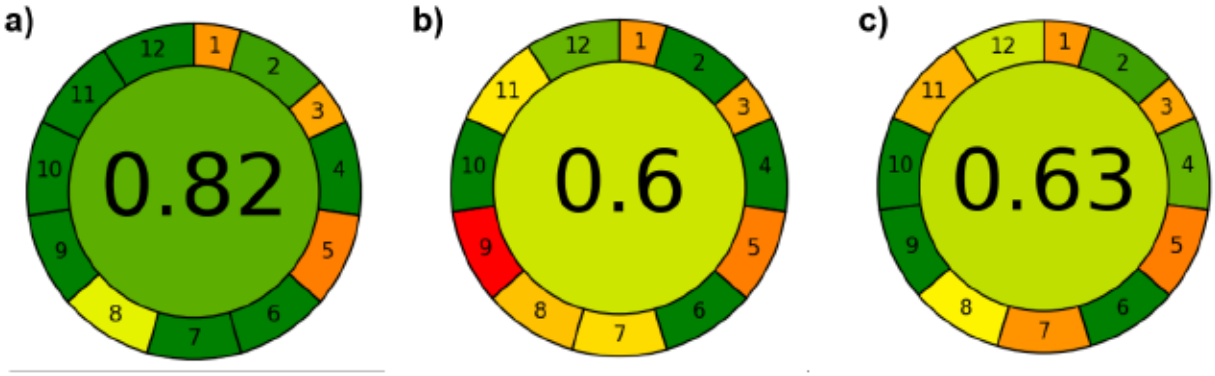

Figure 3.7 Greenness evaluation diagrams derived by the AGREE metric system and program from Pena-Pereira et al. (2020)[24] for a) the IC-IPAD method presented in this work, b) the IC-ESI-MS method published by Armbruster et al. (2019)[28] and c) the LC-UV/vis method published by Nowack (1997)[30].

Application example: DTPMP oxidation by manganese dioxide

To demonstrate the suitability of the method described for laboratory APP transformation studies, DTPMP and its major electroactive TPs were quantified in the course of DTPMP oxidation by manganese dioxide. Measured concentrations over the course of the sequence were corrected using continuously measured check standards (1 µM, see Figure C.12 and Table C.5 for the correction function).

Each sample was measured in triplicates. Figure 3.8 shows DTPMP transformation alongside the formation of TPs over time. While DTPMP concentrations decreased continuously, known (IDMP, AMPA) and unknown compounds appeared in the chromatogram, the latter were labeled with letters (see Figure 3.8, 24.5 h). While some of the TPs (AMPA, IDMP) just increased, others decreased in concentration over the course of the experiment (D, E after 0.7 h) and, therefore, seem to represent intermediate products. For better depiction of the low concentrated analyte peaks, see Figure C.13. DTPMP is almost completely transformed after 3 hours. The similarity of the 3-hour and 24.5-hour samples demonstrates that the transformation products remain stable, with minimal changes occurring between these timepoints.

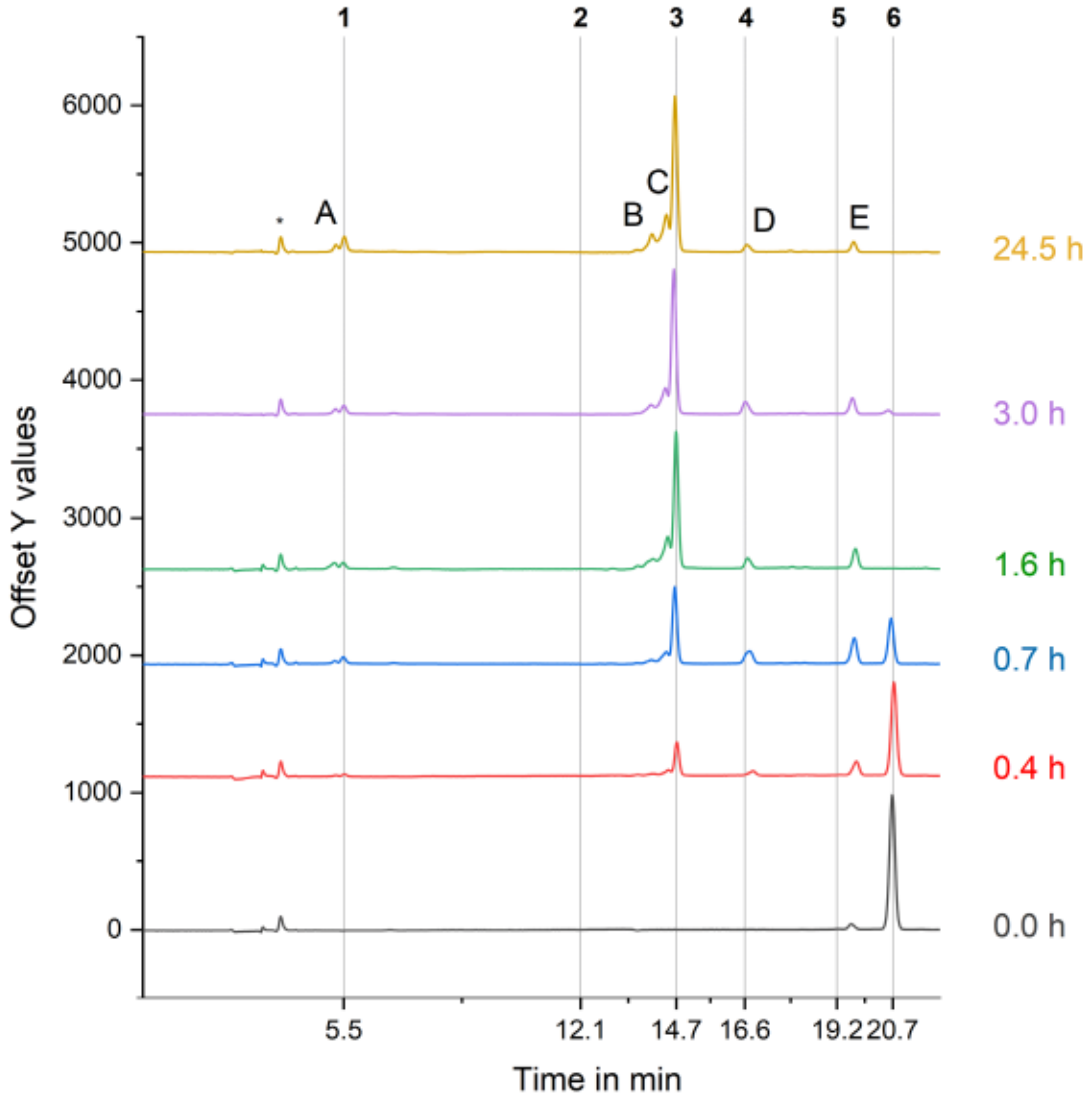

Figure 3.8 Stacked chromatograms of five different sampling points from the DTPMP transformation experiment (aqueous phase) with MnO_2 shown after blank subtraction. The respective time in hours is denoted next to each

chromatogram. The numbers denote the following compounds: 1 = AMPA, 2 = Glyphosate, 3 = IDMP, 4 = ATMP, 5 = EDTMP, 6 = DTPMP. The asterisk denotes the injection peak. Unknown TPs formed are labeled with letters. Optimized chromatographic and amperometric parameters as described in the caption of Figures 3.2 and 3.5 3) were employed.

IDMP and AMPA were identified by RT assignment and standard addition (see Figure C.14 & 15). However, the identification via standard addition is not a definite identification and thus needs to be verified by either plausibility and/or by identification methods such as IC-MS/MS. IDMP and AMPA are well-described as APP transformation products in literature[7,12,15] and are thus plausible and expected. In addition, AMPA has been identified using LC-MS/MS[16]. Contrary, the positive result of the ATMP standard addition (Figure C.15) illustrates the deficiency of this approach as the formation of ATMP (which would require a C-P bond formation) can be excluded in the conducted experiment. Thus, this peak represents a different compound coeluting with ATMP, probably also exhibiting 3-4 phosphonate groups.

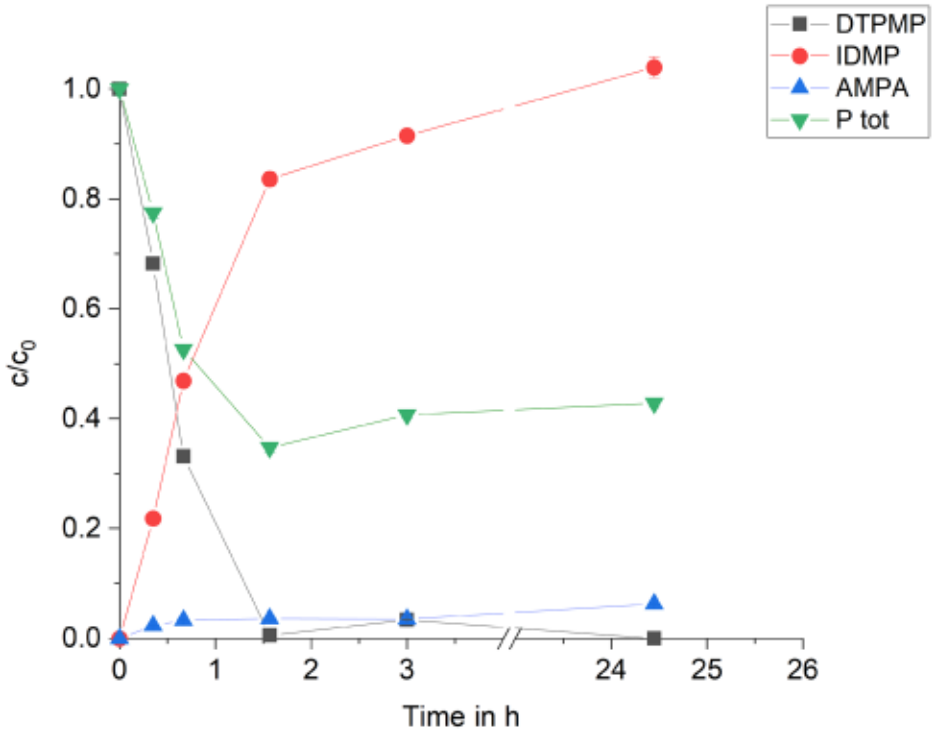

Figure 3.9 Total concentration profiles of DTPMP, IDMP, and AMPA normalized to the initial DTPMP concentration during DTPMP oxidation by MnO_2 using 0.1 g/L MnO_2 at pH 6 in an anoxic environment. "P tot" represents the phosphorus mass balance, which includes total P from all quantified compounds. Error bars represent standard deviations of triple measurements. Optimized chromatographic and amperometric parameters as described in the caption of Figures 3.2 and 3.5 3) were employed.

Finally, the concentration profiles of the identified compounds DTPMP, IDMP, and AMPA versus time were plotted. Figure 3.9 shows the total concentrations (aqueous + sorbed) of the three

compounds and the weighted phosphorus mass balance (P_{tot}). The highest standard deviation was found for IDMP after 24.5 h (σ = 10.54 µM, σ_r = 1.1 %). The weighted P_{tot} including DTPMP, IDMP, and AMPA amounts to 37.1 ±0.5 % at the end of the experiment.

Thus, the developed method i) gives a good overview of the formed (electroactive) transformation products and ii) allows the accurate quantification of TPs using external calibration with standards.

Other unknown transformation products showing a signal on the detector (A-E) could tentatively be identified by the respective standards and ultimately by high-resolution mass spectrometry (HRMS). For the determination of orthophosphate and other non-electroactive compounds different analytical methods are required.

3.5 Conclusion

The IC-IPAD method developed in this study represents a cost-effective and green method for the simultaneous quantification and monitoring of APPs and their transformation products in transformation studies. The method is suitable for the intended application of APP quantification in laboratory experiments and allows the monitoring of the environmentally relevant transformation products AMPA, glyphosate, and IDMP. This was demonstrated for a DTPMP transformation experiment with MnO_2. MDLs between 0.014 µM (AMPA) and 0.104 µM (DTPMP) were achieved, while external calibration showed excellent linearity from 0.05 to 20 µM. This new method is superior in terms of environmental friendliness due to low energy consumption, elimination of any derivatization reactions and organic solvents in the mobile phase, and better simultaneous quantification of six analytes. However, unambiguous identification of unknown analytes and differentiation of coeluting compounds is not possible with this method due to the inherent limitations of the detection employed. If structural elucidation is required, the separation system could be hyphenated with tandem HRMS using a membrane suppressor system, while quantification could be performed using the method presented here. Future integration of green APP extraction methods could enhance the method's sensitivity in complex environmental matrices, potentially extending its application range to natural samples.

3.6 References

(1) Rott, E.; Steinmetz, H.; Metzger, J. W. Organophosphonates: A Review on Environmental Relevance, Biodegradability and Removal in Wastewater Treatment Plants. *Science of The Total Environment* **2018**, *615*. https://doi.org/10.1016/j.scitotenv.2017.09.223.

(2) Studnik, H.; Liebsch, S.; Forlani, G.; Wieczorek, D.; Kafarski, P.; Lipok, J. Amino Polyphosphonates - Chemical Features and Practical Uses, Environmental Durability and Biodegradation. *N Biotechnol* **2015**, *32* (1), 1–6. https://doi.org/10.1016/j.nbt.2014.06.007.

(3) Wang, S.; Sun, S.; Shan, C.; Pan, B. Analysis of Trace Phosphonates in Authentic Water Samples by Pre-Methylation and LC-Orbitrap MS/MS. *Water Res* **2019**, *161*, 78–88. https://doi.org/10.1016/j.watres.2019.05.099.

(4) Industrieverband Körperpflege- und Waschmittel e.V. *Nachhaltigkeit in Der Wasch-, Pflege- Und Reinigungsmittelbranche in Deutschland*; 2021. https://www.ikw.org/fileadmin/IKW_Dateien/downloads/Haushaltspflege/2021_IKW_Nachhaltigkeitsbericht.pdf (accessed 2024-06-11).

(5) Nowack, B. The Behavior of Phosphonates in Wastewater Treatment Plants of Switzerland. *Water Res* **1998**, *4* (12), 1271–1279.

(6) Nowack, B. Aminopolyphosphonate Removal during Wastewater Treatment. *Water Res* **2002**, *36*, 4636–4642.

(7) Nowack, B.; Stone, A. T. Degradation of Nitrilotris(Methylenephosphonic Acid) and Related (Amino)Phosphonate Chelating Agents in the Presence of Manganese and Molecular Oxygen. *Environ Sci Technol* **2000**, *34* (22), 4759–4765. https://doi.org/10.1021/es0000908.

(8) Nowack, B.; Stone, A. T. Homogeneous and Heterogeneous Oxidation of Nitrilotrismethylenephosphonic Acid (NTMP) in the Presence of Manganese(II, III) and Molecular Oxygen. *Journal of Physical Chemistry B* **2002**, *106* (24), 6227–6233. https://doi.org/10.1021/jp014293+.

(9) Nowack, B.; Stone, A. T. Manganese-Catalyzed Degradation of Phosphonic Acids. *Environ Chem Lett* **2003**, *1* (1), 24–31. https://doi.org/10.1007/s10311-002-0014-3.

(10) Klinger, J.; Lang, M.; Sacher, F.; Brauch, H. J.; Maier, D.; Worch, E. Formation of Glyphosate and AMPA during Ozonation of Waters Containing

Ethylenediaminetetra(Methylenephosphonic Acid). *Ozone Sci Eng* **1998**, *20* (2), 99–110. https://doi.org/10.1080/01919519808547279.

(11) Marks, R. G. H.; Rockel, S. P.; Kerpen, K.; Somnitz, H.; Martin, P. R.; Jochmann, M. A.; Schmidt, T. C. Effects of PH-Dependent Speciation on the Photolytic Degradation Mechanism of Phosphonates. *J Photochem Photobiol A Chem* **2023**, 115327. https://doi.org/10.1016/j.jphotochem.2023.115327.

(12) Marks, R. G. H.; Drees, F.; Rockel, S.; Kerpen, K.; Jochmann, M. A.; Schmidt, T. C. Mechanistic Investigation of Phosphonate Photolysis in Aqueous Solution by Simultaneous LC-IRMS and HRMS Analysis. *J Photochem Photobiol A Chem* **2023**, *439*, 114582. https://doi.org/10.1016/j.jphotochem.2023.114582.

(13) Lesueur, C.; Pfeffer, M.; Fuerhacker, M. Photodegradation of Phosphonates in Water. *Chemosphere* **2005**, *59* (5). https://doi.org/10.1016/j.chemosphere.2004.10.049.

(14) Kuhn, R.; Jensch, R.; Bryant, I. M.; Fischer, T.; Liebsch, S.; Martienssen, M. Photodegradation of Ethylenediaminetetra(Methylenephosphonic Acid) – The Effect of the System Configuration. *J Photochem Photobiol A Chem* **2020**, *388*. https://doi.org/10.1016/j.jphotochem.2019.112192.

(15) Kuhn, R.; Jensch, R.; Bryant, I. M.; Fischer, T.; Liebsch, S.; Martienssen, M. The Influence of Selected Bivalent Metal Ions on the Photolysis of Diethylenetriamine Penta(Methylenephosphonic Acid). *Chemosphere* **2018**, *210*, 726–733. https://doi.org/10.1016/j.chemosphere.2018.07.033.

(16) Röhnelt, A.; Martin, P.; Athmer, M.; Bieger, S.; Buchner, D.; Karst, U.; Huhn, C.; Schmidt, T.; Haderlein, S. Glyphosate Is a Transformation Product of a Widely Used Aminopolyphosphonate Complexing Agent [Preprint in Review]. *Nat Commun* **2024**. https://doi.org/10.21203/rs.3.rs-4692988/v1.

(17) Venditti, S.; Kiesch, A.; Hansen, J. Fate of Glyphosate and Its Metabolite AminoMethylPhosponic Acid (AMPA) from Point Source through Wastewater Sludge and Advanced Treatment. *Chemosphere* **2023**, *340*, 139843. https://doi.org/10.1016/j.chemosphere.2023.139843.

(18) Schwientek, M.; Rügner, H.; Haderlein, S. B.; Schulz, W.; Wimmer, B.; Engelbart, L.; Bieger, S.; Huhn, C. Glyphosate Contamination in European Rivers Not from Herbicide

Application? *Water Res* **2024**, *263*, 122140. https://doi.org/10.1016/j.watres.2024.122140.

(19) Keith, L. H.; Gron, L. U.; Young, J. L. Green Analytical Methodologies. *Chemical Reviews*. June 2007, pp 2695–2708. https://doi.org/10.1021/cr068359e.

(20) Tobiszewski, M. Metrics for Green Analytical Chemistry. *Analytical Methods* **2016**, *8* (15), 2993–2999. https://doi.org/10.1039/c6ay00478d.

(21) Tobiszewski, M.; Marć, M.; Gałuszka, A.; Namieśnik, J. Green Chemistry Metrics with Special Reference to Green Analytical Chemistry. *Molecules* **2015**, *20* (6), 10928–10946. https://doi.org/10.3390/molecules200610928.

(22) Armenta, S.; Garrigues, S.; de la Guardia, M. Green Analytical Chemistry. *Trends in Analytical Chemistry* **2008**, *27* (6), 497–511. https://doi.org/10.1016/j.trac.2008.05.003.

(23) Rani, A.; Singh, H.; Kaur, G.; Singh, J. Introduction to Green Analytical Chemistry. In *Green Chemical Analysis and Sample Preparations*; Springer International Publishing: Cham, 2022; pp 1–27. https://doi.org/10.1007/978-3-030-96534-1_1.

(24) Pena-Pereira, F.; Wojnowski, W.; Tobiszewski, M. AGREE - Analytical GREEnness Metric Approach and Software. *Anal Chem* **2020**, *92* (14), 10076–10082. https://doi.org/10.1021/acs.analchem.0c01887.

(25) Fürhacker, M.; Lesueur, C.; Pfeffer, M.; Köllensperger, G.; Popp, M.; Mentler, A. *Phosphonate - AMPA (Aminomethylphosphonsäure). Herkunftsabschätzung, Umweltkonzentrationen Und Photolyseabbau*; Vienna, 2005.

(26) Schmidt, C. K.; Raue, B.; Brauch, H. J.; Sacher, F. Trace-Level Analysis of Phosphonates in Environmental Waters by Ion Chromatography and Inductively Coupled Plasma Mass Spectrometry. *Int J Environ Anal Chem* **2014**, *94* (4), 385–398. https://doi.org/10.1080/03067319.2013.831410.

(27) Klinger, J.; Sacher, F.; Brauch, H.-J.; Maier, D. Determination of Organic Phosphonates in Aqueous Samples Using Liquid Chromatography/ Particle-Beam Mass Spectrometry. *Acta hydrochim. hydrobiol.* **1997**, *25* (2), 79–86.

(28) Armbruster, D.; Rott, E.; Minke, R.; Happel, O. Trace-Level Determination of Phosphonates in Liquid and Solid Phase of Wastewater and Environmental Samples by

IC-ESI-MS/MS. *Anal Bioanal Chem* **2019**, *412* (20), 4807–4825. https://doi.org/10.1007/s00216-019-02159-5.

(29) Weiss, J.; Hägele, G. Lonen-Chromatographische Analyse Anorganischer Und Organischer Komplexbildner. *Fresenius Z Anal Chem* **1987**, *348*, 46–50.

(30) Nowack, B. Determination of Phosphonates in Natural Waters by Ion-Pair High-Performance Liquid Chromatography. *J Chromatogr A* **1997**, *773*, 139–146.

(31) Nowack, B.; Stone, A. T. The Influence of Metal Ions on the Adsorption of Phosphonates onto Goethite. *Environ Sci Technol* **1999**, *33* (20), 3627–3633. https://doi.org/10.1021/es9900860.

(32) Popov, K.; Rönkkömäki, H.; J Lajunen, L. H. Critical Evaluation of Stability Constants of Phosphonic Acids (IUPAC Technical Report). *Pure Appl. Chem.* **2001**, *73* (10), 1641–1677.

(33) Nowack, B. Environmental Chemistry of Phosphonates. *Water Res* **2003**, *37* (11), 2533–2546. https://doi.org/10.1016/S0043-1354(03)00079-4.

(34) Tewari, M.-J. K.; van Stroe-Bieze, S. Analysis of Amine-Containing Phosphonates in Detergent Powders by Anion-Exchange Chromatography with Pulsed Amperometric Detection. *J Chromatogr A* **1997**, *771*, 155–161.

(35) Armbruster, D.; Müller, U.; Happel, O. Characterization of Phosphonate-Based Antiscalants Used in Drinking Water Treatment Plants by Anion-Exchange Chromatography Coupled to Electrospray Ionization Time-of-Flight Mass Spectrometry and Inductively Coupled Plasma Mass Spectrometry. *J Chromatogr A* **2019**, *1601*, 189–204. https://doi.org/10.1016/j.chroma.2019.05.014.

(36) Ibáñez, M.; Pozo, Ó. J.; Sancho, J. V.; López, F. J.; Hernández, F. Residue Determination of Glyphosate, Glufosinate and Aminomethylphosphonic Acid in Water and Soil Samples by Liquid Chromatography Coupled to Electrospray Tandem Mass Spectrometry. *J Chromatogr A* **2005**, *1081* (2), 145–155. https://doi.org/10.1016/j.chroma.2005.05.041.

(37) Hanke, I.; Singer, H.; Hollender, J. Ultratrace-Level Determination of Glyphosate, Aminomethylphosphonic Acid and Glufosinate in Natural Waters by Solid-Phase Extraction Followed by Liquid Chromatography–Tandem Mass Spectrometry:

Performance Tuning of Derivatization, Enrichment and Detection. *Anal Bioanal Chem* **2008**, *391* (6), 2265–2276. https://doi.org/10.1007/s00216-008-2134-5.

(38) Poiger, T.; Buerge, I. J.; Bächli, A.; Müller, M. D.; Balmer, M. E. Occurrence of the Herbicide Glyphosate and Its Metabolite AMPA in Surface Waters in Switzerland Determined with On-Line Solid Phase Extraction LC-MS/MS. *Environmental Science and Pollution Research* **2017**, *24* (2), 1588–1596. https://doi.org/10.1007/s11356-016-7835-2.

(39) Pinto, E.; Soares, A. G.; Ferreira, I. M. P. L. V. O. Quantitative Analysis of Glyphosate, Glufosinate and AMPA in Irrigation Water by in Situ Derivatization–Dispersive Liquid–Liquid Microextraction Combined with UPLC-MS/MS. *Analytical Methods* **2018**, *10* (5), 554–561. https://doi.org/10.1039/C7AY02722B.

(40) Alonso, B.; Griffero, L.; Bentos Pereira, H.; Pareja, L.; Pérez Parada, A. Determination of Glyphosate and AMPA in Freshwater and Soil from Agroecosystems by 9-Fluorenylmethoxycarbonyl Chloride Derivatization and Liquid Chromatography - Fluorescence Detection and Tandem Mass Spectrometry. *MethodsX* **2022**, *9*, 101730. https://doi.org/10.1016/j.mex.2022.101730.

(41) Piriyapittaya, M.; Jayanta, S.; Mitra, S.; Leepipatpiboon, N. Micro-Scale Membrane Extraction of Glyphosate and Aminomethylphosphonic Acid in Water Followed by High-Performance Liquid Chromatography and Post-Column Derivatization with Fluorescence Detector. *J Chromatogr A* **2008**, *1189* (1–2), 483–492. https://doi.org/10.1016/j.chroma.2008.01.074.

(42) Läubli, M.; Brand, B.; Aeschlimann, A.; Zierfels, G. *Glyphosat Und AMPA in Trinkwasser [White Paper]*; 2016. https://www.metrohm.com/de_de/applications/whitepaper/wp-010.html (accessed 2024-11-04).

(43) Wimmer, B.; Pattky, M.; Zada, L. G.; Meixner, M.; Haderlein, S. B.; Zimmermann, H. P.; Huhn, C. Capillary Electrophoresis-Mass Spectrometry for the Direct Analysis of Glyphosate: Method Development and Application to Beer Beverages and Environmental Studies. *Anal Bioanal Chem* **2020**, *412* (20), 4967–4983. https://doi.org/10.1007/s00216-020-02751-0.

(44) Chen, M. X.; Cao, Z. Y.; Jiang, Y.; Zhu, Z. W. Direct Determination of Glyphosate and Its Major Metabolite, Aminomethylphosphonic Acid, In Fruits and Vegetables by Mixed-Mode Hydrophilic Interaction/Weak Anion-Exchange Liquid Chromatography Coupled with

Electrospray Tandem Mass Spectrometry. *J Chromatogr A* **2013**, *1272*, 90–99. https://doi.org/10.1016/j.chroma.2012.11.069.

(45) Fedorowski, J.; LaCourse, W. R. A Review of Pulsed Electrochemical Detection Following Liquid Chromatography and Capillary Electrophoresis. *Anal Chim Acta* **2015**, *861*, 1–11. https://doi.org/10.1016/j.aca.2014.08.035.

(46) LaCourse, W. R. *Pulsed Electrochemical Detection in High Performance Liquid Chromatography*, 1st ed.; Wiley & Sons Ltd: New Jersey, 1997.

(47) Johnson, D. C.; Dobberpuhl, D.; Roberts, R.; Vandeberg, P. Review: Pulsed Amperometric Detection of Carbohydrates, Amines and Sulfur Species in Ion Chromatography-the Current State of Research. *J Chromatogr* **1993**, *640*, 79–96.

(48) Weiss, J. *Handbook of Ion Chromatography*, 4th ed.; Wiley-VCH: Weinheim, 2016.

(49) Röhnelt, A. M.; Martin, P. R.; Buchner, D.; Haderlein, S. B. Transformation of Iminodi(Methylene Phosphonate) on Manganese Dioxides - Passivation of the Mineral Surface by (Formed) Mn2+. *Environ Sci Technol* **2023**, *57* (32), 11958–11966. https://doi.org/10.1021/acs.est.3c01838.

(50) Welch, L. E.; LaCourse, W. R.; Mead, D. A.; Johnson, D. C.; Hu, T. Comparison of Pulsed Coulometric Detection and Potential-Sweep Pulsed Coulometric Detection for Underivatized Amino Acids in Liquid Chromatography. *Anal Chem* **1989**, *61*, 555–559.

(51) US EPA. *Definition and Procedure for the Determination of the Method Detection Limit, Revision 2*; 2016. https://www.epa.gov/sites/default/files/2016-12/documents/mdl-procedure_rev2_12-13-2016.pdf (accessed 2024-01-05).

(52) Slingsby, R.; Pohl, C.; Saini, C. Approaches to Sample Pretreatment in the Determination of Perchlorate in Real World Samples. *Anal Chim Acta* **2006**, *567*, 57–65. https://doi.org/10.1016/j.aca.2006.01.043.

(53) Kim, H. S.; Koo, Y. J.; Lee, M.; Pack, E. C.; Jang, D. Y.; Lee, S. H.; Lim, K. M.; Choi, D. W. An Optimised Method for the Rapid Analysis of Condensed Phosphates in Fishery and Processed Marine Food Products Using Ion Chromatography and Microwave Sample Processing. *Food Additives and Contaminants - Part A* **2020**, *37* (2), 205–215. https://doi.org/10.1080/19440049.2019.1693634.

(54) Rohrer, J.; Avdalovic, N. A Practical Guide for Amino Acid Determinations by High-Performance Anion-Exchange Chromatography with Integrated Pulsed Amperometric Detection. In *Ion Chromatography: Instrumentation, Techniques and Applications*; 2021; Vol. 13, pp 269–286. https://doi.org/10.1016/B978-0-12-813075-9.00013-3.

(55) Martens, D. A.; Loeffelmann, K. L. Automatic Generation of Ultra-Pure Hydroxide Eluent for Carbohydrate Analysis of Environmental Samples. *J Chromatogr A* **2004**, *1039*, 33–37. https://doi.org/10.1016/j.chroma.2003.12.064.

(56) Johnson, D. C.; LaCourse, W. R. Pulsed Electrochemical Detection at Noble Metal Electrodes in Liquid Chromatography. *Electroanalysis* **1992**, *4* (4), 367–380. https://doi.org/10.1002/elan.1140040404.

(57) Jaworska, J.; Van Genderen-Takken, H.; Hanstveit, A.; Van De Plassche, E.; Feijtel, T. Environmental Risk Assessment of Phosphonates, Used in Domestic Laundry and Cleaning Agents in the Netherlands. *Chemosphere* **2002**, No. 47, 655–665.

(58) Gledhill, W. E.; Feijtel, T. C. J. Environmental Properties and Safety Assessment of Organic Phosphonates Used for Detergent and Water Treatment Applications. In *The Handbook of Environmental Chemistry – Detergents*; 1992; pp 261–285. https://doi.org/10.1007/978-3-540-47108-0_8.

(59) Tintrop, L. K.; Salemi, A.; Jochmann, M. A.; Engewald, W. R.; Schmidt, T. C. Improving Greenness and Sustainability of Standard Analytical Methods by Microextraction Techniques: A Critical Review. *Anal Chim Acta* **2023**, *1271*. https://doi.org/10.1016/j.aca.2023.341468.

(60) Lorenzo-Parodi, N.; Kaziur-Cegla, W.; Schmidt, T. C. Automation and Optimization of the Sample Preparation of Aromatic Amines for Their Analysis with GC–MS. *Green Analytical Chemistry* **2023**, *6*. https://doi.org/10.1016/j.greeac.2023.100071.

(61) Mejías, C.; Arenas, M.; Martín, J.; Santos, J. L.; Aparicio, I.; Alonso, E. Green Assessment of Analytical Procedures for the Determination of Pharmaceuticals in Sewage Sludge and Soil. *Crit Rev Anal Chem* **2023**, 1–14. https://doi.org/10.1080/10408347.2023.2276294.

(62) Jonnalagadda, R.; Rathinam, S.; Chandrasekar, V. Development and Greenness Assessment of Analytical Quality by Design Optimised Eco-Friendly UV Spectrophotometric Methods for Analysis of Two Natural Antioxidants in Pure and

Formulation. *Journal of Natural Remedies* **2023**, *23* (4), 1475–1490. https://doi.org/10.18311/jnr/2023/33662.

4 Glyphosate is a transformation product of a widely used aminopolyphosphonate complexing agent

Anna M. Röhnelt[1], Phillipp R. Martin[1,#], Mathis Athmer[2], Sarah Bieger[3], Daniel Buchner[1], Uwe Karst[2], Carolin Huhn[3], Torsten C. Schmidt[4], Stefan B. Haderlein[1]

[1]*Environmental Mineralogy, Center for Applied Geoscience, University of Tübingen, Tübingen, Germany*

[2]*Institute of Inorganic and Analytical Chemistry, University of Münster, Münster, Germany*

[3]*Institute of Physical and Theoretical Chemistry, Department of Chemistry, University of Tübingen, Tübingen, Germany*

[4]*Instrumental Analytical Chemistry and Center for Water and Environmental Research (ZWU), University of Duisburg-Essen, Essen, Germany*

[#]*Current address: Division for Environmental Geosciences, Centre for Microbiology and Environmental Systems Science of Vienna, Vienna, Austria*

Status in the publication process: Manuscript accepted for publication by *Nature Communications*. Resubmitted after revisions at February 11, 2025. Preprint available at https://www.researchsquare.com/article/rs-4692988/v1.

Author Contributions:

A.M.R.: Conceptualization, Methodology, Validation, Formal Analysis, Investigation, Writing – Original Draft, Visualization, Project Administration

P.R.M.: Conceptualization, Methodology, Validation, Funding Acquisition, Writing – Review & Editing

M.A.: Methodology, Investigation, Formal Analysis (all regarding IC-ICP-MS), Writing – Review and Editing

S.B.: Investigation, Formal Analysis (all regarding NMR measurements), Writing – Review and Editing

D.B.: Conceptualization, Funding Acquisition, Writing – Review & Editing

U.K.: Supervision, Writing – Review and Editing

C.H.: Conceptualization, Writing – Review and Editing

T.C.S.: Supervision, Writing – Review and Editing

S.B.H.: Conceptualization, Supervision, Resources, Writing – Review & Editing

4.1 Abstract

We demonstrate that the broad-spectrum herbicide glyphosate is a stable transformation product of diethylenetriamine penta(methylenephosphonate) (DTPMP), a chelating agent widely used in household and industrial applications. Glyphosate was formed at near-neutral pH in buffered ultrapure water and sterile-filtered wastewater, but only in the presence of manganese. Dissolved Mn^{2+} and O_2 or suspended MnO_2 (with and without dissolved O_2) led to glyphosate, that remained stable even after complete DTPMP transformation. Maximum glyphosate yields varied with reaction conditions and ranged from 0.03 to 0.42 mol-%. The ubiquitous presence of manganese in natural and engineered systems underscores the potential importance of Mn-driven DTPMP transformation as a previously overlooked source of glyphosate in aquatic systems. While further research is needed to evaluate the factors controlling the product spectrum and glyphosate yields from DTPMP transformation in technical and natural settings, our results challenge the current paradigm that herbicide application is the sole source of environmental glyphosate contamination. Consequently, current strategies and approaches to protect water resources from glyphosate contamination need to be reconsidered and expanded.

4.2 Introduction

The aminomonophosphonate glyphosate is the most widely used herbicide worldwide[1]. It is a non-selective herbicide, mostly used to kill weeds that compete with crops. Its utilization has significantly increased following the introduction of genetically modified herbicide-tolerant crops, which allowed for extended glyphosate application periods[1,2]. According to the US National Pesticide Information Center (NPIC) the typical half-life of glyphosate is relatively short (1.5 months)[3] but highly variable in soils ranging from few days to several years[4–7]. Environmental persistence of glyphosate is reflected by its frequent detection in ground and surface waters[8–13].

The major transformation product (TP) of glyphosate in the environment is aminomethylphosphonate (AMPA), which exhibits a longer half-life than glyphosate[7,11].

Glyphosate pollution of water bodies so far has exclusively been attributed to herbicide applications[14]. Yet, a recent study revealed negative removal rates for glyphosate and AMPA in municipal wastewater treatment plants[15], while another study highlighted municipal wastewaters as a significant source for glyphosate and AMPA in surface waters in Europe[12]. As the high and rather constant loads of glyphosate and AMPA in wastewater effluents over the year are not compatible with herbicide applications, a different source was suspected[12]. Aminopolyphosphonates (APPs), which are widely used in laundry detergents in the EU[16], are known precursors of aminomethylphosphonate (AMPA)[17–21]. Since the basic structure of glyphosate is already present in certain APPs (see Fig. 4.1), APPs are suspected precursors for glyphosate, too[12,22].

Phosphonate consumption (APPs as well as N-free analogues) in Europe was 49,000 metric tons per year in 2012[16]. Detergents and bleaches are major applications for phosphonates. 7,613 metric tons were used in household detergent and cleaning applications in Germany in 2019[23]. The three commercially most relevant APPs are aminotris(methylene phosphonate) (ATMP), ethylenediaminetetra(methylene phosphonate) (EDTMP) and diethylenetriamine penta(methylene phosphonate) (DTPMP)[16].

While the predominant removal process for DTPMP and other polyphosphonates in wastewater treatment plants (WWTPs) is commonly attributed to sorption onto sewage sludge[16,24,25], recent studies underscore the need to critically examine also the transformation pathways of these compounds[12,15].

Transformation of APPs (photolysis, Mn^{2+}/O_2, MnOOH) with AMPA, iminodi(methylene phosphonate) (IDMP) and phosphate as major TPs (see Fig. 4.1) is well documented in the literature[17–19,26–28]. However, evidence for glyphosate formation is limited to ozonation of EDTMP in drinking water[22] and is lacking under environmentally relevant conditions. The formation of glyphosate from APPs requires the presence of an ethylene moiety on the nitrogen atom of the APP molecule, whose terminal carbon can ultimately be oxidized to a carboxylic acid. Among the high-volume APPs, only EDTMP and DTPMP exhibit this structural feature, the latter one being quantitatively the most significant[29].

Klinger *et al.*[22] proposed a reaction scheme for the formation of glyphosate from EDTMP by ozone, a strong oxidant widely used in water treatment. The authors proposed an aldehyde as an

intermediate after a C-N bond cleavage within the ethylene moiety and further oxidation of this aldehyde to the carboxylic acid required for the formation of glyphosate.[20]

Besides ozone, manganese oxide minerals (MnO_x) are strong oxidizing agents that are important not only in technical systems but also in the environment[30]. They are often formed by microbial oxidation of dissolved Mn^{II}, leading to amorphous structures with high surface areas[30,31]. Manganese minerals are ubiquitous, not only present in soils and sediments but also in substantial concentrations in sewage sludge[32]. The significance of manganese for the oxidation of ATMP and other APPs including DTPMP has early been recognised by Nowack & Stone[27,28,33]. Recently, the transformation of IDMP by manganese dioxide was investigated in detail revealing AMPA and PO_4^{3-} as main TPs[26]. The transient formation of *N*-formyl-AMPA (F-AMPA) suggests oxidation of the terminal carbon of an *N*-methyl-AMPA intermediate to an aldehyde after C–P bond cleavage of IDMP. In analogy to the oxidation of EDTPM by ozone, further oxidation of this terminal carbon might lead to the carboxylic acid – in this case with a methylene moiety as IDMP is the precursor.

Therefore, it is conceivable that manganese oxide minerals or dissolved manganese may lead to glyphosate formation from APPs bearing an ethylene moiety (see Fig. 4.1) in technical and environmental systems.

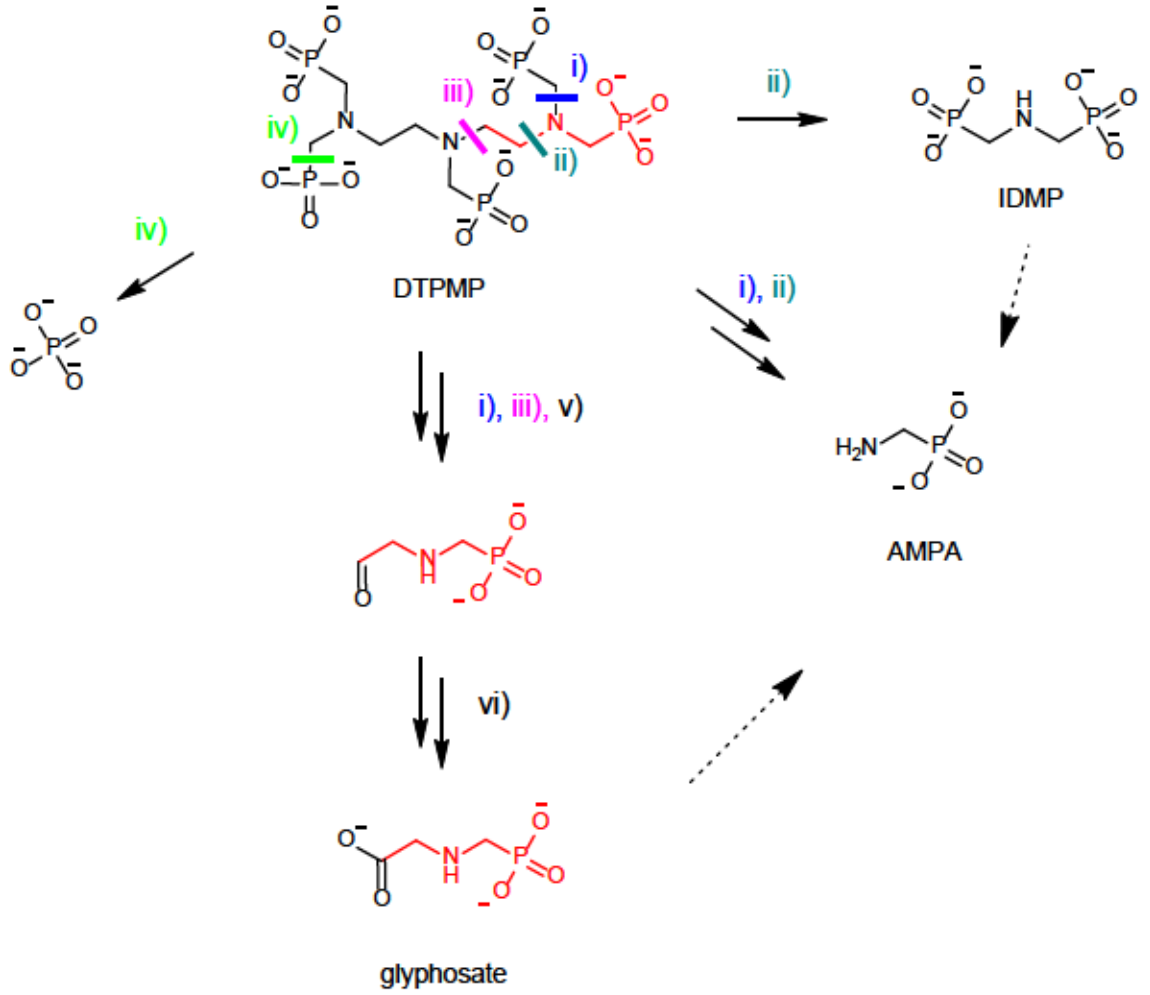

Figure 4.1 Schematic representation of the formation of phosphate, AMPA, IDMP and glyphosate (proposed) from DTPMP. Phosphate can form via one C-P bond cleavage (iv), IDMP is formed via one C-N bond cleavage (ii), while AMPA is formed via two C-N bond cleavages (i, ii). We propose one pathway for the formation of glyphosate from DTPMP via two C-N bond cleavages (i, iii) and oxidation of the terminal C first to the aldehyde (v) and then to the carboxylic acid (vi). The symmetry of the DTPMP molecule, which contains five phosphonate groups, allows multiple equivalent bond cleavages to lead to the same resultant product. For clarity, only one representative option for each potential cleavage is illustrated. All compounds are depicted in their fully deprotonated forms.

Here, we present the results of systematic laboratory experiments on the formation of glyphosate and AMPA as TPs of DTPMP oxidation by manganese dioxide and dissolved manganese and oxygen. The study was designed to capture relevant environmental conditions regarding pH and the presence or absence of dissolved oxygen.

4.3 Results & Discussion

We report the results of laboratory batch experiments designed to elucidate the effects of MnO_2 mineral concentrations (0.1 g/L vs. 1 g/L), dissolved Mn^{2+} (1 mM) and the presence or absence of O_2 (atmosphere/21 vol.-% O_2 vs N_2 atmosphere) on the transformation of 1 mM DTPMP. The experiments were carried out in purified water (buffered at pH 6) as well as in sterile-filtered wastewater (pH 8) as matrix. The pH values were monitored and are depicted in Figure D.1. Control experiments without manganese oxides or dissolved Mn^{2+} generally showed no reactivity towards DTPMP (see Supplementary Figure D.2).

DTPMP transformation by manganese at pH 6

In aqueous solution buffered at pH 6, DTPMP was completely transformed by MnO_2 within ≤ 24 h under all conditions studied (see Fig. 4.2). With 1.0 g/L MnO_2 under oxic conditions (fastest reaction kinetics), complete DTPMP transformation was observed after 20 min, while for 0.1 g/L MnO_2 under anoxic conditions (slowest reaction kinetics) complete DTPMP transformation was observed after 24 hours. Under oxic conditions with 1 mM Mn^{2+} the slowest transformation kinetics of DTPMP were observed and complete DTPMP transformation was reached only after >130 hours (see Fig. D.3).

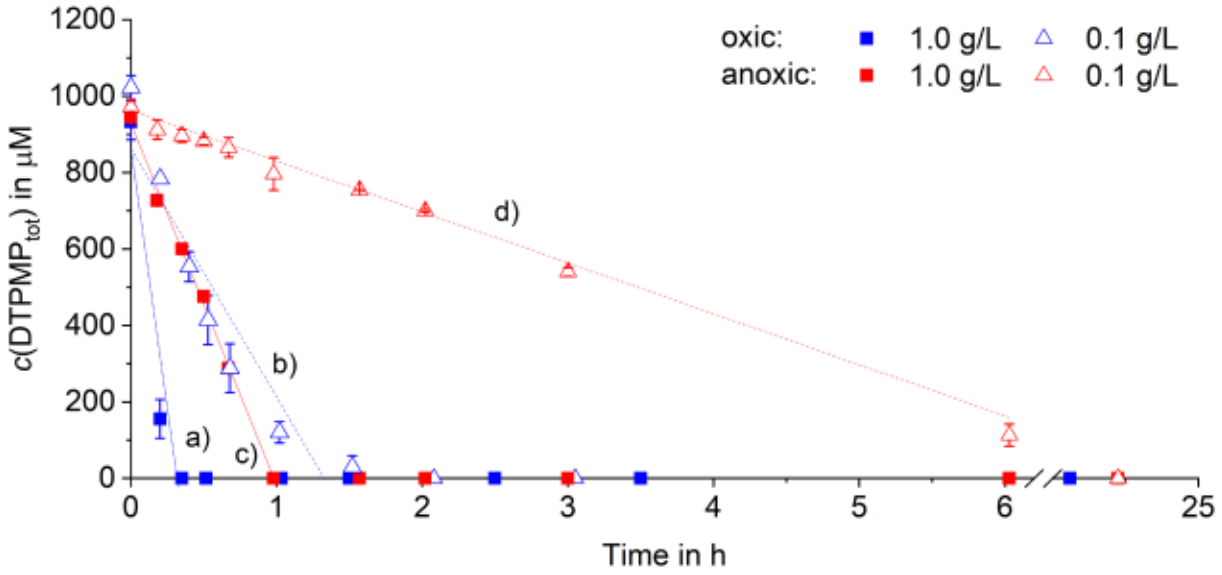

Figure 4.2 Total (aqueous and sorbed) DTPMP concentrations quantified using IC-PAD as a function of time and pseudo-first order fits (see Table 4.1) for all four experiments with MnO_2 in aqueous MES buffer (pH 6) a) 1.0 g/L MnO_2 oxic conditions, b) 0.1 g/L MnO_2 oxic conditions, c) 1.0 g/L MnO_2 anoxic conditions, d) 0.1 g/L MnO_2 anoxic conditions. Error bars represent absolute errors between experimental duplicates.

To evaluate the DTPMP transformation kinetics, pseudo 0th-order rate constants were determined as no higher reaction order adequately described the kinetics across all four MnO_2 experiments. These constants were derived by linear regression considering the time intervals described in Table 4.1. This approach allowed for a comparative kinetic analysis of the four MnO_2 experiments.

In the absence of dissolved oxygen, the transformation of DTPMP followed a pseudo-0th order rate law with R^2 values of >0.98. The presence of dissolved oxygen accelerated the reaction and changed the rate law as indicated by the deviation from pseudo-0th order kinetics ($R^2 \cong 0.85$). Both MnO_2 concentration and the presence of O_2 concentrations enhanced DTPMP transformation kinetics, with the fastest rates for 1.0 g/L MnO_2 under oxic conditions, followed by 1.0 g/L MnO_2 under anoxic conditions. Both experiments (oxic and anoxic) containing 0.1 g/L MnO_2 exhibited slower reaction kinetics than 1.0 g/L, while the reaction containing 0.1 g/L under anoxic conditions showed the slowest reaction. Normalization of the reaction rate constants to the specific surface area (k_{norm}) provided further insights into the role of oxygen and available surface area. k_{norm}-values showed that the oxic experiments were faster compared to their anoxic counterparts.

The rate enhancing role of oxygen may be related to multiple processes involving different redox states of manganese as reported in literature. Under oxic conditions, Mn^{2+} (formed by the reduction of Mn^{IV} [26,30]) is known to catalyze DTPMP (and ATMP, EDTMP) oxidation by O_2 (Mn^{2+}/O_2) in homogeneous solution[28,34]. However, the much slower reaction kinetics of DTPMP in homogeneous solution (1 mM Mn^{2+} and O_2) compared to the heterogeneous systems found in this study clearly show that the strongly enhancing role of O_2 in MnO_2 experiments must be due to processes other than mere Mn^{2+}/O_2 interaction, probably involving the formation of Mn^{III} on the mineral surface.

Manganese minerals with elevated Mn^{III} content appear to be more reactive oxidants [30,35,36]. In heterogeneous systems containing Mn^{2+} and MnO_2, Mn^{III} can be formed by comproportionation and be associated with the mineral surface or reside in solution[35]. Furthermore, MnO_2 can catalyze the oxidation of Mn^{II} by O_2 to Mn^{III} [37]. Finally, MnO_2 itself may act as a direct oxidant but also as a catalyst in connection with O_2 [38].

Previous research on IDMP transformation using the same sample of MnO_2 demonstrated that roughly two electrons are accepted by MnO_2 per transformation of one IDMP molecule[26]. Thus, the electron-accepting capacity of 0.1 g/L MnO_2, which corresponds to 1.1 mM MnO_2, cannot explain the complete transformation of 1 mM DTPMP to smaller transformation products, which

are partially further oxidized. Moreover, as normalized reaction rate constants both under oxic and anoxic conditions were higher for low mineral concentrations (0.1 g/L vs. 1.0 g/L) a catalytic role of MnO_2 next to its direct oxidation activity is evident.

Table 4.1 Pseudo-0th order reaction rate constants (k) and those reaction rate constants normalized to the surface area (k_{norm}) for DTPMP transformation in the four experiments with MnO_2 in MES buffer. The standard errors of the linear regression are given as ±x. R^2 is the regression coefficient of the linear regression from the start of the experiment until complete DTPMP transformation (24 h excluded for 0.1 g/L anoxic due to low data point density). The linear section indicates the time interval/timepoints included in the linear regression.

c(MnO_2)	**1.0 g/L**	**0.1 g/L**	**1.0 g/L**	**0.1 g/L**
O_2	**oxic**	**oxic**	**anoxic**	**anoxic**
k in µM/h	2729 ± 800	650 ± 106	946 ± 26	133 ± 3
k_{norm} in µmol/(m^2*h)	42 ± 12	101 ± 16	14.7 ± 0.4	20.6 ± 0.5
R^2	0.842	0.859	0.996	0.988
Linear section in h	0-0.35	0-1.5	0-0.67	0-6.0

Formation of TPs from DTPMP

During DTPMP transformation, the formation of various phosphorus-containing TPs was monitored in the aqueous phase using ion chromatography (IC) coupled to inductive-coupled plasma mass spectrometry (ICP-MS). Figure 4.3 shows an exemplary chromatogram (1 g/L MnO_2, anoxic conditions, reaction time of 2 h, aqueous phase) next to a mix-standard of 30 ppb P (0.97 µM) per compound. The main TPs identified based on retention times and reference compounds in all experiments were IDMP and phosphate, consistent with previous studies[16–18,28]. Based on the initial DTPMP concentration, IDMP formation reached up to 97 mol-% (0.1 g/L MnO_2, anoxic conditions), while PO_4^{3-} formation peaked at 153 mol-% (1.0 g/L MnO_2, oxic conditions). Regarding phosphate, the maximum molar yield amounts to 500 mol-%, due to DTPMP's five phosphonate moieties. DTPMP, IDMP, and PO_4^{3-} concentrations over time in the aqueous phase are depicted in Supplementary Figure D.4.

In the exemplary chromatogram shown in Figure 4.3, a double peak is visible at the retention time of AMPA (83.0 s), while a triple peak is observed around the retention time of glyphosate (167.5 s). Both peaks, even if considered to be the respective compounds, were below the instrumental LODs (0.9 ppb P for AMPA and 1.7 ppb P for glyphosate) and therefore represent an almost negligible fraction within the TP spectrum. Thus, it is not surprising that the formation of glyphosate has so far been mostly overlooked.

To verify glyphosate and AMPA formation during DTPMP transformation, we used FMOC derivatization and subsequent quantification by means of reversed-phase high-performance liquid chromatography (RP-HPLC) coupled to a triple-quadrupole (QQQ) mass spectrometer, an established trace analysis method for glyphosate and AMPA[39–41].

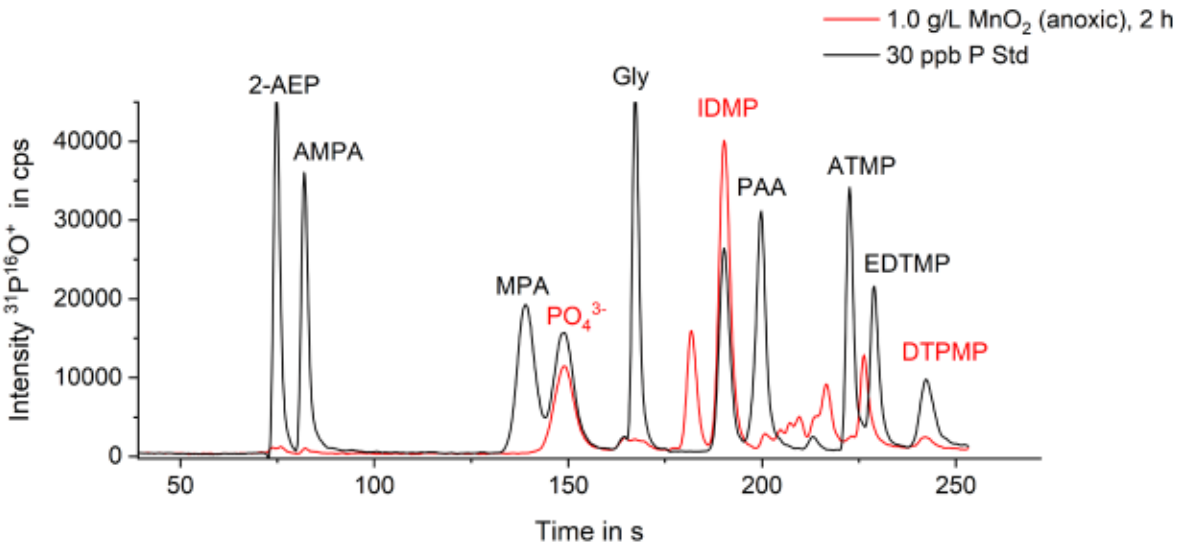

Figure 4.3 Phosphorus-selective IC-ICP-MS chromatogram of the aqueous fraction of duplicate A of the experiment containing 1.0 g/L MnO_2 under anoxic conditions, reaction time 2 h (red, see Fig. 4.2 c), overlayed by the chromatogram of a standard mix including the denoted compounds (black, 30 ppb P per compound). The sample was diluted 1:1000 to match the calibration range. Abbreviations for standard compounds not described in the text: 2-AEP = 2-aminoethylphosphonate, MPA = methylphosphonate, PAA = phosphonoacetic acid.

Glyphosate and AMPA formation from DTPMP

The formation of glyphosate as well as AMPA was observed in all experiments with MnO_2 (see Fig. 4.4). While AMPA is the main TP of glyphosate in the environment[7,11,42], the main path for AMPA formation from DTPMP is via two C–N bond cleavages (see Fig. 4.1).

Glyphosate and AMPA yields were calculated in mol-% based on the analyzed initial DTPMP concentration. The maximum molar yields for the experiments conducted at pH 6 within the

timespans presented in Figure 4.4 were 0.16 mol-% (1.6 µM) for glyphosate and 10.13 mol-% (95 µM) for AMPA. Clearly, the concentration of oxygen and MnO_2 affected the glyphosate and AMPA formation kinetics and maximum observable yields.

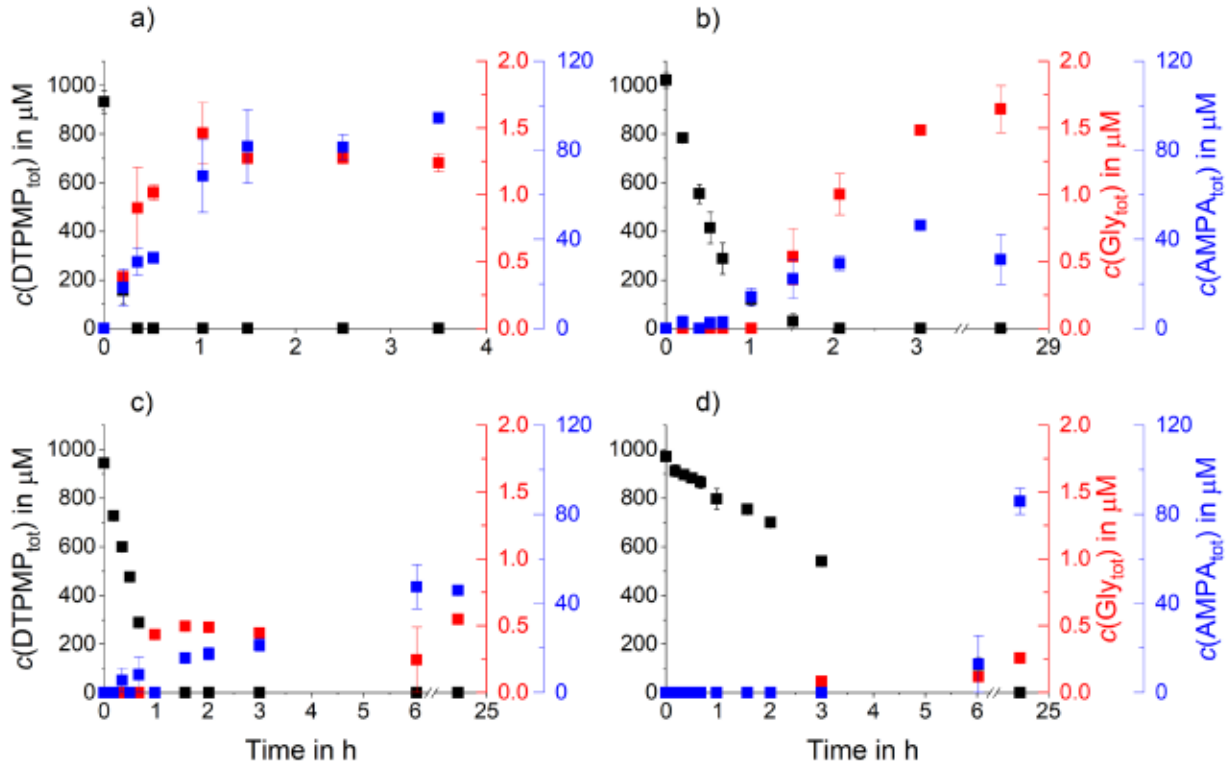

Figure 4.4 Total DTPMP (black), glyphosate (red) and AMPA (blue) concentrations during DTPMP oxidation by MnO_2 in four different experiments in MES buffer (pH 6). DTPMP was quantified using IC-IPAD (see Fig. 4.2), AMPA and glyphosate using LC-QQQ. a) 1.0 g/L MnO_2 oxic, b) 0.1 g/L MnO_2 oxic, c) 1.0 g/L MnO_2 anoxic, d) 0.1 g/L MnO_2 anoxic. Error bars represent absolute errors between experimental duplicates.

Both compounds formed fastest in the presence of 1.0 g/L MnO_2 under oxic conditions (Fig. 4.4a) reaching their maximum concentration after 1 hour. A similar maximum concentration of glyphosate was reached with 0.1 g/L MnO_2 under oxic conditions but only after approximately 28 hours compared to 1 hour (Fig. 4.4b).

With 0.1 g/L MnO_2 under anoxic conditions (Fig. 4.4d) no AMPA was observed within the first four hours. After 6 hours, AMPA was detected in comparably low concentrations around 12 µM increasing up to 98 µM after 24 hours, while a maximum glyphosate yield of 0.3 µM was detected after 24 hours.

Continued glyphosate and AMPA formation after complete DTPMP consumption (see Fig. 4.4 a, b and c) suggests the presence of intermediates that are further transformed to glyphosate and/or AMPA. The presence of such intermediates is further supported by a lag phase before glyphosate and AMPA formation, as observed for 0.1 g/L MnO_2 under oxic conditions (Fig. 4.4 b). Glyphosate and AMPA concentrations only rose after 1.5 and 1 hour, respectively, even though DTPMP was almost completely transformed at that time.

The maximum concentrations of AMPA and glyphosate formed differed between the four experiments (see Table 4.2). Under anoxic conditions, significantly lower glyphosate yields (0.03 and 0.06 mol-%) compared to oxic conditions (both 0.16 mol-%) were observed, either due to lower glyphosate formation or rapid subsequent transformation. However, for AMPA this trend is not discernible (see Table 4.2), potentially due to the numerous reaction pathways leading to AMPA.

To elucidate the significance of heterogeneous (MnO_2) and homogeneous (Mn^{2+}/O_2) oxidation reactions on product formation, an experiment with 1 mM DTPMP and 1 mM dissolved Mn^{2+} ($MnCl_2$) was conducted under oxic conditions (buffered at pH 6). Neither glyphosate nor AMPA formation was observed within the first 24 hours (see Fig. 4.5 a). After 137 hours (approximately 5.5 days), however, 6.3 ± 0.2 mol-% AMPA and 0.06 ± 0.01 mol-% glyphosate were quantified. AMPA and glyphosate concentrations stayed almost constant until 185 h yielding 6.8 ± 0.7 mol-% (AMPA) and 0.07 ± 0.00 mol-% (glyphosate). The oxidation of glyphosate and AMPA on manganese oxides has been extensively studied and both compounds can be oxidized by MnO_x [43–46]. Thus, further investigations are required to better understand the stability and further transformation of glyphosate and AMPA in consecutive reactions.

To account for longer reaction times, the experiment for the most reactive system (1 g/L MnO_2, oxic) was repeated but now sampled over 96 hours (see Supplementary Fig. D.5). AMPA concentrations increased until the end of the experiment and reached a maximum of 206 µM (24 mol-%) after 96 hours (4 days). Glyphosate was detected up to a maximum of 1.1 µM (0.1 mol-%), but no clear trend in concentrations could be deduced.

This experiment demonstrates that AMPA and glyphosate – even in the most reactive suspension after 4 days – are not completely transformed. This is remarkable, as the oxidation of glyphosate and AMPA on manganese oxides has been extensively studied and both compounds can be oxidized by MnO_x [43–46]. Thus, further investigations are required to better understand the stability and further transformation of glyphosate and AMPA in consecutive reactions. The accumulation

of TPs during the experiment creates a complex matrix that may impede the reaction between AMPA or glyphosate and MnO_2. These TPs potentially occupy the mineral surface, reducing the active sites available for further reactions. Two scenarios are consistent with these findings: (i) the built-up of a TP matrix hinders glyphosate and AMPA transformation by diminishing the reactivity of MnO_2 through sorption, or (ii) the rate of glyphosate and AMPA formation exceeds their transformation rate in parallel reactions.

Formation of glyphosate and AMPA from DTPMP in wastewater matrix

To address the environmental relevance of the observations in pure water, experiments containing 1 g/L MnO_2 and 1 mM Mn^{2+} were conducted in wastewater (pH 8, sterile filtrated; see the Methods section for details on the wastewater sample). In control experiments with unspiked wastewater with and without MnO_2 or Mn^{2+}, negligible glyphosate and AMPA concentrations were occasionally detected (see Fig. D.6). Dissolved manganese in the wastewater sample was below the detection limit (<0.04 mg/L).

DTPMP transformation kinetics with 1.0 g/L MnO_2 in the wastewater matrix were slower than in MES buffer at pH 6 (see Fig. D.7 a versus b) in line with a lower oxidation potential of manganese oxides at higher pH[47,48], as well as increased electrostatic repulsion between DTPMP and the mineral surface (point of zero charge of 5.6)[30,49]. Furthermore, differences between the experiments with MES buffer and wastewater are likely due to the complex wastewater-matrix containing organics (such as other complexing agents) and cations (e.g., calcium), which were reported to influence APP transformation and sorption[18,50]. Glyphosate and AMPA yields with 1 g/L MnO_2 in wastewater were up to 0.06 mol-% (glyphosate) and 10.3 mol-% (AMPA) after 168 hours. However, in wastewater spiked with 1 mM Mn^{2+}, DTPMP transformation kinetics were faster and had higher glyphosate and AMPA yields compared to MES-buffered pure water at pH 6 (see Fig. D.5.) In wastewater spiked with 1 mM Mn^{2+}, the highest glyphosate yield (0.42 mol-%) of all experiments conducted in this study was observed (see Table 4.2), albeit only after 240 h. Possibly, the reaction kinetics are faster at pH 8 due to stronger complex formation of Mn^{II} and DTPMP, such as shown for ATMP[28]. At higher pH, less protons compete with metal ions present in solution and DTPMP is more negatively charged[51]. Furthermore, Mn^{III} complexes might play a role at higher pH. While the stability of Mn^{III} complexes varies depending on the ligand, certain ligands including desferrioxamine B show higher stability of Mn^{III} complexes at pH values between 7 and 11[52].

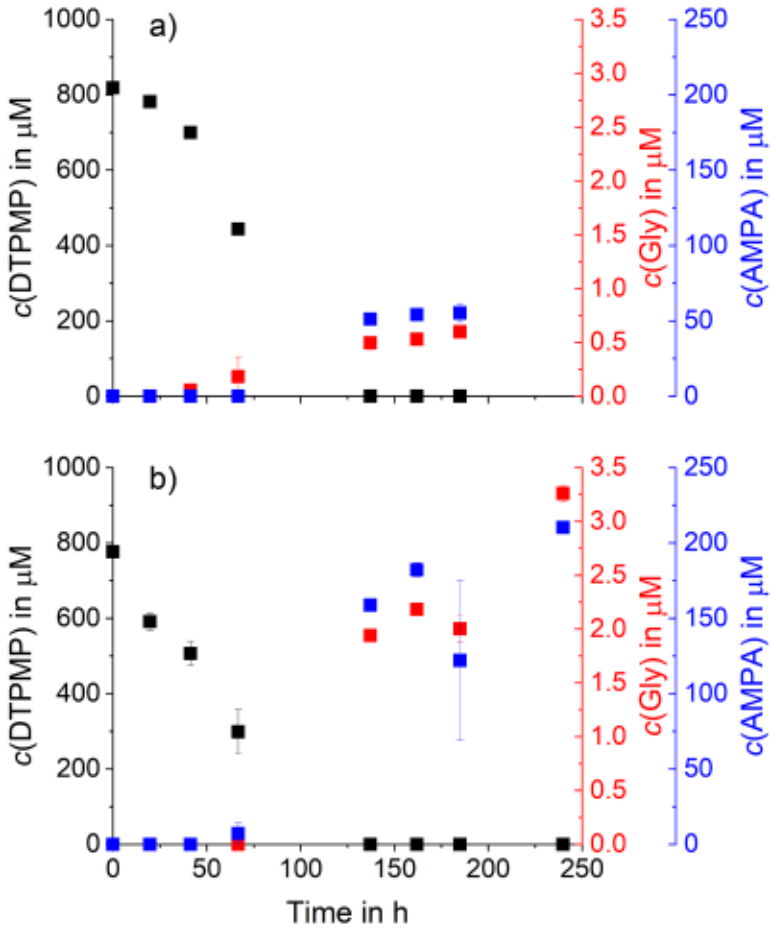

Figure 4.5 DTPMP (black), glyphosate (red) and AMPA (blue) concentrations during oxidation of 1 mM DTPMP by 1 mM Mn^{2+} in the experiments containing **a)** pure 20 mM MES buffer (pH 6) and **b)** wastewater (pH 8) as matrices. DTPMP was quantified using IC-IPAD, glyphosate and AMPA were quantified using LC-QQQ. Error bars represent absolute errors between experimental duplicates.

Table 4.2 Maximum total AMPA and glyphosate yields given in mol-% of the initial quantified DTPMP concentration at the denoted timepoints. Errors for AMPA and glyphosate yields represent absolute errors between duplicates. MES denotes experiments in aqueous 20 mM MES buffer at pH 6, while WW stands for sterile-filtered wastewater at pH 8. The timepoint denotes the time of maximum observed AMPA resp. glyphosate formation.

$c(MnO_2)$ in g/L	$c(Mn^{2+})$ in mM	O_2	Matrix	$AMPA_{max}$ in mol-%	Timepoint in h	Gly_{max} in mol-%	Timpoint in h
1.0	-	oxic	MES	10.1 ± 0.2	3.5	0.16 ± 0.02	1.0
0.1	-	oxic	MES	4.5 ± 0.2	3.0	0.16 ± 0.01	28
1.0	-	anoxic	MES	5.0 ± 1.0	6.0	0.06 ± 0.00	24
0.1	-	anoxic	MES	10.1 ± 0.5	24	0.03 ± 0.00	24
1.0	-	oxic	WW	10.3 ± 0.3	168	0.06 ± 0.01	168
-	1.0	oxic	MES	6.7 ± 0.7	185	0.07 ± 0.00	185
-	1.0	oxic	WW	27.1 ± 0.5	240	0.42 ± 0.01	240

4.4 Conclusion

Polyphosphonates as replacements for polyphosphates and polycarboxylates in detergents, laundry products and other applications have been considered critical due to their persistence. However, they have been accepted in applications because they were not considered toxicologically relevant. Despite their reportedly high recalcitrance attributed to the high stability of the C–P bond[29,53–55], APPs can be transformed in the presence of manganese, which occurs ubiquitously in WWTPs, soils & sediments, yielding phosphate, IDMP and AMPA as major products.

Our study demonstrates that manganese potentially plays a key role in converting the widely used complexing agent DTPMP in a multi-step reaction to the herbicide glyphosate. The reaction proceeds at circumneutral pH at MnO_2 minerals both in the absence and presence of dissolved oxygen but also in homogeneous solution in the presence of Mn^{2+}/O_2, even in wastewater. Under all conditions studied, AMPA and glyphosate were transformation products, AMPA up to 27.1 mol-% and glyphosate up to 0.42 mol-%. Both the kinetics and yield of DTPMP transformation products were heavily influenced by the reaction conditions (MnO_2 concentration and presence of O_2 and pH/matrix). Once DTPMP was completely transformed, the concentrations of

glyphosate and AMPA remained constant or even increased within 1 to 10 days of kinetic experiments. The persistence of glyphosate and AMPA towards the end of the experiment in the presence of excess MnO_2 is remarkable as both compounds can be oxidized by unreacted MnO_2 minerals[42–46].

The comparatively high glyphosate yield of the experiment containing 1 mM Mn^{2+} in wastewater under oxic conditions, relative to all other experiments, underlines the relevance of both MnO_2 and aqueous Mn^{2+} in environmental and technical systems. This finding underlines the relevance of manganese-driven oxidation reactions in glyphosate and AMPA formation from DTPMP. The distribution between Mn^{II} and Mn^{III}/Mn^{IV} species in the environment is known to depend on various conditions such as pH, microbial activity, and O_2 levels[56,57]. Our results demonstrate that both Mn^{II}/O_2 and Mn^{IV} can lead to glyphosate and AMPA formation, suggesting that these processes may occur under a wide range of environmental conditions.

Overall, this study provides experimental evidence for conversion of a widely used non-toxic commodity compound into a highly debated pesticide[1,2,5,58] under environmentally relevant reaction conditions. While we could demonstrate that the reaction is chemically feasible in the laboratory, future research should elucidate in detail how environmental conditions affect glyphosate formation from DTPMP and related APPs, the formation and identification of key intermediates and field studies including yields in wastewater treatment plants.

In addition, our findings may also provide clues for revisiting APP biotransformation studies. All bacterial growth media used in published APP biotransformation studies contain dissolved manganese[55,59–63]. Thus, manganese-driven oxidation may occur in parallel with or instead of biotransformation of DTPMP and other APPs. Martin et al (2022)[34] showed that even at a molar ratio of 1:100 (Mn:ATMP), ATMP was completely degraded within 30 hours. Thus, it is conceivable that in biotransformation studies under oxic conditions in the presence of dissolved Mn^{2+}, microorganisms may utilize chemical transformation products of APPs, such as phosphate, IDMP, or AMPA, as a phosphorus source rather than or in addition to directly metabolizing the target APPs.

Overall, our work offers a scientific basis to rationalize recent and unexpected findings of elevated glyphosate concentrations in European WWTP effluents[12,15] and suggests that manganese may play a crucial role in this phenomenon, potentially serving as a key factor in understanding the underlying processes.

4.5 Methods

Chemicals

All chemicals were purchased from Merck (Darmstadt, Germany) in the highest available purity, if not described differently. The manganese dioxide (Manganese^{IV}oxide, ≥98%; MnO_2, Batch No. 168267405) was has been purchased from Carl Roth (Karlsruhe, Germany). $MnCl_2$ tetrahydrate (p.a., ≥99%) was purchased from Merck (Darmstadt, Germany) The MnO_2 specifications can be found in "Methods – Mineral Characterization" and the Supplementary Information. DTPMP was purchased as solid acid from Zschimmer and Schwarz (Lahnstein, Germany) under the name "Cublen D 900 GR" (CAS: 15827-60-8). In order to ascertain the purity of the DTPMP, a ^{31}P-{^{1}H}-NMR measurement was conducted, showing a purity of >98.6 % regarding P (nuclear magnetic resonance spectroscopy (NMR) measurements, for details, see below). Glyphosate PESTANAL (≥98.0 %), AMPA (99%), IDMP (≥97 %), ATMP (≥97.0 %), 2-aminoethylphosphonic acid (99 %), methylphosphonic acid (99 %) and phosphonoacetic acid (98 %) solids were purchased from Sigma Aldrich (St Louis, MO, USA). EDTMP was purchased as solid acid from Zschimmer and Schwarz (Lahnstein, Germany) under the name "Cublen ELC 950". The purity of EDTMP was determined to be >98.6 % regarding P using ^{31}P-{^{1}H}-NMR (see below). Isotope-labelled glyphosate (i) and AMPA (ii) were purchased from LGC Standards Ltd. (Teddington, England) (i) and HPC Standards GmbH (Cunnersdorf, Germany) (ii). Phosphate standard solution (1000 mg/L PO_4^{3-} in H_2O) for preparation of IC-ICP-MS phosphonate standards was purchased from Merck (Darmstadt, Germany).

Sodium hydroxide for IC-IPAD eluent preparation and analyte desorption from the manganese dioxide was purchased as a 49-51% aqueous solution from Supelco (Merck, Darmstadt, Germany), NaH_2PO_4 (p.a., ≥99%) for analyte desorption from Roth (Karlsruhe, Germany) and sodium acetate trihydrate for IC-IPAD eluent preparation from Chemsolute (Renningen, Germany). 2-(*N*-morpholino)ethanesulfonic acid (MES) buffer (≥99%) for the DTPMP transformation experiments was purchased from Carl Roth. Sodium acetate for IC-IPAD eluent preparation was delivered by Chemsolute (Renningen, Germany).

The cation exchange resin in proton form (Dowex 50 W X 8, 100-200 mesh, ≥1.7 eq/L) used to remove dissolved manganese was purchased from Carl Roth.

The water used for the experiments and IC-PAD measurements was purified by an ultrapure water purification system (Barnstead, GenPure Pro, Thermo Scientific, Waltham, MA, USA) down to a conductivity below 0.06 µS/cm. For IC-ICP-MS analysis (dilutions and eluent preparation),

doubly distilled water from an Aquatron A4000D system (Barloworld Scientific, Nemours, France) was used.

Fluorenylmethoxycarbonyl chloride (FMOC Cl, 98 %) and sodium tetraborate decahydrate (borate, p.a.) used for the derivatization of glyphosate and AMPA were purchased from Carl Roth resp. Honeywell/Fluka (Charlotte, NC, USA). Dichloromethane (DCM, HPLC grade) for washing the derivatized samples was bought from Fisher Scientific (Waltham, MA, USA). For LC analysis with a triple quadrupole mass spectrometer (LC-QQQ) the eluent was prepared using LC/MS-grade acetonitrile (ACN, ≥99.9%) from Honeywell/Riedel-de Haën (Seelze, Germany), LC/MS grade water (Fisher Scientific, Loughborough, UK) and NH4Ac (p.a., ≥98%) from Sigma Aldrich (St Louis, MO, USA).

Nitric acid (HNO_3, 65%, for analysis) for IC-ICP-MS measurements was purchased from Thermo Fisher Scientific (Bremen, Germany) and purified with a DST-1000 acid purification system from Savillex (Eden Prairie, MN, USA). For IC-ICP-MS eluent preparation, aqueous ammonia solution (25-27 %, for trace analysis) was purchased from VWR International LLC (Radnor, PA, USA) and diethylenetriaminepentaacetic acid (DTPA) from Honeywell/Fluka (Charlotte, NC, USA). The IC-ICP-MS post-column internal standard (1000 µg/L indium in 2% aqueous HNO_3) was purchased from Sigma-Aldrich (St. Louis, MO, USA).

Deuterium oxide (D_2O, 99.9 atom% D) for NMR measurements was obtained from Sigma- Aldrich (Steinheim, Germany).

Design of DTPMP transformation experiments

The experiments (duplicates with one control) were conducted in 50 mL centrifugation tubes (polypropylene, Fisher Scientific, Waltham, MA, USA) in the presence of ambient air or in the glovebox (N_2 atmosphere, $c(O_2) < 10$ ppm) (Unilab from MBRAUN, Garching, Germany) at room temperature (21±1 °C). For the glovebox experiments, DTPMP stock solution, MES buffer solution and deionized water were purged with N_2 for one hour under rapid stirring before transfer into the glovebox. Then, DTPMP, MES buffer and water were mixed to yield concentrations of 1 mM DTPMP and 20 mM MES. After mixing, the first aliquot of 5 mL was taken as t_0 sample. Then, solid MnO_2 was added, to reach a concentration of 0.1 or 1.0 g/L. The reaction suspensions were shaken in an overhead-shaker at a speed of 25 rpm. At defined time points derived from pilot tests, a well suspended 4 mL aliquot of the suspension was taken, centrifuged (15 min,

20,000 rcf), and filtered (0.2 µM PES syringe filter, BGB Analytik, Lörrach, Germany)[26]. To desorb residual analytes from the mineral pellet after centrifugation and sampling the supernatant (aqueous phase), the mineral pellet was treated with 0.1 M NaOH and 0.1 M NaH_2PO_4 in the ultrasonic bath for 30 minutes[64]. To account for possible parallel homogenous Mn^{II}-catalyzed oxidation by O_2 initiated by formed Mn^{2+}, an additional experiment with 1 mM $MnCl_2$ (no MnO_2) under oxic conditions was conducted. The experiments using 1.0 g/L MnO_2 and 1 mM Mn^{2+} /O_2 as oxidant/catalyst were repeated in wastewater (pH 8).

The homogeneous reactions were quenched by the addition of cation exchange resin to the aliquot taken from the reaction solution to bind Mn^{2+}.

Samples were stored in the dark at -20 °C until analysis. Prior to analysis, samples were thawed, treated with cation exchange resin (if not done before freezing) and diluted for the respective measurement purpose.

The wastewater was sampled at 10 am on September 9, 2024 from the municipal wastewater treatment plant in Lustnau (Tübingen, SW Germany), after the screen and grit chamber, but before the primary settling tank. The wastewater was then filtered with different filter systems: I) coffee filter (Melitta, Minden, Germany), II) folded filters 595 ½ (Whatman Int. Ltd, Buckinghamshire, UK), III) glass fibre round filters GF 55 (Schleicher & Schuell, Dassel, Germany) and finally IV) sterile S-PAK 0.22 µm filters (Merck, Darmstadt, Germany). This filtered wastewater was used undiluted as matrix for the experiments. The initial pH of the wastewater was 8. The changes in pH development over time are shown in Fig. D.1. Detailed information regarding the composition of the wastewater is provided below.

Quantification of DTPMP

Quantification of DTPMP was performed according to the IC-IPAD (ion chromatography coupled to integrated amperometric detection) method published by Röhnelt *et al.* (2025)[65]. A 930 Compact IC Flex ion chromatograph (Metrohm, Herisau, Switzerland) was used, equipped with an anion exchange column (Dionex IonPac AS16, 2x250 mm, Thermo Fisher Scientific, Waltham, United States), a suitable guard column (Dionex IonPac AG16, 2x50 mm) and an amperometric detector (Wall-Jet Cell, Metrohm). The Wall-Jet cell was equipped with a gold working electrode, a Pt auxiliary electrode and an Ag/AgCl reference electrode (all Metrohm). The detector method potential vs. time profile is depicted in Supplementary Fig. D.8. The dosing units for i) sample

uptake and ii) concentration gradient were both of the type "800 Dosino" (Metrohm), with i) 2 mL and ii) 5 mL cylinder volume.

To prevent CO_2 dissolution into the eluents, an overpressure of 0.5 bar N_2 was applied to both eluent bottles (gas-tight plastic bottles, Metrohm). 15 mM NaOH served as eluent A, while 50 mM NaOH with 400 mM sodium acetate served as eluent B. The gradient profile is depicted in Supplementary Table D.1.

Quantification was performed by external calibration (0.01-20 µM) and normalization to repeatedly injected control standards.

Total DTPMP concentrations were analyzed by combining sorbed and aqueous fractions prior to measuring.

Quantification of AMPA and glyphosate

AMPA and glyphosate were quantified using reversed phase (RP) liquid chromatography (LC) coupled to triple quadrupole mass spectrometry (QQQ-MS) after derivatization using FMOC chloride[39–41]. The sample was diluted 1:2 (glyphosate) respectively 1:100 (AMPA) with ultrapure water and the respective isotope-labelled standard was added to reach a final concentration of 50 µg/L. Then, 10-15 mg of the cation exchange resin were added to 1 mL of the diluted sample and shaken for 30 min. After sedimentation of the resin, 900 µL of the supernatant were sampled and mixed with 200 µL 80 mM borate buffer and 200 µL 40 mM FMOC chloride in acetonitrile. The sample, which turned milky immediately, was let to rest for 30 min. Afterwards, the clear aqueous phase was washed twice using 2 mL DCM, each. The now derivatized samples were stored in the dark at 4 °C until measurement. Repeated measurements showed the stability of the derivatized samples over several months.

The liquid chromatography (1290 Infinity II, Agilent, Santa Clara, CA, USA) was coupled to a triple quadrupole (QQQ) mass spectrometer (6470 LC/TQ, Agilent, Stadt/LAND), equipped with an AJS source. A reversed phase column (Agilent Poroshell 120 EC-C18 2.7 µm, 2.1 x 100 mm + 2.1 x 5 mm pre-column) was used to separate the derivatized compounds. The derivatized analytes were measured in positive ionization mode with a cell accelerator voltage of 5 V.

2.5 mM aqueous ammonium acetate (A) and acetonitrile (B) served as mobile phases. The concentration gradient profile is provided in Supplementary Table D.2. A sample of 1 µL was

injected together with 0.2 µL internal standard (200 µg/L glufosinate-FMOC). The column was heated to 40 °C and the flow rate was set to 0.3 mL/min. The MS parameters and fragment ions used for quantification can be found in Supplementary Table D.3.

Limits of detection (LOD) and quantification (LOQ) were calculated for each measurement sequence based on the standard deviation of the linear response and the slope of the calibration curve (5-200 µg/L (glyphosate), 5-500 µg/L (AMPA), ISTD 50 µg/L each) following the International Council for Harmonisation (ICH) Q2(R1) guideline[66]. Table D.4 provides the LOD/LOQ values derived for every measurement sequence.

The aqueous and sorbed fractions were analyzed separately, with the sorbed fractions representing a minor part of the investigated compounds (see Supplementary Fig. D.9).

Quantification of phosphorus-containing TPs using IC-ICP-MS

For the detection of all phosphorus-containing compounds, a prepFAST IC system (Elemental Scientific, Omaha, NE, USA) was connected to an iCAP TQ inductively coupled plasma mass spectrometer (ICP-MS) (Thermo Fisher Scientific, Bremen, Germany).

The prepFAST IC system was equipped with an anion exchange column CF-Cr-01 (50 × 4 mm) (Elemental Scientific, Omaha, NE, USA) and the injection volume was set to 50 µL. The chromatographic separation was performed with a flow rate of 1000 µL/min and a post-column internal standard flow rate of 100 µL/min indium in 2% nitric acid (1 µg/L). 300 µg/L DTPA in water (pH 9.2) served as eluent A, while eluent B consisted of 150 mM ammonium nitrate with 300 µg/L DTPA in water (pH 9.2). For the chromatographic separation, a five-step gradient was employed, which is described in Supplementary Table D.5.

Analysis was conducted in QQQ mode with oxygen as a reaction gas. Phosphorus was detected as $^{31}P^{16}O^{+}$ and indium as $^{115}In^{+}$ with individual dwell times of 100 ms. Quantification was performed by external calibration. Unknown TPs were quantified using the calibration function of the nearest polyphosphonate standard. The LOD was determined by the 3σ criteria, and the LOQ was determined by the 10σ criteria respectively.

Due to the desorption protocol using 0.1 M NaH_2PO_4 as competitive sorbent, with this method, just the aqueous phase of the heterogenous experiments could be analyzed.

Nuclear Magnetic Resonance Spectroscopy (NMR)

To assure the purity of the DTPMP (EDTMP) purchased commercially, a ^{31}P-{^{1}H}-NMR measurement was conducted (NMR department, Chemistry Department, University of Tübingen). ^{31}P-NMR-spectroscopy is a suitable analytical tool to characterize the purity of phosphonates, due to the 100% natural abundance of ^{31}P and the wide range of chemical shifts and high sensitivity of the method.[67]

10 mg DTPMP (EDTMP) and 600 µL of deuterated water (D_2O) were mixed and vortexed for 5 s. Afterwards, 600 µL were transferred to an NMR glass tube. The measurement was performed on a Bruker AMX 600 MHz NMR spectrometer (Bruker, Billerica, MA, USA), operating at 242.94 MHz for phosphorous observation with a zgpg30 pulse program. The acquisition parameters used for this experiment with 1D sequence with power-gated decoupling and a 30 ° flip angle were as follows: number of scans: 64, spectral width: 96153.84 Hz, offset (O1): -12146.85 Hz, acquisition time: 0.34 seconds, relaxation delay (d1): 2.00 s. The spectrum was quantitatively evaluated using the Bruker Top Spin 4.1.4 software.

DTPMP: in the ^{31}P-{^{1}H}-NMR-spectrum (Fig. D.10), two main signals with an intensity ratio of 1:4 can be seen, which represent the phosphonate-group in the middle of DTPMP (δ (ppm): 12.94) and the four phosphonate groups of DTPMP attached to the outer amine-moieties (δ (ppm): 9.23). Impurities are marked with an asterisk. The sum of all signal-integrals is normalized to 100. Impurities of DTPMP contributed with 1.37 %. Thus, the purity of the DTPMP regarding the P content was >98.6 %.

EDTMP: In the ^{31}P-{^{1}H}-NMR-spectrum of EDTMP, shown in Fig. D.11, we can see one signal attributed to EDTMP representing all chemically equivalent phosphonate-groups (δ (ppm): 8.76). Impurities are marked with an asterisk. The sum of all signal-integrals is normalized to 100. Impurities containing phosphorous of the analyzed EDTMP amount to only 3.40 %. The used EDTMP in the experiments is therefore of high purity with 96.6%.

Mineral Characterization

The point of zero charge (pH_{PZC}) of the manganese dioxide was determined to be pH 5.6 ± 0.1 by zeta potential measurements. The X-ray diffractogram (see Fig. D.12) showed a mostly amorphous structure, interspersed with some crystalline domains (pyrolusite, akhtensite). The

specific surface area (SSA) was determined to be 64.5 ± 0.2 m^2/g using the Brunauer-Emmett-Teller (BET) method. Measurement details as well as further specifications can be found in the Supplementary Information.

Wastewater Characterization

The wastewater sample taken from the WWTP in Lustnau (Tübingen, Germany) on September 9, 2024, had a pH value of 7.94. The dissolved organic carbon (DOC) measured as non-purgeable organic carbon (NPOC), was determined to be 11.6 mg/L. Dissolved iron and manganese concentrations were both below the detection limit of 0.04 mg/L (Mn) and 0.02 mg/L (Fe). Supplementary Table D.6 summarizes the results of the wastewater sample characterization using IC with conductivity detection and MP-AES (for analytical methods see the Supplementary Information). Supplementary Table D.7 contains additional information on a 24h-mixed wastewater sample monitored by the WWTP Lustnau. The sampling point for the latter lies after the screen but before the grit chamber. Due to heavy rainfall the day and night before wastewater sampling the wastewater volume treated in the WWTP in Lustnau (Tübingen, Germany) on September 9, 2024, amounted to ~80 000 m^3/d compared to 25 000 – 30 000 m^3/d on an average dry day.

4.6 References

(1) Benbrook, C. M. How Did the US EPA and IARC Reach Diametrically Opposed Conclusions on the Genotoxicity of Glyphosate-Based Herbicides? *Environ Sci Eur* **2019**, *31* (1). https://doi.org/10.1186/s12302-018-0184-7.

(2) Tarazona, J. V.; Court-Marques, D.; Tiramani, M.; Reich, H.; Pfeil, R.; Istace, F.; Crivellente, F. Glyphosate Toxicity and Carcinogenicity: A Review of the Scientific Basis of the European Union Assessment and Its Differences with IARC. *Arch Toxicol* **2017**, *91* (8), 2723–2743. https://doi.org/10.1007/s00204-017-1962-5.

(3) Henderson, A. M. ; Gervais, J. A. ; Luukinen, B. ; Buhl, K. ; Stone, D. ; Strid, A. ; Cross, A. ;; Jenkins, J. *Glyphosate Technical Fact Sheet*. http://npic.orst.edu/factsheets/archive/glyphotech.html (accessed 2024-06-11).

(4) U.S. Environmental Protection Agency. *Glyphosate Reregistration Eligibility Decision (RED)*; Washington, D.C., 1993. https://www3.epa.gov/pesticides/chem_search/reg_actions/reregistration/red_PC-417300_1-Sep-93.pdf (accessed 2024-06-11).

(5) Caiati, C.; Pollice, P.; Favale, S.; Lepera, M. E. The Herbicide Glyphosate and Its Apparently Controversial Effect on Human Health: An Updated Clinical Perspective. *Endocr Metab Immune Disord Drug Targets* **2019**, *20* (4), 489–505. https://doi.org/10.2174/1871530319666191015191614.

(6) Eberbach, P. Applying Non-Steady-State Compartmental Analysis to Investigate the Simultaneous Degradation of Soluble and Sorbed Glyphosate (N-(Phosphonomethyl)Glycine) in Four Soils. *Pestic Sci* **1998**, *52* (3), 229–240. https://doi.org/10.1002/(SICI)1096-9063(199803)52:3<229::AID-PS684>3.0.CO;2-O.

(7) András Székács; Béla Darvas. Forty Years with Glyphosate. In *Herbicides: Properties, Synthesis and Control of Weeds*; 2012; pp 247–287.

(8) Coupe, R. H.; Kalkhoff, S. J.; Capel, P. D.; Gregoire, C. Fate and Transport of Glyphosate and Aminomethylphosphonic Acid in Surface Waters of Agricultural Basins. *Pest Manag Sci* **2012**, *68* (1), 16–30. https://doi.org/10.1002/ps.2212.

(9) Borggaard, O. K.; Gimsing, A. L. Fate of Glyphosate in Soil and the Possibility of Leaching to Ground and Surface Waters: A Review. *Pest Manag Sci* **2008**, *64* (4), 441–456. https://doi.org/10.1002/ps.1512.

(10) Rendón-Von Osten, J.; Dzul-Caamal, R. Glyphosate Residues in Groundwater, Drinking Water and Urine of Subsistence Farmers from Intensive Agriculture Localities: A Survey in Hopelchén, Campeche, Mexico. *Int J Environ Res Public Health* **2017**, *14* (6). https://doi.org/10.3390/ijerph14060595.

(11) Tresnakova, N.; Stara, A.; Velisek, J. Effects of Glyphosate and Its Metabolite AMPA on Aquatic Organisms. *Applied Sciences (Switzerland)* **2021**, *11* (19). https://doi.org/10.3390/app11199004.

(12) Schwientek, M.; Rügner, H.; Haderlein, S. B.; Schulz, W.; Wimmer, B.; Engelbart, L.; Bieger, S.; Huhn, C. Glyphosate Contamination in European Rivers Not from Herbicide Application? *Water Res* **2024**, *263*, 122140. https://doi.org/10.1016/j.watres.2024.122140.

(13) Battaglin, W. A.; Meyer, M. T.; Kuivila, K. M.; Dietze, J. E. Glyphosate and Its Degradation Product AMPA Occur Frequently and Widely in U.S. Soils, Surface Water, Groundwater, and Precipitation. *J Am Water Resour Assoc* **2014**, *50* (2), 275–290. https://doi.org/10.1111/jawr.12159.

(14) Brovini, E. M.; Cardoso, S. J.; Quadra, G. R.; Vilas-Boas, J. A.; Paranaíba, J. R.; Pereira, R. de O.; Mendonça, R. F. Glyphosate Concentrations in Global Freshwaters: Are Aquatic Organisms at Risk? *Environmental Science and Pollution Research* **2021**, *28* (43), 60635–60648. https://doi.org/10.1007/s11356-021-14609-8.

(15) Venditti, S.; Kiesch, A.; Hansen, J. Fate of Glyphosate and Its Metabolite AminoMethylPhosponic Acid (AMPA) from Point Source through Wastewater Sludge and Advanced Treatment. *Chemosphere* **2023**, *340*, 139843. https://doi.org/10.1016/j.chemosphere.2023.139843.

(16) Rott, E.; Steinmetz, H.; Metzger, J. W. Organophosphonates: A Review on Environmental Relevance, Biodegradability and Removal in Wastewater Treatment Plants. *Science of The Total Environment* **2018**, *615*. https://doi.org/10.1016/j.scitotenv.2017.09.223.

(17) Kuhn, R.; Jensch, R.; Bryant, I. M.; Fischer, T.; Liebsch, S.; Martienssen, M. Photodegradation of Ethylenediaminetetra(Methylenephosphonic Acid) – The Effect of the

System Configuration. *J Photochem Photobiol A Chem* **2020**, *388*. https://doi.org/10.1016/j.jphotochem.2019.112192.

(18) Kuhn, R.; Jensch, R.; Bryant, I. M.; Fischer, T.; Liebsch, S.; Martienssen, M. The Influence of Selected Bivalent Metal Ions on the Photolysis of Diethylenetriamine Penta(Methylenephosphonic Acid). *Chemosphere* **2018**, *210*, 726–733. https://doi.org/10.1016/j.chemosphere.2018.07.033.

(19) Marks, R. G. H.; Drees, F.; Rockel, S.; Kerpen, K.; Jochmann, M. A.; Schmidt, T. C. Mechanistic Investigation of Phosphonate Photolysis in Aqueous Solution by Simultaneous LC-IRMS and HRMS Analysis. *J Photochem Photobiol A Chem* **2023**, *439*, 114582. https://doi.org/10.1016/j.jphotochem.2023.114582.

(20) Grandcoin, A.; Piel, S.; Baurès, E. AminoMethylPhosphonic Acid (AMPA) in Natural Waters: Its Sources, Behavior and Environmental Fate. *Water Research*. Elsevier Ltd 2017, pp 187–197. https://doi.org/10.1016/j.watres.2017.03.055.

(21) Jaworska, J.; Van Genderen-Takken, H.; Hanstveit, A.; Van De Plassche, E.; Feijtel, T. Environmental Risk Assessment of Phosphonates, Used in Domestic Laundry and Cleaning Agents in the Netherlands. *Chemosphere* **2002**, No. 47, 655–665.

(22) Klinger, J.; Lang, M.; Sacher, F.; Brauch, H. J.; Maier, D.; Worch, E. Formation of Glyphosate and AMPA during Ozonation of Waters Containing Ethylenediaminetetra(Methylenephosphonic Acid). *Ozone Sci Eng* **1998**, *20* (2), 99–110. https://doi.org/10.1080/01919519808547279.

(23) Industrieverband Körperpflege- und Waschmittel e.V. *Nachhaltigkeit in Der Wasch-, Pflege- Und Reinigungsmittelbranche in Deutschland*; 2021. https://www.ikw.org/fileadmin/IKW_Dateien/downloads/Haushaltspflege/2021_IKW_Nachhaltigkeitsbericht.pdf (accessed 2024-06-11).

(24) Nowack, B. The Behavior of Phosphonates in Wastewater Treatment Plants of Switzerland. *Water Res* **1998**, *4* (12), 1271–1279.

(25) Nowack, B. Aminopolyphosphonate Removal during Wastewater Treatment. *Water Res* **2002**, *36*, 4636–4642.

(26) Röhnelt, A. M.; Martin, P. R.; Buchner, D.; Haderlein, S. B. Transformation of Iminodi(Methylene Phosphonate) on Manganese Dioxides - Passivation of the Mineral

Surface by (Formed) Mn2+. *Environ Sci Technol* **2023**, *57* (32), 11958–11966. https://doi.org/10.1021/acs.est.3c01838.

(27) Nowack, B.; Stone, A. T. Homogeneous and Heterogeneous Oxidation of Nitrilotrismethylenephosphonic Acid (NTMP) in the Presence of Manganese(II, III) and Molecular Oxygen. *Journal of Physical Chemistry B* **2002**, *106* (24), 6227–6233. https://doi.org/10.1021/jp014293+.

(28) Nowack, B.; Stone, A. T. Degradation of Nitrilotris(Methylenephosphonic Acid) and Related (Amino)Phosphonate Chelating Agents in the Presence of Manganese and Molecular Oxygen. *Environ Sci Technol* **2000**, *34* (22), 4759–4765. https://doi.org/10.1021/es0000908.

(29) Gledhill, W. E.; Feijtel, T. C. J. Environmental Properties and Safety Assessment of Organic Phosphonates Used for Detergent and Water Treatment Applications. In *The Handbook of Environmental Chemistry – Detergents*; 1992; pp 261–285. https://doi.org/10.1007/978-3-540-47108-0_8.

(30) Remucal, C. K.; Ginder-Vogel, M. A Critical Review of the Reactivity of Manganese Oxides with Organic Contaminants. *Environmental Sciences: Processes and Impacts* **2014**, *16* (6), 1247–1266. https://doi.org/10.1039/c3em00703k.

(31) Post, J. E. Manganese Oxide Minerals: Crystal Structures and Economic and Environmental Significance. *Proc. Natl. Acad. Sci. USA* **1999**, *96*, 3447–3454.

(32) Roskosch, A.; Heidecke, P. *Klärschlammentsorgung in Der Bundesrepublik Deutschland*; 2018. https://www.umweltbundesamt.de/publikationen/klaerschlammentsorgung-in-der-bundesrepublik (accessed 2024-10-21).

(33) Nowack, B.; Stone, A. T. Manganese-Catalyzed Degradation of Phosphonic Acids. *Environ Chem Lett* **2003**, *1* (1), 24–31. https://doi.org/10.1007/s10311-002-0014-3.

(34) Martin, P. R.; Buchner, D.; Jochmann, M. A.; Elsner, M.; Haderlein, S. B. Two Pathways Compete in the Mn(II)-Catalyzed Oxidation of Aminotrismethylene Phosphonate (ATMP). *Environ Sci Technol* **2022**, *56* (7), 4091–4100. https://doi.org/10.1021/acs.est.1c06407.

(35) McKendry, I. G.; Kondaveeti, S. K.; Shumlas, S. L.; Strongin, D. R.; Zdilla, M. J. Decoration of the Layered Manganese Oxide Birnessite with Mn(Ii/Iii) Gives a New Water Oxidation

Catalyst with Fifty-Fold Turnover Number Enhancement. *Dalton Transactions* **2015**, *44* (29), 12981–12984. https://doi.org/10.1039/c5dt01436k.

(36) Ouyang, H.; Wu, C.; Qiu, X.; Tanaka, K.; Ohnuki, T.; Yu, Q. New Insight of Mn(III) in δ-MnO2 for Peroxymonosulfate Activation Reaction: Via Direct Electron Transfer or via Free Radical Reactions. *Environ Res* **2023**, *217*, 114874. https://doi.org/10.1016/j.envres.2022.114874.

(37) Junta, J. L.; Hochella Jr, M. F. Manganese (II) Oxidation at Mineral Surfaces: A Microscopic and Spectroscopic Study. *Geochimica et Cosmochimica Act* **1994**, *58* (22), 4985–4999.

(38) Lyu, Y.; Li, C.; Du, X.; Zhu, Y.; Zhang, Y.; Li, S. Catalytic Oxidation of Toluene over MnO2 Catalysts with Different Mn (II) Precursors and the Study of Reaction Pathway. *Fuel* **2020**, *262*, 116610. https://doi.org/10.1016/j.fuel.2019.116610.

(39) Poiger, T.; Buerge, I. J.; Bächli, A.; Müller, M. D.; Balmer, M. E. Occurrence of the Herbicide Glyphosate and Its Metabolite AMPA in Surface Waters in Switzerland Determined with On-Line Solid Phase Extraction LC-MS/MS. *Environmental Science and Pollution Research* **2017**, *24* (2), 1588–1596. https://doi.org/10.1007/s11356-016-7835-2.

(40) Hanke, I.; Singer, H.; Hollender, J. Ultratrace-Level Determination of Glyphosate, Aminomethylphosphonic Acid and Glufosinate in Natural Waters by Solid-Phase Extraction Followed by Liquid Chromatography–Tandem Mass Spectrometry: Performance Tuning of Derivatization, Enrichment and Detection. *Anal Bioanal Chem* **2008**, *391* (6), 2265–2276. https://doi.org/10.1007/s00216-008-2134-5.

(41) Ibáñez, M.; Pozo, Ó. J.; Sancho, J. V.; López, F. J.; Hernández, F. Residue Determination of Glyphosate, Glufosinate and Aminomethylphosphonic Acid in Water and Soil Samples by Liquid Chromatography Coupled to Electrospray Tandem Mass Spectrometry. *J Chromatogr A* **2005**, *1081* (2), 145–155. https://doi.org/10.1016/j.chroma.2005.05.041.

(42) Sun, M.; Li, H.; Jaisi, D. P. Degradation of Glyphosate and Bioavailability of Phosphorus Derived from Glyphosate in a Soil-Water System. *Water Res* **2019**, *163*. https://doi.org/10.1016/j.watres.2019.07.007.

(43) Moller, S. R.; Wallace, A. F.; Zahir, R.; Quadery, A.; Jaisi, D. P. Effect of Temperature on the Degradation of Glyphosate by Mn-Oxide: Products and Pathways of Degradation. *J Hazard Mater* **2024**, *461*, 132467. https://doi.org/10.1016/j.jhazmat.2023.132467.

(44) Paudel, P.; Negusse, A.; Jaisi, D. P. Birnessite-Catalyzed Degradation of Glyphosate: A Mechanistic Study Aided by Kinetics Batch Studies and NMR Spectroscopy. *Soil Science Society of America Journal* **2015**, *79* (3), 815–825. https://doi.org/10.2136/sssaj2014.10.0394.

(45) Li, H.; Jaisi, D. P. Competition of Sorption and Degradation Reactions during Glyphosate Degradation by Ferrihydrite/δ-Manganese Oxide Composites. *ACS Earth Space Chem* **2019**, *3* (7), 1362–1370. https://doi.org/10.1021/acsearthspacechem.9b00127.

(46) Barrett, K. A.; McBride, M. B. Oxidative Degradation of Glyphosate and Aminomethylphosphonate by Manganese Oxide. *Environ Sci Technol* **2005**, *39* (23), 9223–9228. https://doi.org/10.1021/es051342d.

(47) Tari, I.; Hirai, T. Potential-PH Relations of Synthetic Beta Manganese Dioxide in NH4Cl Solutions. *Electrochim Acta* **1981**, *26*, 1657–1660.

(48) Stone, A. T. Reductive Dissolution of Manganese(III/IV) Oxides by Substituted Phenols. *Environ Sci Technol* **1987**, *21* (17), 979–988.

(49) Sigg, L.; Stumm, W. *Aquatische Chemie - Einführung in Die Chemie Natürlicher Gewässer*; vdf Hochschulverlag AG an der ETH Zürich, 2016. https://doi.org/10.3218/3768-5.

(50) Martínez, R. J.; Farrell, J. Understanding Nitrilotris(Methylenephosphonic Acid) Reactions with Ferric Hydroxide. *Chemosphere* **2017**, *175*, 490–496. https://doi.org/10.1016/j.chemosphere.2017.02.015.

(51) Tomson, B.; Kan, A. T.; Oddo, J. E. Acid/Base and Metal Complex Solution Chemistry of the Polyphosphonate DTPMP versus Temperature and Ionic Strength. *Langmuir* **1994**, *10*, 1442–1449.

(52) Duckworth, O. W.; Sposito, G. Siderophore-Manganese (III) Interactions. I. Air-Oxidation of Manganese(II) Promoted by Desferrioxamine B. *Environ Sci Technol* **2005**, *39* (16), 6037–6044. https://doi.org/10.1021/es050275k.

(53) Nowack, B.; Stone, A. T. The Influence of Metal Ions on the Adsorption of Phosphonates onto Goethite. *Environ Sci Technol* **1999**, *33* (20), 3627–3633. https://doi.org/10.1021/es9900860.

(54) Ruffolo, F.; Dinhof, T.; Murray, L.; Zangelmi, E.; Chin, J. P.; Pallitsch, K.; Peracchi, A. The Microbial Degradation of Natural and Anthropogenic Phosphonates. *Molecules* **2023**, *28* (19). https://doi.org/10.3390/molecules28196863.

(55) Schowanek, D.; Verstraete, W. Phosphonate Utilization by Bacterial Cultures and Enrichments from Environmental Samples. *Appl Environ Microbiol* **1990**, *56* (4), 895–903.

(56) Geszvain, K.; Butterfield, C.; Davis, R. E.; Madison, A. S.; Lee, S. W.; Parker, D. L.; Soldatova, A.; Spiro, T. G.; Luther, G. W.; Tebo, B. M. The Molecular Biogeochemistry of Manganese(II) Oxidation. *Biochem Soc Trans* **2012**, *40* (6), 1244–1248. https://doi.org/10.1042/BST20120229.

(57) Luther, G. W. Manganese(II) Oxidation and Mn(IV) Reduction in the Environment - Two One-Electron Transfer Steps versus a Single Two-Electron Step. *Geomicrobiol J* **2005**, *22* (3–4), 195–203. https://doi.org/10.1080/01490450590946022.

(58) Myers, J. P.; Antoniou, M. N.; Blumberg, B.; Carroll, L.; Colborn, T.; Everett, L. G.; Hansen, M.; Landrigan, P. J.; Lanphear, B. P.; Mesnage, R.; Vandenberg, L. N.; Vom Saal, F. S.; Welshons, W. V.; Benbrook, C. M. Concerns over Use of Glyphosate-Based Herbicides and Risks Associated with Exposures: A Consensus Statement. *Environmental Health* **2016**, *15* (1). https://doi.org/10.1186/s12940-016-0117-0.

(59) Steber, J.; Wierich, P. Properties of Aminotris(Methylenephosphonate) Affecting Its Environmental Fate: Degradability, Sludge Adsorption, Mobility in Soils, and Bioconcentration. *Chemosphere* **1987**, *16* (6), 1323–1337.

(60) Riedel, R.; Meißner, K.; Kaschubowski, A.; Benndorf, D.; Martienssen, M.; Braun, B. Laundry Isolate Delftia Sp. UBM14 Capable of Biodegrading Industrially Relevant Aminophosphonates. *Microorganisms* **2024**, *12* (8). https://doi.org/10.3390/microorganisms12081664.

(61) Riedel, R.; Commichau, F. M.; Benndorf, D.; Hertel, R.; Holzer, K.; Hoelzle, L. E.; Mardoukhi, M. S. Y.; Noack, L. E.; Martienssen, M. Biodegradation of Selected Aminophosphonates by the Bacterial Isolate Ochrobactrum Sp. BTU1. *Microbiol Res* **2024**, *280*. https://doi.org/10.1016/j.micres.2024.127600.

(62) Drzyzga, D.; Forlani, G.; Vermander, J.; Kafarski, P.; Lipok, J. Biodegradation of the Aminopolyphosphonate DTPMP by the Cyanobacterium Anabaena Variabilis Proceeds via

a C–P Lyase-Independent Pathway. *Environ Microbiol* **2017**, *19* (3), 1065–1076. https://doi.org/10.1111/1462-2920.13616.

(63) Riedel, R.; Krahl, K.; Buder, K.; Böllmann, J.; Braun, B.; Martienssen, M. Novel Standard Biodegradation Test for Synthetic Phosphonates. *J Microbiol Methods* **2023**, *212*. https://doi.org/10.1016/j.mimet.2023.106793.

(64) Wimmer, B.; Neidhardt, H.; Schwientek, M.; Haderlein, S. B.; Huhn, C. Phosphate Addition Enhances Alkaline Extraction of Glyphosate from Highly Sorptive Soils and Aquatic Sediments. *Pest Manag Sci* **2022**, *78* (6), 2550–2559. https://doi.org/10.1002/ps.6883.

(65) Röhnelt, A. M.; Martin, P. R.; Marks, R. G. H.; Buchner, D.; Weiss, J.; Schmidt, T. C.; Haderlein, S. B. Green Quantification of Amino(Poly)Phosphonates Using Ion Chromatography Coupled to Integrated Pulsed Amperometric Detection. *Anal Bioanal Chem* **2025**. https://doi.org/10.1007/s00216-025-05747-w.

(66) International Council for Harmonisation of Technical Requirements. *ICH Harmonised Guideline - Validation of Analytical Procedures Q2(R2)*. https://database.ich.org/sites/default/files/ICH_Q2%28R2%29_Guideline_2023_1130.pdf (accessed 2024-06-12).

(67) Oromí-Farrús, M.; Minguell, J. M.; Oromi, N.; Canela-Garayoa, R. A Reliable Method for Quantification of Phosphonates and Their Impurities by ^{31}P NMR. *Anal Lett* **2013**, *46* (12), 1910–1921. https://doi.org/10.1080/00032719.2013.780239.

5 General Conclusion and Outlook

5.1 Conclusion

5.1.1 Short Summary of Main Findings

This thesis presents significant contributions to our understanding of APPs and their environmental fate together with new approach for APP quantification. **Chapter 2** elucidated the oxidation of IDMP on manganese dioxide. Next to revealing AMPA and phosphate as the main transformation products of IDMP, the combination of concentration data and CSIA results underlined the role of different surface complexes and the inhibiting effect of formed Mn^{2+} by sorbing to the mineral surface. Following this, **chapter 3** presents the development and validation of a novel, environmentally friendly analytical method using IC-IPAD for simultaneous quantification of six amino(poly)phosphonates (A(P)Ps). This method enables the concurrent monitoring of higher molecular weight APPs, such as DTPMP, alongside their mono- and biphosphonate transformation products like IDMP and AMPA, thereby consolidating multiple analytical procedures previously required for comprehensive A(P)P analysis into a single, efficient approach. Finally, **chapter 4** uses the newly developed analytical method and previously derived knowledge about IDMP transformation, to investigate the manganese-driven oxidation of DTPMP. It was demonstrated that glyphosate, a broad-spectrum herbicide, and AMPA are stable transformation products, thus manganese-driven oxidation of DTPMP was revealed as a previously unrecognized pathway for potential glyphosate formation in the environment and technical systems.

The three parts of this thesis collectively fulfill the general aims of this work by elucidating transformation pathways, developing new analytical tools, and revealing unexpected sources of controversial environmental contaminants. However, new research questions and fields of research have opened up through the results of this thesis and other recent works on APPs.

5.1.2 Critical contextualization within the scientific framework

In general, polyphosphonates – including APPs – are **reported to be chemically stable**, which is attributed to the stability of the C-P bond[1–4]. Consistent with this, **sorption to sewage sludge** is considered the primary elimination route for APPs in WWTPs[5,6].

However, recent research revealed APPs to be not so stable after all: Kuhn *et al.* (2018 + 2020)[7,8] as well as Marks *et al.* (2023a and b)[9,10] showed UV-induced transformation of EDTMP, DTPMP and ATMP. The transformation products usually comprised – inter alia – the respective phosphonate reduced by one methylphosphonate group (e.g., IDMP forms from ATMP). Nowack & Stone (2000)[11] already showed ATMP, EDTMP and DTPMP to be transformed by Mn^{2+}/O_2. This work now provides even more information on the manganese-driven oxidation of DTPMP and its TPs and proves that transformation and glyphosate formation is even possible in a wastewater matrix. IDMP, AMPA and PO_4^{3-} – as also shown in this work – are widely known and proven TPs of APP transformation[7–9,12–14], while this work and Klinger *et al.* (1998)[15] added glyphosate as a minor TP to the portfolio. **Chapter 2** of this work showed IDMP to be readily transformed to AMPA and PO_4^{3-} by manganese dioxide. AMPA and glyphosate are also shown to be efficiently transformed by Mn oxides[16–19]. Hence, it is scientific consensus that ATMP, EDTMP and DTPMP can all be chemically degraded to smaller aminophosphonates and ultimately to phosphate. Rott *et al.* (2020)[20] investigated the partitioning of amine-free and amine-containing polyphosphonates (PPs) between the aqueous and sorbed phase in rivers. The study found lower concentrations of APPs compared to the amine-free PPs PBTC and HEDP in all environmental compartments, despite their higher use volumes. This suggests that APPs may be less stable or more prone to degradation in the environment compared to PBTC and HEDP[20]. The authors noted that the lower concentrations of APPs could be due to their higher biodegradability or transformation processes occurring in WWTPs or the environment.

Two very recent studies on glyphosate and AMPA concentrations in wastewater treatment plant (WWTP) influents, effluents and receiving waters revealed two crucial insights: i) WWTP effluents appear to be the main source for glyphosate and AMPA in surface waters[21] and ii) negative removal rates for AMPA and glyphosate were found in WWTPs – which implies they are formed or released within the WWTPs[12]. As stated above, glyphosate and AMPA are proven TPs of APPs.

These discoveries raise considerable doubt on the long-accepted assumption that sorption to sewage sludge represents the main elimination route for APPs in WWTPs[6,22].

Those concerns are further supported by the fact that studies investigating sorption of APPs to sewage sludge neglected the analysis of i) the sorbed phase and/or ii) transformation products[23,24]. The absence of analytes in the aqueous phase was taken as proof for sorption, without confirming that the analytes are sorbed on the sludge or mineral. The deduction "As

phosphonates are not biodegradable, the elimination must be due to sorption processes"[24] must therefore be strongly contradicted.

Engelbart & Bieger *et al.* (2024)[25] showed the transformation of ^{13}C-labelled DTPMP in sewage sludge, together with the formation of corresponding ^{13}C-glyphosate and ^{13}C-AMPA. This now unequivocally proves glyphosate and AMPA formation from DTPMP in sewage sludge and rules out the possibility of mere desorption causing their negative removal rates in WWTPs. Although it seems plausible from the current state of research that manganese is the missing link for DTPMP transformation in sewage sludge and glyphosate formation thereof, this still needs to be proven beyond doubt, as sewage sludge is a quite complex matrix with a plethora of potential reactants.

Another important field to which this work provides valuable insights is the reported **biotransformation of APPs**. Biotransformation of natural and synthetic monophosphonates including glyphosate is a widely studied and elucidated field[4,26,27]. Biotransformation of APPs on the contrary have not been studied as extensively. Prior to the 2000's, some studies on the biotransformation of APPs have been conducted[3,5,28]. Following a brief hiatus, publications on this topic resumed from 2017 onwards[29–32]. In general, APPs are regarded to be not readily biodegradable[22].

The role of manganese-driven APP oxidation has been investigated in this and previous work[11,33]. Martin *et al.* 2022[33] could show, that even at a molar Mn^{2+}:ATMP ratio of 1:100, ATMP is completely transformed by Mn^{2+}/O_2 after 30 hours. **Chapter 4** of this work showed that DTPMP can be effectively transformed by MnO_2 or Mn^{2+}/O_2 even in a wastewater matrix. Careful examination of published biotransformation studies revealed that all were conducted under aerobic conditions and all bacterial growth media contained manganese: $MnCl_2$ was contained in the trace element solution SL-8 used by Riedel *et al.* (2023, 2024a and 2024b)[30–32], in the Bg11 medium used by Drzyzga & Lipok (2017)[29], the AAP-medium used by Steber & Wierich (1986 and 1987)[28,34] and the trace metal solution used by Schowanek & Verstraete (1990)[3]. The studies of Riedel *et al.* (2023, 2024a, 2024b)[30–32] miss negative (abiotic) controls involving the respective APP and non-inoculated bacterial growth medium. Thus, in these studies the abiotic transformation of APPs in the microcosms in addition to or instead of biotransformation cannot be ruled out. Steber & Wierich (1987)[28] (i), Schowanek & Verstraete (1990)[3] (ii) as well as Drzyzga & Lipok (2017)[29] (iii) conducted such abiotic controls. They observed abiotic ATMP (i, ii and iii) and DTPMP (ii and iii) transformation in non-inoculated growth media within a couple of days. Steber & Wierich (1987)[28] could even show ATMP degradation in pure natural water. The recent

study by Engelbart & Bieger *et al.* (2024)[25] examining DTPMP transformation in sewage sludge additionally did not observe enhanced DTPMP transformation rates in sludge containing viable microbial communities compared to azide-treated sludge (the azide-treatment suppresses microbial activity).

However, bacterial growth was observed in all cited biotransformation studies, when the respective APP presented the only initial P-source. The early work of Steber & Wierich (1987)[28] provides important insights: Biodegradation experiments using ^{14}C-labelled ATMP and monitoring of the $^{14}CO_2$ evolution revealed that CO_2 was in fact produced from ATMP.

The results of this thesis and recently published findings together with the missing and the conducted abiotic controls give rise to significant doubt that biotransformation of APPs was in fact monitored. It seems rather conceivable that the microbes used P-containing TPs from abiotic transformation – e.g. PO_4^{3-} – as their phosphorus sources.

Consequently, it appears advisable to critically evaluate, revise or, if necessary, repeat studies on APP sorption onto sewage sludge, APP biotransformation, and earlier investigations into APP processes in WWTPs.

In order to do that, the APP quantification method developed in **chapter 3** provides a useful tool. **Analysis of APPs** is challenging, therefore, the available methods for APP analysis without derivatization are still scarce (see **chapter 3**). Even though aspects of green analytical chemistry (GAC) have gained increasing attention over the past two decades[35,36], these principles are still not incorporated into recent method development processes[37,38]. This can sometimes be attributed to higher priorities (e.g., trace analysis) or merely the availability of specific devices and processes.

The IC-PAD method described in **chapter 3** does offer a green and low-cost alternative for the quantification of AMPA, glyphosate, IDMP, ATMP, EDTMP and DTPMP down to <1 µM. APP concentrations in wastewater influents have been determined between <0.05-2 µM[5], while wastewater effluent concentrations were detected between 1.1 and 2.7 µg/L (2-6 nM)[38]. Hence, for monitoring APP concentrations in real samples previous enrichment would be necessary. However, the method was initially developed for the green and low-cost quantification of laboratory samples, where concentrations are adjustable. The elucidated inconsistencies in previous APP research as well as glyphosate being a TP emphasize the need for controlled laboratory experiments investigating transformation and sorption of APPs. The biggest advantage of this method is the simultaneous analysis of the mono- and bisphosphonates in one run together

with the APPs. Until now, separate analytical methods needed to be applied[37–42]. The applicability of the IC-PAD method has been demonstrated in **chapter 3** and **chapter 4**.

The revelation of **glyphosate** as a (minor) **TP of manganese-driven DTPMP oxidation** is perhaps the most striking discovery of this thesis. While **chapter 4** of this work demonstrated that the formation of glyphosate is chemically feasible under environmentally relevant conditions, a recent study has actually shown the transformation of DTPMP and the formation of glyphosate in sewage sludge[25]. Those findings challenge the conventional view of glyphosate sources in the environment, which typically focused on agricultural runoff[39,43–45]. Now, the substances DTPMP (and EDTMP), previously classified harmless, need to be regarded as "glyphosate precursors" and require more scrutiny.

The glyphosate debate extends far beyond the scientific community, encompassing a diverse array of stakeholders including the general public, corporate entities, and legal professionals. As glyphosate containing weed-control formulas were previously regarded as the only glyphosate source, those new findings offer new perspectives on environmental pollution and accountabilities. However, the environmental and toxicological impacts of long-term exposure to glyphosate in surface waters in the range of 0.2-1 µg/L[21] still need to be investigated. The multitude of studies conducted on glyphosate's cancerogenicity did not lead to a scientific consensus until now[46,47]. Hence, even if a new glyphosate contamination route is identified, it is advised not to extrapolate from limited evidence to the environmental implications.

In conclusion, this research has significantly advanced our understanding of APP transformations in environmental and engineered systems. By elucidating the mechanisms of IDMP oxidation on MnO_2, developing a novel analytical method for APP quantification, and discovering an unexpected pathway for glyphosate formation from DTPMP, this work challenges existing paradigms about APP fate and transformation. These findings have important implications for environmental risk assessment, water quality management, and the regulation of APPs and their transformation products. The unexpected formation of glyphosate from a widely used complexing agent underscores the need for a more comprehensive approach to assessing the environmental impact of seemingly benign chemicals. As we continue to unravel the complex behavior of APPs in the environment, it becomes clear that our understanding of these compounds and their potential impacts is still evolving, necessitating ongoing research and reevaluation of current practices.

5.2 Outlook

Building on the insights gained from this thesis, several avenues for **immediate follow-up research** are proposed.

Despite the insights of **chapter 2** and **4** of this thesis and previous work, several questions on the exact mechanism of oxidative transformation of amino(poly)phosphonates (A(P)Ps) on MnO_2 remain unanswered. What is the underlying mechanism to the heterogenous as well as the homogenous reaction? While our findings suggest initial C-P bond cleavage followed by C-N bond cleavage during IDMP oxidation on MnO_2, based on near-equimolar phosphate yields and substoichiometric AMPA yields, definitive confirmation of this mechanism requires further investigation. Further, the role of Mn^{III} on the mineral surface and in the aqueous phase remains unclear: To which extent and where is – if at all – Mn^{III} involved? This will probably deviate for different aminophosphonates and APPs due to differing chelating capabilities and therefore different Mn^{III} stabilities in solution. Elucidating the involvement of Mn^{III} in these reactions would provide crucial insights into the redox dynamics at the mineral-water interface, potentially revealing rate-limiting steps and intermediates in the oxidation process, which could significantly enhance our understanding of A(P)P transformation mechanisms in both engineered and natural systems.

To investigate the mechanism and succession of bond cleavages, either isotope-labelling[48] or nitrogen CSIA present helpful tools. By e.g. using isotope-labelled water ($H_2{}^{18}O$), one could monitor if and where the heavy water oxygen is inserted into the TPs[49]. Nitrogen CSIA of IDMP in addition to carbon CSIA could provide insights if nitrogen involving bonds are cleaved primarily in the reaction progress. To investigate the formation of Mn^{III}, one could make use of chelating agents leading to Mn^{III}-complexes with distinct UV/vis absorption. By stabilizing potential Mn^{III} in solution with strong ligands such as desferrioxamine B (DFOB) or Cd-porphyrin (TCPP), Mn^{III} could be made visible[50–52]. However, those methods still face some challenges due to the redox instability of DFOB or the oxidation of formed Mn^{II} complexes by molecular oxygen to Mn^{III} [50]. The investigation of the Mn oxidation states on the mineral surface could be realized by means of X-ray photo-electron spectroscopy. This helps to elucidate the role of Mn^{2+} sorbed to the mineral surface, e.g. if it undergoes comproportionation with Mn^{IV} to form Mn^{III} and how different Mn oxidation states enhance or inhibit the heterogenous reaction.

Especially for the oxidation of DTPMP on MnO_2 (**chapter 4**) the identification of unknown TPs is still pending. Further, the questions arose: In which matrices is the reaction possible? Which

parameters effect the glyphosate and AMPA yield? How long are glyphosate and AMPA stable in different reaction matrices?

Those research questions could be answered by conducting further laboratory experiments as described in **chapter 4** using different matrices and adding different parameters such as inorganic cations, anions or natural organic matter. Elucidation of the reaction mechanism would require different analytical methods. Using high-resolution mass spectrometry (HRMS) could shed light on the so far unknown TPs. Those, especially intermediate products, could already present indicators for the underlying reaction mechanism. The use of isotope-labelled glyphosate, present in the solution from the start, could trace if glyphosate is formed and transformed in parallel and thus shed light on glyphosate's stability in the reaction suspension.

The IC-PAD method could be expanded, by introducing more external standards. Some TPs of DTPMP transformation reactions are not easily commercially available, thus, to further investigate APP transformation, those standards would need to be self-synthesized. A higher degree of applicability could be achieved by the inclusion of sample preparation steps like purification and pre-concentration, which would potentially allow the measurement of natural samples in the future.

Building upon the short-term projections and immediate follow-up work outlined in the previous section, several **long-term research directions** emerge that could potentially reshape our understanding of APPs and their environmental fate over the coming years to decades.

Firstly, the discovery of glyphosate formation from APPs in natural and technical systems necessitates detailed investigations into the mechanisms and conditions of this transformation. Future research should focus on identifying the primary locations of APP degradation and glyphosate formation, whether in sewer systems, WWTPs, surface waters, or soil environments. The specific processes leading to glyphosate formation need to be elucidated, with particular attention to the role of manganese. While our research has highlighted the potential significance of manganese-driven oxidation, it remains to be seen whether this is the predominant mechanism in complex environmental matrices and systems.

Additionally, the stability and persistence of the formed glyphosate in these systems require thorough examination. The environmental implications of continuous, low-level glyphosate entry into aquatic ecosystems demand comprehensive study. Research should focus on the long-term

effects on aquatic organisms and plants, as even low concentrations might lead to chronic toxicity or alterations in ecosystem dynamics. This work together with other recent findings underline the necessity for the development of new long-term monitoring programs to capture subtle, cumulative effects. Moreover, the potential for APP-derived glyphosate formation may reignite discussions on the long-term toxicity and carcinogenicity of glyphosate for humans. The scientific community and regulatory bodies may need to reassess the risks associated with glyphosate exposure, considering this newly identified, continuous source. This reassessment should include epidemiological studies that account for potential low-level, chronic exposure from non-agricultural sources.

From an analytical perspective, the findings of this thesis, along with other recent research, underscore the need for routine analysis of APPs, particularly EDTMP and DTPMP, alongside glyphosate and AMPA in WWTPs and surface waters. Establishing appropriate sampling frequencies, time points, and locations will be crucial for deriving meaningful data on the occurrence and fate of these compounds. This shift in analytical focus will require equipping routine laboratories with instruments capable of performing easy, green, robust, and cost-efficient A(P)P analysis. Further research in sample preparation, automation, and analytical techniques will be necessary to meet this demand.

On a broader scale, this thesis highlights the critical importance of thoroughly investigating widely used chemicals for both direct and indirect environmental and health effects before their large-scale environmental release. The unexpected formation of a controversial herbicide from a supposedly benign chelating agent serves as a stark reminder of the potential for unforeseen consequences in chemical usage. It is hoped that these findings will contribute to a shift towards more rigorous scrutiny and comprehensive risk assessment of chemicals prior to their widespread application.

5.3 References

(1) Nowack, B.; Stone, A. T. The Influence of Metal Ions on the Adsorption of Phosphonates onto Goethite. *Environ Sci Technol* **1999**, *33* (20), 3627–3633. https://doi.org/10.1021/es9900860.

(2) Gledhill, W. E.; Feijtel, T. C. J. Environmental Properties and Safety Assessment of Organic Phosphonates Used for Detergent and Water Treatment Applications. In *The Handbook of Environmental Chemistry – Detergents*; 1992; pp 261–285. https://doi.org/10.1007/978-3-540-47108-0_8.

(3) Schowanek, D.; Verstraete, W. Phosphonate Utilization by Bacterial Cultures and Enrichments from Environmental Samples. *Appl Environ Microbiol* **1990**, *56* (4), 895–903.

(4) Ruffolo, F.; Dinhof, T.; Murray, L.; Zangelmi, E.; Chin, J. P.; Pallitsch, K.; Peracchi, A. The Microbial Degradation of Natural and Anthropogenic Phosphonates. *Molecules* **2023**, *28* (19). https://doi.org/10.3390/molecules28196863.

(5) Nowack, B. The Behavior of Phosphonates in Wastewater Treatment Plants of Switzerland. *Water Res* **1998**, *4* (12), 1271–1279.

(6) Rott, E.; Steinmetz, H.; Metzger, J. W. Organophosphonates: A Review on Environmental Relevance, Biodegradability and Removal in Wastewater Treatment Plants. *Science of The Total Environment* **2018**, *615*. https://doi.org/10.1016/j.scitotenv.2017.09.223.

(7) Kuhn, R.; Jensch, R.; Bryant, I. M.; Fischer, T.; Liebsch, S.; Martienssen, M. The Influence of Selected Bivalent Metal Ions on the Photolysis of Diethylenetriamine Penta(Methylenephosphonic Acid). *Chemosphere* **2018**, *210*, 726–733. https://doi.org/10.1016/j.chemosphere.2018.07.033.

(8) Kuhn, R.; Jensch, R.; Bryant, I. M.; Fischer, T.; Liebsch, S.; Martienssen, M. Photodegradation of Ethylenediaminetetra(Methylenephosphonic Acid) – The Effect of the System Configuration. *J Photochem Photobiol A Chem* **2020**, *388*. https://doi.org/10.1016/j.jphotochem.2019.112192.

(9) Marks, R. G. H.; Rockel, S. P.; Kerpen, K.; Somnitz, H.; Martin, P. R.; Jochmann, M. A.; Schmidt, T. C. Effects of PH-Dependent Speciation on the Photolytic Degradation Mechanism of Phosphonates. *J Photochem Photobiol A Chem* **2023**, 115327. https://doi.org/10.1016/j.jphotochem.2023.115327.

(10) Marks, R. G. H.; Drees, F.; Rockel, S.; Kerpen, K.; Jochmann, M. A.; Schmidt, T. C. Mechanistic Investigation of Phosphonate Photolysis in Aqueous Solution by Simultaneous LC-IRMS and HRMS Analysis. *J Photochem Photobiol A Chem* **2023**, *439*, 114582. https://doi.org/10.1016/j.jphotochem.2023.114582.

(11) Nowack, B.; Stone, A. T. Degradation of Nitrilotris(Methylenephosphonic Acid) and Related (Amino)Phosphonate Chelating Agents in the Presence of Manganese and Molecular Oxygen. *Environ Sci Technol* **2000**, *34* (22), 4759–4765. https://doi.org/10.1021/es0000908.

(12) Venditti, S.; Kiesch, A.; Hansen, J. Fate of Glyphosate and Its Metabolite AminoMethylPhosponic Acid (AMPA) from Point Source through Wastewater Sludge and Advanced Treatment. *Chemosphere* **2023**, *340*. https://doi.org/10.1016/j.chemosphere.2023.139843.

(13) Jaworska, J.; Van Genderen-Takken, H.; Hanstveit, A.; Van De Plassche, E.; Feijtel, T. Environmental Risk Assessment of Phosphonates, Used in Domestic Laundry and Cleaning Agents in the Netherlands. *Chemosphere* **2002**, No. 47, 655–665.

(14) Lesueur, C.; Pfeffer, M.; Fuerhacker, M. Photodegradation of Phosphonates in Water. *Chemosphere* **2005**, *59* (5). https://doi.org/10.1016/j.chemosphere.2004.10.049.

(15) Klinger, J.; Lang, M.; Sacher, F.; Brauch, H. J.; Maier, D.; Worch, E. Formation of Glyphosate and AMPA during Ozonation of Waters Containing Ethylenediaminetetra(Methylenephosphonic Acid). *Ozone Sci Eng* **1998**, *20* (2), 99–110. https://doi.org/10.1080/01919519808547279.

(16) Barrett, K. A.; McBride, M. B. Oxidative Degradation of Glyphosate and Aminomethylphosphonate by Manganese Oxide. *Environ Sci Technol* **2005**, *39* (23), 9223–9228. https://doi.org/10.1021/es051342d.

(17) Li, H.; Joshi, S. R.; Jaisi, D. P. Degradation and Isotope Source Tracking of Glyphosate and Aminomethylphosphonic Acid. *J Agric Food Chem* **2016**, *64* (3), 529–538. https://doi.org/10.1021/acs.jafc.5b04838.

(18) Li, H.; Jaisi, D. P. Competition of Sorption and Degradation Reactions during Glyphosate Degradation by Ferrihydrite/δ-Manganese Oxide Composites. *ACS Earth Space Chem* **2019**, *3* (7), 1362–1370. https://doi.org/10.1021/acsearthspacechem.9b00127.

(19) Li, H.; Wallace, A. F.; Sun, M.; Reardon, P.; Jaisi, D. P. Degradation of Glyphosate by Mn-Oxide May Bypass Sarcosine and Form Glycine Directly after C-N Bond Cleavage. *Environ Sci Technol* **2018**, *52* (3), 1109–1117. https://doi.org/10.1021/acs.est.7b03692.

(20) Rott, E.; Happel, O.; Armbruster, D.; Minke, R. Behavior of PBTC, HEDP, and Aminophosphonates in the Process of Wastewater Treatment. *Water (Switzerland)* **2020**, *12* (1). https://doi.org/10.3390/w12010053.

(21) Schwientek, M.; Rügner, H.; Haderlein, S. B.; Schulz, W.; Wimmer, B.; Engelbart, L.; Bieger, S.; Huhn, C. Glyphosate Contamination in European Rivers Not from Herbicide Application? *Water Res* **2024**, *263*, 122140. https://doi.org/10.1016/j.watres.2024.122140.

(22) European Phosphonates Association. *Input to the Revision of the EU Ecolabels Related to Detergents*; 2015. https://www.phosphonates.org/images/Images/Documents/EPA%20phosphonate%20input%20detergent%20Ecolabel.pdf (accessed 2022-11-28).

(23) Nowack, B. Aminopolyphosphonate Removal during Wastewater Treatment. *Water Res* **2002**, *36*, 4636–4642.

(24) Nowack, B. Determination of Phosphonates in Natural Waters by Ion-Pair High-Performance Liquid Chromatography. *J Chromatogr A* **1997**, *773*, 139–146.

(25) Engelbart, L.; Bieger, S.; Thompson, K. J.; Bader, T.; Kramer, M.; Haderlein, S.; Röhnelt, A.; Martin, P.; Buchner, D.; Bloch, R.; Rügner, H.; Huhn, C. De Novo Formation of Glyphosate and AMPA in Sewage Sludge from Phosphonates Used as Antiscalants and Bleach Stabilizers in Households and Industry (WR91151). *submitted to Water Research* **2024**.

(26) András Székács; Béla Darvas. Forty Years with Glyphosate. In *Herbicides: Properties, Synthesis and Control of Weeds*; 2012; pp 247–287.

(27) Borggaard, O. K.; Gimsing, A. L. Fate of Glyphosate in Soil and the Possibility of Leaching to Ground and Surface Waters: A Review. *Pest Manag Sci* **2008**, *64* (4), 441–456. https://doi.org/10.1002/ps.1512.

(28) Steber, J.; Wierich, P. Properties of Aminotris(Methylenephosphonate) Affecting Its Environmental Fate: Degradability, Sludge Adsorption, Mobility in Soils, and Bioconcentration. *Chemosphere* **1987**, *16* (6), 1323–1337.

(29) Drzyzga, D.; Forlani, G.; Vermander, J.; Kafarski, P.; Lipok, J. Biodegradation of the Aminopolyphosphonate DTPMP by the Cyanobacterium Anabaena Variabilis Proceeds via a C–P Lyase-Independent Pathway. *Environ Microbiol* **2017**, *19* (3), 1065–1076. https://doi.org/10.1111/1462-2920.13616.

(30) Riedel, R.; Meißner, K.; Kaschubowski, A.; Benndorf, D.; Martienssen, M.; Braun, B. Laundry Isolate Delftia Sp. UBM14 Capable of Biodegrading Industrially Relevant Aminophosphonates. *Microorganisms* **2024**, *12* (8). https://doi.org/10.3390/microorganisms12081664.

(31) Riedel, R.; Krahl, K.; Buder, K.; Böllmann, J.; Braun, B.; Martienssen, M. Novel Standard Biodegradation Test for Synthetic Phosphonates. *J Microbiol Methods* **2023**, *212*. https://doi.org/10.1016/j.mimet.2023.106793.

(32) Riedel, R.; Commichau, F. M.; Benndorf, D.; Hertel, R.; Holzer, K.; Hoelzle, L. E.; Mardoukhi, M. S. Y.; Noack, L. E.; Martienssen, M. Biodegradation of Selected Aminophosphonates by the Bacterial Isolate Ochrobactrum Sp. BTU1. *Microbiol Res* **2024**, *280*. https://doi.org/10.1016/j.micres.2024.127600.

(33) Martin, P. R.; Buchner, D.; Jochmann, M. A.; Elsner, M.; Haderlein, S. B. Two Pathways Compete in the Mn(II)-Catalyzed Oxidation of Aminotrismethylene Phosphonate (ATMP). *Environ Sci Technol* **2022**, *56* (7), 4091–4100. https://doi.org/10.1021/acs.est.1c06407.

(34) Steber, J.; Wierich, P. Properties of Hydroxyethane Diphosphonate Affecting Its Environmental Fate: Degradability, Sludge Adsorption, Mobility in Soils, and Bioconcentration. *Chemosphere* **1986**, *15* (7), 929–945.

(35) Armenta, S.; Garrigues, S.; de la Guardia, M. Green Analytical Chemistry. *TrAC - Trends in Analytical Chemistry* **2008**, *27* (6), 497–511. https://doi.org/10.1016/j.trac.2008.05.003.

(36) Tobiszewski, M.; Marć, M.; Gałuszka, A.; Namieśnik, J. Green Chemistry Metrics with Special Reference to Green Analytical Chemistry. *Molecules*. MDPI AG June 1, 2015, pp 10928–10946. https://doi.org/10.3390/molecules200610928.

(37) Wang, S.; Sun, S.; Shan, C.; Pan, B. Analysis of Trace Phosphonates in Authentic Water Samples by Pre-Methylation and LC-Orbitrap MS/MS. *Water Res* **2019**, *161*, 78–88. https://doi.org/10.1016/j.watres.2019.05.099.

(38) Armbruster, D.; Rott, E.; Minke, R.; Happel, O. Trace-Level Determination of Phosphonates in Liquid and Solid Phase of Wastewater and Environmental Samples by IC-ESI-MS/MS. *Anal Bioanal Chem* **2019**, *412* (20), 4807–4825. https://doi.org/10.1007/s00216-019-02159-5.

(39) Hanke, I.; Singer, H.; Hollender, J. Ultratrace-Level Determination of Glyphosate, Aminomethylphosphonic Acid and Glufosinate in Natural Waters by Solid-Phase Extraction Followed by Liquid Chromatography–Tandem Mass Spectrometry: Performance Tuning of Derivatization, Enrichment and Detection. *Anal Bioanal Chem* **2008**, *391* (6), 2265–2276. https://doi.org/10.1007/s00216-008-2134-5.

(40) Alonso, B.; Griffero, L.; Bentos Pereira, H.; Pareja, L.; Pérez Parada, A. Determination of Glyphosate and AMPA in Freshwater and Soil from Agroecosystems by 9-Fluorenylmethoxycarbonyl Chloride Derivatization and Liquid Chromatography - Fluorescence Detection and Tandem Mass Spectrometry. *MethodsX* **2022**, *9*. https://doi.org/10.1016/j.mex.2022.101730.

(41) Tewari, M.-J. K.; van Stroe-Bieze, S. Analysis of Amine-Containing Phosphonates in Detergent Powders by Anion-Exchange Chromatography with Pulsed Amperometric Detection. *J Chromatogr A* **1997**, *771*, 155–161.

(42) Weiss, J.; Hägele, G. Lonen-Chromatographische Analyse Anorganischer Und Organischer Komplexbildner. *Fresenius Z Anal Chem* **1987**, *348*, 46–50.

(43) Van Bruggen, A. H. C.; He, M. M.; Shin, K.; Mai, V.; Jeong, K. C.; Finckh, M. R.; Morris, J. G. Environmental and Health Effects of the Herbicide Glyphosate. *Science of the Total Environment*. Elsevier B.V. March 1, 2018, pp 255–268. https://doi.org/10.1016/j.scitotenv.2017.10.309.

(44) Grandcoin, A.; Piel, S.; Baurès, E. AminoMethylPhosphonic Acid (AMPA) in Natural Waters: Its Sources, Behavior and Environmental Fate. *Water Res* **2017**, *117*, 187–197. https://doi.org/10.1016/j.watres.2017.03.055.

(45) Bento, C. P. M.; Yang, X.; Gort, G.; Xue, S.; van Dam, R.; Zomer, P.; Mol, H. G. J.; Ritsema, C. J.; Geissen, V. Persistence of Glyphosate and Aminomethylphosphonic Acid in Loess Soil under Different Combinations of Temperature, Soil Moisture and Light/Darkness. *Science of the Total Environment* **2016**, *572*, 301–311. https://doi.org/10.1016/j.scitotenv.2016.07.215.

(46) Benbrook, C. M. How Did the US EPA and IARC Reach Diametrically Opposed Conclusions on the Genotoxicity of Glyphosate-Based Herbicides? *Environ Sci Eur* **2019**, *31* (1). https://doi.org/10.1186/s12302-018-0184-7.

(47) Myers, J. P.; Antoniou, M. N.; Blumberg, B.; Carroll, L.; Colborn, T.; Everett, L. G.; Hansen, M.; Landrigan, P. J.; Lanphear, B. P.; Mesnage, R.; Vandenberg, L. N.; Vom Saal, F. S.; Welshons, W. V.; Benbrook, C. M. Concerns over Use of Glyphosate-Based Herbicides and Risks Associated with Exposures: A Consensus Statement. *Environmental Health* **2016**, *15* (1). https://doi.org/10.1186/s12940-016-0117-0.

(48) Sun, M.; Li, H.; Jaisi, D. P. Degradation of Glyphosate and Bioavailability of Phosphorus Derived from Glyphosate in a Soil-Water System. *Water Res* **2019**, *163*. https://doi.org/10.1016/j.watres.2019.07.007.

(49) Li, H.; Jaisi, D. P. An Isotope Labeling Technique to Investigate Atom Exchange during Phosphate Sorption and Desorption. *Soil Science Society of America Journal* **2015**, *79* (5), 1340–1351. https://doi.org/10.2136/sssaj2015.04.0158.

(50) Kim, B.; Lingappa, U. F.; Magyar, J.; Monteverde, D.; Valentine, J. S.; Cho, J.; Fischer, W. Challenges of Measuring Soluble Mn(III) Species in Natural Samples. *Molecules* **2022**, *27* (5). https://doi.org/10.3390/molecules27051661.

(51) Jones, M. R.; Oldham, V. E.; Luther, G. W.; Mucci, A.; Tebo, B. M. Distribution of Desferrioxamine-B-Extractable Soluble Manganese(III) and Particulate MnO 2 in the St. Lawrence Estuary, Canada. *Mar Chem* **2019**, *208*, 70–82. https://doi.org/10.1016/j.marchem.2018.11.005.

(52) Duckworth, O. W.; Sposito, G. Siderophore-Manganese (III) Interactions. I. Air-Oxidation of Manganese(II) Promoted by Desferrioxamine B. *Environ Sci Technol* **2005**, *39* (16), 6037–6044. https://doi.org/10.1021/es050275k.

A - Supporting information to chapter 1

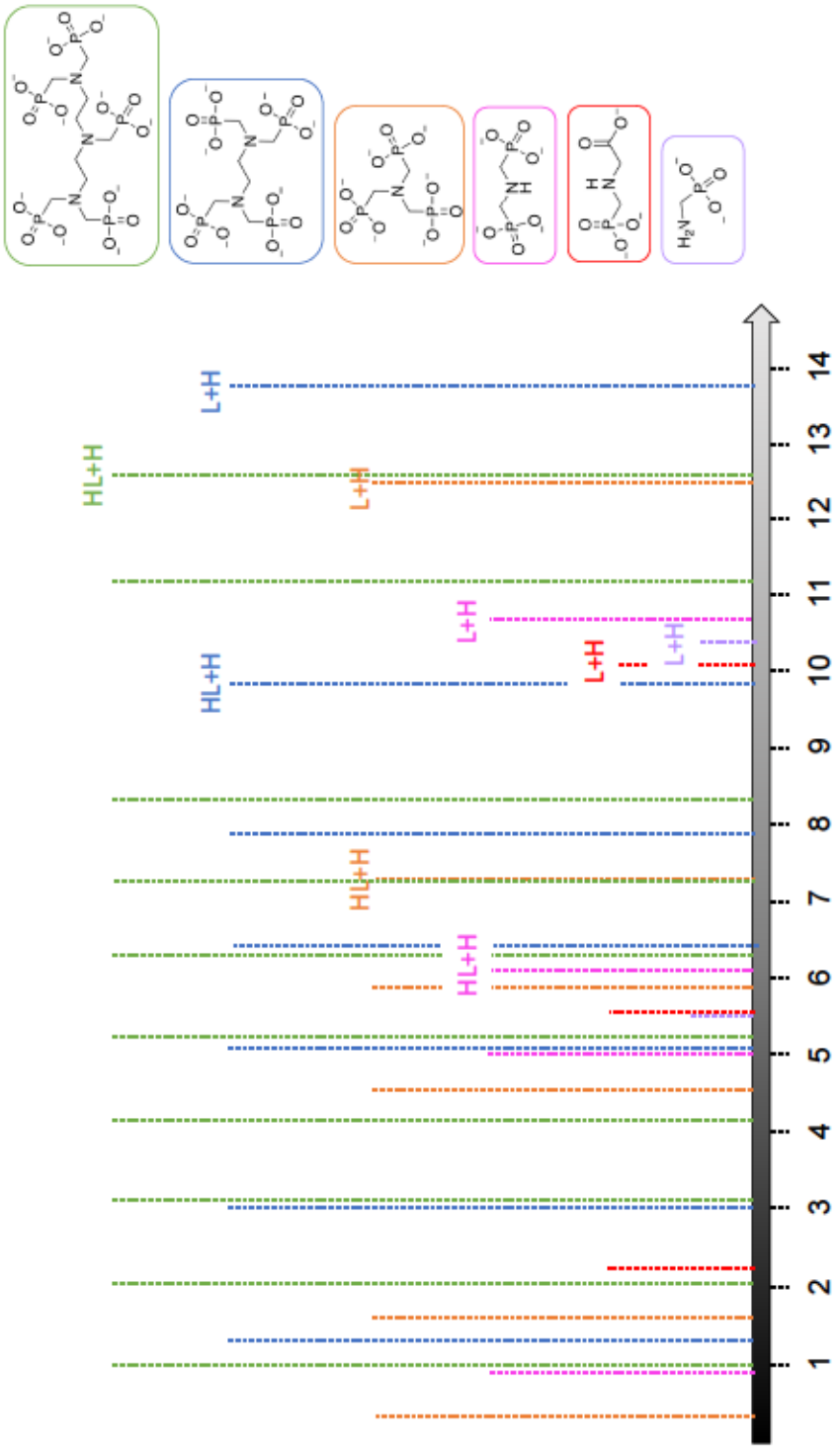

Figure A.1 pKa values of the six aminophosphonates mainly investigated in this thesis: AMPA, glyphosate, IDMP, ATMP, EDTMP and DTPMP. The pKa values are taken from Popov et al. 2001 (EDTMP, AMPA), Tomson et al. 1994 (DTPMP), Graf et al. 2022 (glyphosate), Deluchat et al. 1997 (ATMP) and Motekaitis & Mortell 2006 (glyphosate, IDMP).

B - Supporting information to chapter 2

INTRODUCTION

Speciation of IDMP, AMPA and PO_4^{3-}

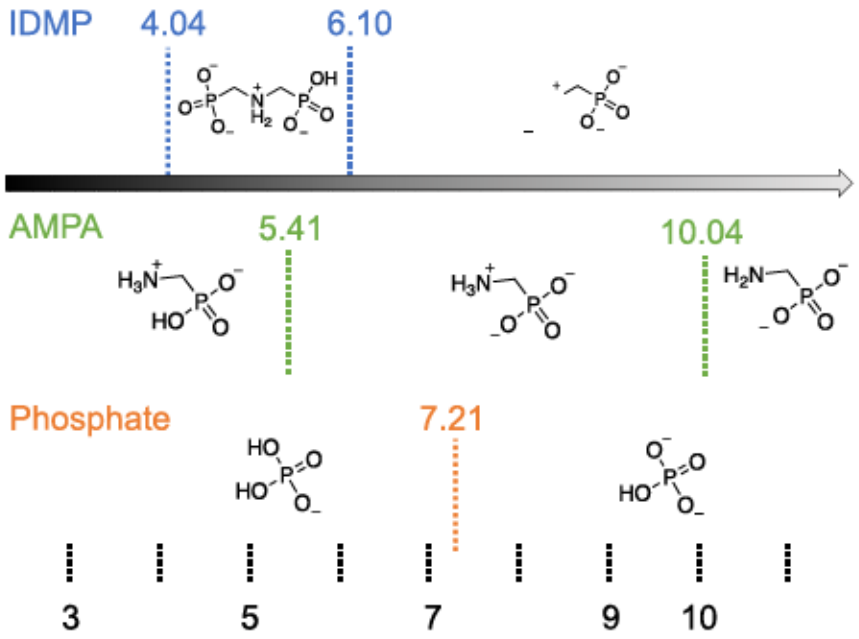

Figure B.1 Speciations of IDMP, AMPA and phosphate between pH 3 and 11. pKa values for an ionic strength of 0.1 M, taken from Popov et al.[1].

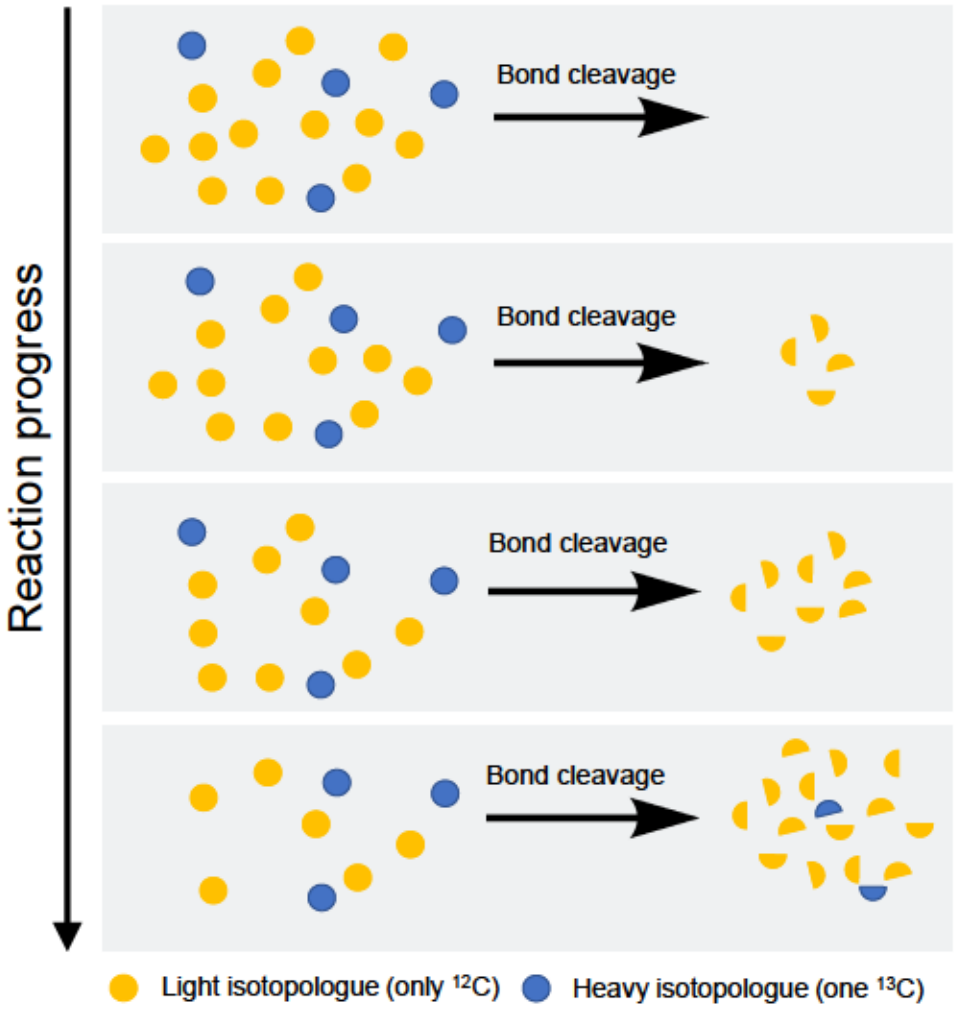

Figure B.2 Schematic explanation of the kinetic isotope effect, resp. ^{13}C enrichment in the reactant during a C-bond cleavage reaction.

Effects of buffer on IDMP oxidation on MnO_2

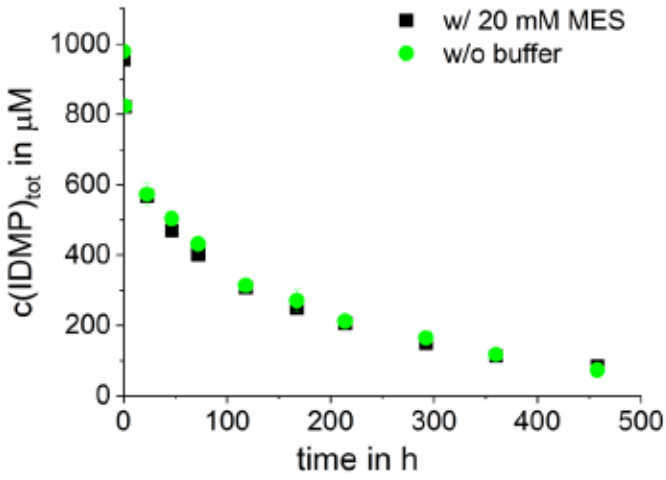

Figure B.3 Comparison of two experiments containing 1.7 g/L $MnO_{2/com}$ with and without buffer (20 mM MES). Error bars represent the absolute error between duplicates.

AMPA+IDMP quantification using the IC-ECD flow gradient method

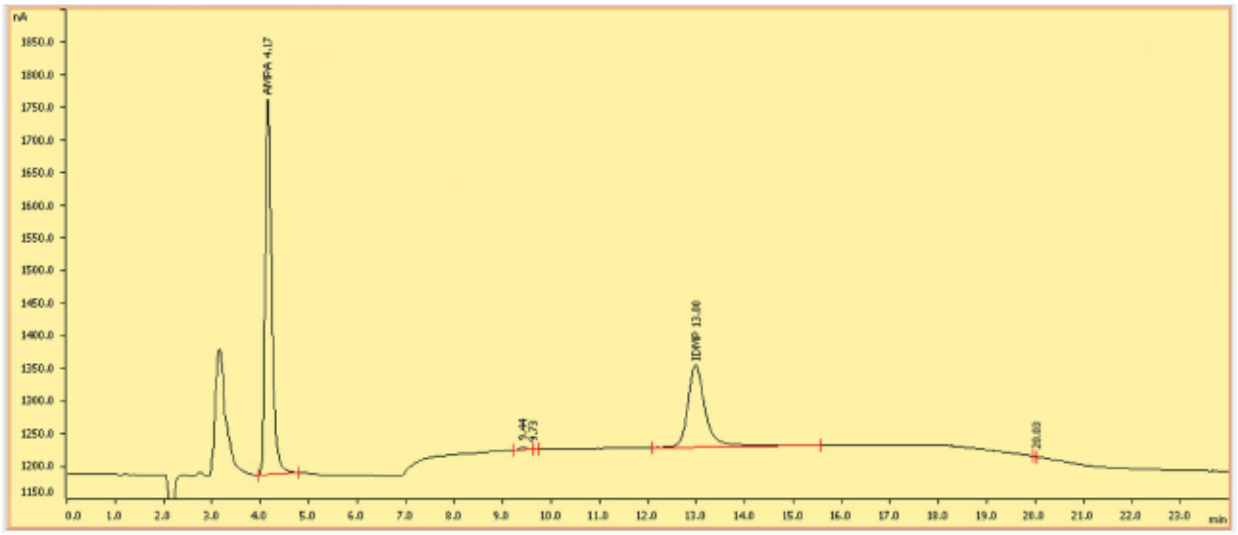

Figure B.4 Chromatogram of simultaneous IDMP and AMPA quantification using IC-ECD with a flow gradient method (see Figure B.2). RT(AMPA) = 4.17 min, RT(IDMP) = 13.00 min.

The IC-ECD measurements had a total length of 24 min, each, and were conducted using a flow gradient (see Table B.1 **a)**). The detector was set to the "flexiPAD" mode (Table B.1 **b)**), running a new cycle every 900 ms. Analyte signals have been integrated (measurement period) between 370 and 790 ms, thus measurement time was 420 ms starting every 900 ms. The according detector range was 200 µA.

Table B.1 a) Flow gradient method, b) detector method "flexiPAD" used for IDMP and AMPA quantifications using IC-ECD.

a) Flow Gradient		
Time in min	**Flow in mL min^{-1}**	**Curve**
0.0	0.4	
7.0	1.2	Step
18.0	1.2	Linear
21.0	0.4	Linear
24.0	0.4	Linear

b) Detector Method flexiPAD			
Time period in ms	**Sum time in ms**	**Start potential in V**	**End potential in V**
370	370	0.0	0.0
150	520	0.0	0.25
110	630	0.25	0.25
120	750	0.25	0.0
50	800	0.0	0.0
40	840	-1.0	-1.0
60	900	0.6	0.6

MP-AES

Aqueous manganese in the centrifuged and filtered samples was quantified by a 4200 MP–AES, equipped with a SPS 3 autosampler, a cyclonic spray chamber and an easy–fit torch (Agilent Technologies, Santa Clara, United States). The selected wavelength was 403.076 nm. The read time and gas nebulizer gas flow were set to 5 s and 0.85 L/min, respectively. Samples were diluted prior to analysis 1:4, with a final concentration of 1 % (v/v) HNO_3. External standards in the range between 0.1 mg/L and 25.0 mg/L were used for quantification ($R^2 > 0.9999$).

LC-IRMS

LC-IRMS measurements: Devices, measuring/oxidation conditions and further analytical parameters

Separation of IDMP from other components was achieved using an UltiMate3000 HPLC-system equipped with an anion exchange column (Shodex IC NI-424, 100x4.6 mm) (Showa Denko, Tokyo, Japan) held constant at 40 °C. The mobile phase (2.5 mM NaH_2PO_4 acidified to pH 2.6 by H_3PO_4) was delivered at a flow rate of 0.5 mL/min. The separation unit was coupled to the IRMS (Delta V Plus IRMS, Thermo Fisher Scientific, Bremen, Germany) via the interface (LC-IsoLink, Thermo Fisher Scientific, Bremen, Germany). Complete oxidation was achieved by flow rates of 50 µL/min (1.5 M H_3PO_4) resp. 75 µL/min (60 g/L $Na_2S_2O_8$), with the oxidation reactor set to 99.9 °C. Stability of the oxidation conditions and therefore δ-values were checked by external standards (0.1-1 mM IDMP), while ion source performance was monitored by four CO_2 reference gas peaks; the third one served as "set-zero" for the calculation of δ-values. Each experimental duplicate was measured in triplicates (n = 6). The standard deviation of those six measurements presents the standard deviation used in this work.

Moving Mean approach for LPIA of IDMP

The limit of precise isotope analysis (LPIA) was determined to be 50 µM IDMP following the moving mean method by Jochmann *et al.*[2].

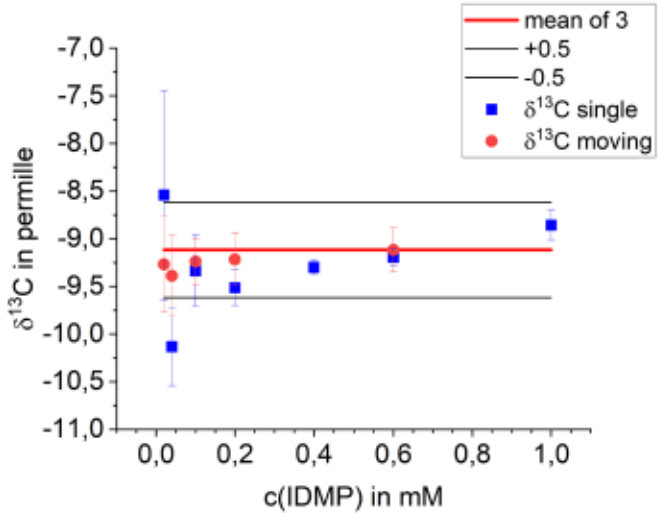

Figure B.5 Moving mean approach for IDMP using a $Na_2S_2O_8$ concentration of 60 g/L (75 µL/min) and 1.5 M H_3PO_4 (50 µL/min).

LC-HRMS-IRMS measurements

Identification (and quantification) of the transformation products *N*-formyl-aminomethylphosphonate (F-AMPA) and hydroxymethylphosphonate (HMP) were achieved by the hyphenation of a LC-IRMS (Thermo Dionex Ultimate 3000, Thermo Fisher Scientific Inc., Waltham, USA; Delta V Advantage IRMS, Thermo Fisher Scientific, Bremen, Germany) holding an anion exchange column (IC NI-424, 4.6 mm ID x 100 mm L + 4.6 mm ID x 10 mm L, Shodex, München, Germany) with a high-resolution mass spectrometer (QExactive Orbitrap, Thermo Fisher Scientific Inc., Waltham, USA) using a flow-splitter (QuickSplit, 610-PO10-06, ASI, Richmond US). The column temperature was 20 °C, stabilized by a high temperature HPLC 200 column oven (SIM GmbH, Oberhausen, Germany). The injected sample volume was 10 µL. The flow rate of the eluent (4 mM sulfuric acid in water, pH 3) was set to 400 µL min^{-1}. A constant split ratio between IRMS to HRMS was adjusted to 1:13.3. Due to this split ratio, most of the eluent flow was led to the IRMS (370 ± 2 µL min^{-1}), while only a small portion was led to the HRMS (30 ± 2 µL min^{-1}).

For oxidation of the analytes before entering the IRMS, phosphoric acid (1.5 M in water) and sodium persulfate (100 g L^{-1} in water) were added as oxidizing reagents to the eluent stream at a flow rate of 40 µL min^{-1} each via a T-piece. The oxidation reactor was heated to 100 °C, which induces the formation of sulphate radicals.

$MnO_{2/syn}$ synthesis

The protocol for the synthesis of $MnO_{2/syn}$ via the reduction of $KMnO_4$ by H_2O_2 under acidic conditions was adapted from Villegas *et al.*[3]. First, 7.2 mL concentrated nitric acid (EMSURE, Merck, Darmstadt, Germany) was added to 72 mL 1 % (v/v, equivalent to 426 mM) hydrogen peroxide (30 %, for analysis, Merck). Afterwards, 75 mL of a 274 mM KMnO4 (EMSURE, Merck) solution was added to the acidic hydrogen peroxide solution with approximately 1.5 mL/min under constant rapid stirring. After a reaction time of 60 min, stirring was stopped and the particles were allowed to settle for another 60 min. The residue was washed several times with ultrapure water, until it showed a conductivity ≥ 1.5 µS/cm. The residue was then vacuum filtrated and dried at 80 °C for 24 h. The dried mineral was crushed in a mortar and stored in a desiccator over silica gel up to its final use.

Mineral Characterization:

Scanning electron microscopy (SEM): Zeiss Crossbeam 550 Focused Ion Beam – Scanning Electron Microscope (FIB-SEM) (Zeiss, Oberkochen, Germany), operated in secondary electron (SE) mode using an accelerating voltage of 2 kV. The samples were mounted onto aluminum stubs (Ø 12 mm) using a carbon adhesive tab and coated with ca. 8 nm Au using a BAL-TEC™ SCD 005 sputter coater.

Brunauer-Emmett-Teller method (BET): Gemini VII 2390 (Micrometrics, Norcross, GA, United States) by nitrogen sorption-desorption isotherms. Samples were degassed before analysis overnight under vacuum at 120 °C.

Point of Zero Charge: Zetasizer Nano ZSP (Malvern Pananalytical, Malvern, United Kingdom) in folded capillary zeta cells at 20 °C. Measurements were conducted in triplicates with 10 to 15 runs, each. For analysis, 50 mg/L MnO_2 suspensions were prepared in 10 mM NaCl + 10 mM MES buffer and the pH was adjusted by 0.1 M or 1 M NaOH and HCl. The point of zero charge was determined by plotting the zeta potential as function of the adjusted pH and subsequent regression of the linear part of the data sets

Pyrophosphate (PP) extraction of Mn^{III}: Mn^{III}-content of the two minerals was identified via PP-extraction and subsequent spectroscopic quantification. For extraction of available Mn^{III}, 1 mM (0.087 g/L) or 17 mM (1.5 g/L) MnO_2 was suspended in 20 mM PP (pH 7) and shaken on an overhead shaker for 24 h. Afterwards, the suspension was centrifuged at 14 000 rcf for 15 min and the supernatant was analyzed at 258 nm (UV5Bio, Mettler Toledo, Greifensee, Switzerland). The concentration of Mn^{III}-PP was calculated based on the molar absorption coefficient at 258 nm of 6750 (M cm)-1. The MnIII-content was then normalized to the BET surface area.

Powder X-ray diffraction (XRD): was performed using a D8 Discover (Bruker, Billerica, MA, United States) equipped with a Cu-source (Cu-K α radiation, λ = 1.54184 Å) with a beam voltage and current of 40 kV and 20 mA, respectively.

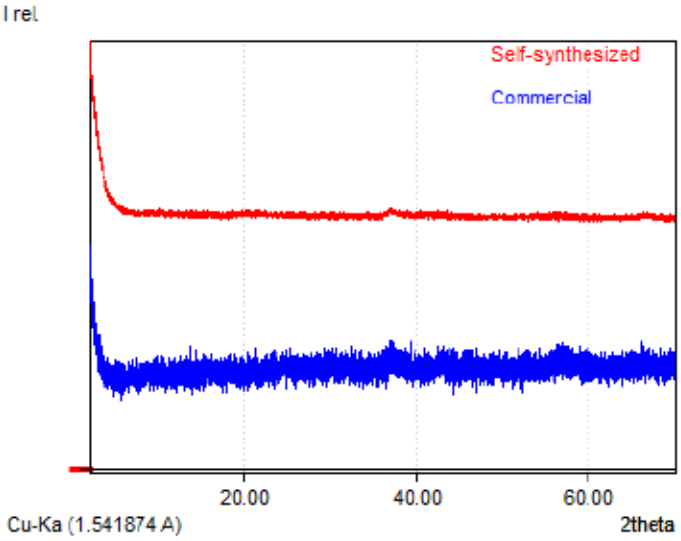

Figure B.6 X-ray diffractograms of $MnO_{2/syn}$ and $MnO_{2/com}$ showing no distinct peaks and thus exhibiting an amorphous structure.

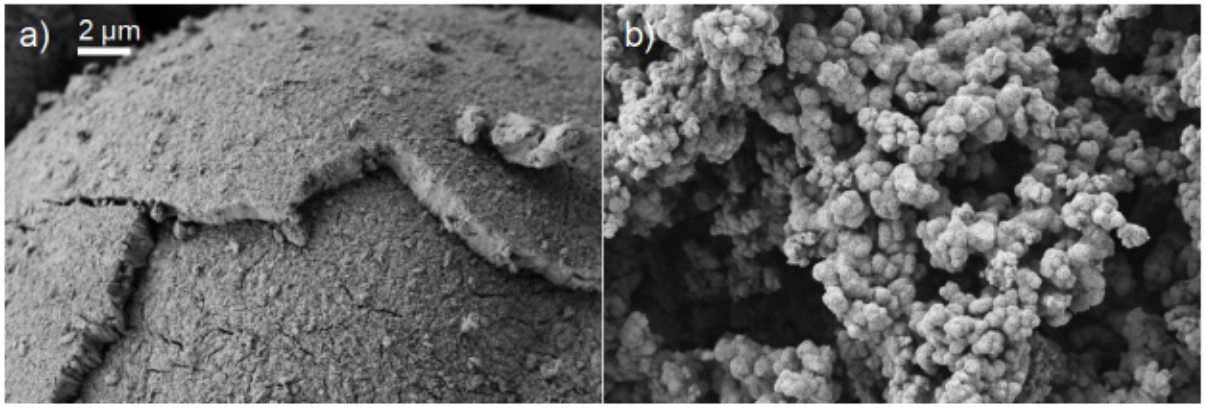

Figure B.7 Scanning Electron Microscopy (SEM) pictures of a) $MnO_{2/com}$ and b) $MnO_{2/syn}$.

Both minerals show no peaks in the X-ray diffractograms and therefore reveal an amorphous structure. The extractable Mn^{III}-content was 1 % of total manganese for $MnO_{2/com}$ and 5 % for $MnO_{2/syn}$ (in % of total manganese). With regard to the different surface areas, both show an extractable Mn^{III}-content of 1.76 nmol/m^2. Further, total reflection X-ray fluorescence (TXRF) revealed just minor amounts of other monovalent cations in both minerals (K: ca. 0.01 molar ratio vs Mn for $MnO_{2/syn}$, Ca: 0.3 molar ratio vs Mn for $MnO_{2/com}$ and $MnO_{2/syn}$), which validates the low Mn^{III} content.

$MnO_{2/syn}$ exhibits a five times greater specific surface area (SSA) than $MnO_{2/com}$: 326 ± 1 m^2/g versus 64.5 ± 0.2 m^2/g. The SEM pictures affirm the strong difference in SSA and show that we deal with a highly porous structure in case of $MnO_{2/syn}$. While the $MnO_{2/syn}$ exhibits a very ordered flower-like structure which is common for synthetic birnessite (McKendry et al., 2015), $MnO_{2/com}$ appears far less porous and much denser.

The minerals also differed a lot regarding their point of zero charge (pH_{pzc}), which is 2.3 ± 0.1 ($MnO_{2/syn}$) resp. 5.6 ± 0.1 ($MnO_{2/com}$).

RESULTS AND DISCUSSION

F-AMPA analysis

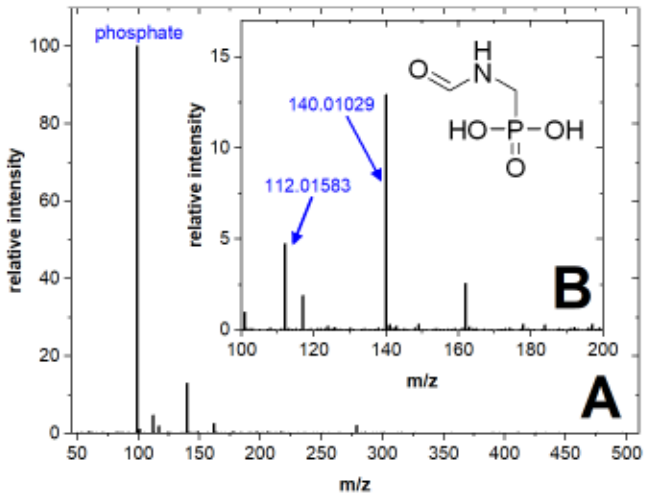

Figure B.8 Panel **A**: Mass spectrum of an IDMP transformation experiment containing 1.7 g/L $MnO_{2/com}$, but no buffer, in the mass range of 50-500 m/z. Panel **B**: Zoom in the mass range of 100-200 m/z.

The concentrations of F-AMPA were calculated based on F-AMPA LC-IRMS peak areas (see Figure B.8) – identified by the respective HRMS m/z – assuming an identical oxidation efficiency to IDMP.

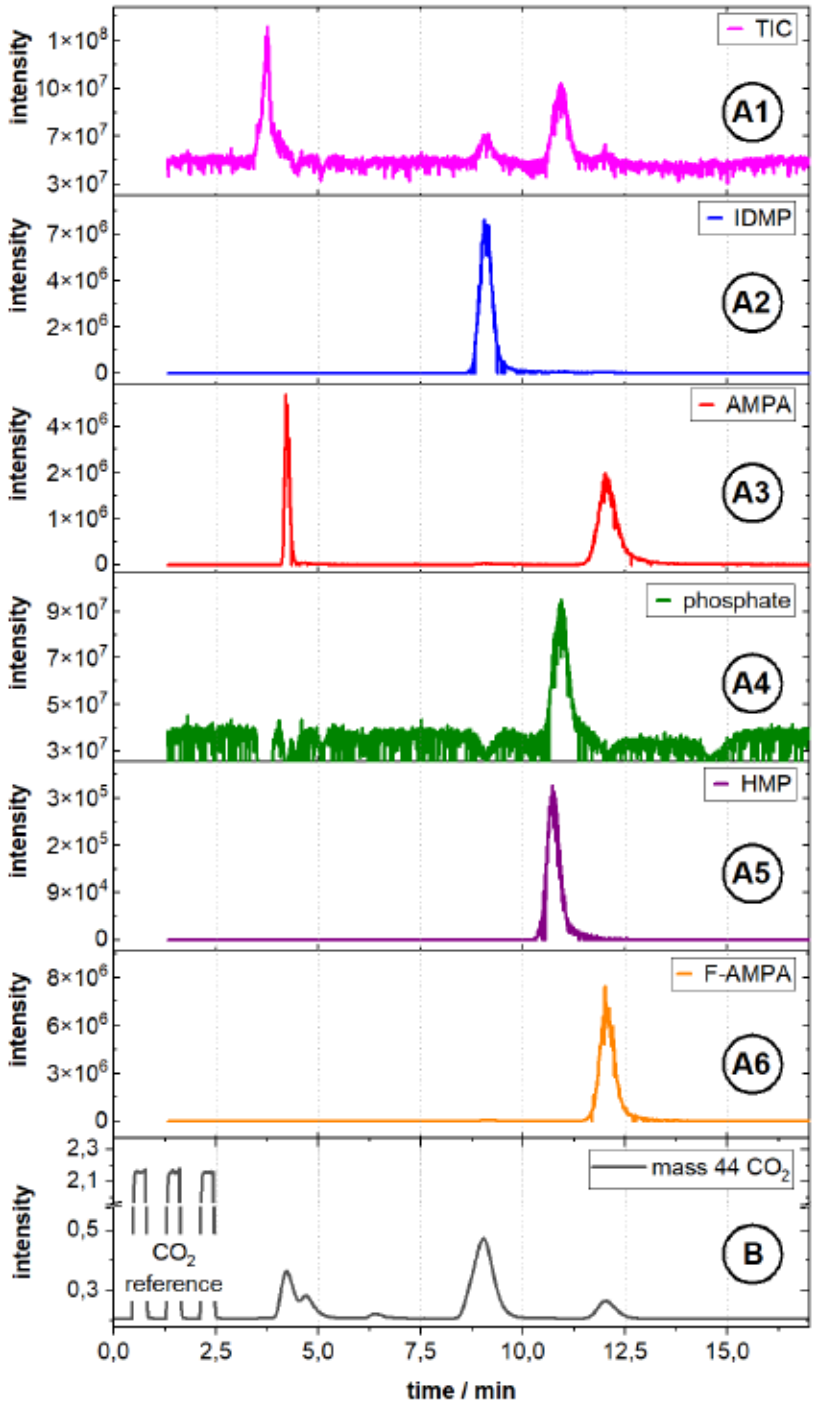

Figure B.9 Simultaneous analysis of an IDMP transformation experiment containing 1.7 g/L $MnO_{2/com}$, but no buffer, by LC-IRMS-HRMS. Panel **A1** to **A6** show the analysis with HRMS. The total ion current (TIC) is plotted against the time. Extracted ion chromatograms (EIC) were extracted for IDMP, AMPA, o-PO_4, HMP, and F-AMPA. Panel B presents the IRMS mass trace of CO_2 at mass 44. The HRMS and IRMS measurements have a retention time offset of 1.3 minutes. For the presentation of the data, the retention time was adjusted accordingly. HPLC conditions: Flow rate 0.4 $mLmin^{-1}$, eluent water (pH~3, H_2SO_4). Oxidation conditions: 40 $\mu Lmin^{-1}$ phosphoric acid (1.5 M), 40 $\mu Lmin^{-1}$ sodium peroxydisulfate solution (100 gL^{-1} in H2O). Injection volume 10 µL.

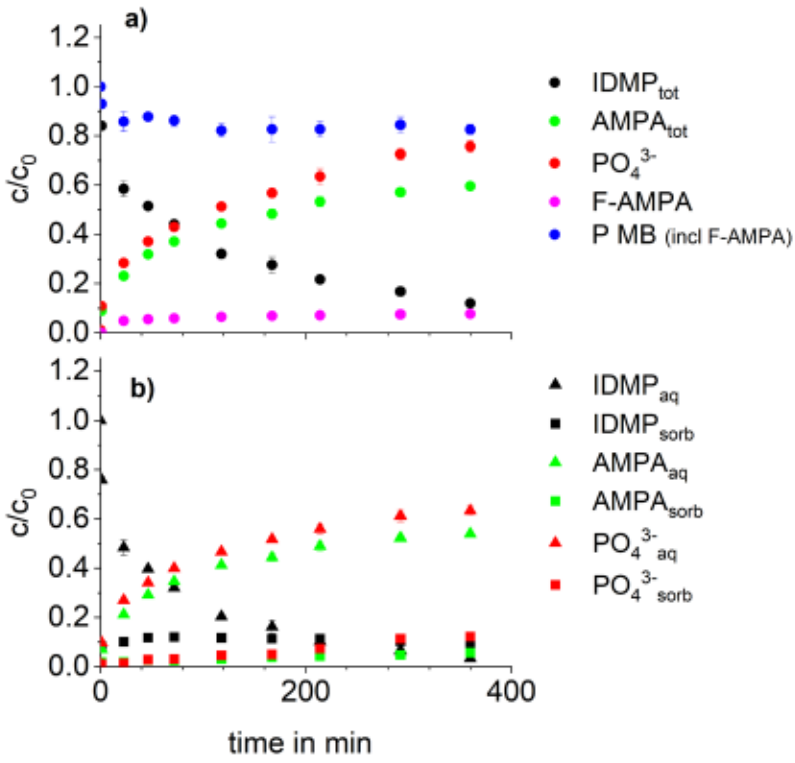

Figure B.10 Full data set for an experiment containing 1.7 g/L $MnO_{2/com}$ (no buffer), including F-AMPA concentrations. F-AMPA has just been found in the aqueous phase. Error bars represent absolute deviations of duplicates.

Subsequent AMPA transformation

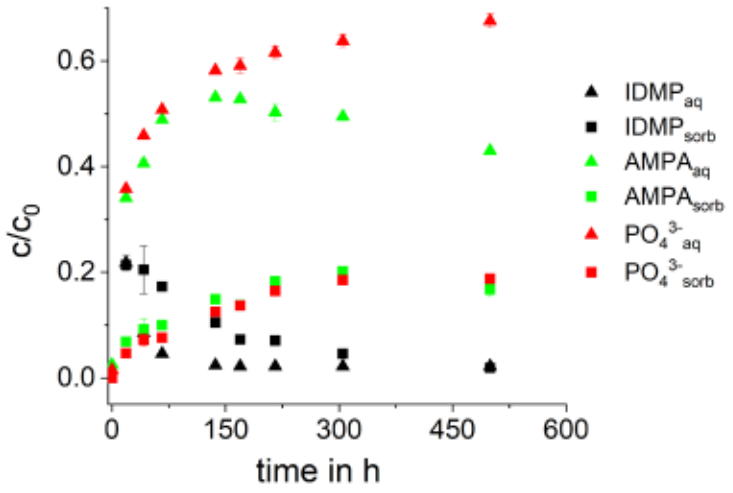

Figure B.11 Aqueous and sorbed concentrations of IDMP, AMPA and phosphate normalized to the initial IDMP concentration of the IDMP transformation experiment containing 3.4 g/L $MnO_{2/com}$. Observation for a longer period of time, until AMPA transformation occurred in the same reaction suspension. Error bars represent the absolute deviation between duplicates.

Kinetics: Zero order approximation

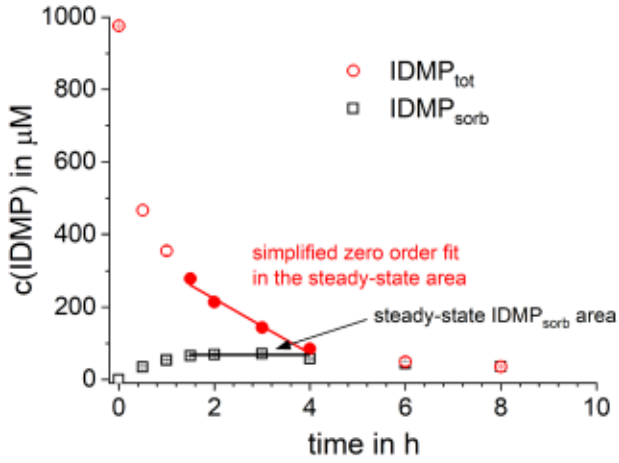

Figure B.12 Schematic explanation of the derivation of the zero-order rate constant in the quasi-steady state area, exemplary for 1.7 g/L $MnO_{2/syn}$ and 1 mM IDMP.

Sorption Data

Sorption of Mn^{2+} onto MnO_2:

Sorption data of Mn^{2+} on MnO_2 were fitted using the Freundlich model[4]:

$$c_{sorb} = K_F \cdot {c_{aq}}^n$$

With c_{sorb} = surface loading of the mineral with Mn^{2+}, K = Freundlich constant and c_{aq} = aqueous Mn^{2+} concentration. The calculated parameters were n = 0.36 ± 0.04 [0.43 ± 0.04] and K_F = 0.66 ± 0.22 [0.31 ± 0.10] for 0.67 g/L $MnO_{2/syn}$ [3.4 g/L $MnO_{2/com}$].

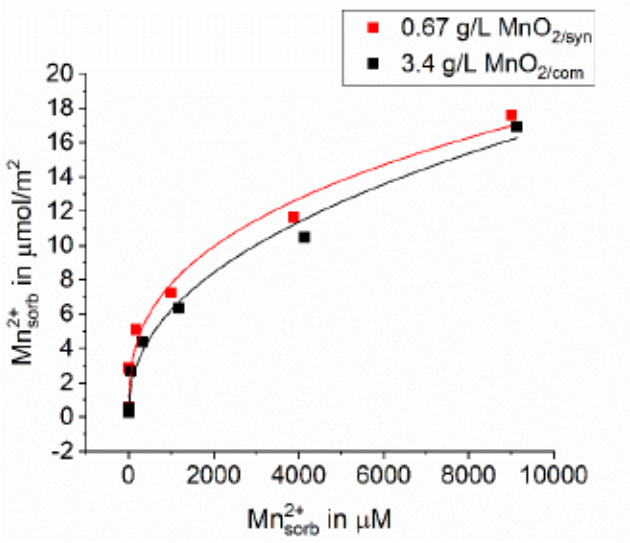

Figure B.13 Mn^{2+} sorption isotherms fitted by the Freundlich model for 0.67 g/L $MnO_{2/syn}$ and 3.4 g/L $MnO_{2/com}$ at pH 6 containing 20 mM MES buffer.

Effect of Mn^{2+} formation/addition

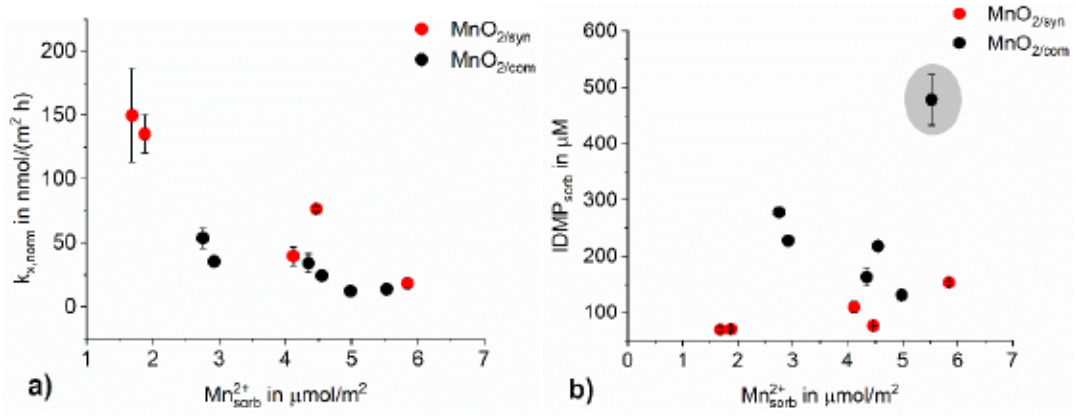

Figure B.14 Relationship between the sorbed Mn^{2+} concentration in µmol/m² at the end of the respective experiment and **a)** the normalized zero-order reaction rate $k_{x,norm}$ and **b)** the maximum sorbed IDMP concentration in µmol/L (indicating how much IDMP has been sorbed from the suspension) for the two investigated manganese dioxides $MnO_{2/syn}$ and $MnO_{2/com}$. Error bars in y represent the standard error of the zero-order reaction rate (**a)**), resp. the deviation between duplicates (**b)**). The validation experiment with $MnO_{2/com}$ and a Mn^{2+} starting concentration of 1 mM is included; it probably differs from the other experiments in **b)** due to the high initial presence of Mn^{2+}(highlighted with a grey circle).

Loading of the mineral with different amounts of Mn^{2+} prior to addition of IDMP to the suspension revealed a clear positive relationship between sorbed Mn^{2+} and sorbed IDMP. Sorbed Mn^{2+} was calculated via the difference between total added and measured Mn^{2+}_{aq} after sorption – before any IDMP was present. IDMP has been desorbed from the mineral and quantified as described in the manuscript.

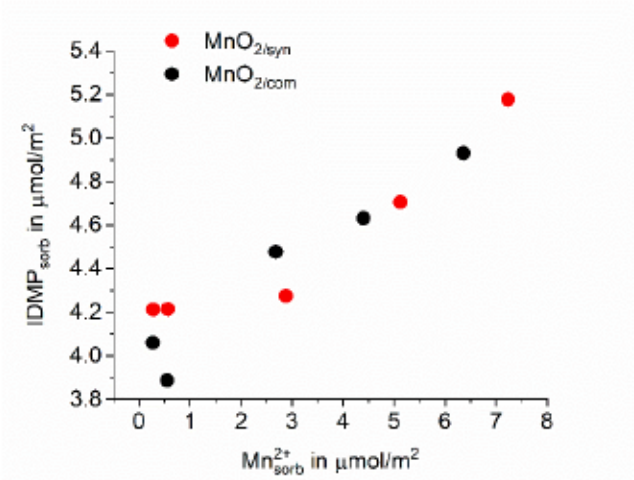

Figure B.15 Sorption experiment: Effect of sorbed Mn^{2+} (prior) on IDMP sorption onto the MnO_2 surface.

Isotope Section

Carbon isotopic fractionation during IDMP sorption onto Al_2O_3

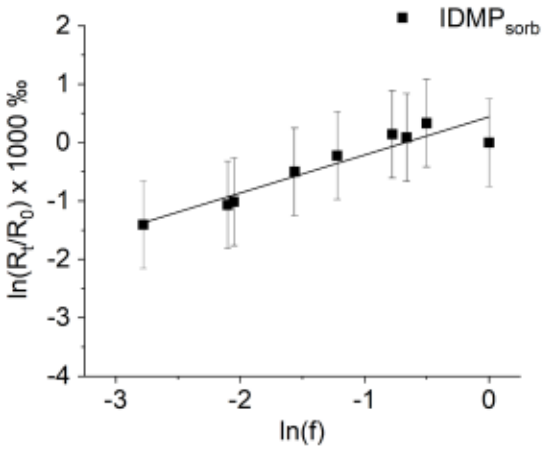

Figure B.16 Double-logarithmic Rayleigh plot for sorption of IDMP onto Al_2O_3. The calculated enrichment factor is ε_C = 0.65 ± 0.09 ‰ and is therefore regarded insignificant (measurement uncertainty of ± 0.5 ‰).

Graphical explanation of scenarios I and II described in the manuscript:

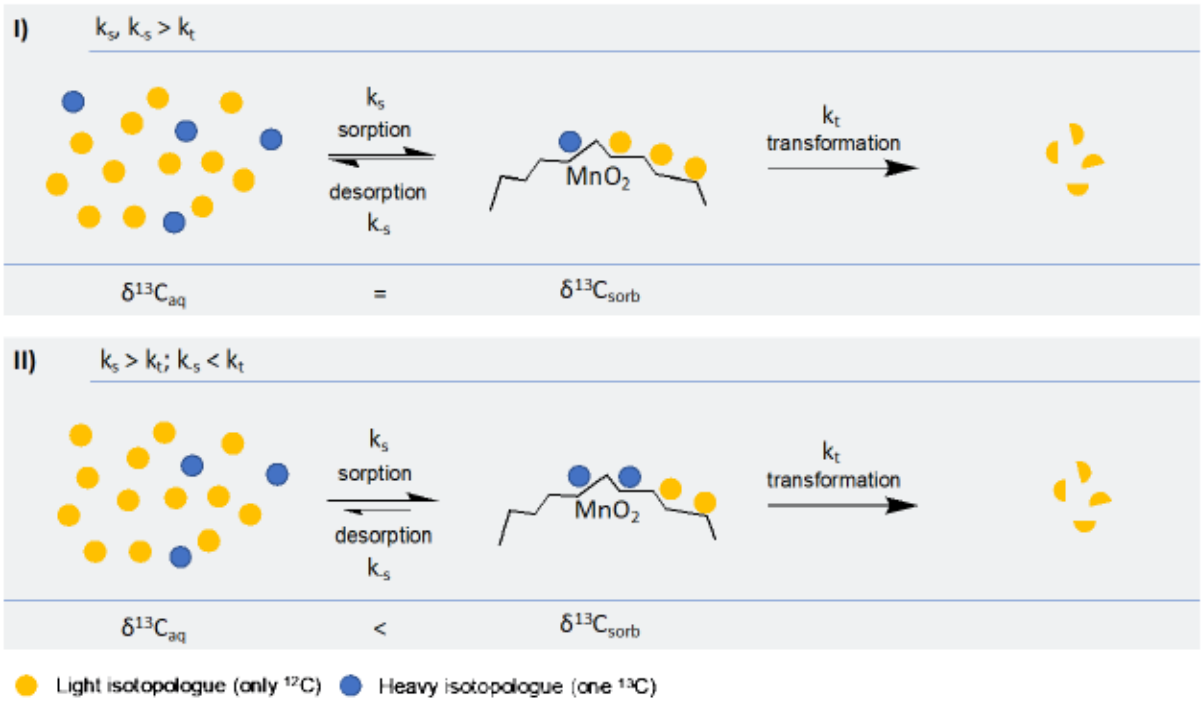

Figure B.17 Graphical depiction of the two scenarios described in the manuscript. In both scenarios, isotope fractionation is caused by the transformation step and is not masked by sorption (not leading to isotope fractionation). In scenario I, sorption and desorption are quite fast and thus a quick equilibrium between sorbed and aqueous phase is established. Thus, we find the same ^{13}C enrichment in the sorbed and in the aqueous phase. In scenario II, desorption is slow compared to transformation, as such the ^{13}C enrichment on the mineral (sorbed phase) is higher, as establishment of an equilibrium between sorbed and aqueous phase is quite slow. Additionally, k_t is higher (transformation is faster) in I) than in II).

Detailed Rayleigh plots

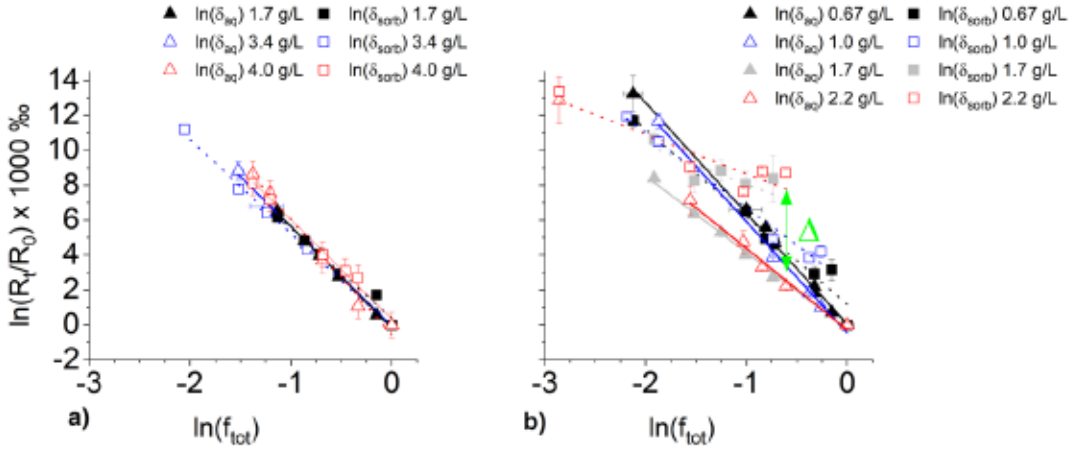

Figure B.18 Double logarithmic Rayleigh plots of aqueous and sorbed IDMP phases of seven IDMP transformation experiments: **a)** $MnO_{2/com}$ in concentrations of 1.7, 3.4 and 4.0 g/L, **b)** $MnO_{2/syn}$ in concentrations of 0.67, 1.0, 1.7 and 2.2 g/L. The δ-values are plotted versus the total remaining fraction of IDMP ($m_{tot} = m_{aq} + m_{sorb}$). Linear regressions are indicated by solid (aq) and dashed (sorb) lines, respectively. Errors of the normalized isotopic composition represent the standard deviations of all six isotopic measurements (triplicate analyses of duplicate experiments), while errors of the fraction represent the errors of IDMP quantification between duplicates experiments. The green delta indicates the deviation between aqueous and sorbed phase.

Enrichment factors

Table B.2 Enrichment factors (slope) and intercepts of double logarithmic Rayleigh equations of different IDMP transformation experiments. The remaining IDMP in the aqueous (aq) and sorbed (sorb) phase has been measured.

MnO_2	Phase	Slope in ‰	Intercept in ‰
1.7 g/L com	aq	-5.82 ± 0.74	-0.17 ± 0.51
	sorb	-5.11 ± 0.74	0.41 ± 0.51
	SUM	-5.68 ± 0.18	0.09 ± 0.12
3.4 g/L com	aq	-5.71 ± 0.62	-0.08 ± 0.66
	sorb	-5.38 ± 0.46	-0,14 ± 0.61
	SUM	-5.29 ± 0.11	0.00 ± 0.11
4.0 g/L com	aq	-6.58 ± 0.61	-0.54 ± 0.54
	sorb	-5.60 ± 0.60	0.34 ± 0.50
	SUM	-6.03 ± 0.19	-0.21 ± 0.12
0.67 g/L syn	aq	-6.33 ± 0.40	0.05 ± 0.37
	sorb	-5.00 ± 0.40	1.18 ± 0.37
	SUM	-6.28 ± 0.15	0.11 ± 0.09
1.0 g/L syn	aq	-6.37 ± 0.48	-0.46 ± 0.45
	sorb	-4.29 ± 0.40	2.42 ± 0.54 (w/o t_0)
	SUM	-5.64 ± 0.09	-0.12 ± 0.06
1.7 g/L syn	aq	-4.39 ± 0.48	-0.25 ± 0.59
	sorb	-2.20 ± 0.95	5.87 ± 1.35 (w/o t_0)
	SUM	-4.75 ± 0.13	-0.04 ± 0.10
2.2 g/L syn	aq	-4.67 ± 0.62	-0.29 ± 0.60
	sorb	-2.25 ± 0.40	6.41 ± 0.63 (w/o t_0)
	SUM	-4.64 ± 0.18	-0.03 ± 0.08

References

(1) Popov, K.; Rönkkömäki, H.; J Lajunen, L. H. *Critical Evaluation of Stability Constants of Phosphonic Acids (IUPAC Technical Report)*; Brazil, 2001; Vol. 73.

(2) Jochmann, M. A.; Blessing, M.; Haderlein, S. B.; Schmidt, T. C. A New Approach to Determine Method Detection Limits for Compound-Specific Isotope Analysis of Volatile Organic Compounds. *Rapid Communications in Mass Spectrometry* **2006**, *20* (24), 3639–3648. https://doi.org/10.1002/rcm.2784.

(3) Villegas, J. C.; Garces, L. J.; Gomez, S.; Durand, J. P.; Suib, S. L. Particle Size Control of Cryptomelane Nanomaterials by Use of H2O2 in Acidic Conditions. *Chemistry of Materials* **2005**, *17* (7), 1910–1918. https://doi.org/10.1021/cm048391u.

(4) Sigg, L.; Stumm, W. *Aquatische Chemie - Einführung in Die Chemie Natürlicher Gewässer*; vdf Hochschulverlag AG an der ETH Zürich, 2016. https://doi.org/10.3218/3768-5.

C - Supporting information to chapter 3

INTRODUCTION

Table C.1 Compilation of published and validated APP quantification methods and their key parameters.

Reference	APPs	Column	Eluents	Derivatization	Detector
Wang et al. 2019[1]	DTPMP, EDTMP, ATMP, HDTMP (PBTC, HEDP)	LC (ZORBAX Eclipse Plus C18)	H2O, ACN (0.1 % Formic acid)	Trimethylsilyl-diazomethane	HESI-MS/MS (QQQ)
Fürhacker et al. 2005[2]	DTPMP, EDTMP, ATMP	IC (Dionex AG7-AS7)	H2O (1 % MeOH), 100 mM HNO3 (1 % MeOH)	-	ICP-MS (QQQ)
Schmidt et al. 2014[3]	DTPMP, EDTMP, ATMP, HDTMP (HEDP)	IC (Thermo IonPac AS16)	H_2O, NaOH, (addition of DTPA)	-	ICP-MS
Armbruster et al. 2019[4]	DTPMP, EDTMP, ATMP (PBTC, HEDP)	IC (Thermo IonPac AS16)	H_2O, NAOH, MeOH	-	ESI-MS/MS (QQQ)
Klinger et al. 1997[5]	DTPMP, EDTMP, ATMP, HDTMP (PBTC, HEDP)	LC (Merck LiChrospher 100 Diol)	Isopropyl alcohol, n-Hexane	Diazomethane	Particle beam (PB)-MS
Tewari et al. 1997[6]	DTPMP, EDTMP	IC (Thermo AS11)	0-200 mM NaOH	-	PAD (Au WE, Ag/AgCl RE)
Wong et al. 1987[7]	DTPMP, EDTMP, ATMP, HEDTMP (HEDP)	IC (Waters IC Pak A)	Nitric Acid (15 mM)	-	RID
Weiss & Hägele 1987[8]	DTPMP, EDTMP, ATMP (HEDP)	IC (HPIC AS7, Dionex)	30-70 mM HNO_3	Post-colµmn: Complex formation with Fe^{III}	UV/vis absorption
Nowack 1997[9]	DTPMP, EDTMP, ATMP (HEDP)	LC (ion-pair chromatography using RP colµmn: PLRP-S, polymer labs)	20 mM $NaHCO_3$ and 1 mM tetrabutylammonium bromide in H_2O	Pre-column: Complex formation with Fe^{III}	UV/vis absorption
Vaeth, Sladek & Kenar 1987[10]	ATMP, EDTMP, DTPMP	IC (HPIC AS7, Dionex)	3.2 mM EDTA + 0.17 mM KCl, pH 5.1	Post-colµmn: oxidation to phosphate by persulfate, then derivatization using molybdenum blue	UV/vis absorption

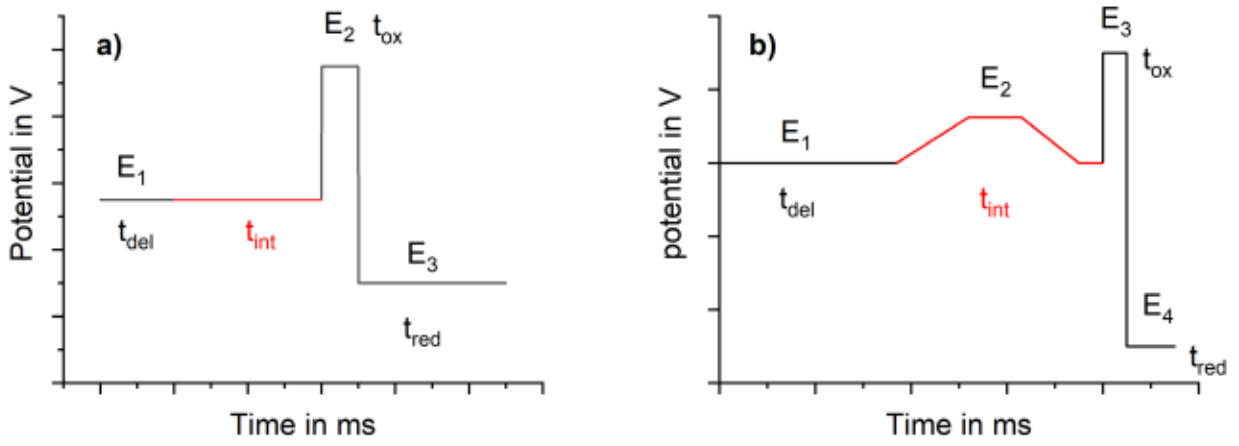

Figure C.1 Exemplary potential cycles of a) PAD (corresponding to mode I detection) and b) integrated PAD (corresponding to mode II detection).

Background on Pulsed Amperometric Detection (PAD)

In PAD, a short potential sequence including a high oxidation and a low reducing potential, typically lasting <1 second is repetitively applied. This is particularly advantageous when analytes and/or transformation products strongly adsorb onto the electrode surface and was primarily developed for the analysis of carbohydrates[11]. After the oxidation step, a higher oxidation potential is applied to oxidatively remove residual analyte and/or transformation products from the WE. In the successive reduction step, a low reduction potential is applied to reduce the formed gold oxide back to gold. To prevent monitoring non-faradaic current, a delay time is required prior to the measurement interval, allowing charging currents to decay[11,12]. A schematic depiction of a PAD waveform is provided in Figure C.1 **a**. Developments regarding PAD and instrumentation allow this detector to be coupled to high-pressure liquid chromatography (HPLC) systems with purely aqueous eluents, despite the inherent sensitivity of pulsed amperometric detection toward pressure and pH.

Table C.2 Explanation of different potentials and times applied in the IPAD waveform (see Fig S1 b)[11,13]

Potential/Time	Description
E_1	Starting (prior to onset of oxide formation) and ending potential of the scan (more negative than oxide dissolution)
E_2	Maximum potential of the scan for optimal analyte oxidation
E_3	Oxidation potential to initiate formation of "cleaning oxide"
E_4	Reduction potential to initiate dissolution of inert oxide
t_{del}	Delay time: Allow the charging current to decay, before the faradaic current produced by redox reactions at the electrodes is recorded
t_{int}	Integration time: Measurement signal is recorded
t_{ox}	Time for application of the oxidation potential E_3
t_{red}	Time for application of the reduction potential E_4

EXPERIMENTAL SECTION

Purity of DTPMP & EDTMP

Nuclear magnetic resonance spectroscopy (NMR)

To assure the purity of the acquired EDTMP, ^{1}H- and ^{31}P-{^{1}H}-NMR measurements were conducted (NMR department, Chemistry Department, University of Tübingen).

10 mg EDTMP (DTPMP) and 600 µL of deuterated water (D_2O) were mixed and vortexed for 5 s. Afterwards, 600 µL were transferred to an NMR glass tube. The measurement was performed on a Bruker AMX 600 MHz NMR spectrometer (Bruker, Billerica, MA, USA), operating at 600.13 MHz for hydrogen observation with a zg30 pulse program and at 242.94 MHz for phosphorous observation with a zgpg30 pulse program. The acquisition parameters used for this experiment with 1D sequence with power-gated decoupling and a 30 ° flip angle were as follows for ^{1}H (^{31}P): number of scans: 32 (64), spectral width: 12019.23 Hz (96153.84 Hz), offset (O1): 3705.80 Hz (-12146.85 Hz), acquisition time: 2.73 s (0.34 s), relaxation delay (d1): 1.00 s (2.00 s). The spectrum was quantitatively evaluated using the Bruker Top Spin 4.1.4 software.

Results

^{31}P-NMR-spectroscopy, due to its 100% natural abundance, wide range of chemical shift and high sensitivity[14], is a suitable analytical tool to characterize the purity of phosphonates.

EDTMP

In the ^{31}P-{^{1}H}-NMR-spectrum of EDTMP, shown in Figure C.2, we can see one signal attributed to EDTMP representing all chemically equivalent phosphonate-groups (δ (ppm): 8.76) Impurities are marked with "*". The sum of all signal-integrals is normalized to 100. Impurities containing phosphorous of the analysed EDTMP amount to only 3.40 %. The used EDTMP in the experiments is therefore of high purity with 96.6%. The ^{1}H-NMR-spectrum is shown in Figure C.3. Therein we can see the signals attributed to EDTMP in a ratio of 4:8. The singulet represents the protons of the ethylenediamine moiety in the middle (δ (ppm): 3.88) and the duplet represents the protons of the four phosphonate groups attached to the amine-moieties (δ (ppm): 3.52). Impurities are marked with "*". The sum of all signal-integrals is normalized to 100. Impurities of the analysed EDTMP amount to only 2.52%. The used EDTMP in the experiments is therefore of high purity with 97.48%.

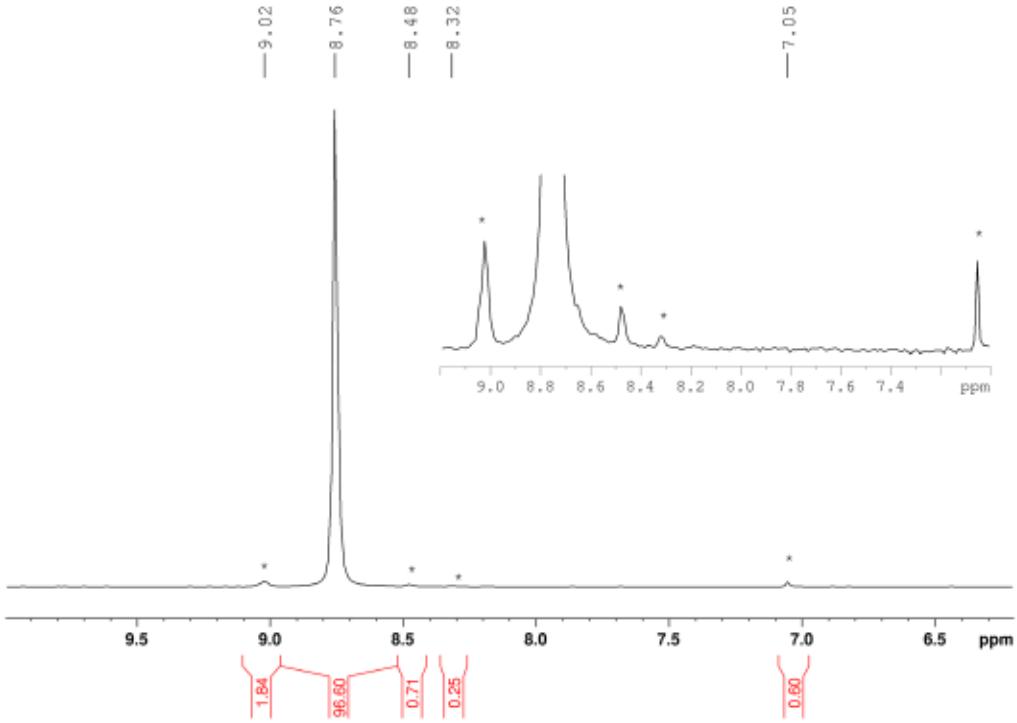

Figure C.2 ^{31}P-{^{1}H}-NMR-spectrum of EDTMP in D_2O. δ (ppm): 8.76. Impurities are marked with "*". The sum of integrals is normalized to 100.

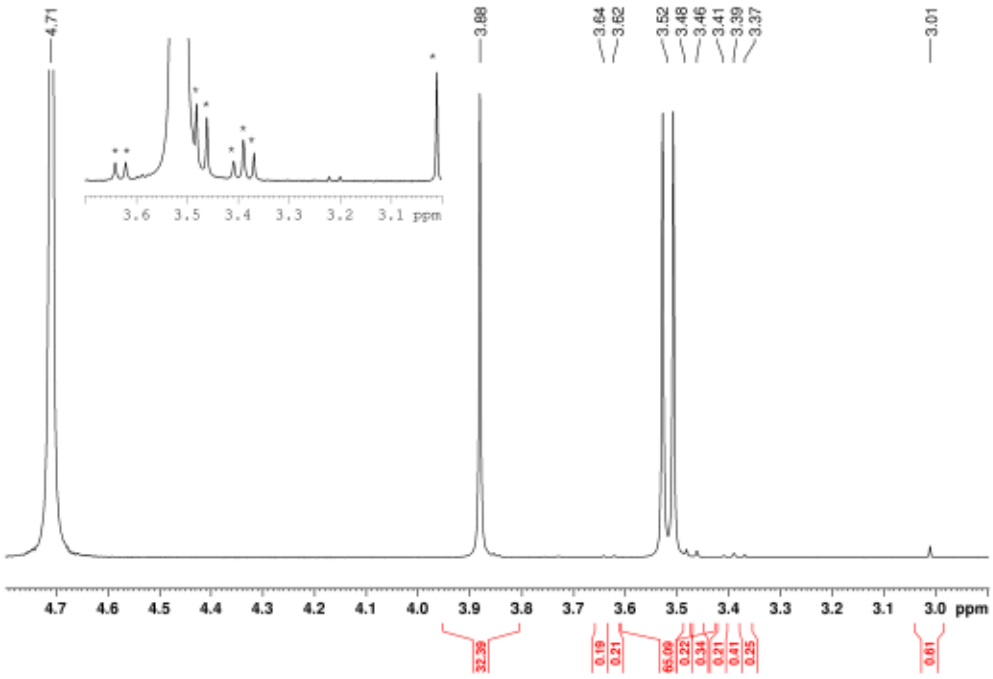

Figure C.3 ^{1}H-NMR-spectrum of EDTMP in D_2O. δ (ppm): 9.23, 12.94. Impurities are marked with "*". The sum of integrals is normalized to 100.

DTPMP

In the ^{31}P-{^{1}H}-NMR-spectrum (Fig. C.4), two main signals in a ratio of 1:4 can be seen, which represent the phosphonate-group in the middle of DTPMP (δ (ppm): 12.94) and the four phosphonate groups of DTPMP attached to the outer amine moieties (δ (ppm): 9.23). Impurities are marked with an asterisk. The sum of all signal-integrals is normalized to 100. Impurities of the analysed DTPMP contribute 1.37 %. The purity of the DTPMP used in the experiments is therefore >98.6 %.

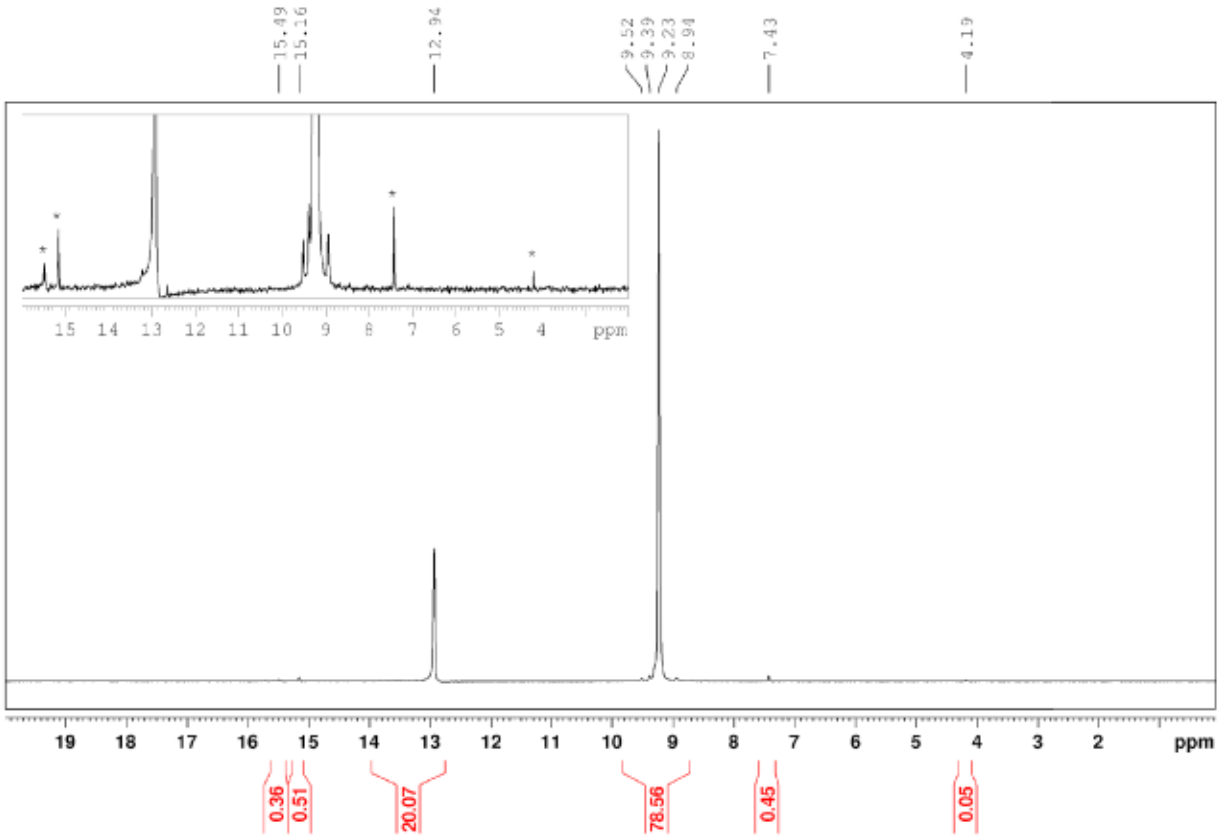

Figure C.4 ^{31}P-{^{1}H}-NMR-spectrum of DTPMP in D_2O. δ (ppm): 9.23, 12.94. Impurities are marked with an asterisk. The sum of integrals is normalized to 100.

Instrumentation

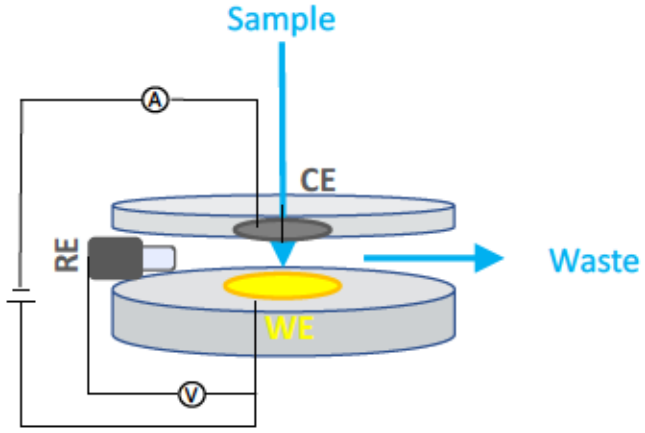

Figure C.5 Schematic depiction of the Wall-Jet cell geometry used for amperometric detection throughout this work. RE = reference electrode, WE = working electrode, CE = counter electrode.

RESULTS AND DISCUSSION

Chromatographic separation

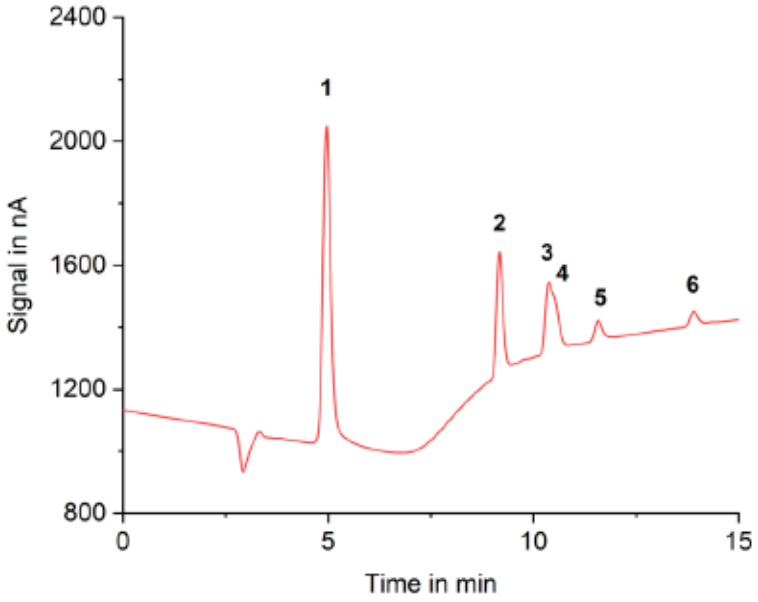

Figure C.6 Chromatogram of a 10 µM multi-phosphonate standard using pure NaOH eluents. Chromatographic conditions: column: Thermo Scientific Dionex AS16 (2x5 + 2x250mm), 30 °C; eluents: A 10 mM NaOH, B 150 mM NaOH, 30 °C, (no column regeneration with 300 mM NaOH for months); gradient profile: B 0-17 min 20-80 % B, 17-20 min 80 % B; 20.1-40 min 0 % B; detection: amperometric detection with gold WE, Pt CE and AG/AgCl RE, waveform as depicted in Figure 3.5 3) with E_2 = 0.27 V; injection volume: 50 µL; 10 µM of 1 = AMPA, 2 = glyphosate, 3 = IDMP, 4 = ATMP, 5 = EDTMP, 6 = DTPMP.

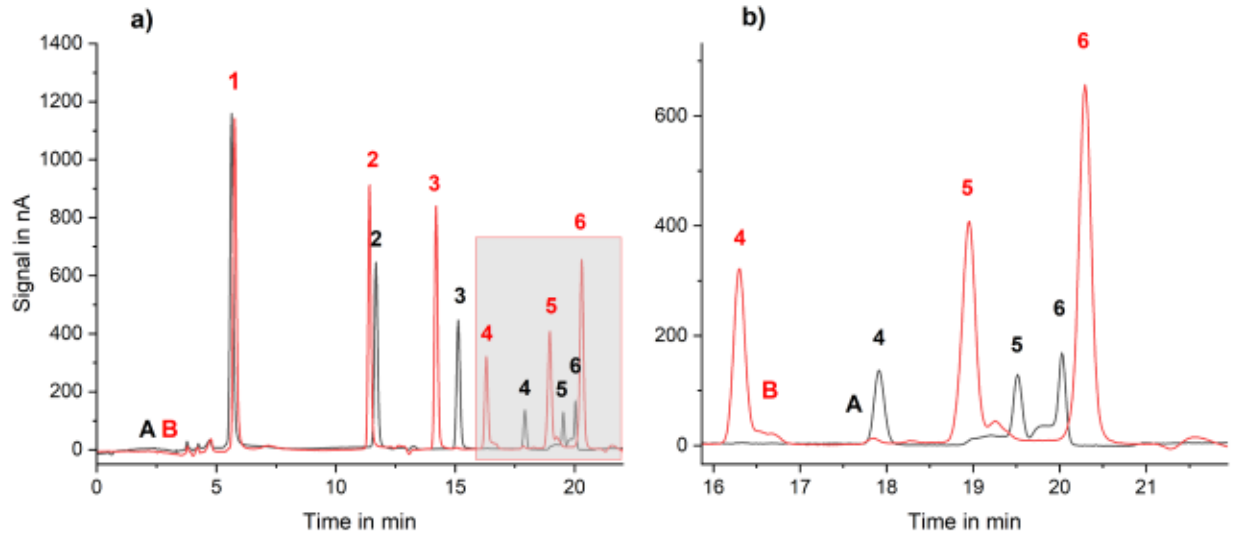

Figure C.7 Two chromatograms of the same 10 µM multi-standard using different gradient profiles and eluents B (**A:** 50 mM NaOH and 400 mMMNaOAc, **B**: 15 mM NaOH and 400 mM NaOAc), shown after blank substraction. **a)** shows the full chromatogram, **b)** displays a magnification of the grey rectangle in **a)**. The chromatographic conditions for **B** correspond to those in the caption of Figure 3.2. Chromatographic conditions for **A**: column: Thermo Scientific Dionex AS16 (2x5 + 2x250 mm) at 30 °C; eluents **A**: 15 mM NaOH, **B**: 50 mM NaOH + 400 mM NaOAc; flow rate: 0.3 mL/min; gradient profile: 0-6 min 0 % B, 6-14 min 10-30 % B, 14-18 min 30-100 % B, 18-19 min 100 % B, 20.1-22 min 0 % B, post run: 8 min with 100 % eluent A at 0.6 mL/min; detection: amperometric detector with gold WE, Pt CE and Ag/AgCl RE, 35 °C; waveform: see Figure 3.5 3); injection volume: 50 µL; 10 µM of: 1 = AMPA, 2 = glyphosate, 3 = IDMP, 4 = ATMP, 5 = EDTMP, 6 = DTPMP.

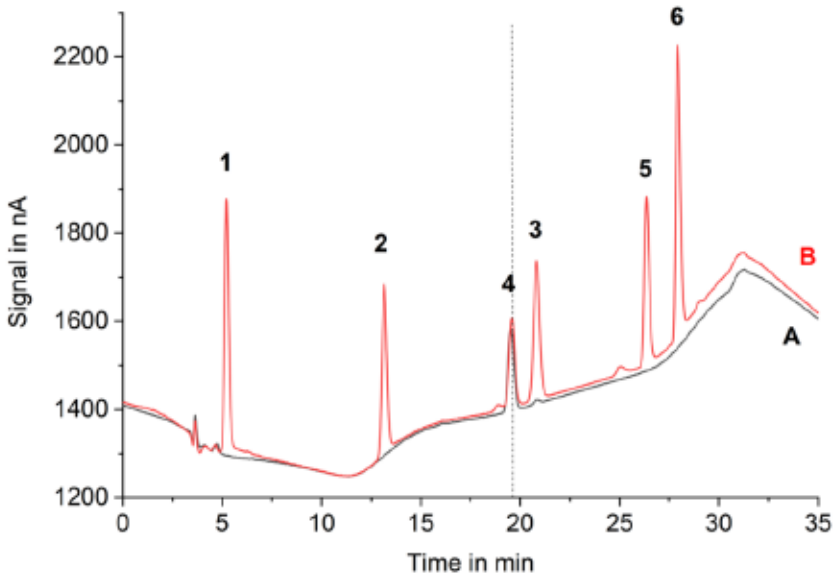

Figure C.8 Chromatograms of **A** a single ATMP standard and **B** a multi-phosphonate standard. Chromatographic conditions: column: Thermo Scientific Dionex AS16 (2x5 + 2x250 mm) at 30 °C, eluents: A 20 mM NaOH, B 50 mM NaOH + 400 mM NaOAc, 30 °C, (no column regeneration with 300 mM NaOH for months); gradient profile: 0-5 min 10 % B, 5-13 min 10-30 % B, 17-30 min 30-100 % B, 17-20 min 100 % B, 20.1-40 min 0 % B; detection: amperometric detection with gold WE, Pt CE and AG/AgCl RE, waveform as depicted in Figure 3.5 **3)** with E_2 = 0.25 V; injection volume 50 µL. 10 µM of 1 = AMPA, 2 = glyphosate, 3 = IDMP, 4 = ATMP, 5 = EDTMP, 6 = DTPMP.

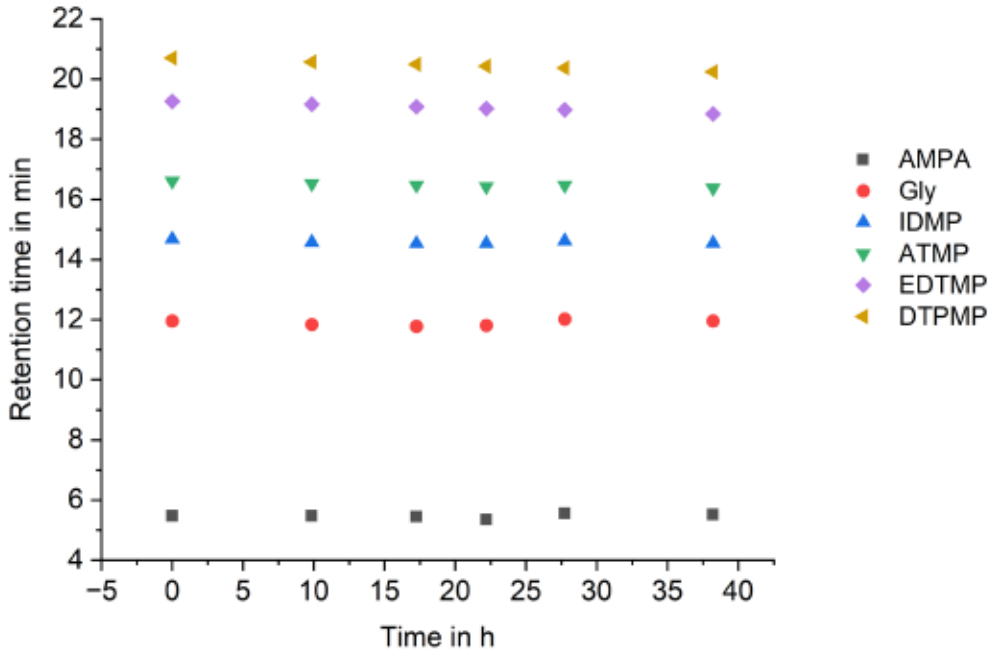

Figure C.9 Retention time of the six investigated analytes in repetitive measurements of a 1 µM multi-standard over 38 hours using the final optimized method presented in the text. Chromatographic conditions: see caption of Figure 3.2.

(Integrated) pulsed amperometric detection

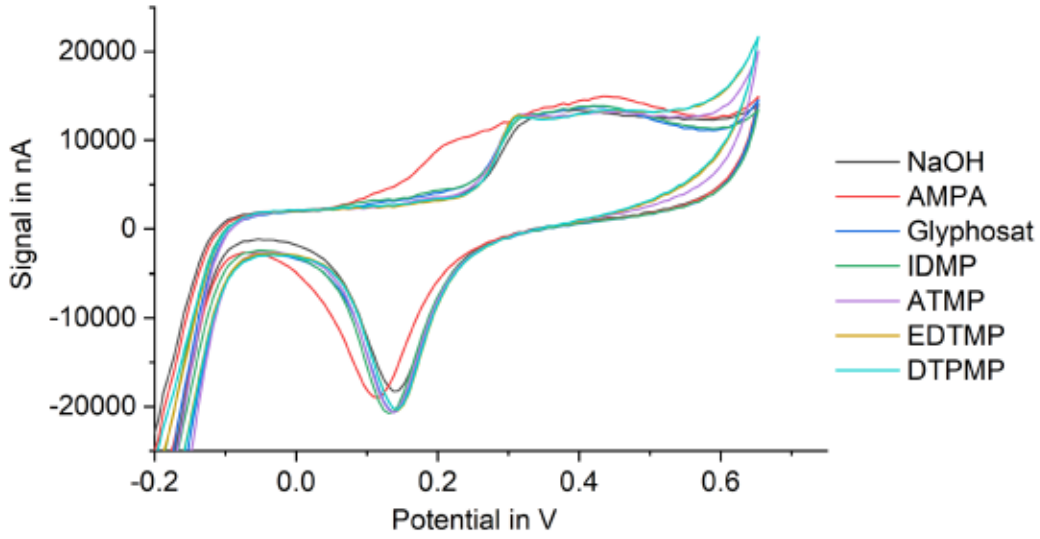

Figure C.10 Cyclovoltammograms of 0.5 mM of the respective aminophosphonate in 0.1 M NaOH background solution, next to the pure background solution.

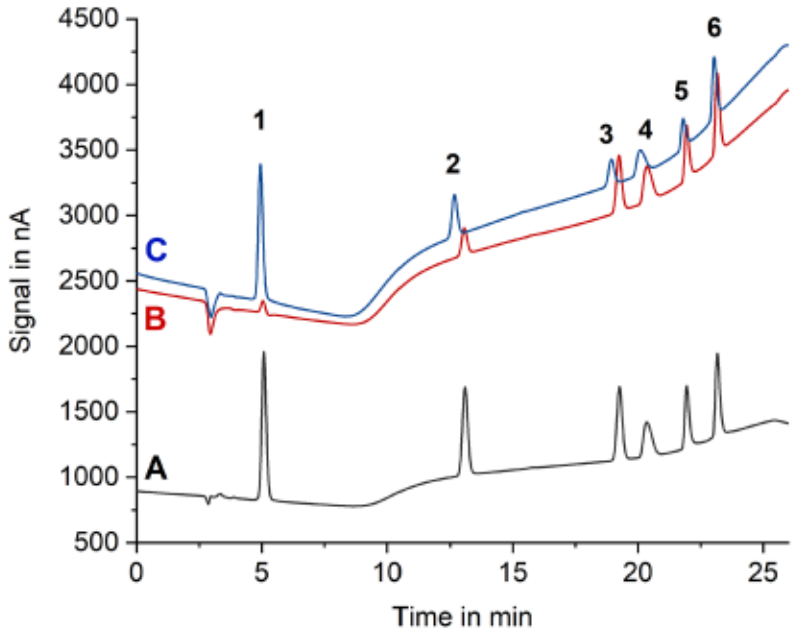

Figure C.11 Chromatogram recorded using IPAD (**A**) compared to two chromatograms recorded using PAD (**B** & **C**). Chromatographic conditions: **A**, **B** & **C**: Column: Thermo Scientific Dionex AS16 (2x5 + 2x250mm), 30 °C; eluents: A: 15 mM NaOH, B: 50 mM NaOH + 400 mM NaOAc. Gradient profile:0-5 min 10 % B, 5-13 min 10-30 % B, 13-17 min 30-100 % B, 17-20 min 100 % B, 20.1-40 min 0 % B; detection: amperometric detector with gold WE, Pt CE and Ag/AgCl RE. Waveforms: **A**: IPAD waveform similar to Figure 3.4 **3**) with E_2 = 0.27 V, **B**: PAD waveform similar to Figure 3.4 **2**) with E_1 = 0.15 V, C: PAD waveform similar to Figure 3.5 **2**) with E_1 = 0.27 V; compounds: 10 µM of 1 = AMPA, 2 = glyphosate, 3 = IDMP, 4 = ATMP, 5 = EDTMP, 6 = DTPMP; injection volume: 50 µL.

Screening of detector parameters:

Table C.3 Detector method changes and resulting peak areas of all six analytes in nA*min. Benchmark method applies an IPAD waveform with E_2 = 0.25 V, as depicted in Figure 3.5 **3**). PAD indicates, that PAD has been applied as depicted in Figure 3.4 **2**). If not indicated otherwise, IPAD has been applied. The potential numbers (E_1, E_2, …) for PAD and IPAD are explained in Figure C.1 and Table C.2.

Method change compared to benchmark	Area in nA*min					
	AMPA	glyph	IDMP	ATMP	EDTMP	DTPMP
-	277.12	109.65	106.60	123.75	50.31	102.43
-	256.66	119.15	117.84	149.30	68.03	120.89
E_2 = 0.23 V	212.90	114.68	120.08	157.18	70.13	121.13
E_2 = 0.21 V	133.63	100.78	124.22	167.99	74.50	120.53
E_2 = 0.27 V	270.50	145.32	127.28	155.31	74.12	127.54
t_{int} = 750 ms (only trapez)	292.26	145.53	139.87	147.63	70.93	122.65
Change order of E_3 and E_4	262.78	118.27	120.98	172.09	67.46	114.56
Change order of E_3 and E_4 and change t_{ox} & t_{red} (40 vs 60 ms)	247.22	115.74	110.14	149.08	56.56	98.09
Change order of E_3 and E_4 and t_{ox} & t_{red} both 50 ms	261.51	109.14	110.67	158.52	59.02	104.66
PAD, E_1=0.15	22.02	56.60	111.60	103.04	89.89	135.96
PAD, E_1=0.27	237.69	90.24	52.81	70.98	50.49	103.01

Table C.4 Exact potentials and times of the final optimized IPAD waveform.

Time in ms	Start potential in V	End potential in V	Integration
0 - 370	0.0	0.0	
370 - 520	0.0	0.0 – 0.27	Start
520 - 630	0.27	0.27	
630 - 750	0.27	0.0	End
750 - 800	0.0	0.0	
800 - 840	-1.0	-1.0	
840 - 900	0.6	0.6	

Greenness

To ensure the highest possible comparability between the three methods and transparency, all criteria have been assigned with the default weight of 2, except for the **principle 1** "Direct analytical techniques" and **3** "In-situ measurements", which were assigned the weight 1. As all compared methods are off-line methods conducting batch analysis, **principles 1** and **3** are irrelevant for this comparison. The second point that needs clarification concerns **principle 8** "Number of detectable analytes in a single run": One major advantage of the presented IC-IPAD method is its ability to measure all six analytes presented above – AMPA, glyphosate, IDMP, ATMP, EDTMP, and DTPMP – in the same chromatographic run. While existing polyphosphonate methods sometimes included other substances, e.g. HEDP, PBTC or sulfate, in this work we solely focus on the six substances mentioned above. Thus, if a method is able to quantify sulfate, nitrate, PBTC and EDTMP, the "number of detectable analytes" will be counted one (EDTMP) in this comparison. Last but not least the "amount of sample needed" (**principle 2**) needs clarification. Due to the different concentration ranges of the samples measured in the three methods (natural samples vs. laboratory batch experiments) and the required preconcentration steps for natural samples, the "amount of sample needed" was not comparable. Therefore, the injection volumes were drawn for comparison instead.

Application example: DTPMP oxidation by MnO_2

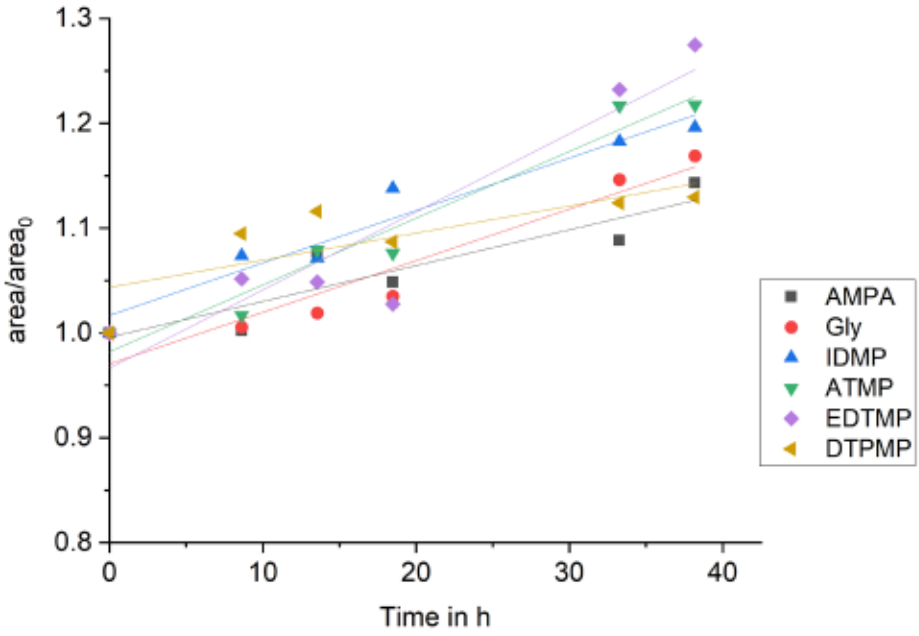

Figure C.12 Normalized peak areas of the six analytes in 1 µM multi-phosphonate check standards over time. The peak areas are all normalized to the peak area of the respective analyte measured at timepoint zero. From the linear regression (see below) a correction factor – relative increase per hour – has been calculated for each analyte, which was then applied to the sample measurements, see equation below.

Correction of sample concentrations:

The corrected concentration is derived by subtracting the product of correction factor (f), time (t) in hours, and initially calculated concentration (c_{int}) from the initially calculated concentration.

$$c_{corr} = c_{init}(1 - f \cdot t)$$

Table C.5 Calculated correction parameters from the 1 µM check standards shown in Figure C.9.

Analyte	Relative increase after 38 hours	r^2 of linear regression	Correction factor f (rel. increase/h)
AMPA	1.143404	0.8274	0.003755
Glyphosate	1.168947	0.9218	0.004424
IDMP	1.196055	0.9434	0.005134
ATMP	1.217679	0.9563	0.005701
EDTMP	1.274751	0.8727	0.007195
DTPMP	1.129571	0.6225	0.003393

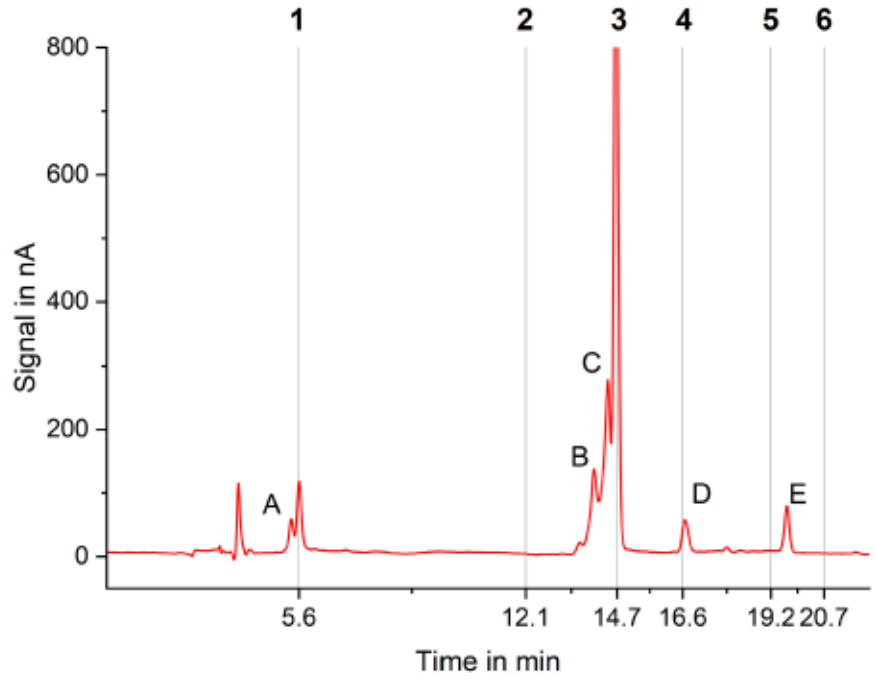

Figure C.13 Chromatogram of the aqueous phase of the DTPMP/MnO_2 transformation experiment after 3.0 hours applying blank subtraction. For better depiction of the low concentrated TPs, the y-axis maximum was decreased below the IDMP peak height. Unknown TPs were assigned the letters A-E. Chromatographic conditions as described in the caption of Figure 3.2. Compounds: 1 = AMPA, 2 = glyphosate, 3 = IDMP, 4 = ATMP, 5 = EDTMP, 6 = DTPMP; injection volume: 50 µL.

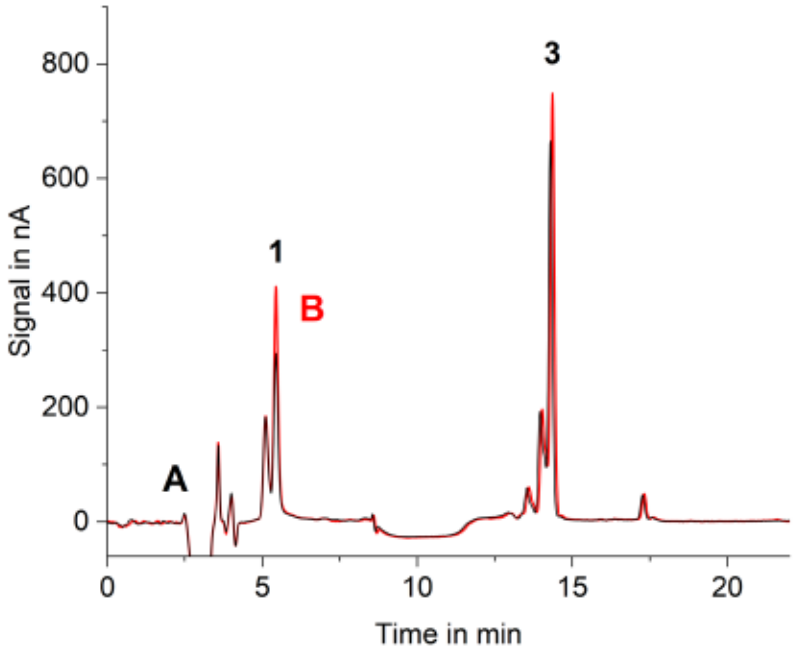

Figure C.14 Chromatograms of the sorbed fraction of the sampling point after 0.67 h, with (**A**) and without (**B**) standard addition of 1 µM AMPA (**1**) and IDMP (**2**). Chromatographic conditions as described in the caption of Figure 3.2.

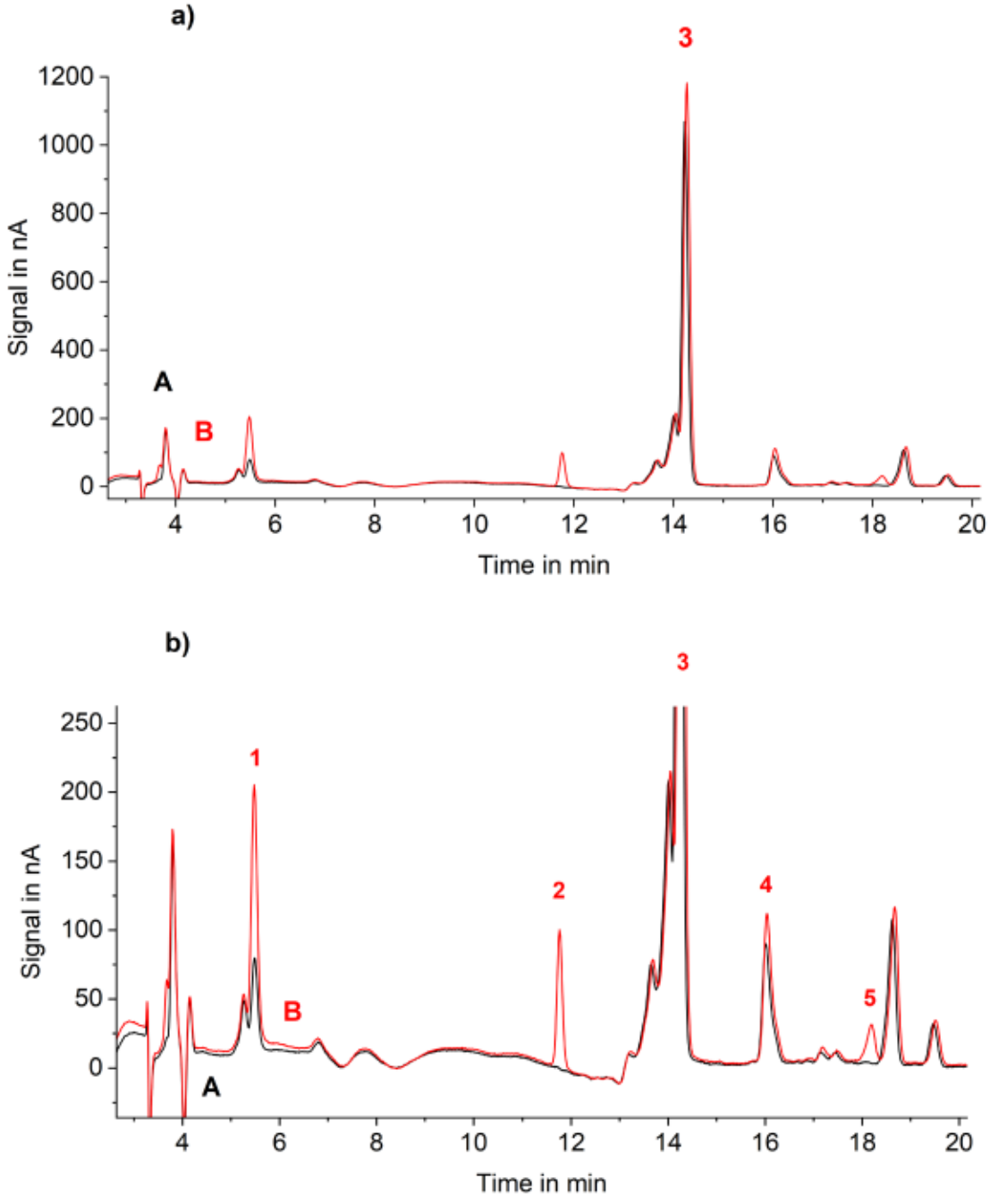

Figure C.15 Chromatograms of the aqueous phase of the DTPMP/MnO_2 transformation experiment after 3.0 hours applying blank subtraction. **A** shows the pure sample, while **B** shows a sample with standard addition of 1 µM AMPA (**1**), glyphosate (**2**), IDMP (**3**), ATMP (**4**), and EDTMP (**5**). **a)** shows the full chromatogram, while **b)** shows y-axis magnification. Chromatographic conditions as described in the caption of Figure 3.2.

References

(1) Wang, S.; Sun, S.; Shan, C.; Pan, B. Analysis of Trace Phosphonates in Authentic Water Samples by Pre-Methylation and LC-Orbitrap MS/MS. *Water Res* **2019**, *161*, 78–88. https://doi.org/10.1016/j.watres.2019.05.099.

(2) Fürhacker, M.; Lesueur, C.; Pfeffer, M.; Köllensperger, G.; Popp, M.; Mentler, A. *Phosphonate - AMPA (Aminomethylphosphonsäure). Herkunftsabschätzung, Umweltkonzentrationen Und Photolyseabbau*; Vienna, 2005.

(3) Schmidt, C. K.; Raue, B.; Brauch, H. J.; Sacher, F. Trace-Level Analysis of Phosphonates in Environmental Waters by Ion Chromatography and Inductively Coupled Plasma Mass Spectrometry. *Int J Environ Anal Chem* **2014**, *94* (4), 385–398. https://doi.org/10.1080/03067319.2013.831410.

(4) Armbruster, D.; Müller, U.; Happel, O. Characterization of Phosphonate-Based Antiscalants Used in Drinking Water Treatment Plants by Anion-Exchange Chromatography Coupled to Electrospray Ionization Time-of-Flight Mass Spectrometry and Inductively Coupled Plasma Mass Spectrometry. *J Chromatogr A* **2019**, *1601*, 189–204. https://doi.org/10.1016/j.chroma.2019.05.014.

(5) Klinger, J.; Sacher, F.; Brauch, H.-J.; Maier, D. Determination of Organic Phosphonates in Aqueous Samples Using Liquid Chromatography/ Particle-Beam Mass Spectrometry. *Acta hydrochim. hydrobiol.* **1997**, *25* (2), 79–86.

(6) Tewari, M.-J. K.; van Stroe-Bieze, S. Analysis of Amine-Containing Phosphonates in Detergent Powders by Anion-Exchange Chromatography with Pulsed Amperometric Detection. *J Chromatogr A* **1997**, *771*, 155–161.

(7) Wong, D.; Jandik, P.; Jones, W. R.; Hagenaars, A. Ion Chromatography of Polyphosphonates with Direct Refractive Index Detection. *J Chromatogr* **1987**, *389*, 279–285.

(8) Weiss, J.; Hägele, G. Lonen-Chromatographische Analyse Anorganischer Und Organischer Komplexbildner. *Fresenius Z Anal Chem* **1987**, *348*, 46–50.

(9) Nowack, B. Determination of Phosphonates in Natural Waters by Ion-Pair High-Performance Liquid Chromatography. *J Chromatogr A* **1997**, *773*, 139–146.

(10) Vaeth, E.; Sladek, P.; Kenar, K. Ionen-Chromatographie von Polyphosphaten Und Phosphonaten. *Fresenius Z Anal Chem* **1987**, *329*.

(11) Weiss, J. *Handbook of Ion Chromatography*, 4th ed.; Wiley-VCH: Weinheim, 2016.

(12) Fedorowski, J.; LaCourse, W. R. A Review of Pulsed Electrochemical Detection Following Liquid Chromatography and Capillary Electrophoresis. *Anal Chim Acta* **2015**, *861*, 1–11. https://doi.org/10.1016/j.aca.2014.08.035.

(13) LaCourse, W. R. *Pulsed Electrochemical Detection in High Performance Liquid Chromatography*, 1st ed.; Wiley & Sons Ltd: New Jersey, 1997.

(14) Oromí-Farrús, M.; Minguell, J. M.; Oromi, N.; Canela-Garayoa, R. A Reliable Method for Quantification of Phosphonates and Their Impurities by ^{31}P NMR. *Anal Lett* **2013**, *46* (12), 1910–1921. https://doi.org/10.1080/00032719.2013.780239.

D - Supporting information to chapter 4

RESULTS AND DISCUSSION

pH control in conducted experiments

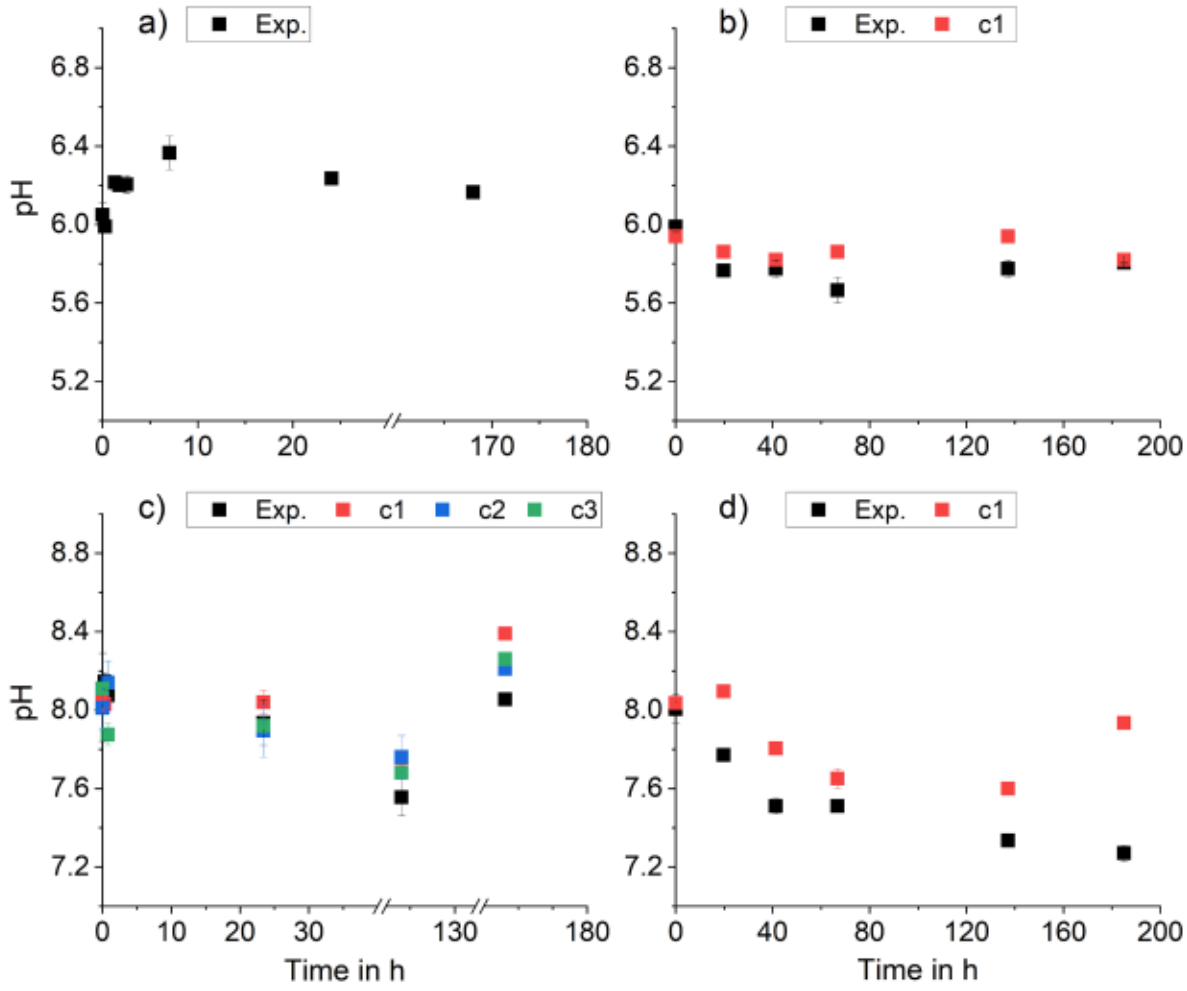

Figure D.1 pH values over time in four different DTPMP transformation experiments (Exp.) including several controls (c1-c3, respectively). a): Exp.: 1.0 g/L MnO_2 oxic in MES (black); b): Exp.: 1 mM $MnCl_2$ oxic in MES (black), c1: no $MnCl_2$ (red); c): Exp.: 1.0 g/L MnO_2 oxic in wastewater (black), c1: pure wastewater (red), c2: no MnO_2 (blue), c3: no DTPMP (green); d): Exp.: 1 mM $MnCl_2$ oxic in wastewater (black), c1: no DTPMP (red).

DTPMP stability in the absence of manganese

In the absence of MnO_2 and Mn^{2+} no DTPMP transformation and no AMPA or glyphosate formation could be detected.

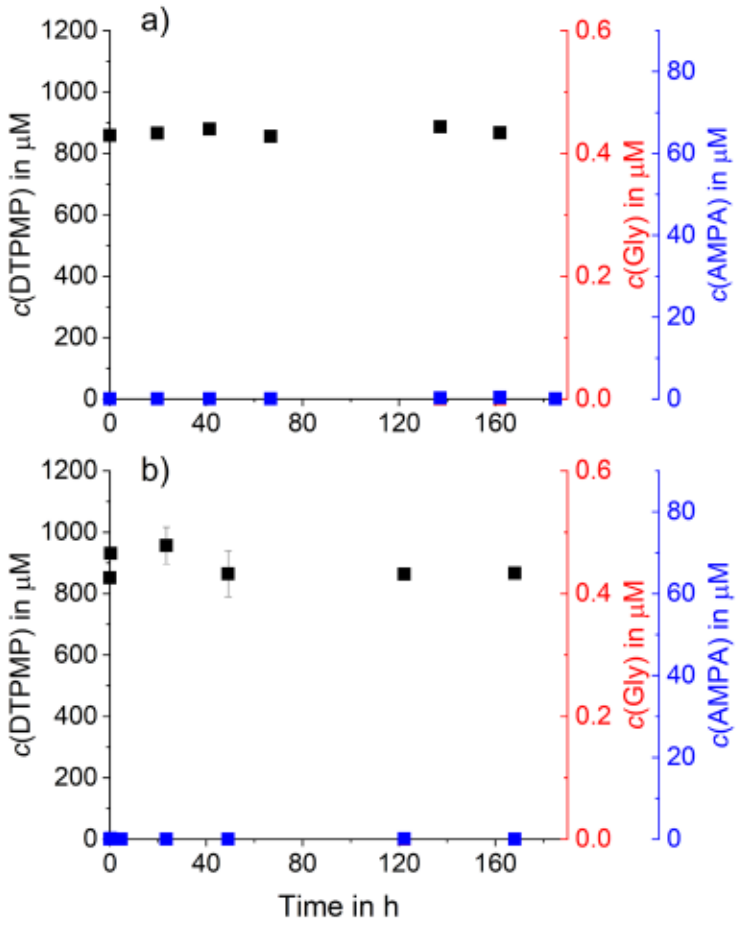

Figure D.2 DTPMP (black), glyphosate (red) and AMPA (blue) concentrations quantified by means of IC-IPAD (DTPMP) and LC-QQQ (glyphosate, AMPA) in two control experiments without manganese in **a)** 20 mM MES buffer (pH 6) and **b)** wastewater (pH 8). DTPMP was quantified using IC-IPAD, while glyphosate and AMPA were quantified using LC-QQQ.

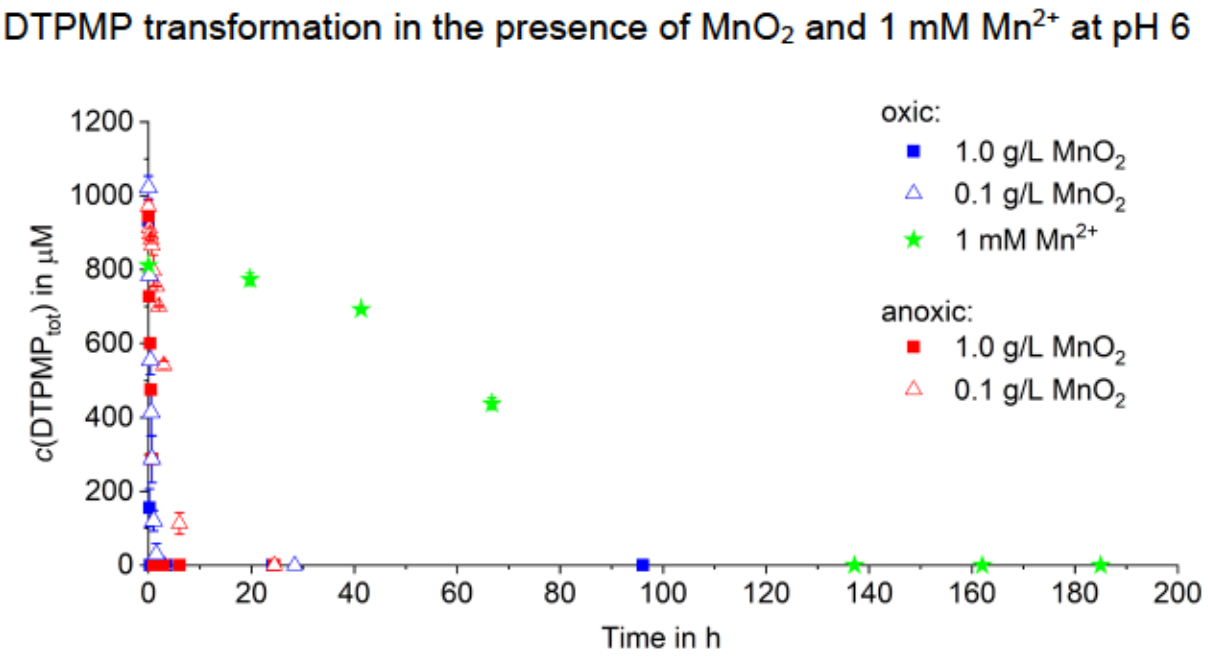

Figure D.3 Total DTPMP concentrations quantified using IC-IPAD as a function of time for all four experiments with MnO_2 (oxic (blue) and anoxic (red)) and one experiment containing 1 mM $MnCl_2$ (oxic, green) in aqueous MES buffer (pH 6). (Figure 2 in the main text amended by the experiment containing 1 mM Mn^{2+} (oxic conditions) at pH 6.) Error bars represent absolute errors between duplicates.

Additional concentration profiles of transformation experiments

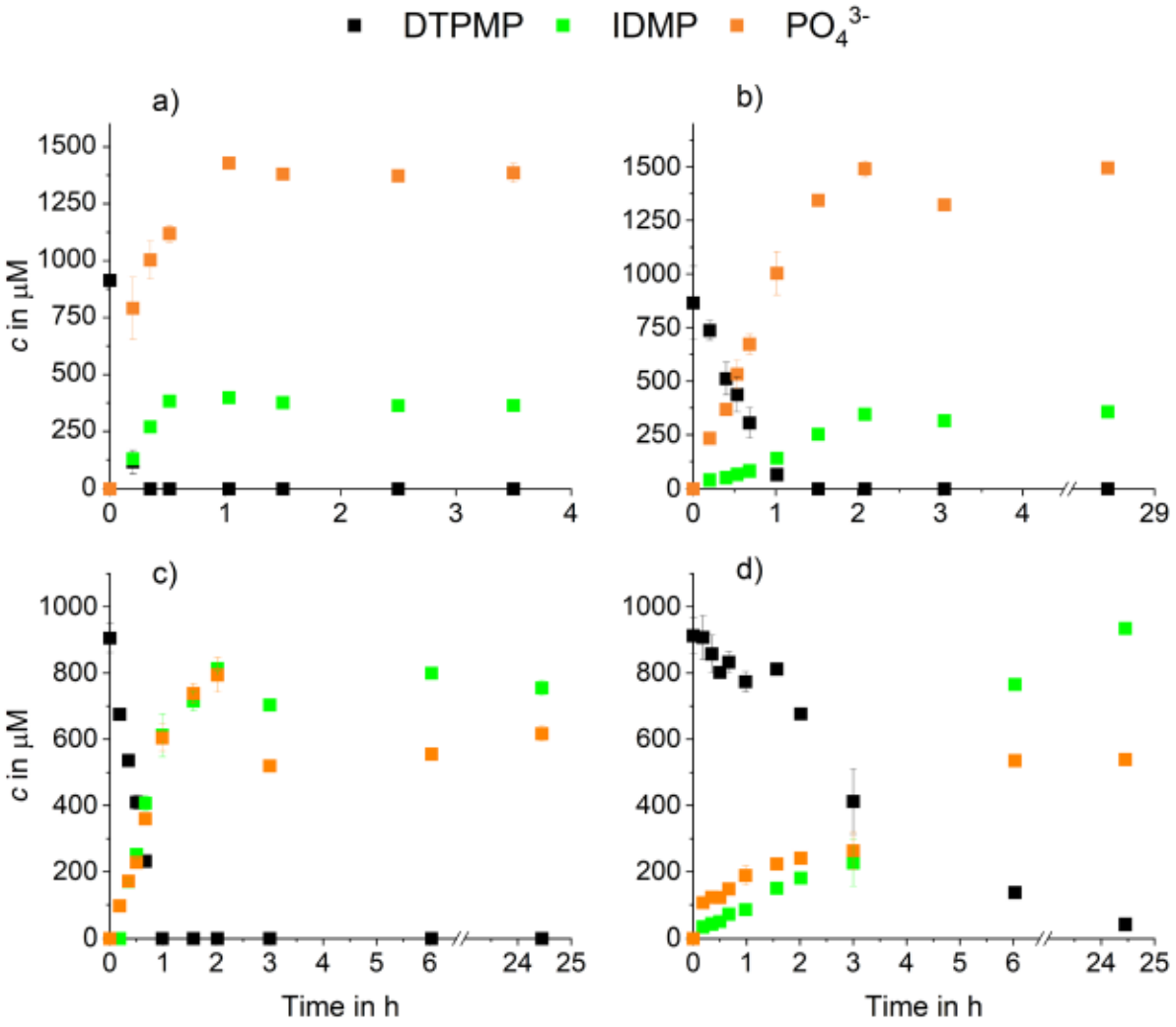

Figure D.4 Aqueous DTPMP (black), IDMP (green) and PO_4^{3-} (orange) concentrations quantified using IC-ICP-MS ($^{31}P^{16}O^+$) during DTPMP oxidation by MnO_2 in four different experiments. a) 1.0 g/L MnO_2 oxic, b) 0.1 g/L MnO_2 oxic, c) 1.0 g/L MnO_2 anoxic, d) 0.1 g/L MnO_2 anoxic. Error bars represent absolute errors between experimental duplicates.

Long-time replica of 1.0 g/L MnO_2 in MES buffer

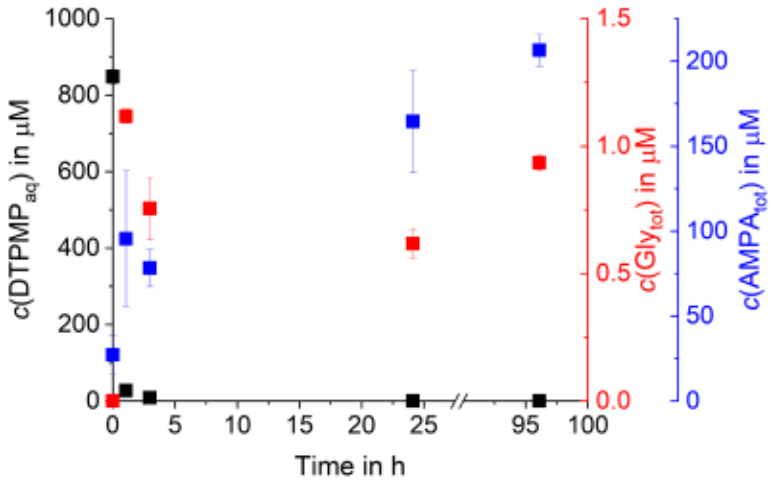

Figure D.5 Aqueous concentrations of DTPMP (back) quantified by means of IC-ICP-MS and total concentrations of glyphosate (red) and AMPA (blue) quantified by means of LC-QQQ in the longtime replica of the experiment using 1.0 g/L MnO_2 in ultrapure buffered water (pH 6) under oxic conditions over 96 hours. Error bars represent absolute errors between experimental duplicates.

AMPA and glyphosate in the DTPMP-free wastewater controls

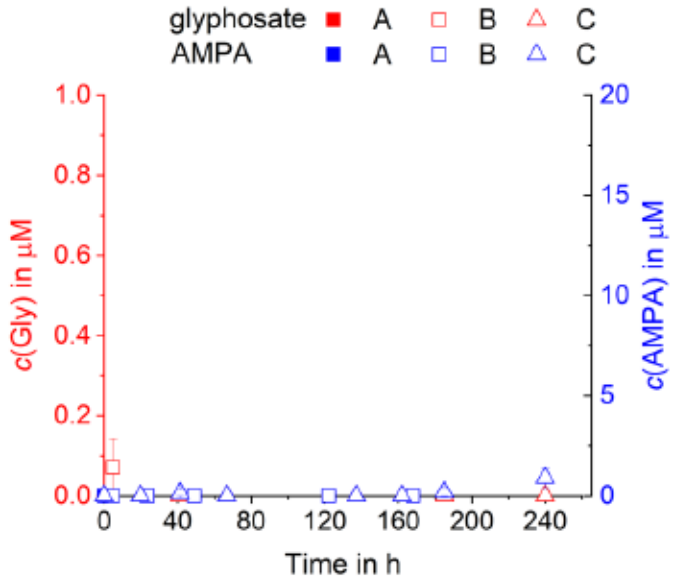

Figure D.6 Glyphosate (red) and AMPA (blue) concentrations quantified by LC-QQQ in control experiments without the addition of DTPMP. A: pure wastewater, B: wastewater with 1.0 g/L MnO_2, C: wastewater with 1 mM $MnCl_2$. Note: Due to data point overlay, not all individual data points are visually distinguishable.

DTPMP transformation by MnO_2 in wastewater vs. MES buffer

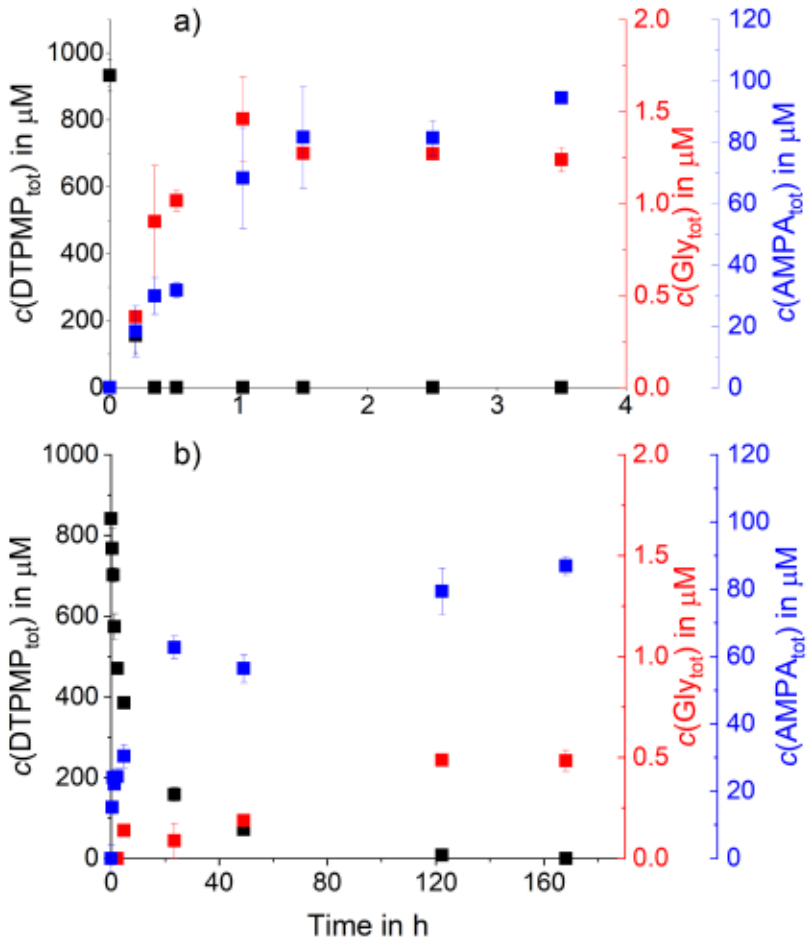

Figure D.7 Total DTPMP (black), glyphosate (red) and AMPA (blue) concentrations quantified by means of IC-IPAD (DTPMP) and LC-QQQ (glyphosate, AMPA) in two experiments containing 1 mM DTPMP and 1.0 g/L MnO_2 in a) 20 mM MES buffer (pH 6) and b) wastewater (pH 8).

METHODS

Quantification of DTPMP

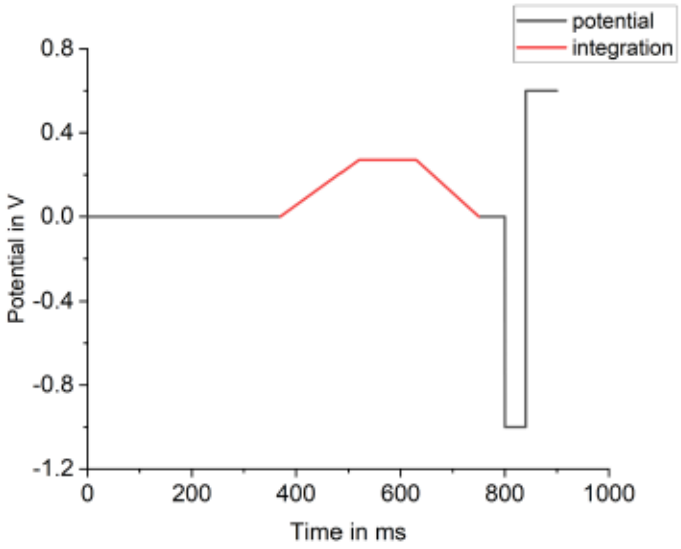

Figure D.8 Detector method or "waveform" for the amperometric detection used in the IC-IPAD method.

Table D.1 Concentration gradient profile of 15 mM NaOH (eluent A) and 50 mM NaOH and 400 mM NaAc (eluent B) for the quantification of DTPMP by IC-IPAD.

Time in min	Share eluent A in %	Share eluent B in %
0.0	100	0
7.1	90	10
15.1	70	30
19.0	0	100
20.0	0	100
20.1	100	0
31.0	100	0

Quantification of AMPA and glyphosate

Table D.2 Concentration gradient profile of 2.5 mM aqueous ammonium acetate (eluent A) and acetonitrile (eluent B) for the quantification of AMPA and glyphosate by LC-QQQ.

Time in min	Share eluent A in %	Share eluent B in %
0.00	95.00	5.00
2.00	95.00	5.00
8.00	30.00	70.00
8.50	0.00	100.00
13.00	0.00	100.00
13.10	95.00	5.00
16.00	95.00	5.00

Table D.3 MS/MS parameters for the quantification of AMPA and glyphosate by LC-QQQ. All compounds were derivatized using FMOC-Cl.

Compound	Precursor ion (*m/z*)	Product ion (*m/z*)	Fragmentor in V	Collision energy in e	Retention time in min
Glyphosate	392	179	100	24	6.15
	392	88	100	16	
$^{13}C_2$, ^{15}N-Glyphosate	395	179	100	24	6.15
	395	91	100	16	
AMPA	334	179	100	11	7.03
	334	112	100	10	
$^{13}C^{15}N$-AMPA	336	179	100	11	7.03
	336	114	100	10	
Glufosinate	404	179	100	24	6.42
	404	136	100	20	

The following table holds LOD/LOQ values for AMPA and glyphosate LC-QQQ measurements derived as stated in the Methods section of the main text.

Table D.4 LOD and LOQ values for glyphosate and AMPA in µg/L for each measurement sequence for the LC-QQQ measurements. The approach used to derive those LOD/LOQ values is described in the Methods section. The controls are displayed below the respective experiment.

Experiment			Glyphosate		AMPA	
Manganese	**O_2**	**matrix**	**LOD**	**LOQ**	**LOD**	**LOQ**
1.0 g/L MnO_2	oxic	MES	10.48	17.44	6.41	10.03
0.1 g/L MnO_2	oxic	MES	5.09	12.13	6.31	10.73
1.0 g/L MnO_2	anoxic	MES	9.80	33.47	9.49	20.94
0.1 g/L MnO_2	anoxic	MES	3.57	6.98	9.49	20.94
1 mM Mn^{2+}	oxic	MES	4.63	8.64	4.42	8.94
- Control 1			4.63	8.64	4.42	8.94
1.0 g/L MnO_2	oxic	wastewater	4.89	10.14	4.42	8.94
- Control 1			3.57	6.98	1.71	4.83
- Control 2			5.50	11.00	5.36	12.04
- Control 3			3.57	6.98	1.71	4.83
1 mM Mn^{2+}	oxic	wastewater	4.63	8.64	5.36	12.04
- Control 1			4.63	8.64	4.42	8.94

Aqueous and sorbed fractions of AMPA and glyphosate

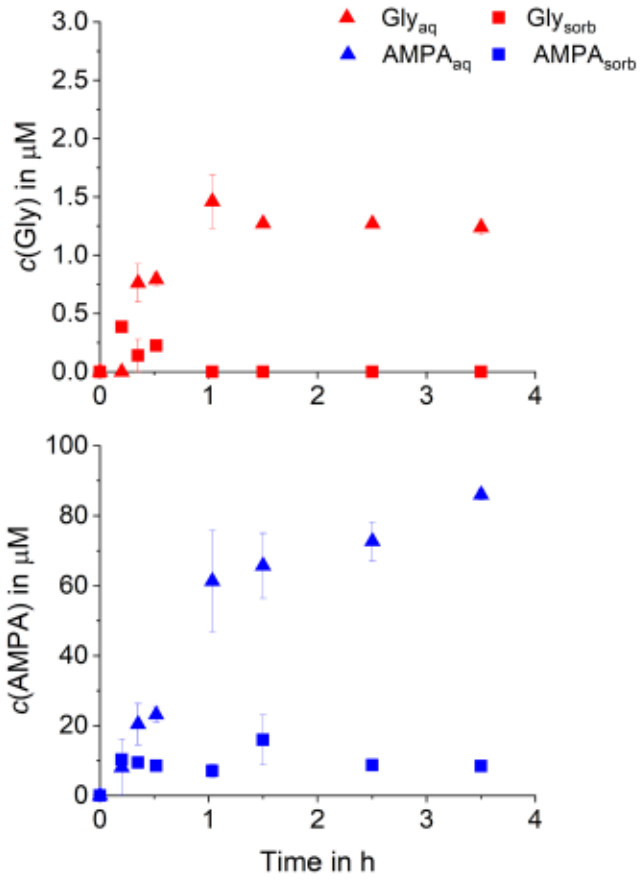

Figure D.9 Aqueous and sorbed glyphosate (red) and AMPA (blue) concentrations quantified by means of LC-QQQ in the experiment with 1.0 g/L MnO_2 under oxic conditions (pH 6). Error bars represent absolute errors between experimental duplicates.

Quantification of phosphorus-containing TPs using IC-ICP-MS

Table D.5 Concentration gradient profile of 300 µg/L aqueous DTPA (pH 9.2) (eluent A) and 150 mM aqueous ammonium nitrate with 300 µg/L DTPA (pH 9.2) (eluent B) for the quantification of P-containing compounds by IC-ICP-MS.

Time in s	Share eluent A in %	Share eluent B in %
0	91.5	8.5
25	86.5	13.5
120	60.0	40.0
155	30.0	70.0
185	12.0	88.0
245	12.0	88.0

Nuclear Magnetic Resonance Spectroscopy (NMR)

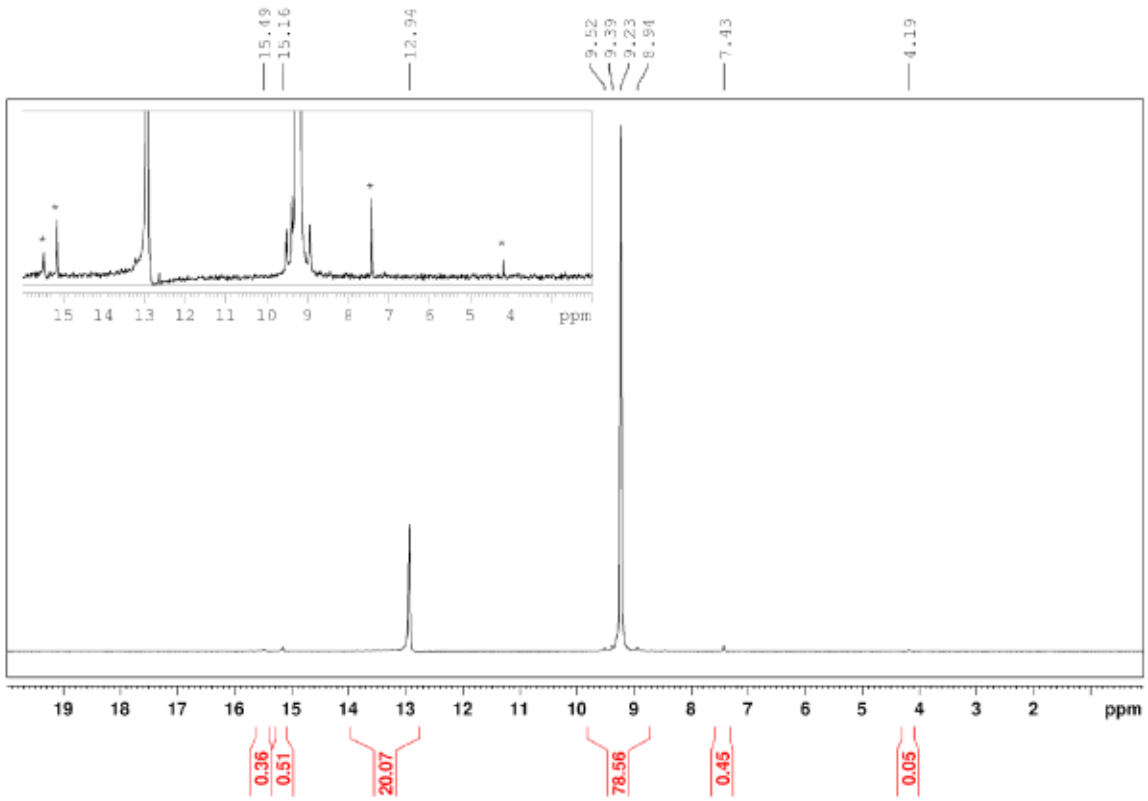

Figure D.10 ^{31}P-{^{1}H}-NMR-spectrum of DTPMP in D_2O measured as stated in the Methods section. δ (ppm): 9.23, 12.94. Impurities are marked with an asterisk. The sum of integrals is normalized to 100.

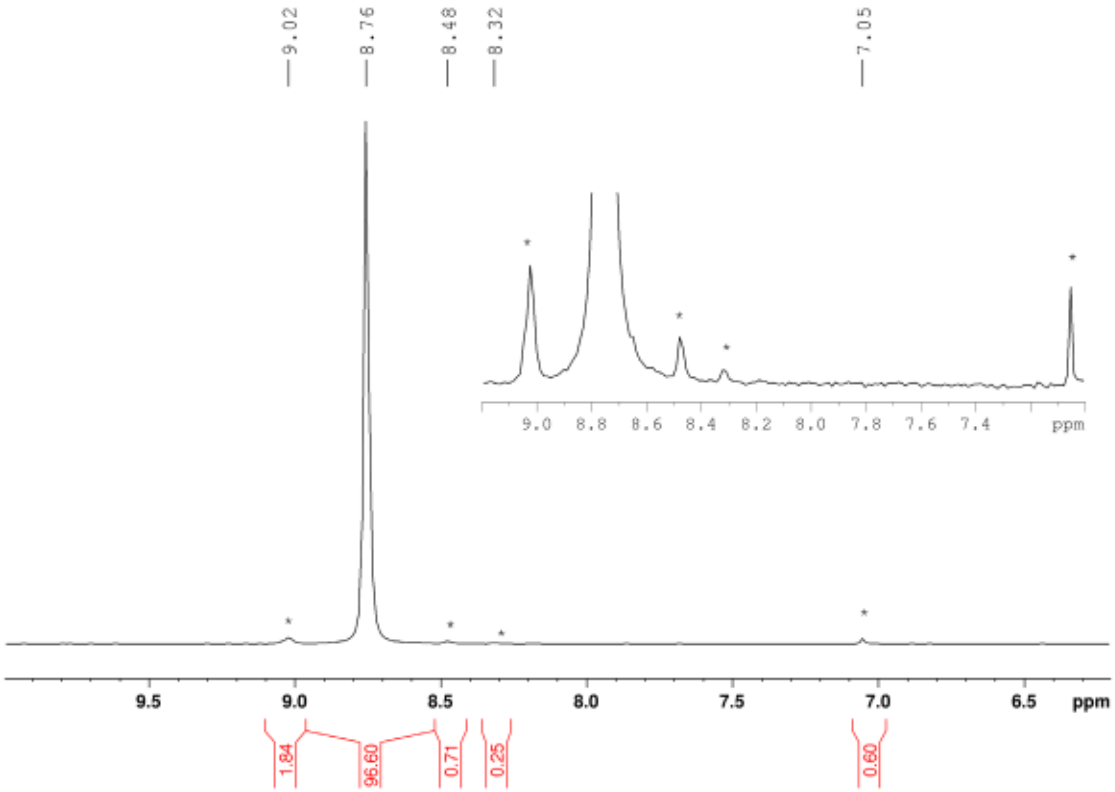

Figure D.11 ^{31}P-{^{1}H}-NMR-spectrum of EDTMP in D_2O measured as stated in the Methods section. δ (ppm): 8.76. Impurities are marked with "*". The sum of integrals is normalized to 100.

Mineral Characterization

Point of zero charge (pH_{PZC})

The pH_{PZC} of the MnO_2 used in this study was analyzed via ζ-potential measurements using a Zetasizer Nano ZSP (Malvern Pananalytical, Malvern, United Kingdom) in folded capillary zeta cells at 20 °C. Measurements were conducted in triplicates with 10 to 15 runs, each. For analysis, 50 mg/L MnO_2 suspensions were prepared in 10 mM NaCl + 10 mM MES buffer and the pH was adjusted by 0.1 M or 1 M NaOH and HCl. The point of zero charge (pH_{PZC}) was determined by plotting the zeta potential as a function of the adjusted pH and subsequent regression of the linear part of the data sets. pH_{PZC} was determined to be 5.6 ± 0.1.

Brunauer-Emmett-Teller method (BET)

The specific surface area (SSA) of the MnO_2 was determined by nitrogen sorption-desorption isotherms using a Gemini VII 2390 (Micrometrics, Norcross, GA, USA). Samples were degassed before analysis overnight under vacuum at 120 °C. SSA was determined at 64.5 ± 0.2 m^2/g.

Powder X-ray diffraction (XRD)

XRD measurements were performed in Göttingen by Volker Karius using an Orion Comet P2 Powder diffractometer (XRD Eigenmann GmbH, Schneittach-Hormersdorf, Germany) equipped with a Cu–source (Cu-Kα radiation, λ_1 = 1.54060 Å, λ_2 = 1.54443 Å) with a $K\alpha_2/K\alpha_1$ relation of 0.5 and a beam voltage and current of 40 kV and 40 mA, respectively. The mineral predominantly exhibits an amorphous structure interspersed with localized crystalline domains consisting of the two polymorphs pyrolusite (β-MnO_2) and akhtenskite (ε-MnO_2).

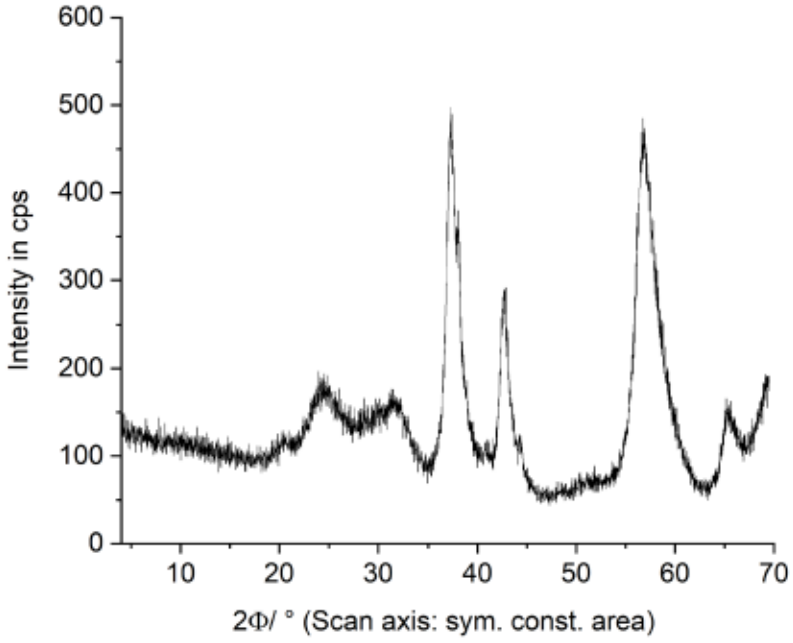

Figure D.12 X-ray diffractogram of the manganese dioxide used in this study. Measurement details are given in the text above.

Further Mineral Analysis

The extractable Mn^{III}-content (quantified by pyrophosphate extraction and UV/vis spectroscopy) was 1 % of total manganese. With regard to the surface area, the extractable Mn^{III}-content was

1.76 nmol/m². Further, total reflection X-ray fluorescence (TXRF) revealed just minor amounts of mono- and bivalent cations (K: <0.001, Ca and Ba: ≤0.03 molar ratio vs Mn), which validates the low Mn^{III}-content.

Wastewater Characterization

Inorganic cation and anion analysis was performed using IC coupled to conductivity detection (CD). The ion chromatograph (930 Compact IC Flex) was equipped with a 919 IC Autosampler plus and two 800 Dosinos (all Metrohm, Filderstadt, Germany) for automated sample dilution and eluent production. On the anion side, a suppressor (MSM Rotor A, Meotrhm) was installed prior to the detector. The column Metrosep A Supp 5 (4.0 x 250.0 mm) was employed for anion analysis, while the Metrosep C6 (4.0x250 mm) was employed for cation analysis (both Metrohm). The eluent on the anion side consisted of 3.2 mM sodium carbonate and 1.0 mM sodium bicarbonate in ultra-pure water and was delivered at a flow rate of 0.7 mL/min. The eluent on the cation side consisted of 4.0 mM nitric acid and 0.7 mM dipicolinic acid delivered at a flow rate of 0.9 mL/min. The injection volume was 20 µL.

Thedissolved organic carbon (**DOC**) was analyzed using a vario TOC cube (Elementar, Langenselbold, Germany). Prior to analysis, the samples were filtered (0.45 µm), acidified to a pH of less than 2 using 32% HCl and purged with synthetic air to remove inorganic carbon. The analysis was conducted in duplicates.

Aqueous manganese and iron in the filtered wastewater sample was quantified by a 4200 MP–AES, equipped with a SPS 3 autosampler, a cyclonic spray chamber and an easy–fit torch (Agilent Technologies, Santa Clara, United States). The selected wavelengths were 403.076 nm (Mn) and 373.486 (Fe). Samples were diluted prior to analysis 1:2, with a final concentration of 1 % (v/v) HNO3. External standards in the range between 0.01 mg/L and 5.0 mg/L were used for quantification ($R^2 > 0.999$). LOD for Mn was determined to be 0.038 mg/L, while the LOD for Fe was determined to be 0.019 mg/L.

Table D.6 Anions and cations quantified in the wastewater sample using ion chromatography with conductivity detection, except for Mn and Fe, which were quantified using microwave-plasma atomic emission spectroscopy (MP-AES), and therefore are not assigned cationic charges.

Anion	*c* in mg/L	Cation	*c* in mg/L
F^-	0.23	Na^+	27.9
Cl^-	39.1	NH_4^+	13.0
NO_2^-	0.7	K^+	7.8
Br^-	0.04	Mg^{2+}	13.3
NO_3^-	7.1	Ca^{2+}	71.3
PO_4^{3-}	3.3	Mn	<0.04
SO_4^{2-}	99.4	Fe	<0.02

Table D.7 Wastewater parameters recorded for a 24-hour mixed sample in the WWTP Lustnau on September 9, 2024. COD stands for "chemical oxygen demand".

Parameter	Value
COD	195 mg/L
P total	2.27 mg/L
Conductivity	691 µS/cm
Temperature	18.8 °C

Acknowledgements

First and foremost, I want to thank Stefan B. Haderlein for taking on the main supervision of my doctoral thesis. Thank you, Stefan, for the opportunity to conduct my PhD thesis in your group and laboratory, thank you for always being available for detailed discussions of data as well as any thoughts or concerns I had throughout the years. Thank you for fostering a relaxed atmosphere in your working group, free from pressure, and for your calming presence in stressful times. I really enjoyed working with you.

Further, I want to thank Torsten C. Schmidt for taking on the Co-supervision of my thesis. Thank you, Torsten, for your regular and valuable feedback in long online meetings and providing me with a more broad-scope perspective on my research. I thank both of you, Stefan & Torsten, for the valuable discussions further shaping my conception of research and ways of thinking. I feel like, no matter where I will go now, those learnings in science and project management will help me on my way ahead.

I would like to thank Philipp R. Martin for the introduction into the phosphonate topic, LC-IRMS and – more general – the field of water chemistry from the laboratory side. I learned a lot from your analytical way of thinking, and our scientific discussions were always very fruitful.

I want to thank the "Happy Office" members Kleanthi Kourtaki and Ruoning Guo for a nice atmosphere. Thank you together with Sara Wild, Cora Strobel and Tamara Pruneddu for the fun lunch times.

Sara, besides that, thank you for your help in the lab, for taking care of the LC-QQQ and especially the (terrible) derivatization procedure. I learned a lot from you. Cora, thank you for interesting conversations about life, science and feminism. I always looked forward to our lunchbreaks and feel to have found an ally in you regarding many views and values.

I thank my diligent HiWis and bachelor students Nora Simon and Hannah Arnold for conducting MnO_2 transformation experiments and helping with the FMOC derivatization. It was a pleasure teaching you.

I want to thank Alwina Mozer and Thomas Kolb from Metrohm, who were always available for discussing problems and sending new spare parts – or even bringing them over from Filderstadt in person. Thank you for your time, the discussions and your ever-present help.

Thanks to my cooperation partners Robert G. H. Marks and Mathis Athmer. Thank you, Robert, for the valuable discussions and great advice on analytical chemistry as well as analyzing some of my samples using your LC-IRMS/HRMS coupling. Thank you, Mathis, for the incredibly pleasant and successful collaboration as well as fruitful discussions. Thank you both for fun conferences!

For the last months of my PhD, I especially want to express my thanks to Joachim Weiss. It was such a blessing to meet you at the Analytica 2024. Thank you for your explanations, your unfiltered honesty, and sharing your expertise. I learned so much from you about ion chromatography, pulsed amperometric detection, and IC problem solving. I am very happy that – with your help– I could finally bring the IC-PAD method chapter to a successful completion.

Especially for the last weeks of my PhD I thank Uwe Karst for advice and help in tricky situations. Thank you for always having an open ear and making time for calls despite your full schedule.

Additionally, I want to thank Sarah Bieger and Markus Kramer from the University of Tübingen for conducting and analyzing the NMR measurements of EDTMP and DTPMP I referred to in my work. In this regard I also want to thank Volker Karius from the university of Göttingen for conducting X-ray diffractograms of the used manganese oxide.

Thank you, Daniel Buchner and Maik A. Jochmann, for your efforts in drafting the DFG proposal and successfully securing the funding my and Roberts PhD theses were based on.

A big thank you to my family, who I could partially just see very rarely. Thanks to all of you, for at least visiting me once in Tübingen, even though the way was long and hard (especially with Deutsche Bahn …). Thanks for the family vacations that allowed me to unwind from work and simply enjoy life. Thanks for always believing in me and supporting any decision.

Finally, I want to thank my life partner Simon Ritter for taking my mind off at the weekends and focusing on “having a good time”. This helped me get through the terrible months of PhD, when it felt like nothing would ever work out.

Statement of Personal Contribution

The work described in the presented thesis was funded by the German Research Foundation (Deutsche Forschungsgemeinschaft).

The following lists delineate my personal contributions to the collaborative publications and manuscripts incorporated in my thesis, "Manganese-driven oxidation of amino(poly)phosphonates – kinetics, processes and product formation". Author contributions are presented in accordance with the CRediT (Contributor Roles Taxonomy) system (https://credit.niso.org/). These detailed attributions precede each chapter containing collaborative work within the thesis.

Chapter 2: Transformation of Iminodi(methylene phosphonate) on Manganese Dioxides – Passivation of the Mineral Surface by (Formed) Mn^{2+}

Authors: Anna M. Röhnelt, Philipp R. Martin, Daniel Buchner, Stefan B. Haderlein

Status in the publication process: Manuscript published.

Röhnelt, A. M., Martin, P. R., Buchner, D., & Haderlein, S. B. (2023). Transformation of Iminodi(methylene phosphonate) on Manganese Dioxides - Passivation of the Mineral Surface by (Formed) Mn2+. *Environmental Science and Technology*, *57*(32), 11958–11966. https://doi.org/10.1021/acs.est.3c01838

Author Contributions:

A.M.R.: Conceptualization, Methodology, Validation, Formal Analysis, Investigation, Writing – Original Draft, Visualization

P.R.M.: Conceptualization, Methodology, Validation, Writing – Review & Editing

D.B.: Funding Acquisition, Writing – Review & Editing

S.B.H.: Funding Acquisition, Supervision, Resources, Writing – Review & Editing

Chapter 3: Green Quantification of Amino(poly)phosphonates using Ion Chromatography coupled to Integrated Pulsed Amperometric Detection

Authors: Anna M. Röhnelt, Philipp R. Martin, Robert G. H. Marks, Daniel Buchner, Joachim Weiss, Torsten C. Schmidt, Stefan B. Haderlein

Status in the publication process: Manuscript published.

Röhnelt, A. M., Martin, P. R., Marks, R. G. H., Buchner, D., Weiss, J., Schmidt, T. C., & Haderlein, S. B. (2025). Green quantification of amino(poly)phosphonates using ion chromatography coupled to integrated pulsed amperometric detection. *Analytical and Bioanalytical Chemistry*. https://doi.org/10.1007/s00216-025-05747-w

Author Contributions:

A.M.R.: Conceptualization, Methodology, Validation, Formal Analysis, Investigation, Writing – Original Draft, Visualization

P.R.M.: Conceptualization, Methodology, Funding Acquisition, Writing – Review & Editing

R.G.H.M.: Conceptualization, Writing – Review and Editing

D.B.: Funding Acquisition, Writing – Review & Editing

J.W.: Validation, Writing – Review and Editing

T.C.S.: Supervision, Writing – Review and Editing

S.B.H.: Funding Acquisition, Supervision, Resources, Writing – Review & Editing

Chapter 4: Glyphosate is a transformation product of a widely used aminopolyphosphonate complexing agent

Authors: Anna M. Röhnelt, Philipp R. Martin, Mathis Athmer, Sarah Bieger, Daniel Buchner, Uwe Karst, Carolin Huhn, Torsten C. Schmidt, Stefan B. Haderlein

Status in the publication process: Manuscript accepted for publication by *Nature Communications*. Resubmitted after revisions at February 11, 2025. Preprint available at https://www.researchsquare.com/article/rs-4692988/v1.

Author Contributions:

A.M.R.: Conceptualization, Methodology, Validation, Formal Analysis, Investigation, Writing – Original Draft, Visualization, Project Administration

P.R.M.: Conceptualization, Methodology, Validation, Funding Acquisition, Writing – Review & Editing

M.A.: Methodology, Investigation, Formal Analysis (all regarding IC-ICP-MS), Writing – Review and Editing

S.B.: Investigation, Formal Analysis (all regarding NMR measurements), Writing – Review and Editing

D.B.: Conceptualization, Funding Acquisition, Writing – Review & Editing

U.K.: Supervision, Writing – Review and Editing

C.H.: Conceptualization, Writing – Review and Editing

T.C.S.: Supervision, Writing – Review and Editing

S.B.H.: Conceptualization, Supervision, Resources, Writing – Review & Editing